ABSTRACT

FLUIDIZATION OF NANOPARTICLES

by
Caroline Hijung Nam

During the past decade, nanoparticles (1-100 nm) and nanocomposites have become the focus of many studies due to the unique properties of nanostructured materials that make them attractive for various applications. Due to their atomic and molecular interactions, nanoparticles and nanocomposites have unique and often favorable catalytic, mechanical, optical, electronic and / or other properties. For instance, nanocrystalline copper is up to 5 times harder than conventional micron sized copper particles. Nanocomposites, such as a homogenous mixture of different nanoparticles, can also exhibit improved properties. Other examples include coating and reacting nanoparticles with a second nanostructured phase. These processes are ideally suited to a fluidization process. However, in order to successfully use these applications, it is necessary to understand how nanoparticles can be fluidized.

This dissertation demonstrates that the fluidization of nanoparticles is indeed possible and in fact, significantly improvable with the addition of external forces or changes in certain conditions. Silica, alumina, and titania nanoparticles, whose sizes range from 7 to 21 nm in diameter, are fluidized in a conventional gravity-driven bed, a vibrated bed, a magnetically assisted bed, a rotating bed, and a bed under supercritical conditions.

The key parameters affecting fluidization quality are examined in each fluidized bed system. An advanced laser and CCD camera system is used to view agglomerates as they are being fluidized. A novel method for estimating fluidized agglomerate size from liquid-fluidization theory and fractal analysis is shown to be in very good agreement with experimental data. Exciting applications in mixing and filtration are also presented.

FLUIDIZATION OF NANOPARTICLES

by
Caroline Hijung Nam

A Dissertation
Submitted to the Faculty of
New Jersey Institute of Technology
In Partial Fulfillment of the Requirements for the Degree of
Doctor of Philosophy in Chemical Engineering

Otto H. York Department of Chemical Engineering

August 2004

APPROVAL PAGE

FLUIDIZATION OF NANOPARTICLES

Caroline Hijung Nam

Dr. Robert Pfeffer, Dissertation Advisor	Date
Distinguished Professor of Chemical Engineering, NJIT	

Dr. Rajesh Davé, Co-Dissertation Advisor	Date
Professor of Mechanical Engineering, NJIT	

Dr. Michael C.Y. Huang, Committee Member	Date
Assistant Professor of Chemical Engineering, NJIT	

Dr. Dana E. Knox, Committee Member	Date
Professor of Chemical Engineering, NJIT	

Dr. Jing Wu, Committee Member	Date
Assistant Professor of Chemical Engineering, NJIT	

BIOGRAPHICAL SKETCH

Author: Caroline Hijung Nam

Degree: Doctor of Philosophy

Date: August 2004

Undergraduate and Graduate Education:

- Doctor of Philosophy in Chemical Engineering,
  New Jersey Institute of Technology, Newark, NJ, 2004

- Bachelor of Engineering in Chemical Engineering,
  The Cooper Union, New York, NY, 2000

Major: Chemical Engineering

Presentations and Publications:

Caroline H. Nam, Robert Pfeffer, Rajesh N. Dave, Jean-Jacques Letourneau, Jacques
Fages, Elizabeth Rodier, "Fluidization of Nanoparticles under Supercritical
Conditions," in preparation, 2004.

Caroline H. Nam, Robert Pfeffer, Rajesh N. Dave, "Fluidization of Nanoparticles in a
Rotating Fluidized Bed," in preparation, 2004.

Caroline H. Nam, Robert Pfeffer, Rajesh N. Dave, Sankaran Sundaresan,
"Aerated Vibrofluidization of Silica Nanoparticles," AIChE Journal,
Vol.50, No. 8, August 2004.

Caroline H. Nam, Robert Pfeffer, Rajesh N. Dave, "Vibrofluidization of Silica
Nanoparticles," Invited Seminar, University of Delaware, March 2004.

Chao Zhu, Guanglian Liu, Qun Yu, Robert Pfeffer, Rajesh N. Dave, Caroline H. Nam,
"Sound Assisted Fluidization of Nanoparticle Agglomerates," Powder
Technology, Vol. 141, pp. 119 – 123, 2004.

Caroline H. Nam, Robert Pfeffer, Rajesh N. Dave, "Vibrofluidization and Magnetically Assisted Fluidization of Nanoparticles," Serial No. 60/490,912, Provisional Patent filed July 2003.

Caroline H. Nam, Robert Pfeffer, Rajesh N. Dave, "Fluidization of Nanoparticles," Proceedings on CD-ROM, 11th International Conference on Fluidization, Naples, Italy, May 2004.

Qun Yu, Caroline H. Nam, Jose Quevedo, Rajesh N. Dave, Chao Zhu, Robert Pfeffer, "Fluidization of Nanoparticles Using External Forces," Work-In-Progress Poster Session of Fluidization XI: Present and Future for Fluidization Engineering, Naples, Italy, May 2004.

Robert Pfeffer, Rajesh N. Dave, Chao Zhu, Caroline H. Nam, Qun Yu, Jose Quevedo, "Fluidization of Silica Nanoparticles Using External Forces," Particles 2004 Conference, Poster Session, Orlando, FL, March 2004.

Robert Pfeffer, Rajesh N. Dave, Chao Zhu, Caroline H. Nam, Jose Quevedo, Qun Yu, "Fluidization of Silica Nanoparticles Using External Forces," 2004 NSF Grantees Conference, Dallas, TX, January, 2004.

Caroline H. Nam, Robert Pfeffer, Rajesh N. Dave, "Aerated Vibrofluidization of Nanoparticles," American Institute of Chemical Engineers Annual Meeting, Indianapolis, IN, November 2002.

Caroline H. Nam, Robert Pfeffer, Rajesh N. Dave, "Aerated Vibrofluidization of Nanoparticles," New Jersey Commission for Science and Technology Review Meeting Poster Session, Newark, NJ, September 2002.

Caroline H. Nam, Robert Pfeffer, Rajesh N. Dave, "Aerated Vibrofluidization of Nanoparticles," Industrial Advisory Board Meeting Poster Session, Newark, NJ, September 2002.

Caroline H. Nam, Robert Pfeffer, "Fluidization of Nanoparticles," Seminar at the Center for Powders and Processes, Albi, France, May 2002.

Caroline H. Nam, Madhuri Kolli, "Fluidization and Granulation in the Rotating Fluidized Bed," Particle Engineering Research Center Meeting at the University of Florida, Gainsville, FL, February 2001.

Karen J. Buechler, Caroline H. Nam, Theresa M. Zawistowski, Richard D. Noble, Carl A. Koval, "Design and Evaluation of a Novel Reactor to Study the Effects of Controlled Periodic Illumination on Photocatalytic Reactions," Industrial and Engineering Chemistry Research, Vol. 38, pp. 1258 – 1263, April 1999.

나의 할머니

오늘의 나는 할머니가 있어서에요

감사 합니다.

영원토록 사랑 해요.

희정

To my Grandma.

I am because of you.

I love you forever.

ACKNOWLEDGMENT

TABLE OF CONTENTS

TABLE OF CONTENTS
(Continued)

Chapter   **Page**

LIST OF TABLES

LIST OF FIGURES

NOMENCLATURE

A = amplitude of vibration (cm)

A_v = cross sectional area of the fluidization chamber (cm^2)

d_{pp} = diameter of primary particle (cm)

d_a = diameter of agglomerate (cm)

D_f = fractal dimension of an agglomerate

f = frequency (Hz)

g = 980 cm/ s^2, acceleration of gravity (cm/s^2)

g_c = 980 gm cm/(gm wt) s^2, conversion factor

H = Hamaker constant (J)

H_{exp} = height of expanded bed at a certain air velocity (cm)

H_{mf} = height of bed at minimum fluidization (cm)

H_o = initial (settled) height of bed before fluidization experiment (cm)

m_a = mass of an agglomerate (g)

n = Richardson-Zaki exponent

N = number of particles in an agglomerate

ΔP = pressure drop (Pa)

r_a = radius of the agglomerate (cm)

r_{pp} = radius of the primary particle (cm)

SA_{pp} = surface area of the primary particle (m^2/g)

u = superficial velocity (cm/s)

u_{mb} = minimum bubbling velocity (cm/s)

$u_{mf} =$ minimum fluidization velocity (cm/s)

$v_a =$ Stokes' settling velocity of an agglomerate (cm/s)

$v_o =$ Stokes' settling velocity of a primary particle (cm/s)

$W =$ weight of the powder bed (g)

$\alpha =$ cross sectional area (m^2)

$\varepsilon =$ total bed voidage

$\varepsilon_e =$ inter-agglomerate voidage

$\varepsilon_m =$ voidage in a packed bed

$\varepsilon_{mf} =$ total voidage at minimum fluidization

$\Gamma =$ vibration intensity

$\phi_e =$ volume fraction of agglomerates in the bed

$\phi =$ volume fraction of primary particles in the bed

$\phi_s =$ sphericity of particle

$\rho_a =$ density of agglomerate (gm/cm^3)

$\rho_b =$ density of the bulk powder (gm/cm^3)

$\rho_f =$ density of fluid (gm/cm^3)

$\rho_g =$ density of fluidizing gas (gm/cm^3)

$\rho_{pp} =$ density of primary particle (gm/cm^3)

$\rho_s =$ density of solids (gm/cm^3)

$u =$ viscosity of gas (gm/cm s)

$\omega =$ angular velocity $= 2\pi f$ (radians/s)

CHAPTER 1

INTRODUCTION

Upon Neil Armstrong's return from the Moon, he described his first steps: "Yes, the surface is fine and powdery. I can kick it up loosely with my toe. It does adhere in fine layers, like powdered charcoal, to the sole and sides of my boots. I only go in a small fraction of an inch, maybe an eighth of an inch, but I can see the footprints of my boots and the treads in the fine, sandy particles (a 1969 conversation transcribed by Jones, 1995)." From these words alone, one can deduce that the Moon's sands are quite different from the sands on the Jersey shore. The dissimilarity can be attributed to the lack of gas on the Moon and the smaller gravitational force compared to Earth's. The key message here that will thematically manifest itself in this dissertation is that powders behave in different ways under different conditions. This dissertation will present the effects of various external forces and environmental conditions on the behavior of fine, nanosized powders during fluidization.

1.1   Nanotechnology: Motivation

Particles are ubiquitous. They are in the ground where crops grow, in rainbows, and even in the words printed on this paper. Due to their high surface to volume ratio, they have very useful applications such as in reactions, catalysis, dispersion, and coating. The technology in developing particle products has only grown in importance since its surge after World War II, when countries were rebuilding their economies.

1

The research since the 1950's and 1960's has shown that certain particle characteristics, such as size, are directly related to their bulk properties. Unique properties can be expected as the size of particles is reduced to the size of molecules. Thus, nanotechnology is predicted to be one of the most significant areas of research.

The basis of nanotechnology is that all materials can be made from atoms and molecules to form nanoparticles, which can be made into nanostructures like coatings, materials with very high surface areas, functional nanodevices, and other materials that have unique properties. The challenge lies not only in the controlled and consistent fabrication of the nanoparticles themselves, but also the subsequent building into nanostructures as the ones described above. Another challenge arises in the handling of the particles since the nanoscale results in poorer flow and higher cohesive forces.

When the challenges are overcome, the implications will be tremendous. A 5 nm particle has about half its atoms at the surface. So techniques that loosely bring together such particles and thus maintain a very high surface area, for example, offer exciting opportunities such as new methods for chemical and electrical energy storage, sensors, tailored catalysts, and drug delivery systems (Koch, 1999). Generally, nanostructures are expected to have new and improved magnetic, optical, mechanical, and / or other properties.

In order to face these challenges, a deep understanding of nanoparticles must be sought. The area that will be focused in this dissertation is that of fluidization of nanoparticles. Fluidization is important in many powder processes in that it allows for smooth flow of particles with ease of handling. It also allows for rapid and homogenous mixing of solids, increased mass and heat transfer coefficients, as well as increased

reaction rates. Understanding the behavior of fluidizing nanoparticles is a big step forward in the field of nanotechnology.

1.2 Background and Applications of Fluidization

By definition, fluidization is simply the lifting of powders by a fluid. The magic that occurs from this levitation is the high fluid – solid contact or as the name fluidization implies, the fluidity of the solids. The intense fluid – solid contact leads to tremendous advantages such as mixing of solids at practically isothermal conditions and ease of transport of solids, and increased rates of heat and mass transfer.

Typically, a bed of powders is said to be fluidized when the pressure drop across the bed, caused by the flow of gas or liquid, balances the weight of the bed. There are several regimes and behaviors of a bed of powders as velocity, properties of the solid particles, properties of the fluidizing medium, and even the design of the fluidization system are varied.

At a low flow rate, the gas or liquid simply percolates through the empty spaces between the particles which renders the bed "fixed" since the particles are immobile. As the flow rate increases, the frictional force between a particle and fluid also increases. At a certain velocity, when the drag force by the moving gas or liquid just about balances the weight of the bed of particles less their buoyancy, the bed is classically said to be at minimum fluidization. The corresponding velocity to a bed that is at minimum fluidization, also known as incipient fluidization, is called the "minimum fluidization velocity," u_{mf}. At velocities above the minimum fluidization velocity, the bed is typically said to be fluidized.

Liquid-solid systems are usually characterized by smooth expansion of the bed and lack of bubbles whereas gas-solid systems are usually characterized by instabilities, low bed expansion, and bubbling. The velocity at which bubbling begins is called the "minimum bubbling velocity", u_{mb}. Smoothly rising beds without bubbles have been dubbed "smoothly fluidized beds," "particulately fluidized beds," or "homogeneously fluidized beds." Unstable, bubbling beds have been called "bubbling fluidized beds," "aggregative fluidized beds," or "heterogeneously fluidized beds."

The properties of the solid particles significantly affect the behavior of fluidization. In 1973, Geldart published a classification of powders with respect to their gas fluidization behavior, which has been used as a staple reference in most gas fluidization papers thereafter (Geldart, 1973). His famous categorization is shown in Figure 1.1. The chart plots density difference and mean particle size. The largest particles, on the order of 1000 microns, are classified as group D which stands for dense. As velocity increases, vigorous movement and spouting occur for group D particles. Group B particles are dense particles like sand particles that are between about 150 and 1000 microns. Group B particles exhibit bubbling behavior when fluidized. Group A particles, less dense and smaller than group B particles, are stand for aeratable which means that they expand very smoothly without bubbling. At higher gas velocities, type A particles will also cause bubbles to form. Group C particles, due to their small size (usually less than 20 microns) and thus a high surface to volume ratio, are very cohesive. The cohesive nature of the powders makes stable fluidization difficult since gas would rather find an easy path instead of fighting though the close friendship between particles to give them all a lift. The easier path usually shows itself in the form of channels or
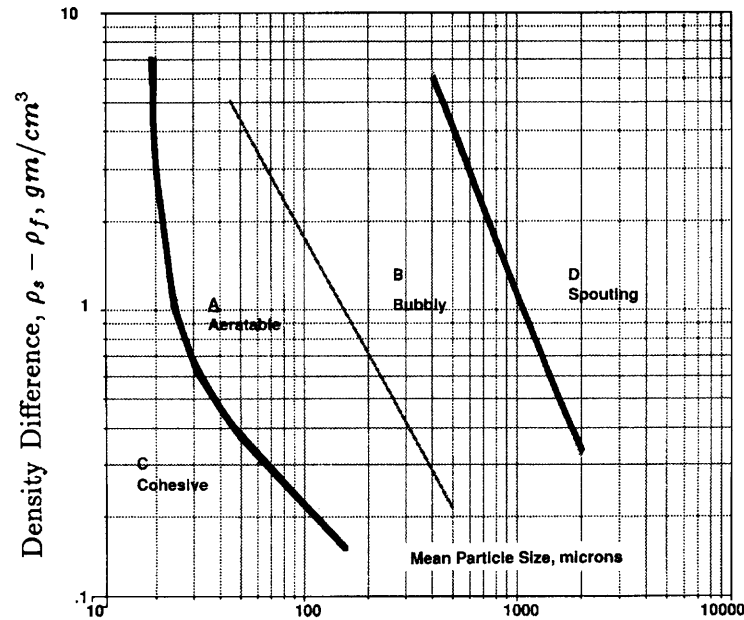
Figure 1.1   Geldart's Particle Classification.
(Geldart, 1973, redrawn by Pell, 1990, pg. 4).

"ratholes." Sometimes, the bed of cohesive powders can spout, eventually forming a stable channel, or even lift as a plug.

Nanoparticles, which will be the focus in this dissertation, are on the extreme end of group C powders according to the Geldart classification. A bed of such particles do indeed form plugging, channeling, spouting, and other typical, non-useful behaviors of Geldart group C powders when exposed to a gas flow. This dissertation will be one of the first to show that fluidization of nanoparticles is certainly possible, the idea of which was seeded by the literature survey that will soon follow.

In addition to powder properties and velocity of the fluidizing medium, the density and viscosity of the fluidizing medium can considerably affect the behavior of the bed. The ordinate in Geldart's classification chart (Figure 1.1) clearly shows the role of density of the fluidizing gas. For example, a type A powder near the border of type B

powders can be pushed into the type B region if the fluidizing gas is much more dense. In addition, density and viscosity reveal their role in some key equations associated with fluidization, which will be discussed later in Chapter 2.

The design of the fluidization system can also appreciably affect fluidization behavior. Typically, chambers with a diameter smaller than 1 inch can add a significant amount of wall effects to the bed of powders. Design of the distributor is also well known to affect the quality of fluidization. As depicted in Figure 1.2, it is important to uniformly distribute the flow of gas or liquid through the bed of solids.

As stated previously, the fluidity of the solids during fluidization is what makes fluidization very appealing for several applications. The knowledge of how various parameters and properties can affect fluidization quality is all the more helpful in developing a wide variety of useful applications, the main goal of which is to treat the solids, whether they be mixed, transported, heated, reacted, or dried, in an efficient and economical way.

Mixing is one application of fluidized beds since fluidization offers vigorous circulation of solids, which can intimately mix different kinds of powders together. Excellent heat exchange and ability to maintain isothermal conditions are advantages of fluidized beds and have been exploited in many physical and chemical applications such as a process to heat cool powders or a process for quenching hot reactions. Coating the solids with another material such as a polymer is also another important application, especially for pharmaceutical industries in their tablet coating processes. Other applications include drying, sizing, agglomeration, synthesis and other types of reactions. Perhaps one of the most famous applications is fluid catalytic cracking (FCC) which was
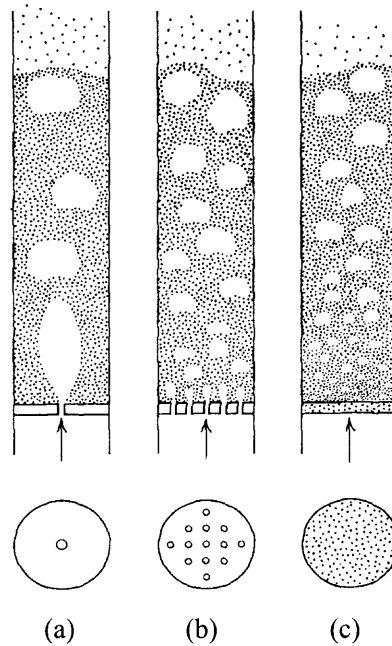
Figure 1.2   The influence of type of gas distributor on the quality of fluidization; (1) single orifice plate, (b) multi-orifice plate, (c) sintered plate.
(extracted from "Fluidization Engineering" by Kunii & Levenspiel, 1969.)

developed for the pressing need for aviation fuel during WWII.   The FCC process took advantage of solids circulation in fluidized beds to help produce about 16,000 m^3 / day which was unparalleled by any other process at the time (Kunii and Levenspiel, 1969). Since its development during WWII, the FCC process has spurred a pursuit of a better understanding of fluidization and its use in the aforementioned applications.

1.3   Literature Survey

Until recently, combining the areas of fluidization and nanoparticles has not been ventured much mainly due to the well-known difficulty of fluidizing such small particles. According to Geldart et al. (1973), the type of fluidization that particles exhibit depends on the size and the density difference between the solid particles and the fluidizing gas.

Based on empirical observations, Geldart et al. (1973) determined that particles whose diameter is smaller than 20 microns and density difference is smaller than 1000 kg/m³, classified as group C powders, are difficult to fluidize since they tend to be very cohesive in a conventional gravity driven fluidized bed. Generally, these powders, as shown in Figure 1.3, will often form cracks, channels, or even lift as a solid plug when exposed to a fluidizing gas with low superficial gas velocity. This behavior is caused by the strong interparticle forces present as the particle size drops below 20 microns. These interparticle forces increase as the surface to volume ratio increase and may significantly exceed the external mechanical forces to which they are subjected.

Through the years, however, groups of researchers (Chaouki et al., 1985, Morooka et al., 1988, Pacek et al., 1990, Iwadate et al., 1998, Wang et al., 1998, Zhou et al., 1999, Wang et al., 2001,) have found that once a high enough superficial gas velocity is reached, the bed of cohesive powders is disrupted and agglomerates or loosely bound aggregates of the fine particles form. If the primary particles are nanoparticles, the agglomerates are fractal and nanostructured. It has been observed that these agglomerates can be fluidized. Some studies have been conducted to study this phenomenon as well as to estimate agglomerate sizes for cohesive powders during fluidization (Iwadate and Horio, 1998; Zhou and Li, 1999; Zhou and Li, 2000; Castellanos et al., 2001; Matsuda et al., 2002; Wang et al., 2002; Werth et al., 2003). In addition to conventionally fluidized beds, there have been external forces introduced to aid in improving fluidization quality of group C micron-sized particles such as vibration (Yoshida et al., 1965; Erdesz and Mujumdar, 1986; Thomas et al., 1989; Thomas and Squires, 1989; Jaraiz et al., 1992; Marring et al., 1994; Benge and Squires, 1995; Marring et al., 1995; Squires and Benge,

1995; Tshabalala and Squires, 1996; Zhu and Li, 1996; Noda et al., 1998; Thomas et al., 1998; Thomas and Squires, 1998; Thomas et al., 2000; Venkatesh at al., 1998; Mori et al., 1990; Castellanos et al., 2001; Wank et al., 2001; Castellanos et al., 2002; Dutta and Dullea, 1991; Youzhi et al., 1998; Tasirin et al., 2001; Tasirin and Anuar, 2001; Mawatari et al., 2002; Yi et al., 2002; Mawatari et al., 2003), magnetic assistance (Rosensweig et al., 1981; Malhotra and Muhumdar, 1987; Zhu et al., 2003; Thivel et al., 2004), acoustic waves (Chirone et al., 1992; Xu and Zhu, 2004; Zhu et al., 2004), and rotation (Mutsers and Rietema, 1977; Levy et al., 1978; Takahashi et al., 1984; Fan et al., 1985; Watano et al., 1993; Tardos et al., 1998; Watano et al., 1999; Arastoopour et al., 2004; Watano et al., 2004; Chen, 1987; Kao et al., 1987; Qian et al., 2001; Matsuda et al., 2001; Ding et al., 2002). There have also been studies investigating the effects of temperature and pressure on fluidizability (Mogan et al., 1969; Chitester et al., 1984; Tsutsumi et al., 1995; Yates, 1995; Lettieri et al., 2000; Marzocchella and Salatino, 2000; Schreiber et al., 2002; Schreiber et al., 2003; Vogt et al., 2004; Paola and Riccardo, 2004).

In the 1980's and early 1990's, several research groups tried to develop a theory of particle collision based on the kinetic theory approach of Chapman and Cowling (1970), Sinclair and Jackson (1989), and Ding and Gidaspow (1990). The kinetic theory approach is based on the oscillation of particles. Without the use of empirical equations, kinetic theory allows for the determination of, for example, the pressure and viscosity. It determines the turbulent kinetic energy of the particles and is based on particle collisions. There have been several modifications to this approach such as in the work of Louge et al. (1991) who included the effects of both gas turbulence and particle collision. Mathiesen et al. (1999) modified the theory for the solid phase and two

different particle sizes. While kinetic theory modeling will not be used here, it is important to note that this type of model can be used to describe hydrodynamic properties such as flow conditions, fluidization velocity, bubbling velocity, and settling velocity. The following sections of the dissertation will focus on and review the previous studies conducted with group C powders in the areas of conventional fluidized beds, fluidized beds with external force assistance, and fluidized beds at varying temperatures and pressures.
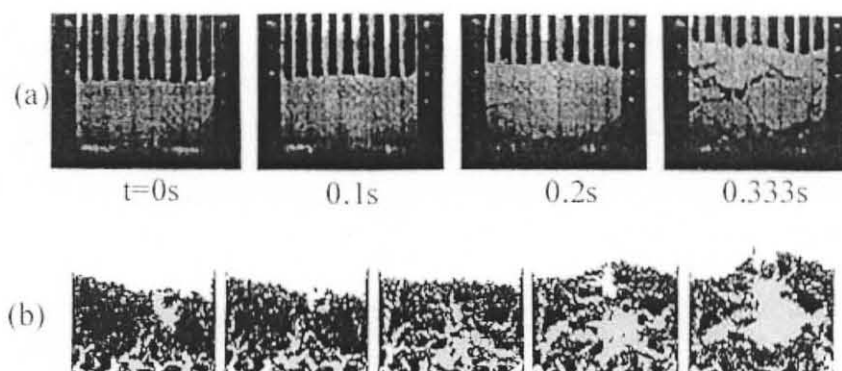
Figure 1.3 Agglomerate formation in initial stage of fluidization of cohesive fine powder beds. (a) photographs of 2-D bed, (b) snapshots of DEM simulation. (Iwadate et al., pg. 224)

1.3.1 Studies on Conventional Fluidization of Group C Particles

The idea that gas-fluidization of fine particles could be stable was investigated as early as the 1960s (Jackson, 1963; Pigford and Baron, 1965; Molerus, 1967). Experimental studies started to appear shortly after by groups such as Baerns (1966), Massimilla et al. (1972), and Mutsers and Rietema (1977). The latter group pointed out that the cohesive forces between particles resulted in a mechanically strong, powder structure that helped lead to agglomerating fluidization at high enough velocities. The diameters of the

particles used in the aforementioned study were between 19 and 128 microns.

In 1980, Abrahamsen and Geldart used cracking catalyst of 51 microns, ballotini glass beads of various sizes between 43 and 71 microns, and alumina particles of various sizes between 21 to 71 microns to correlate minimum bubbling velocity to the properties of the fluidizing gas and the size of the powders. Furthering quantitative analysis, Liss et al. (1984) was one group to correlate pressure drop across the bed and minimum fluidization velocity to the cohesive force between the particles. Liss et al. (1984) were able to induce a stickiness between the particles with a sintering mechanism and quantitatively analyze cohesion during fluidization. They concluded that higher pressure drops can be accounted for by an additive cohesion force in a force balance equation. This idea will later be refuted by the author in Chapter 3.

Chaouki et al. (1985), one of the first groups to use nanoparticles for fluidization, found that nanostructured CuO/Al_2O_3 aerogels behaved differently than the commonly seen bubbling fluidization. The fluidized Cu/Al_2O_3 aerogels were made up of a network of linear chains of particles of the order of a few nanometers. They found that, at superficial velocities greatly in excess of the expected minimum fluidization velocity, large agglomerates of the primary particles were formed. These agglomerates fluidized uniformly and expanded in a homogeneous manner. This experiment provided a means of dispersing, and thus putting the nanostructured aerogels having a specific surface area as large as 400 m^2/g to practical use. These investigators observed that at very low gas velocities preferential channeling occurs, but the channels are so weak that with increasing gas velocity, the particles start forming agglomerates at the top of the bed until the bed becomes smoothly fluidized without bubbling. This process is illustrated in

Figure 1.4. The particles form loose stable agglomerates that look like snowflakes and are fluidized at velocities much higher than the buoyancy condition of the primary particles.

Low velocity, preferential channeling

Normal fluidization Negligible inter-particle forces

Plug rise Very high interparticle forces

"Chunking"
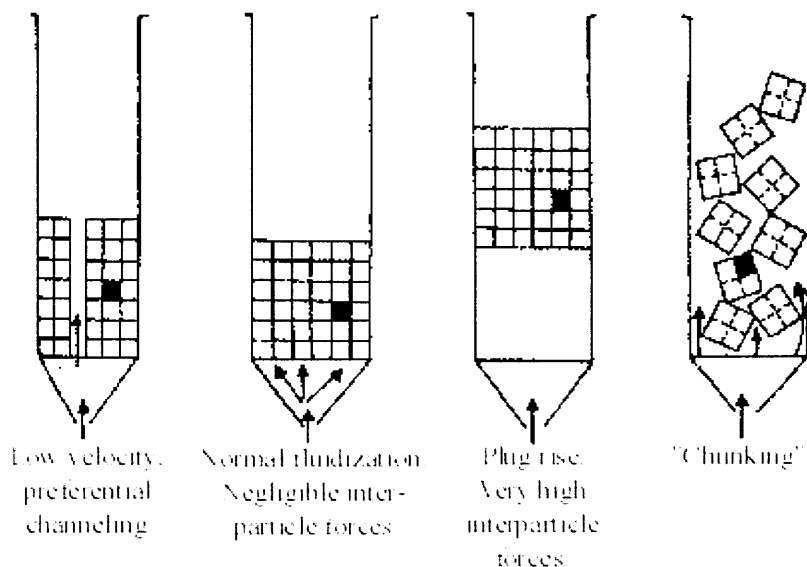
Figure 1.4 Descriptive hydrodynamic behavior of aerogels.
(Chaouki et al., pg 119)

On the other end of the fluidization spectrum, Morooka et al. (1988) observed agglomerate fluidization with bubbles. They reported a steep rise in bed height when fluidizing Ni, Si_3N_4 , SiC, Al_2O_3 and TiO_2 particles, all of submicron size. From their model, they found that the mean diameter of agglomerates varied from 180 to 700 μm. The mean primary particle size varied from 20 to 500 nm.

Similarly, Pacek and Nienow (1990) fluidized ultrafine, very dense, hard metal Geldart group C powders via self-agglomeration. As the gas velocity was increased, the powder transformed into agglomerates. At higher gas velocities, the bed had two layers: a bottom layer with large agglomerates (up to 2 mm in diameter), and a top layer of smaller agglomerates, which fluidized smoothly. At even higher gas velocities, the

entire bed was fluidized and the large agglomerates were broken up into smaller, more stable ones. The bed, at this point, probably reached a state of equilibrium, where the agglomerate growth rate is equal to the rate of size reduction. They also reported that the bed behaved as if fluidizing Geldart group B powders – bubbling occurred at U_{mf}, and bed expansion was low.

The effects of particle shape were observed in a brief study conducted by a few groups such as Judd and Goosen (1989). They found that both pressure fluctuations and bubble size were generally smaller for more spherical particles than for more angled particles that were 30 to 60 microns in diameter. The observations of pressure fluctuations in a fluidized bed of group C powders paved a new direction of research that focused on drag forces and cohesive forces. For example, Khan and Richardson (1990) introduced a method to calculate drag force, pressure drop, and friction factor for a liquid fluidized bed of particles. Despite the fact that this particular research was for liquid fluidization, their results can be applied to gas fluidization of cohesive powders, as will be especially shown in Chapter 2 and subsequent chapters.

Several studies were conducted throughout the 1990s on van der Waals forces and other interparticle forces that could play a role in the stability of gas-fluidized beds. Rietema et al. (1993), for instance, developed a model to explain the effects of various properties such as van der Waals forces, coordination number, and porosity on the stability of a gas fluidized bed of fine particles. Extensive modeling was also conducted by Valverde and Castellanos' group (1998, 2001) who correlated a relationship between tensile strength and other bulk stresses of cohesive powders to voidage and interparticle contact forces. This group also conducted experimental work to study the regimes of

fluidization of fine, micron-sized powders: solid-like, fluid-like, and bubbling (Valverde et al., 2003).

When the bed condition is brought into aggregative fluidization (or bubbling fluidization), collision, coalescence, splitting, and attrition of the agglomerates take place (Iwadate and Horio, 1995, 1998). However, when fluidizing certain agglomerates so that the bed condition is brought into "agglomerate particulate fluidization", a term that was first termed by Wang et al. (2002), what takes place is not the same. Agglomerate particulate fluidization occurs for agglomerates having a much smaller bulk density than those which produce agglomerate bubbling fluidization, another term coined by Wang et al. (2002). In agglomerate particulate fluidization, interparticle forces including van der Waals and electrostatic forces increase significantly with decreasing particle size so that nanoparticles coalesce much more easily than micron sized particles. In addition, they are much more difficult to separate.

Wang, Kwauk, and Li (1998) reported agglomerate bubbling fluidization behavior, when they fluidized particles ranging from 10 nm aerogels to 18 mm alumina powder. They observed larger agglomerates at the bottom of the bed and smaller agglomerates at the top. This is illustrated in Figure 1.5. They also observed better fluidization and more stable agglomerates with a decrease in both primary particle size and bulk density. This implies that different fluidization behavior can be observed for different size and density of primary particles.

Similar to the results found in the work or Wang et al. (1998) and Zhou et al. (1999) found that the bed of agglomerates was fluidized with a higher zone of fluidized bed of small agglomerates and a lower zone of a fixed bed of large agglomerates.
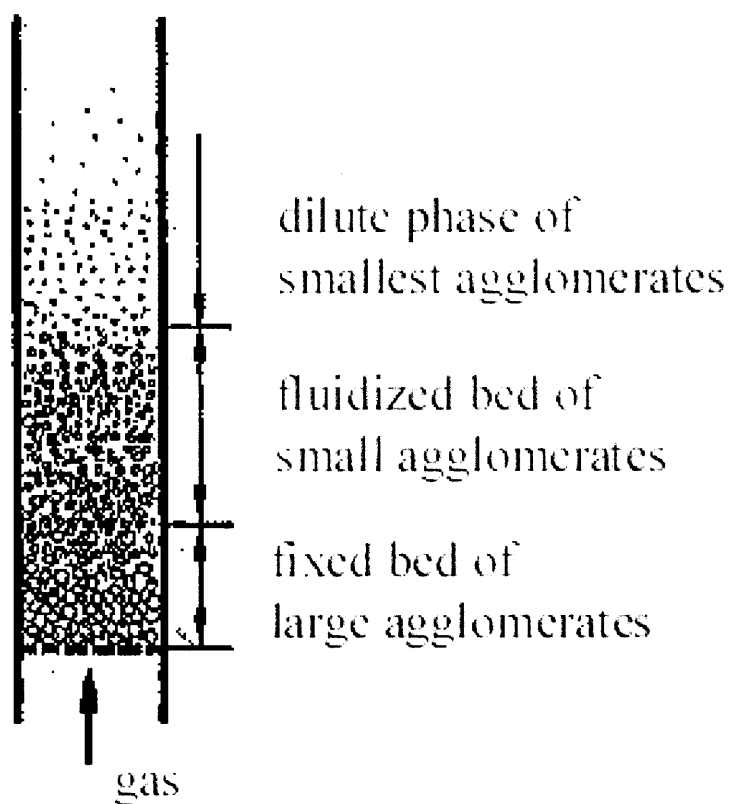
Figure 1.5 Macrostructure of agglomerate fluidized bed.
(Wang et al., pg.384)

Experimentally, they state that their submicron particles formed agglomerates and then fluidize with bubbles, which makes the fluidization behavior aggregative bubbling fluidization.

Aside from bed dimensions, the effects of the bed shape have also been investigated. For example, Tong et al. (2004) investigated the fluidization behavior of fine particles in a conical bed. This cleverly allows for higher superficial velocities toward the bottom of the bed and lower superficial velocities toward the top of the bed. From the literature, it appears that a bed of cohesive powders will typically form larger agglomerates at the bottom of the bed, which would require higher velocities to fluidize. However, larger velocities also lead to greater elutriation from the surface of the bed.

Tong et al. (2004) were able to eliminate plug formations and achieve more uniform sizes of agglomerates throughout the fluidized bed.

Wang et al. (2002) were one of the first to use fumed silica, similar to those that were used for this dissertation. When fluidizing a variety of fumed SiO_2 powders with void fraction as high as 98-99% and very low bulk densities, Wang et al. (2002) found similar results as Chaouki et al. (1985). Because their expanded beds appeared similar to those seen in solid-liquid fluidization systems, they have coined the phenomenon agglomerate particulate fluidization. In both studies, the agglomerates were so light and porous that they moved easily with the gas, resulting in a high degree of mixing. Their large size allowed for a high terminal velocity so the powders remained in the bed, which expanded uniformly up to ten times the initial fixed bed height.

In light of the idea that the properties of the agglomerates are the significant factors affecting fluidization behavior, it seems slightly contradictory that Wang et al. (2002) also state that "the hydrodynamic dimension of the fluidized agglomerates can be derived from the particulate behavior." This statement implies that the fluidization behavior can be derived from the particulate behavior as well as the agglomerate behavior. A comprehensive study needs to be conducted about the relationships between the primary particles and agglomerates and between the agglomerates and fluidization behavior. Their assertion that "the distance between [the SiO_2 powders is] enlarged by the abundant porous 3D netlike structures and the strong cohesive forces usual between tiny particles are effectively diminished and the packed bed does not harden" implies that the agglomerating particulate fluidization behavior will only work for certain particles. Subsequent studies should include finding powders that form the 3D netlike structure and

any correlation between the properties of the primary particles. It is clear that the surface modification of the primary particles affected some important results like bed expansion and superficial gas velocity. For example, the hydrophobic surface-coated silica powders exhibited higher bed expansion ratios than the hydrophilic powders.

Jung and Gidaspow (2002) also worked with fumed silica in their fluidization experiments. They achieved fluidization of 10 nm fumed silica without large bubbles. From their data, they were able to set up a kinetic theory to simulate the sedimentation process and thus determine a solids stress modulus and an agglomerate size. Yu et al. (2004) were able to fluidize carbon nanotubes and observe a pressure drop hysteresis, which gave light to the hydrodynamics of the powder. Like Jung and Gidaspow (2002), Yu et al. (2004) see the importance of modeling and understanding the rheology and hydrodynamics of such ultrafine particles. It is clear from the literature thus far that a relationship between the characteristics of the primary particles, agglomerate properties, and macroscopic flow behavior is needed to understand fluidization behavior of ultrafine particles. It appears that the physical properties of the agglomerates strongly affect the behavior of fluidization.

1.3.2 Studies on the Effect of External Forces on Fluidization

Fluidizing nanoparticles using external forces is a novel idea. However, the use of external forces for the fluidization of micron sized particles dates back to as early as 1965. The work of Yoshida et al. (1965) is an early example that involves applying vibrations to a distributor of a fluidized bed for particles on the order of 500 microns. While 500 micron particles are many orders of magnitude larger than the nanoparticles described in

this dissertation, the idea of using an additional force to assist in fluidization is shared. Figure 1.6 illustrates a set of results from the work of Yoshida et al. (1965). The most significant result they found was that the minimum fluidization velocity was significantly reduced with the vibratory assistance.
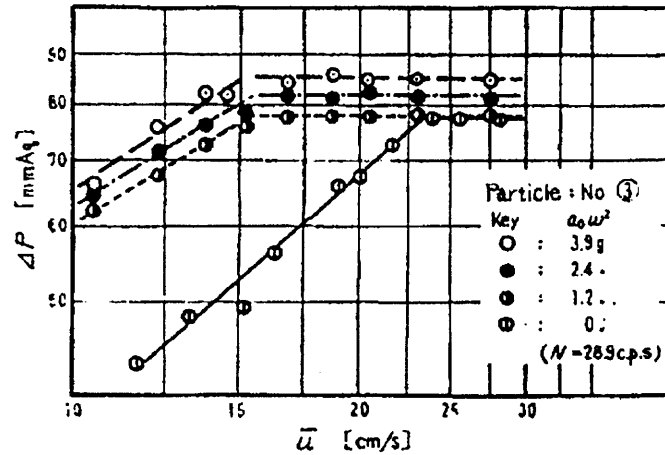
Figure 1.6 Effect of mechanical vibrations on the plot of superficial velocity vs. pressure drop for sand particles (546 microns).
(Yoshida et al., 1965, pg. 876)

Erdesz and Mujumdar (1986), whose powders ranged from 150 microns to almost 3 mm in diameter, also found that vibration helped to decrease the minimum fluidization velocity. Strangely, they also found that the pressure drop plateau decreases with the mechanical agitation despite the constant bed weight. Malhotra and Mujumdar (1987) continued the study by correlating flow characteristics and heat-transfer rates in an aerated, vibrated fluidized bed. The particles used ranged from 325 microns to over 2 mm, which are much larger than Geldart group C particles. Slightly smaller particles, 40 microns to almost 1 mm in size, were used by Squires' group in several shallow bed studies for various applications (Thomas et al., 1989; Thomas and Squires, 1989, Squires

and Benge, 1995; Benge and Squires, 1995; Tshabalala and Squires, 1996; Thomas and Squires, 1998; Thomas et al., 1998; Thomas et al., 2000). They identified different states of the vibrated bed and showed that under certain conditions, there is significant gas-to-solid contact, which is an important aspect for reactions and catalytic fluid beds. However, the purpose of including these non-group-C studies is to show that generally, vibration has been a very good modification to conventional fluidized beds. Vibrational assistance has helped overcome some drawbacks that might arise such as gas bypassing and elutriation. Vibration also appears to considerably lower the minimum fluidization velocity.

Vibration of cohesive, fine powders did not start progressing until the early 1990s. Mori et al. (1990) were one of the first to propose the vibro-fluidized bed to fluidize group C particles. They observed that lower gas velocities are needed to fluidize group C particles with vibration than without. Mori et al. (1990) introduce some applications of this process such as drying and humidity control of powders that were commonly thought to be very difficult to control. Dutta and Dullea (1991) also investigated the effects of vibration on the fluidization of particles that were between 4 and 12 microns in size. They found that not only is pressure drop slightly lower with vibration, but also that the bed expansion is much higher and elutriation of powders is much lower than without vibration. Some of their major results are shown in Figure 1.7.

Jaraiz et al. (1992) also made a significant contribution to the relatively new field of vibrated beds of fine particles with their study estimating interparticle forces from expansion and pressure drop experiments. They found that vibration helped to collapse any plug formation and channels as well as to help expand the bed and fluidize it more

smoothly. Their experimental results for various powders of 1.4 to 27 microns are summarized in Figure 1.8.
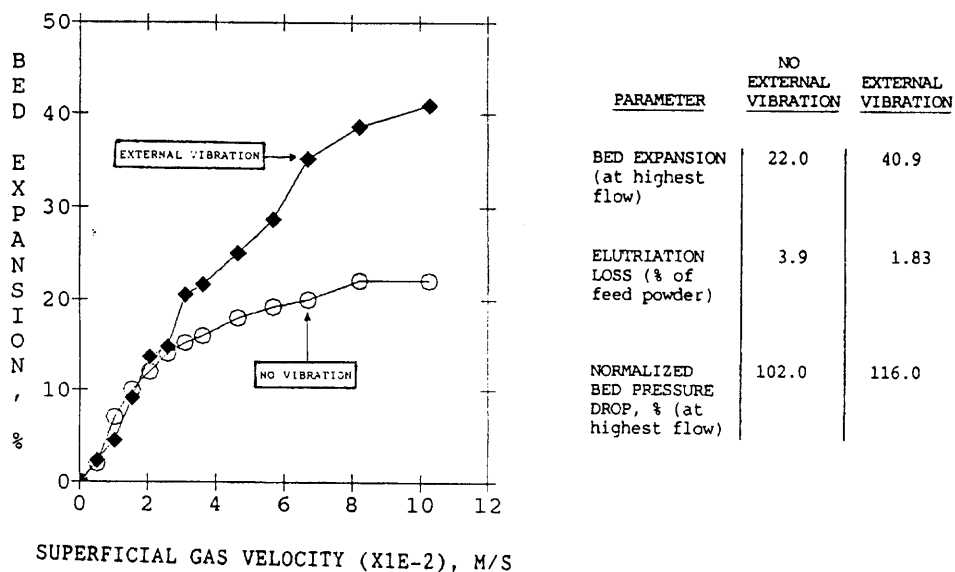
Figure 1.7 Effect of external vibration on bed expansion (left) and a summary of results from experiments with and without vibration (right).
(Dutta and Dullea, 1991, pg. 45)
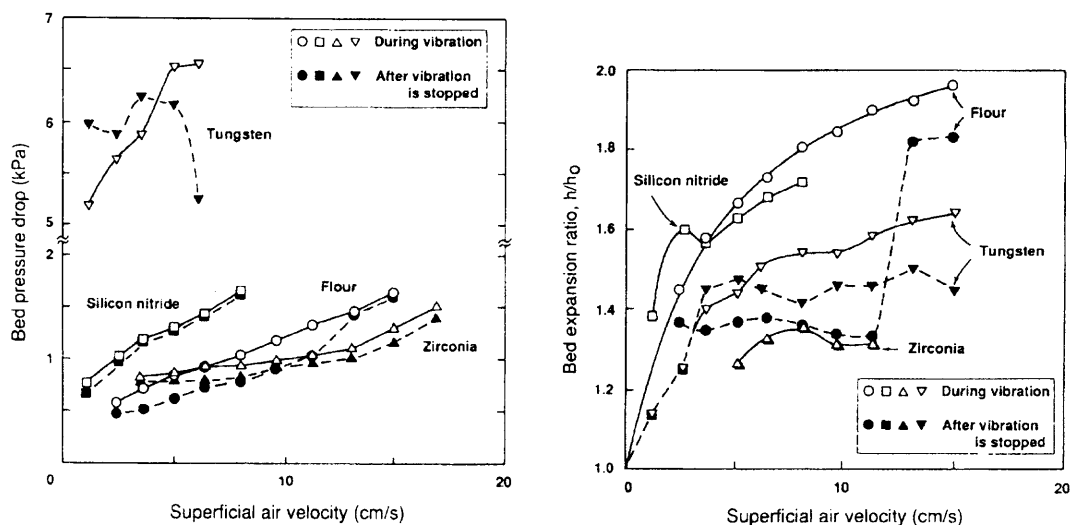
Figure 1.8 Pressure drop in vibrated beds followed by vibration turned off (left) and bed expansion of a vibrated fluidized bed followed by vibration turned off (right).
(Jaraiz et al., 1992, p. 27)

Marring et al. (1994) fluidized 35 to 80 micron glass beads and 7 to 100 micron potato starch in a bed with a vibrating distributor, an apparatus similar to the one used by Yoshida et al. (1965). They were able to control the degree of cohesivity by varying moisture content of the powders and found that the vibrational intensity needed to successfully fluidize the powders was proportional to the degree of cohesivity. Marring et al. (1994) found that not only did vibration help decrease the minimum fluidization velocity, but also to reduce bed voidage and to achieve smoother fluidization. Marring et al. (1995) soon published another study investigating the use of aeration and vibration for discharge of potato starch from silos. This study showed an application in that with a little aid, even cohesive powders can discharge smoothly and easily. Another application was demonstrated in the work by Youzhi et al. (1998), who were able to separate a binary mixture of relatively large particles in a vibrating fluidized bed. This particular application will echo itself in the mixing section of Chapter 8 of this dissertation.

Simulations and computer modeling work entered the scene in the late 1990s to try to describe the phenomena that occurs during vibrated fluidization experiments. Venkatesh at al. (1998), for example, developed computer simulations that suggested alternating cycles of agglomeration and breakage of fluidizing agglomerates. While the particles used in the simulation were very large, approximately 3 mm, the concept of agglomeration and deagglomeration, illustrated in Figure 1.9, will repeat for the fluidization of nanoparticles discussed in this dissertation.

Noda et al. (1998) conducted experiments to observe any phenomenological changes with change in pressure for vibrated fluidized beds. Particles used were fine
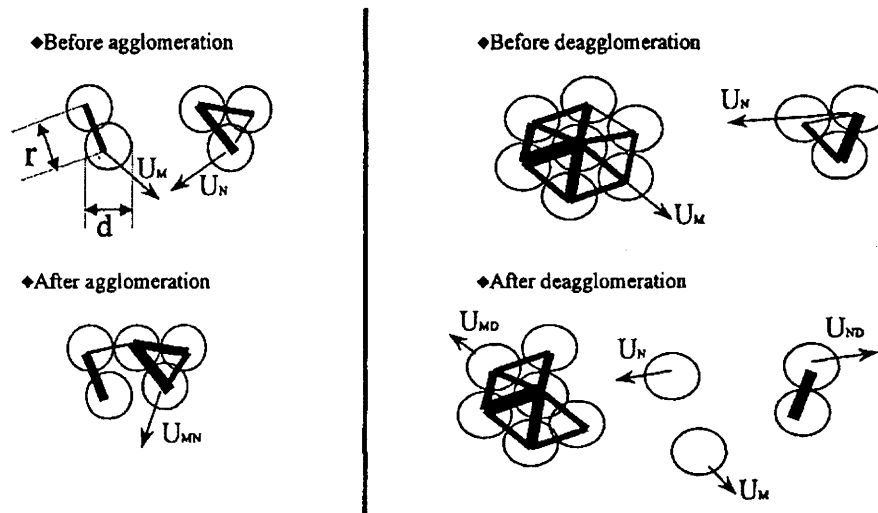
Figure 1.9 Agglomeration and deagglomeration mechanisms as proposed by Venkatesh et al. (1998). U = particle velocity vector; Subscripts are particles or agglomerate labels.
(Venkatesh et al., 1998, pg. 213)
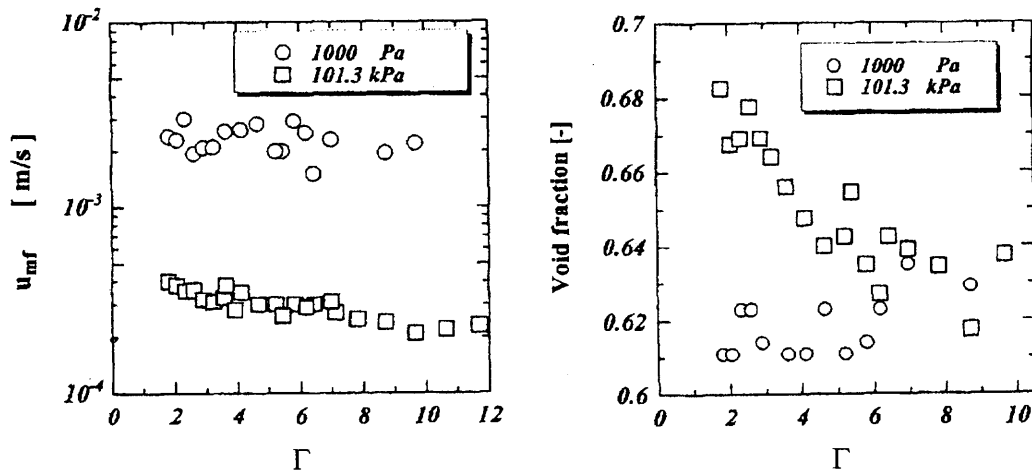
Figure 1.10 Effect of vibrational intensity (Γ) on minimum fluidization velocity (left) and void fraction at u_{mf} (right) at 1 kPa and 101.3 kPa.
(Noda et al., 1998)

glass beads that were about 6 microns in diameter. As depicted in Figure 1.10, Noda et al. (1998) found that at reduced pressures, the minimum fluidization velocity and void fractions were less variable and more variable, respectively with increasing vibrational intensities. They attribute this behavior to the flow patterns of the bed, which were

observed to be more vigorous in their apparatus under reduced pressure than at atmospheric pressure. Wank et al. (2001) also fluidized fine powders under low pressure. They used 5-11 micron sized boron nitride particles that were found to be lightly bonded agglomerates during fluidization. They found that as the vibrational intensity is increased, agglomerate sizes tended to decrease as well. As a model, they used a force balance that included additive cohesion and vibration terms to calculate minimum fluidization velocity.

Tasirin et al. (2001) vibrofluidized 15, 25, and 35 micron sized cohesive particles; further work was published by Tasirin and Anuar (2001). Like others, Tasirin et al. (2001) and Tasirin and Anuar (2001) found that vibration helped to smooth fluidization as shown in the left portion of Figure 1.11 where there is a clear difference between experiments with vibration and those without. They also measured elutriation rates and were able to determine that in a vibrated fluidized bed, smaller particles elutriated out of the bed less, as shown in the right side of Figure 1.11.

Castellanos et al. (2001) also investigated the effect of vibration on the stability of gas-fluidized beds. They concluded that the response of the fluidized bed is strongly dependent on the average solid volume fraction. Above a certain value of a critical solid volume fraction, the bed is in a solid-like regime where particles are static and sustained by permanent contacts. Below the critical solid volume fraction, the bed is in a fluid-like regime where the powders will agglomerate and are suspended in the fluidizing medium with diffusive dynamics. In the fluid-like regime, vibration helps to expand the bed further as well as to add either surface or bubbling instabilities at some frequencies.
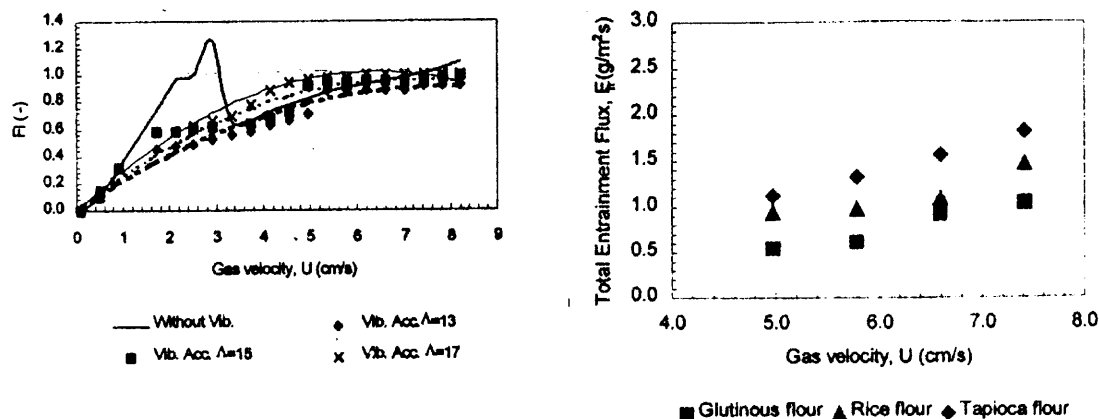
Figure 1.11 Effect of vibration on pressure drop across the bed (left) and Effect of velocity on entrainment flux for 35 micron glutinous flour, 25 micron rice flour, and 15 micron tapioca flour.
(Tasirin et al., 2001)

The effect of particle diameter on vibrofluidization was studied by Mawatari et al. (2002). They used glass beads with diameters ranging from 6 to 100 microns, which are within the Geldart group C and A classifications. For group C powders, they observed a decrease in minimum fluidization velocity with increasing vibrational intensity. For group A powders, they observed no change in minimum fluidization velocity as a function of vibrational intensity. Some of their key results, specifically for the 6 micron powders, are shown in Figure 1.12. Mawatari et al. (2003) published another study that used their experimental data to predict the minimum fluidization velocity. The Ergun equation, a well-known correlation, agreed well with their experimental data, but only for the group A powder experiments. A noticeable difference in experiment and theory was noted for group C powders. The disagreement in data was attributed to the formation of large agglomerates. They concluded that it is necessary to determine the diameter of the agglomerate in order to predict minimum fluidization velocity for the group C powders used in their experiments.

Yi et al. (2002) are another group who examined vibrated fluidized beds. They observed resonance characteristics for a vibrated bed of 40 micron particles. Changes in bed expansion from varying frequency and velocity were recorded and Yi et al. (2002) concluded that when gas velocity and frequency reach certain values, that the bed expansion ratio reaches its maximum. Above these values, while the bed remains at a constant height, the fluidization still remains smooth and stable.

The minimum fluidization velocity and its prediction were investigated by Xu and Zhu (2004). They observed the effects of vibration as well as acoustics, which have been described by Chirone et al. (1992) for example, on a bed of cohesive particles.
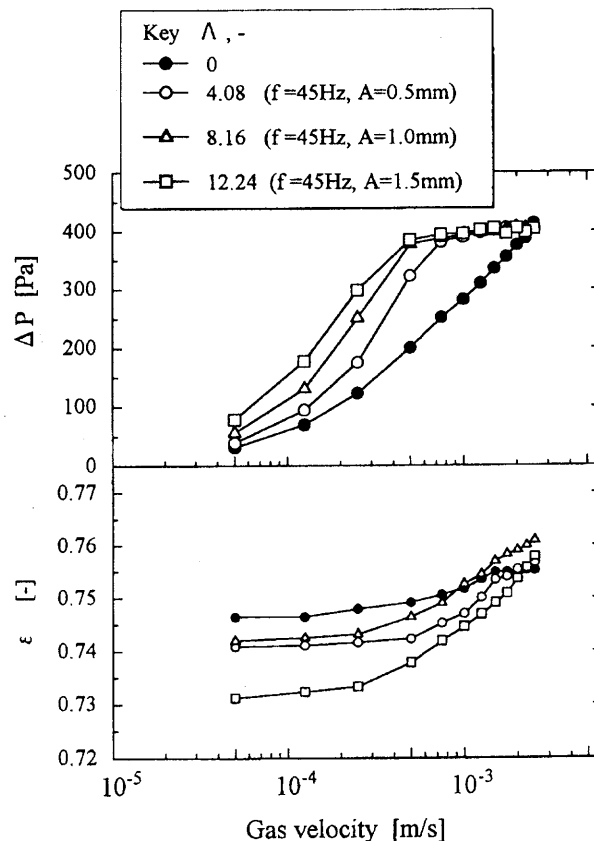
Figure 1.12 Effect of vibrational intensity on pressure drop (top) and void fraction (bottom).
(Mawatari et al., 2002).

Different from the approach made by Mawatari et al. (2003), Xu and Zhu (2004) examined all available methods and theories to calculate minimum fluidization velocity and concluded that none of the available methods were particularly useful for cohesive particles. Such methods include the semi-empirical correlations proposed by Narsimhan (1965), the Ergun-based correlation by Wen and Yu (1966), and the empirical correlation by Leva (1959). These methods assume that the particles fluidize individually, not as agglomerates, and do not consider interparticle forces. As a result, Xu and Zhu tried to derive a universal correlation to predict minimum fluidization velocity, taking into account size, effects of vibration, and interparticle forces that they claimed better agreed with the available data. However, like Wank et al. (2001), Xu and Zhu (2004) used a force balance with additive terms for vibration and interparticle forces, which seems flawed since such terms cannot be simply added (or subtracted) to the weight of the bed. Xu et al. (2004) further analyze these results with more experimental data.

Chirone et al. (1992) fluidized cohesive group C powders in an acoustic field of various sound pressure levels. The fluidization behavior was observed to be bubbleless (APF). According to their model predictions, the sound waves break up channels and improve fluidization quality. They also found that sound waves significantly increase bed expansion ratios. This study inspired the author of this dissertation to design a sound assisted fluidization chamber for nanoparticles upon her return from the Ecole des Mines d'Albi in France where the first vibration studies for nanoparticle fluidization were conducted. The results from these initial vibration studies were very promising for other modes of assistance to successfully fluidize nanoparticles as well. Sound assistance, just as reasoned, enhanced nanoparticle fluidization, the results of which are published by

Zhu et al. (2004). Although the author of this dissertation is a co-author for this article, the results will not be discussed since the results were obtained by another student. There are many other studies in the area of acoustics but since this type of fluidization will not be discussed in this dissertation, these studies will not be reviewed here.

Another type of fluidization aid is magnetic assistance. There have been different ways of incorporating magnets into a fluidized bed system. One way was introduced by Rosensweig et al. (1981) who applied a magnetic field to a bed of ferromagnetic particles. This process led to a very fluid-like, bubbleless, magnetically stabilized bed. The effect of this type of magnetic assistance is depicted in Figure 1.13.

Zhu and Li (1996) added to the Rosensweig et al. (1981) studies by using group C powders. The system was very similar to that of Rosensweig et al. (1981) with a line of magnetic field generators along the length of the bed. Zhu and Li (1996) used 7 to 14 micron magnetic particles and measured bubble size as a function of magnetic field
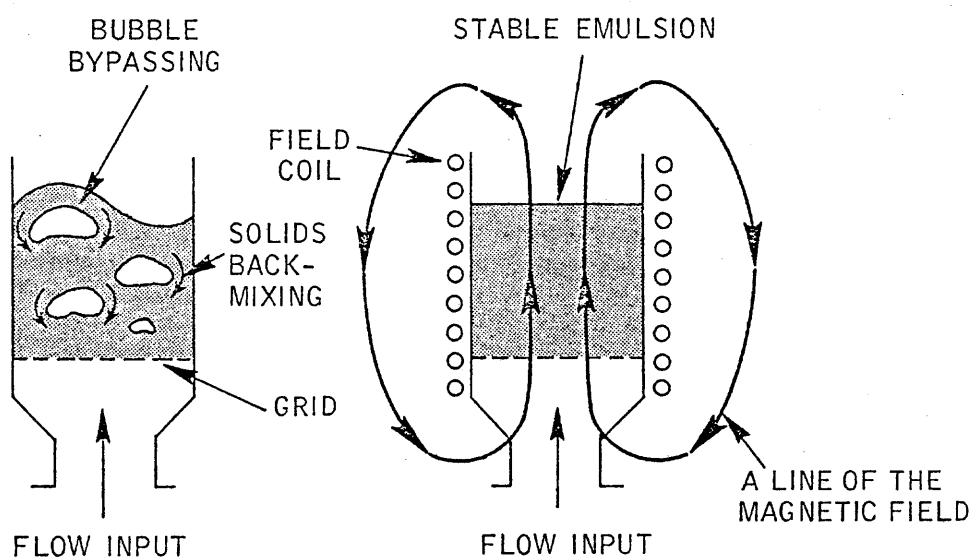
Figure 1.13 Comparison of fluidized solids with flow input alone (left) and with magnetic stabilization (right).
(Rosensweig et al., 1979).

intensity. With increasing magnetic intensity, bubble size decreases. Fluidization quality was said to improve due to the rearrangement of magnetic particles in chain-like structures, which help to break bubbles, and to the improved control of agglomerate size. Rhodes et al. (2001) conducted a similar study but the particles used were 330 to 1600 microns in diameter which are too large for the scope of this dissertation. However, an important concept resulted from their experiments since they found that the use of magnetic fields led to a Geldart group B to A transition. This means that a group C to A transition should also occur, and in fact, is seen in the literature. Thivel et al. (2004) are another group to study magnetically stabilized fluidization. They used a mixture of magnetic particles and non-magnetic particles, from which they were able to obtain similar effects of a system with only magnetic particles.

The literature pertaining to the type of magnetically fluidized bed that this dissertation will describe is limited. Chapter 4 will describe the use of micron sized magnetic particles in a bed of nanoparticles to aid in breaking large agglomerates that form at the bottom of the bed during fluidization. It will be seen that the magnetic particles give a similar type of excitation that vibration provides to break up interparticle forces to allow the bed to expand and fluidize.

Instead of using the conventional gravity-driven bed or beds with the aforementioned types of external force assistance, there have been several experimental and theoretical studies using a rotating fluidized bed (Mutsers and Rietema, 1977; Levy et al., 1978; Takahashi et al., 1984; Chang et al., 1985; Kao et al., 1987; Chen, 1987; Watano et al., 1993; Tardos et al., 1998; Watano et al., 1999; Qian et al., 2001; Matsuda et al., 2001; Qian et al., 2001; Zhu et al., 2003; Matsuda et al., 2001; Ding et al., 2002;

Watano et al., 2004; Arastoopour et al., 2004).   Only some key studies will be described here.   Qian et al. (2001) was one group that used a rotating (or centrifugal field) fluidized bed.   The quality of fluidization was considerably different.   This group found that under a centrifugal force, group C particles can shift to group A, and group A particles can shift to group B.   Based on relatively simple models, Qian et al. (2001) obtained the transition curves between Geldart group A and C particles and between Geldart group A and B particles with increasing "g" as shown in Figure 1.14.   They experimentally confirmed that certain group C particles such as 7 micron alumina and 8 micron glass, which cannot be fluidized in a conventional fluidized bed under low superficial gas velocities, can easily be fluidized smoothly and without channeling in rotating fluidized beds.   It can be seen in Figure 1.14, that 7 μm alumina particles and 8μm glass beads belonging to group C at 1 "g" shift to group A at 7 and 19 (or higher) values of "g".   Using a simple macroscopic model, which equates the forces on an
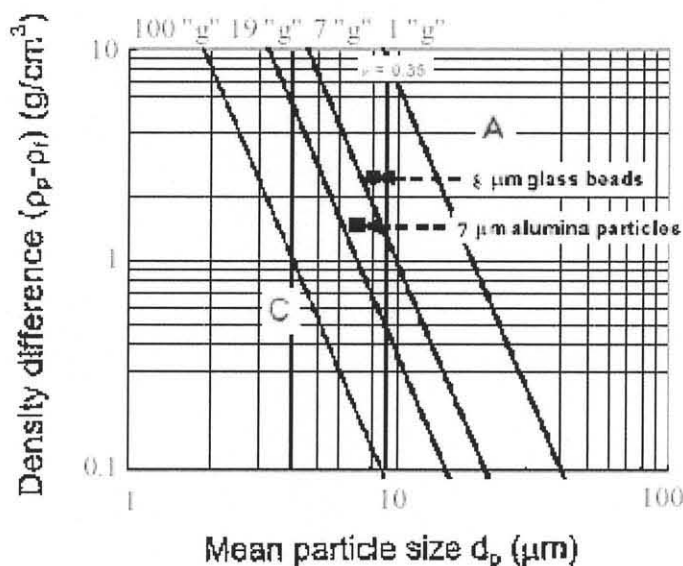
Figure 1.14 Transition curves (group A / group C) as a function of centrifugal acceleration, "g."
(Qian et al., 2001)

individual cohesive particle in a fluidized bed, Qian et al. (2001) developed an equation, which predicts the transition between Geldart group C, and A behavior:

$$\frac{\pi d_p^3}{6}\left(\rho_p - \rho_f\right)g\left(\varepsilon^{-4.8} - \varepsilon\right) = \frac{Al}{24\delta^2}$$, where A is Hamaker's constant $\sim 10^{19}$ J, l is the diameter of the nanoparticle or length of the asperities for micron size particles, $\delta = 0.4$ nm, ε is the void fraction of the bed, and g is the acceleration of gravity in a conventional fluidized bed or the centrifugal acceleration in a rotating fluidized bed.

The above results using micron-sized particles in rotating fluidized beds imply that rotating fluidized beds operating at variable "g" may be the ideal way to fluidize nanoparticles and produce nanocomposites. In fact, with anywhere between 9 and 18.5 "g," Matsuda et al. (2001) fluidized 7 nm TiO_2 in a rotating fluidized bed. At low "g," large agglomerates (0.5-2 mm) were observed near the distributor of the bed, but in the upper region of the bed smaller agglomerates were observed and these were fluidized. This description is similar to the description of agglomerate fluidization in a conventional gravity-driven bed for certain powders (Zhou et al., 1999).

However, at higher values of "g," Matsuda et al. (2001) noted that the agglomerates, especially those near the distributor, became smaller, which was probably due to the larger shearing forces. Interestingly, some bubbles were observed at low "g" but were not observed at higher "g" indicating that the mode of fluidization shifted from bubbling fluidization to particulate fluidization with increasing "g".

In another study, Rietema (1984) pointed out that Geldart's powder classification is correct only when operating at normal temperatures and pressures and in the earth's gravitational field. There are other factors that much be taken into account such as cohesive forces, gas viscosity, the adsorption of gas on the particles, and as this section

suggests, gravitational acceleration. Similar to Qian et al. (2001), Rietema (1984) said that group A powders might behave like group B powders if an increased gravitational force is used or a low-viscosity gas is used. And when a high-viscosity gas is used, group C powders might behave like group A powders. This suggests that the interactions between the gas molecules and particles are very important.

As seen in the above studies, the rotating fluidized bed is capable of creating an environment where the body force exerted on the particles is many times greater than the gravitational force. This is particularly important for fluidization of nanoparticles, in which significant elutriation of particles can be prevented. Overall, fluidizing nanoparticles in a bed with assistance is a novel idea. There have been several studies using external forces for relatively large micron sized particles but none have been recorded in literature for nanoparticles.

1.3.3 Studies on Estimating Agglomerate Size

A number of macroscopic models have been proposed to estimate the size of agglomerates formed in bubbling fluidization and particulate fluidization of cohesive powders (Iwadate and Horio, 1998; Zhou and Li, 1999; Zhou and Li, 2000; Castellanos et al., 2001; Matsuda et al., 2002; Wang et al., 2002; Werth et al., 2003). The interparticle forces present in cohesive powders and their effect on fluidization behavior have also been discussed at length (Fortez et al., 1998; Castellanos et al., 1999; Quintanilla et al., 2001; Valverde et al., 2003). It is believed that in the case of nanoparticles, the agglomerates formed are highly porous and fractal-like in structure, in which the interparticle forces discussed in the aforementioned studies plays an essential role.

There are some studies discussing highly porous media or fractal structures such as the work of Cook (1989), Park and Stephanopoulos (1993), Kantorovich and Bar-ziv (1997), Wu and Lee (1998), Chen and Cai (1999), Rosner and Khalil (1999), Filippov et al. (2000), Larraz (2002), Tang and Raper (2002), Zurita and Rosner (2002), Pirard et al. (2002).

Zhou and Li (1999) estimated agglomerate size via a balance of forces: cohesive force, collision force, kinetic or drag force, gravitational force and buoyancy in the fluidized bed. The agglomerate is said to be in one of two forms: steady or disrupted. The behavior depends on the balance of forces stated above. Their concept is illustrated in Figure 1.15 where the collision of two agglomerates can result in one of three pathways: separation (a), agglomeration (b), and disruption (c). where $F_y + F_c = F_g + F_{va}$ or (kinetic or drag force) + (collision force) = (gravitational force − buoyancy force) + (cohesive force, assumed to be the van der Waals force of attraction). By substituting suitable expressions for each force, their modeling resulted in the following quadratic equation to predict the diameter of the agglomerates:

$$(\rho_a - \rho_f)gd_a^2 - \left[0.33\rho_f u^2 \varepsilon^{-4.8} + \frac{0.996}{\pi}\left(\frac{\pi V^6 \rho_a^3}{k^2}\right)^{1/5}\right]d_a + \frac{A}{4\pi\delta^2} = 0 .$$ This equation

was solved using estimated values of the parameters. Their experimental data was obtained from fluidizing SiC, TiO_2 and SiO_2 particles of diameter from 0.6 to 5 μm. In order to obtain the relative velocity, V, of the agglomerates, Zhou and Li (1999) used the model of Iwadate and Horio (1998), which relates V to the maximum bubble diameter inthe fluidized bed. The size of the agglomerates was solved by trial and error. They obtained values of 330 μm for SiO_2, 520 μm for TiO_2 and 635 μm for SiC, which
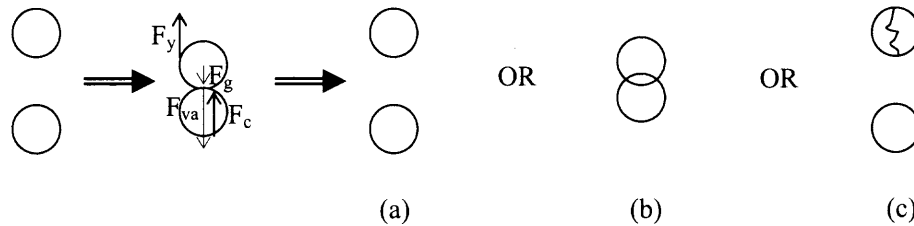
Figure 1.15 Schematic of agglomerate collision model of Zhou et al.
(Zhou and Li, 1999)

compared well with the experimentally measured average agglomerate sizes of 300, 482, 597 μm for these particles, respectively. This model, however, was based on one average agglomerate size when often, the sizes are not uniform throughout the fluidizing bed. The distribution of sizes must be taken into account in future models. Zhou and Li (1999) were not the only ones to incorporate a force balance model in the estimation of agglomerate size. Wank et al. (2001) and Xu and Zhu (2004) were two separate groups who also followed a similar approach to predict agglomerate size, as stated previously.

Iwadate and Horio (1998), another group who used force balances, assumed that the collision force equaled the cohesive force between agglomerates; (cohesive force) =

(collision force) or $\left(\dfrac{Ad_a}{24\delta^2}(1-\varepsilon_a)^2 \right) = 0.166\left(\dfrac{\pi\rho_a^3 V^6}{k^2} \right)^{1/5} d_a^2$. With this model, this

research group compared their data with the data of other research groups that might not have had the same fluidization behavior as they did. In their model, Iwadate and Horio (1998) took into account bubble hydrodynamics which is very important for agglomerating bubbling fluidization but not for agglomerate particulate fluidization where bubbles are not present. Yet this did not prevent them from comparing their data with those of other research groups that had a different fluidization behavior. Chaouki et al. (1985), another group that used force balances, and who reported bubbleless
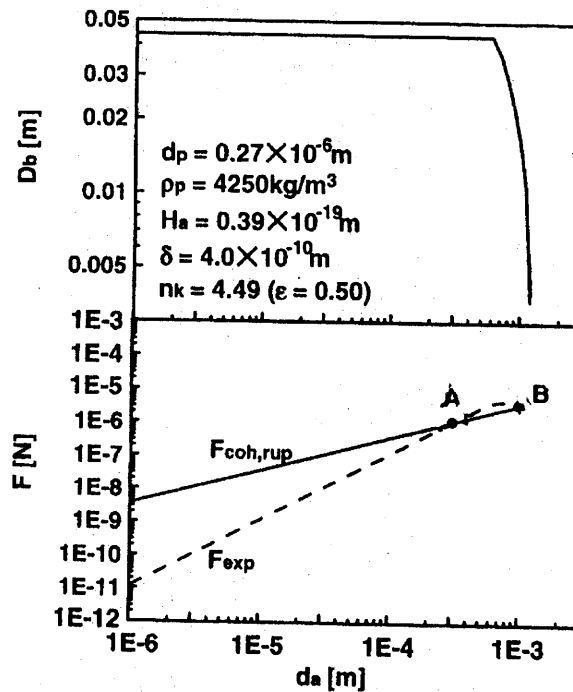
Figure 1.16 Agglomerate size determination from intersection of F_{exp} and $F_{coh,rup}$. (Iwadate and Horio, 1998, pg. 226)

fluidization, estimated agglomerate size by assuming that the difference between the gravitational force and buoyancy force acting on the agglomerate equaled the van der Waals force between the primary particles.

Morooka et al. (1988) predicted agglomerate size via an energy balance, which resulted in a cubic equation for the agglomerate diameter. They assumed that an agglomerate breaks if the collision energy exceeds the energy required to break the agglomerates. Their energy balance simply was (energy generated by laminar shear) + (kinetic energy of an agglomerate) = (energy required to disrupt the agglomerate) or

$$\left(3\pi\mu\Delta u d_a^2\right) + \left(\frac{\pi\rho_a\Delta u^2 d_a^3}{12}\right) = \left(\frac{A\left(1-\varepsilon_a\right)d_a^2}{32\delta d_{pp}\varepsilon_a}\right).$$ As for the few comparative studies

conducted thus far, Zhou and Li (1999) compared their model with those developed by Morooka et al. (1988) and Iwadate and Horio (1998). From their analysis, Zhou and Li

(1999) concluded that their model calculated closer values to the available experimental data. However, their model does not account for the distribution of agglomerate sizes. Iwadate and Horio (1998), as stated before, have also conducted a comparative study of the previous research with their own. They incorporated bubble hydrodynamics in their model and compared results to experimental measurements that included no bubbles. This researcher feels that comparing models from two distinct fluidization behaviors is improper. The study conducted by Iwadate and Horio (1998) is summarized in Figure 1.17.

The structure of nanoparticle agglomerates turns out to be important from not only an applications standpoint but also from a nanoparticle fluidization fundamentals standpoint. The main reason that nanoparticles can fluidize is due to the formation of relatively stable agglomerates that are highly porous. SEM images, discussed in subsequent chapters, have indicated a very loose, fractal structure of nanoparticle

Authors	Model	External force/energy	Cohesion force/energy	Comments
Chaouki et al. [2]	$F_{Ga} = F_{pp}$ Force balance	F_{Ga} $F_{Ga} = \frac{\pi}{6} d_a^3 \rho_a g$ gravity force ≈ drag force	F_{pp} $F_{pp} = \frac{h_w d_p}{16\delta^2}\left[1 + \frac{h_w}{8\pi^2\delta^3 H_r}\right]$ van der Waals force between primary particles	No bubble hydrodynamic effects included.
Morooka et al. [3]	$E_{total} = (E_{kin} + E_{lam})$ $= E_{split}$ Energy balance	$v = U_{mf}$ $E_{total} = (E_{kin} + E_{lam})$ $E_{lam} = 3\pi\mu U_{mf} d_a^2$ $E_{kin} = m U_{mf}^2/2$ laminar shear + kinetic force	E_{split} $E_{split} = \frac{h_w(1-\varepsilon_a)d_a^2}{32\delta^2\varepsilon_a d_p}$ E_{total} energy required to break an agglomerate	No bubble hydrodynamic effects included. If $3\mu U_{mf} < h_w(1-\varepsilon_a)/(32\pi\delta d_{p\varepsilon_a})$, negative d_a is obtained.
Present Work	$F_{exp} = F_{coh,rup}$ Force balance	$\sigma_{expansion}$ $\sigma_{exp} = -P_s$ bubble $F_{exp} = \frac{\pi D_b \rho_s g(-P_s)d_a^2}{2n_k}$ bed expansion force	$F_{coh,rup}$ $F_{coh,rup} = \frac{H_a d_a(1-\varepsilon_a)}{24\delta^2}$ cohesive rupture force	Bed expansion force caused by bubbles is equated with cohesive rupture force.

Figure 1.17 Models of Agglomerate Size Prediction.
(Iwadate and Horio, 1998, pg. 229)

agglomerates. There have been a number of theories and correlations to describe the highly porous particles, such as those shown in Figure 1.18 and Figure 1.19, in terms of voidage, drag force, intraparticle flow, etc. These concepts will later help develop a theory that will be described in detail in the theoretical sections of subsequent chapters (Valverde et al., 2001; Castellanos et al., 2001).

From these studies, it is suspected that the cohesive forces between the primary particles are very important in addition to the forces between agglomerates. It is hypothesized that the agglomerates formed are strongly dependent on the fluidization behavior or vice versa. Part of the goal of this study is to determine what exactly is occurring in the fluidization of nanoparticles. Despite the extensive studies on agglomerate size predictions from gas-solid fluidization, the author used liquid-solid fluidization theory to solve for the agglomerate size. The mixture of gas and nanoagglomerates has hydrodynamic characteristics completely different from those of traditional particles. It is due to the very liquid like behavior of fluidized nanoparticles that led this author to derive theories based on correlations like the Richardson - Zaki
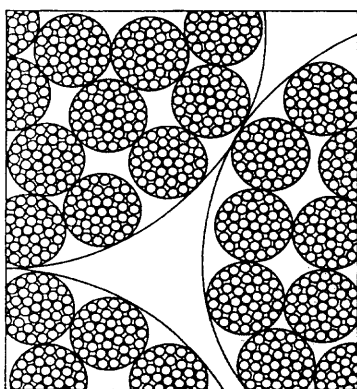
Figure 1.18 Close-up schematic of multiple generation agglomerates forming a fractal, porous material.
(Cook, 1989, pg. 2811).
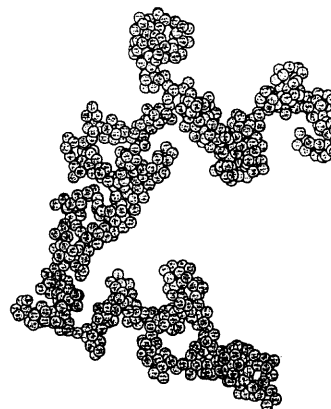
Figure 1.19 A simulated aggregate of 724 particles with a fractal structure.
(Filippov et al., 2000, pg. 5)

(1954) equation, which is normally used for liquid-solid fluidization and sedimentation. This theory will be described in the subsequent chapters of this dissertation.

1.3.4   Studies on Supercritical Fluidization

The idea of fluidizing nanoparticles under supercritical conditions is quite novel and studies pertaining to it, if any prior to this dissertation, are not found in the literature. Thus, studies pertaining to the fluidization of at least micron sized particles under very high pressures will be discussed in this section.

One of the first pertinent studies belongs to Mogan et al. (1969) whose fluidized bed of cracking catalyst was operated under high pressures (300 to 800 psig).   Their objective was to measure elutriation as a way to predict the porosity of the system. They concluded that a combination of the various theories available, such as that of Richardson and Zaki, yielded satisfactory results.   As for fluidization behavior, they visually observed particulate fluidization when using nitrogen and argon and bubbling fluidization when using hydrogen as the fluidizing mediums, for which no explanation was offered.

Another high pressure, nonsupercritical, fluidization set of experiments was conducted by Chitester et al. (1984).   The goal was to investigate the fundamentals of fluidization, such as minimum fluidization velocity, bed voidage, bed expansion, and any bubbling behavior, at pressures as high as 6485 kPa with nitrogen as the fluidizing medium.   Despite the fact that they used particles that were several hundreds of microns large, a possibly pertinent result found was that a turbulent regime was reached at lower gas velocities as the pressure increased.   But at the highest pressure they used, the bed

appears to be particulately fluidized but entrainment is very high. They state, "'smoother' fluidization and excellent mixing at high pressure are confirmed." A similar experimental and modeling study was conducted by Yang et al. (1985).

One key application of high-pressure systems is particle coating since some polymers can be more easily dissolved under high pressures. This application was incorporated into the experimental study conducted by Tsutsumi et al. (1995) who coated fine (approximately 56 microns) catalyst particles with a paraffin wax by a rapid expansion of supercritical fluid solutions (RESS) in a circulating fluidized bed. The goal of their study was to examine the effects of hydrodynamics and solute concentration on coating rate and efficiency. Some of their key results are shown in Figure 1.20. They concluded that because the coating material is deposited directly onto the surface of the catalyst particles without liquid droplets or other binders, there was no significant agglomeration.

Yates (1995) wrote an in-depth review article discussing the effects of temperature and pressure on gas-solid fluidization but only for groups A, B, and D particles. However, just five years later, he and his colleagues wrote a paper (Lettieri et
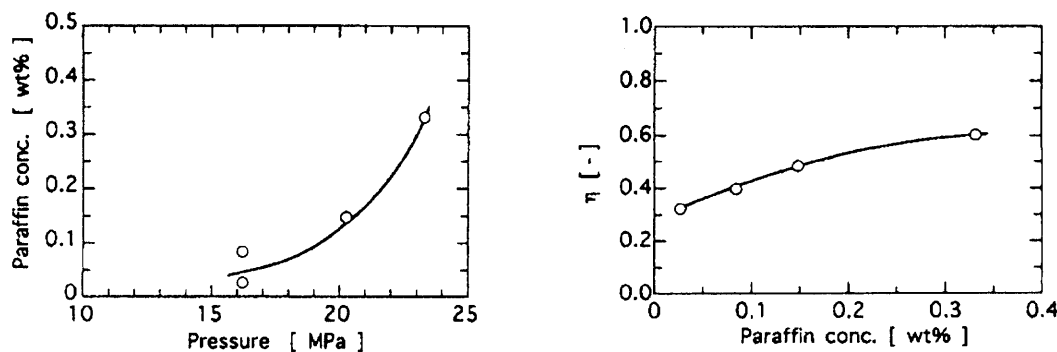
Figure 1.20   Parrafin concentration vs. pressure (left) and coating efficiency vs. paraffin concentration (right).
(Tsutsumi et al., 1995)

al., 2000) discussing the influence of interparticle forces on the fluidization behavior of particles under high temperature, which is a step closer to the supercritical fluidization of nanoparticles discussed in this dissertation. The high temperatures caused their catalyst particles to become more sticky which turned out to be a method for controlling interparticle forces and thus, in a way, mimicking group C powders. The major conclusion was that interparticle forces do not dominate the fluidization behavior but rather, the hydrodynamics do.

Marzocchella and Salatino (2000) fluidized group A and B powders with CO_2 at pressures from ambient to supercritical. They found that the region of homogenous fluidization is broader as the fluid density increases, or in other words, as pressure increases. In comparison to the subcritical experiments, the supercritical conditions resulted in unique data as seen in Figure 1.21. Supercritical conditions allowed for the bed to be fluidized at a lower fluidization velocity and thus had a higher bed voidage according to the Richardson and Zaki (1954) equation., $u=u_o\varepsilon^n$. From visual observations, Marzocchella and Salatino (2000) also mapped the different fluidization regimes in superficial fluid velocity vs. fluid density phase planes. The fluid density at the supercritical conditions used, 80 bars and 35°C, is 480 kg/m3 which correspond to the last set of data points in the mapped plot, Figure 1.22.

The lower minimum fluidization velocities and overall smoother fluidization were taken advantage of in the supercritical coating experiments conducted by Schreiber et al. (2002). This group coated 100 - 200 micron glass beads with paraffin, an example of which is shown in Figure 1.23 (Vogt et al., 2004). The results showed that coating is possible in a supercritical fluidized bed and that further investigations such as

hydrodynamic studies are needed for optimization of this process. The group also coated different particles such as lactose for drug release experiments (Schreiber et al., 2003). Figure 1.24 shows a lactose particle fully coated with paraffin and its release profile, which demonstrated an almost linear dissolution. This showed that the coating process under supercritical conditions is promising since the coating was mostly uniform which enabled a prolongation of the release. Given their experimental data, Schreiber and his colleagues (Vogt et al., 2004) followed their own recommendations from 2002 and investigated the hydrodynamic conditions at which successful coating can occur. Both bubbling and smoothly fluidized (particulate) beds were studied. They concluded that generally, increased flow and increased bubbling yielded a higher quality of coating.

Paola and Riccardo (2004) recently conducted a study that combined the ideas of sound assistance and varying temperature together into a set of fluidization experiments
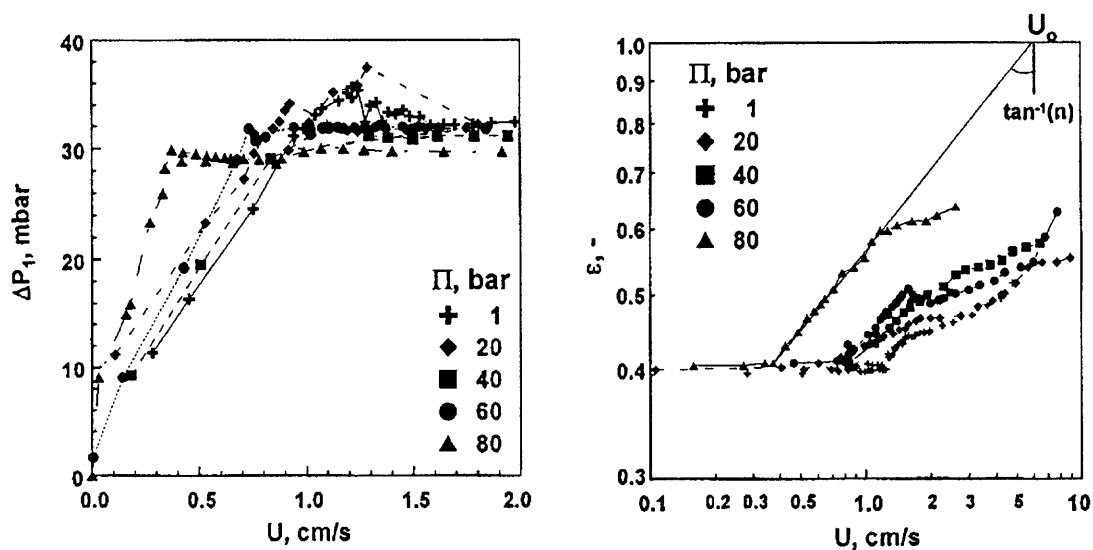
Figure 1.21 Pressure drop vs. superficial fluid velocity (left) and average bed voidage vs. superficial fluid velocity (right) for a bed of 88 micron glass beads.
(Marzocchella and Salatino et al., 2000, pg. 904)
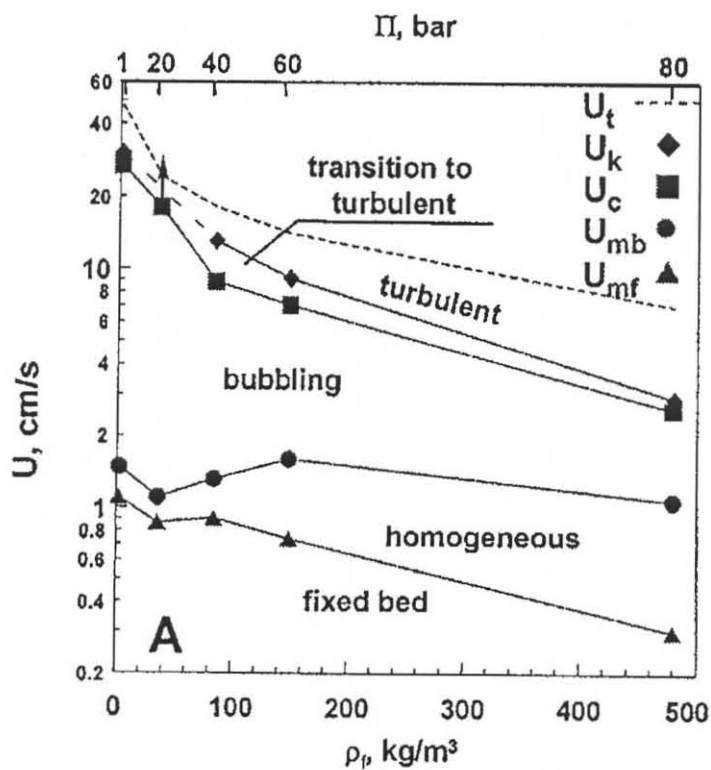
Figure 1.22 Superficial fluid velocities at regime transitions vs. fluid density for 88 micron glass beads.
(Marzocchella and Salatino, 2000, pg. 907)
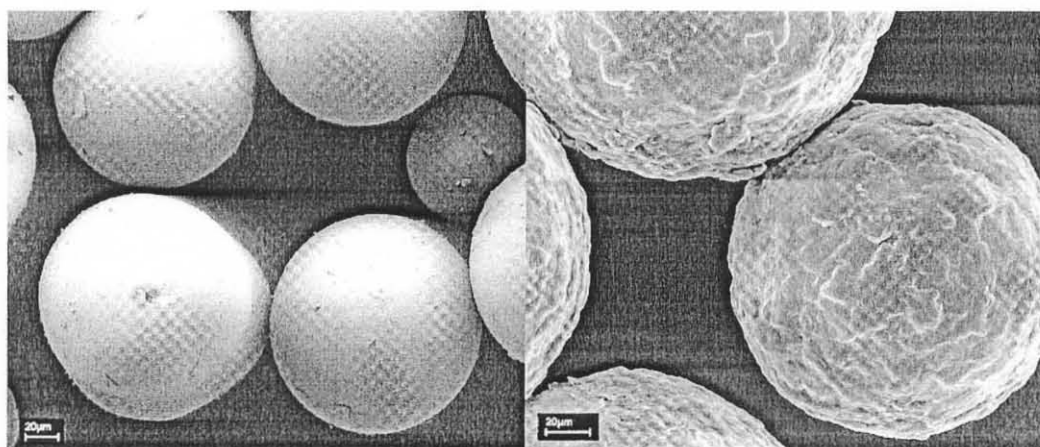
Figure 1.23 Comparison of SEM images of original, uncoated glass beads (left) and coated glass beads (right).
(Vogt et al., 2004, pg. 3)
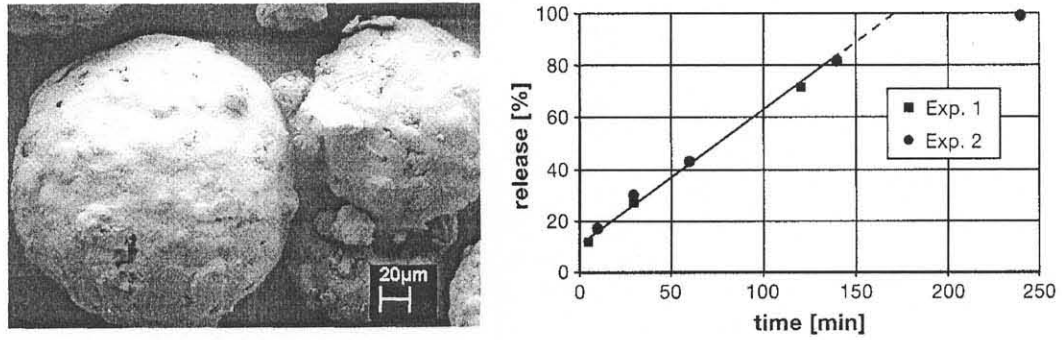
Figure 1.24 SEM image of coated lactose agglomerates (left) and release profile of lactose agglomerates coated with paraffin (right).
(Schreiber et al., 2003, pg. 36, 37)

with various powders including ashes of no more than 80 microns in diameter, which fall under the Geldart group C classification. Their results for the ashes are summarized in Figure 1.25, where it can be seen that temperature had the most notable effect on minimum fluidization velocity (u_{mf}), bed voidage at minimum fluidization conditions (ε_{mf}), size at minimum fluidization conditions (d_{umf}), and the Richardson-Zaki exponent (n). The effect of sound pressure levels made a clear appearance in terminal velocity (u_t) as well as the average particle size at terminal velocity (d_{ut}). Sound assistance was needed to fluidize the ashes since without sound, it would be difficult to achieve any kind of ordinary fluidized state in this particular system and apparatus. As a general conclusion, Paola and Riccardo (2004) remarked that the influence of temperature can be explained on a hydrodynamic basis due to the changes in gas viscosity and density.
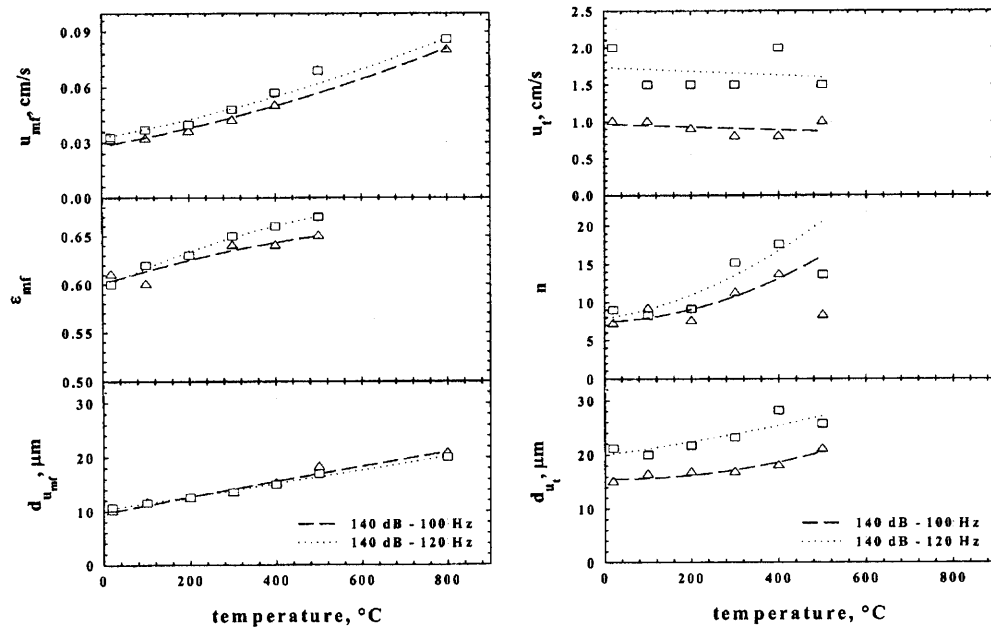
Figure 1.25 Minimum fluidization velocity, bed voidage, average size of particles at minimum fluidization velocity, terminal velocity, Richardson-Zaki exponent, and average size of particles at terminal velocity as a function of temperature at two different sound pressure levels, 140 dB & 100 Hz and 140 dB & 120 Hz, for group C material, ashes. (Paola and Riccardo, 2004, pg. 6).

CHAPTER 2

CONVENTIONAL FLUIDIZED BED

2.1 Introduction and Theory

Conventional fluidization is needed for a basis of comparison when determining any improvement in quality of assisted fluidization or of fluidization under non-ambient conditions. This chapter will focus on conventionally fluidized beds, i.e., no external aids such as vibration, magnetic assistance, and rotation. The theory for "regular" fluidization is well documented and will be summarized below.

At the onset of fluidization, the theory states that the drag force by the flowing gas starts to equal the weight (less buoyancy) of the powder bed. This can be expressed by (pressure drop across the bed)(cross sectional area of the vessel) = (volume of the bed)(solids fraction)(weight of the solids corrected for buoyancy) or by:

$$(\Delta P)(A_v) = W = (A_v H_{mf})(1 - \varepsilon_{mf}) \left((\rho_s - \rho_g) \frac{g}{g_c} \right) \qquad (2.1)$$

where ΔP is the pressure drop across the powder bed, A_v is the cross sectional area of the vessel, W is the weight of the bed, H_{mf} is the height of the bed at minimum fluidization, ε_{mf} is the voidage in the bed at minimum fluidization, ρ_s is the density of the particles, ρ_g is the density of the fluidizing gas, g is the acceleration of gravity, and g_c is a conversion factor. Simplifying and rearranging Equation 2.1 gives:

$$\frac{\Delta P}{H_{mf}} = (1 - \varepsilon_{mf})(\rho_s - \rho_g) \frac{g}{g_c} \qquad (2.2)$$

A lower measured pressure drop than the weight of the bed given by Equation 2.2 could be attributable either to a loss of powder sticking to the wall, powder elutriation, or possibly to some nonuniformities in the gas flow resulting from the relatively porous distributor that was used in the experiments. On the other hand, wall friction (Loezos et al., 2002; Srivastava and Sundaresan, 2002) and cohesion between the bed of particles with a layer of particles adhering tightly to the distributor (Castellanos et al., 1999; Sundaresan, 2003) would result in a higher measured pressure drop than the weight of the bed. Mutsers and Rietema (1977) were the first to suggest that additional terms may need to be included on the right-hand side of Equation 2.2 to account for the higher pressure drop of cohesive powders. They developed a theory, which includes interparticle forces as well as wall friction. Liss et al. (1984) accounted for their high measured pressure drop in a fluidized bed, where the particles were cohesive because of liquid bridge formation, through a term $(6S/d_p)(1 - \varepsilon_{mf})$, which was added to Equation 2.2 on the right-hand side. Here S is the cohesive stress, which is a function of temperature, composition, and particle size distribution.

Ergun (1953) correlated the pressure drop through a fixed bed of uniformly sized particles by the following equation:

$$\frac{\Delta P}{H_{mf}} g_c = 150 \frac{(1-\varepsilon_m)^2}{\varepsilon_m^3} \frac{\mu u}{(\phi_s d_p)^2} + 1.75 \frac{1-\varepsilon_m}{\varepsilon_m^3} \frac{\rho_g u^2}{\phi_s d_p} \qquad (2.3)$$

where μ is the viscosity of the fluidizing medium, ϕ_s is the sphericity of the particle, and d_p is the diameter of the particle. On the right hand side of Equation 2.3, the first part represents the viscous energy losses and the second part represents the kinetic energy losses that a bed will experience under flow. In other words, at low Reynolds numbers

(<20), the kinetic energy loss will be negligible in Equation 2.3 and at high Reynolds numbers (>1000), the viscous energy loss will be negligible in Equation 2.3. At Reynolds numbers between 20 and 1000, neither the viscous nor the kinetic term can be ignored in calculations.

In order to calculate the minimum fluidization velocity, Equation 2.2 and Equation 2.3 are combined to give a quadratic equation for u_{mf}:

$$\left(\frac{1.75}{\phi_s \varepsilon_{mf}^3}\left(\frac{d_p \rho_g}{\mu}\right)^2\right)u_{mf}^2 + \left(\frac{150(1-\varepsilon_{mf})}{\phi_s^2 \varepsilon_{mf}^3}\frac{d_p \rho_g}{\mu}\right)u_{mf} = \frac{d_p^3 \rho_g (\rho_s - \rho_g)g}{\mu^2} \tag{2.4}$$

Based on an agglomerate size of about 50 microns, the Reynolds number is less than 1. The traditional expression for calculating the minimum fluidization velocity based on the Ergun equation for Re < 20 (Kunii and Levenspiel, 1969) is

$$u_{mf} = \frac{(\phi_s d_p)^2}{150}\frac{\rho_s - \rho_g}{\mu}g\left(\frac{\varepsilon_{mf}^3}{1-\varepsilon_{mf}}\right) \tag{2.5}$$

The voidage is complicated to describe since it has been found from this study that there are different voidages within a bed of fluidizing nanoparticles. Because agglomerates are being fluidized, it is important to carefully label the various ways in which one can define voidage. Overall voidage (ε) is defined as the fraction of the total bed volume occupied by the fluid.

$$\varepsilon = 1 - \frac{\rho_b}{\rho_s} \tag{2.6}$$

Here, ρ_s and ρ_b denote the density of the primary nanoparticles (solids) and the apparent density of the bed, respectively. The volume fraction of primary particles in the bed (ϕ) is then equal to $1 - \varepsilon$. As for agglomerate size, a method to estimate the size of highly porous

nanoaggomerates is not readily available in the literature. The modeling work used here will be detailed in Section 2.3.4.

2.2 Experimental Setup, Materials, and Procedure

A schematic of the conventional fluidized bed is shown in Figure 2.1. All beds used were simple, vertical conventional beds with a cylindrical, transparent chamber with a distributor whose purpose is to distribute the fluidizing medium through the chamber. Equipped along the length of the chamber was a series of ports for sampling and pressure measurements. Pressure measurements were made with a pressure transducer (Omega), as depicted in Figure 2.1. Water manometers (Dwyer Mark II) were also used for verifying pressure drop measurements. Sizes, chamber material, and distributors were varied to observe any changes in fluidization behavior. The different bed parameters are summarized in Table 2.1.

The powder bed was placed above the distributor, through which the compressed, bone-dry air flowed. Bone-dry air was used to minimize any humidity effects since liquid bridges between agglomerates can significantly alter the behavior of fluidization. Large agglomerates that may have formed from packaging, storage, and transportation were removed by sieving the as-received powders before each experiment through a 500 micron sieve. Flow rate was measured by rotameters (Gilmont).

The largest of the beds (9.60 cm) was designed somewhat differently than the other very simple, cylindrical beds. The 9.60 cm bed, made of glass and having an expanded cross section at the top, was designed to be somewhat larger than most experimental setups so that wall effects will play less a role. A detailed schematic is

illustrated in Figure 2.2.

The visualization apparatus consisted of (a) a digital camera (SONY) to capture macroscopic behavior of the fluidized bed and its dynamics when expanding, collapsing, and bubbling if any, represented by part 10 in Figure 2.1, and (b) a combination of an argon laser generator (Reliant 1000M, LaserPhysics) with 3-W power and a high-speed CCD camera (LaVision Flowmaster) with an extremely short exposure time, represented by part 9 in Figure 2.1, to capture microscopic attributes of the fluidized bed or more specifically, in situ agglomerate size.

The properties of the powders (Degussa) used for conventional fluidization experiments are listed in Table 2.2. All powders are hydrophilic except for R974 and R972, which were surface treated with dimethyldichlorosilane (DDS) to induce hydrophobicity.
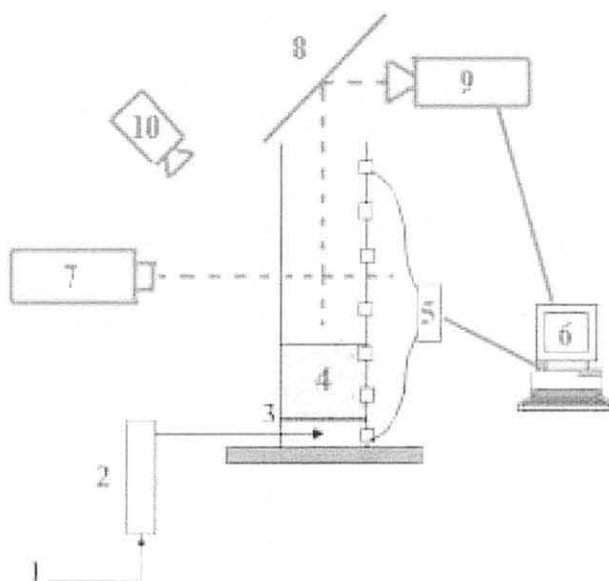
Figure 2.1 Schematic of the conventional fluidized bed. 1: Compressed air; 2: rotameter; 3: distributor; 4:fluidized bed; 5: pressure transducer; 6: computer; 7: laser generator; 8: mirror; 9: CCD camera; 10: digital camera.
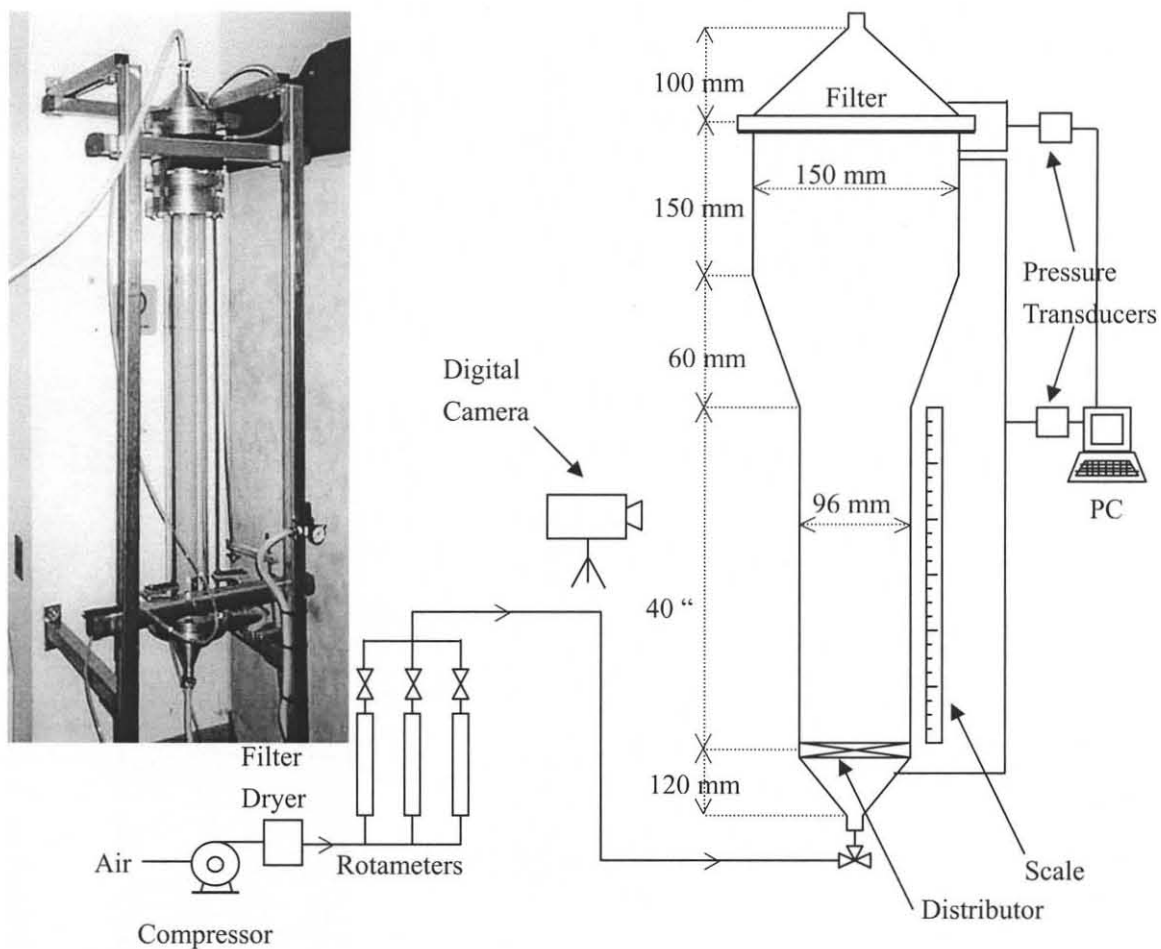
Figure 2.2   Photo and detailed schematic of the largest of the conventional fluidized beds.

To start a typical fluidization experiment, an amount of powder from a sieved batch was carefully measured and slowly placed inside the chamber.   The initial height was recorded after waiting approximately 15 minutes for the bed to settle completely. The flow rate was increased incrementally and the corresponding pressure drop was recorded along with observations of fluidization behavior and expanded height.   Once a definite plateau was reached, the flow rate was decreased incrementally and the corresponding pressure drop, expanded height, and behavior were recorded.   At each

Table 2.1 Summary of Bed Properties

Bed Property	Descriptions of the Types Used
Chamber Diameter	(a) 2.54 cm (b) 6.00 cm (c) 6.25 cm (d) 9.60 cm
Chamber Material	(e) glass / pyrex (f) lexan plastic
Distributor Material	(g) glass (10 microns in pore size) (h) layers of wire meshes (1-2 microns, 40 microns, 100 microns in pore size) (i) sintered metal (1-3 microns in pore size)

Table 2.2 Summary of Powder Properties (values provided by Degussa)

Powder	d_{pp} [nm]	ρ_{pp} [kg/m^3]	ρ_b [kg/m^3]	SA_{pp} [m^2/g]
Silica - R974 (hydrophobic)	12	2200	~30	170
Silica - R972 (hydrophobic)	16	2200	~30	110
Silica - A300 (hydrophilic)	7	2200	~30	300
Silica - A90 (hydrophilic)	20	2200	38-40	90
Alumina - AluC (hydrophilic)	13	4200	50	100
Titania - P25 (hydrophilic)	21	4500	130	50

incremental superficial velocity, sufficient time was given for the bed to reach its true state since it would take a few minutes for the bed to stop expanding from an increase in flow rate.

At each velocity, the macroscopic and microscopic properties were recorded with a digital camera and CCD camera, respectively. The digital camera shots also helped to accurately record bed expansion height. The CCD camera and laser light were used to record agglomerate size and overall shape during fluidization. The laser beam was

located at the surface of the fluidized bed and the camera was focused at the beam. The camera was positioned near the opening of the tube where a mirror was angled at 45°. In this way, no sources of possible distortion, such as the bed wall, would affect the image. Approximately 500 in situ images of each experiment were taken. Each experiment was repeated at least three times and average values were used to represent the experiment.

One method of sampling for SEM (Scanning Electron Microscopy) analysis involved aspirating out particles into a small vial through the ports of the bed. These samples were then gently placed on SEM sample disks for analysis. Another option was to gently dip an SEM sample disc adhered with a double-sided carbon tape into the fluidized bed. The sample disk was then directly used for SEM analysis to determine morphology and size. EDX (Energy Dispersive X-ray) was used in conjunction with the SEM to analyze composition. Other characterization equipment included TEM (Transmission Scanning Microscopy), EELS (Electron Energy Loss Spectroscopy), AFM (Atomic Force Microscopy), and a Beckman- Coulter counter.

2.3   Results and Discussion

2.3.1   Fluidization Behavior

According to Geldart et al. (1973), the type of fluidization behavior exhibited by particles depends on their size and the density difference between the particles and the fluidizing gas. Based on empirical observations, Geldart et al. (1973) determined that particles whose diameter is smaller than 30 microns and density difference is smaller than 1000 kg/m^3, classified as group C powders, are difficult to fluidize in a conventional

gravity-driven fluidized bed.   Generally, these powders would form cracks, channels, or lift as a solid plug when exposed to a fluidizing gas at low superficial gas velocity.   This behavior is mainly caused by the strong interparticle (van der Waals) forces.   The importance of these interparticle forces relative to the weight of the particle increases as the surface-to-volume ratio increases and may significantly exceed the external mechanical forces (such as that attributed to gravity) to which the particles are subjected. As stated in Chapter 1, a number of research groups (Chaouki et al., 1985; Iwadate and Horio, 1998; Li et al., 1990; Morooka et al., 1988; Pacek and Nienow, 1990; Wang, Y., et al., 2002; Wang, Z., et al., 1998; Zhou and Li, 1999) found that once a high enough superficial gas velocity was reached, the interparticle networks were disrupted and agglomerates or loosely bound structures of the ultrafine particles formed.

In this study, the bed of nanoparticles, when exposed to a low flow rate of air below the expected minimum fluidization velocity, exhibited the aforementioned behavior of plug flow, channeling, and / or spouting.   At high flow rates, most group C powders can be fluidized, albeit with high elutriation, due to the formation of agglomerates.   However, it was also observed that the quality of fluidization strongly depends on distributor material, powder material, and chamber diameter.   Aside for the slightly stronger electrostatic effects in the plastic bed than in the glass bed, the chamber material did not have a significant effect on fluidization quality.

Figure 2.3 shows the difference between the fluidization of Silica A300 powders in a bed with a sintered metal distributor and the fluidization of the same powders (10 grams of Silica A300) in the same bed (lexan chamber, 6.25 cm in diameter) except with layers of wire mesh with 40 microns in pore size as the distributor at low velocities.   As

(a) **(b)**
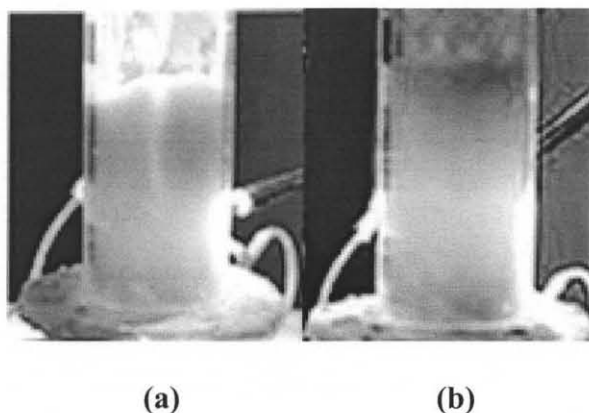
Figure 2.3 Fluidization of 10 grams of Silica A300 powders in a lexan bed (6.25 cm in diameter) with (a) six layers of wire mesh and (b) sintered metal.

seen in the figure, channels and spouting occur in the bed with the wire meshes and smooth fluidization occurs in the bed with the sintered metal distributor. However, at very high velocities, all nanopowders can be fluidized due to the formation of relatively large agglomerates. The difference in behavior from the different distributors results from differences in the uniformity of air distribution in the bed. Overall, the most uniform distribution of air will result in higher fluidization quality. However, with a high degree of uniformity comes a high pressure drop, which in the case of nanoparticles is orders of magnitude higher than the pressure drop across the powder bed. This makes measurement of pressure drop across the bed somewhat difficult since either (a) pressure drop would have to be measured across the distributor and the bed, from which only the small pressure drop across the bed would be needed causing a significant error bar, or (b) pressure drop would have to be measured from slightly above the distributor which often leads to clogging of pressure taps and a slight error in measurement since the bed in its entirety is not accounted for. The bed with the layers of wire mesh, even the one with 1-2 microns in pore size, also gave rise to some instability and relatively large bubbles while the bed with either the sintered metal or glass as the distributor gave rise to, albeit

temporarily, a smoothly fluidized bed with high bed expansion. In other words, although the distribution of air was very uniform, the properties of the cohesive nanopowder can take control of the fluidization behavior as seen in Figure 2.4 where Alumina C started to fluidize smoothly in the glass chamber (9.6 cm in diameter) from the excellent distribution of high-flow air (Figure 2.4b) through a sintered metal distributor in a glass chamber, 9.60 cm in diameter, but eventually collapsed and formed very stable channels (Figure 2.4c). The tortuosity of the pores in the sintered metal and glass distributors significantly helped increase uniformity of flow.

Powder material also had an influence on fluidization quality. Silica A90, Alumina C, and Titania P25 all were more susceptible to characteristic group C behavior

(a)   (b)   (c)
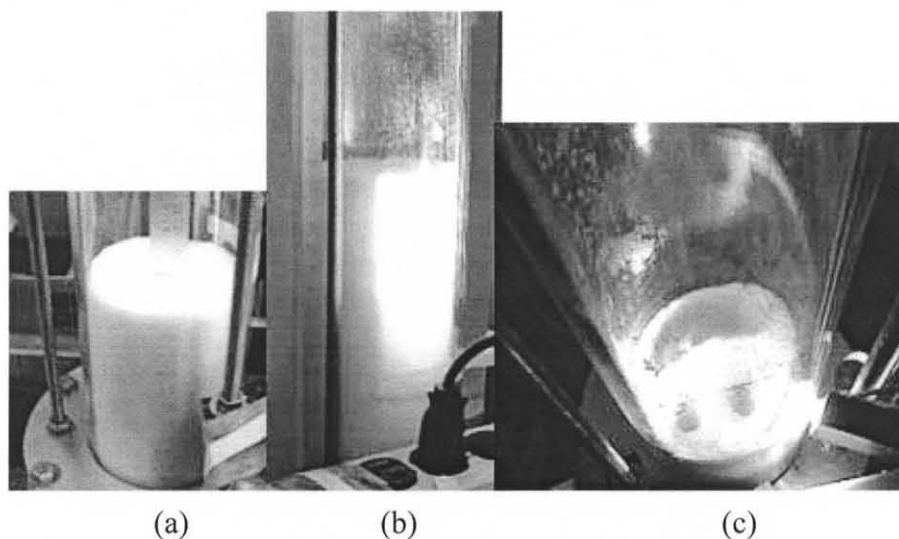
Figure 2.4 Behavior of a conventionally fluidized Alumina C bed in a glass chamber (9.6 cm in diameter) with a sintered metal distributor at (a) 0 s, (b) 1 minutes, and (c) 2 minutes and thereafter.

such as channeling, plugging, and spouting which can be overcome by relatively high superficial velocities. Silicas R972, R974, and A300 were easily fluidizable at high velocities with substantial bed expansion. Alumina C and Titania P25 both have bulk densities much higher than the other nanoparticles, which could explain why fluidization

was more difficult than with the lighter, fluffier particles. However, Silica A90, has a similar bulk density to the other silicas and yet, was difficult to fluidize in the conventional bed. The reason could be attributed to the agglomerate structure. The silicas R974, R972, and A300 have smaller diameters and higher surface areas compared to that of A90. This means that there are very strong interparticle forces that can possibly hold an agglomerate structure together that is needed for the fluidization of nanoparticles. In other words, it is possible that the agglomerate structure is so strong that the agglomerates are so strong that the agglomerates are too large to be readily fluidized. Perhaps the interparticle forces between the Silica A90 particles are not strong enough to maintain the agglomerate structure needed for fluidization to occur. Overall, the Silica R974, Silica R972, and Silica A300 exhibited smoother and more stable fluidization than Silica A90, Alumina C, and Titania P25 in the conventional fluidized bed. In the terms coined by Wang et al. (2002), Silica R974, Silica R972, and Silica A300 can be categorized as powders that exhibit APF behavior (agglomerate particulate fluidization) whereas Silica A90, Alumina C, and Titania P25 can be categorized as powders that exhibit ABF behavior (agglomerate bubbling fluidization).

Chamber diameter also affected fluidization behavior. Generally, fluidized beds should be at least 2.54 cm (1 inch) in diameter because any lower would give rise to appreciable wall effects. However, for nanoparticles, 1 inch for a conventionally fluidized bed is too small since plugs would form on a consistent basis. The chamber that was 6 cm (2.4 inches) in diameter was just right for a lab-scale apparatus for the fluidization of the silicas R974, R972, and A300. Silica A90, Alumina C, and Titania P25 exhibited slightly better fluidization in the 2.4 inch bed but still showed typical group

C fluidization characteristics. The 9 cm (3.5 inch) bed also proved to be an acceptable size to achieve vigorous fluidization for silicas R974, R972, and A300. Again, Silica A90, Alumina C, and Titania P25 showed slightly better fluidization quality in the 3.5 inch bed.

2.3.2   Pressure Drop

The pressure drops across the sintered metal distributor and the glass distributor were very large relative to the pressure drop across the nanoagglomerates. The layers of wire meshes had a much smaller pressure drop associated with it but a somewhat poorer distribution of air. Adding 3 mm glass beads below the distributor of wire meshes helped to distribute the air more uniformly. In this way, the pressure drop across the entire bed may be measured which is important for accuracy in all calculations using experimental data. In the case of using the sintered metal distributor or the glass distributor, pressure would be measured from a location above but near the distributor which often would lead to clogged pressure taps and a small inaccuracy in pressure drop since not all of the powder bed would be accounted for. Therefore, in order to measure the pressure drop across the entire powder bed, six layers of wire mesh were used as the distributor for the following experiments. The lexan chamber with a diameter of 6.25 cm was used for all experiments as well. This also means that the initial height of each powder should be at least 6.25 cm. In order to comply to this guideline, 10.0 grams of Silica R974, 10.0 grams of Silica R972, 11.0 grams of Silica A300, 15.0 grams of Silica A90, 14.0 grams of Alumina C, and 40.0 grams of Titania P25 were used for the experiments. Using more powder would only affect the absolute pressure drop and bed

expansion measurements. Non-dimensionalized values would remain practically the same.

In all of the experiments performed, the measured pressure drop across the bed at high gas velocities, above the minimum fluidization velocity, approximately equaled the weight of the bed per unit cross-sectional area, as given by the force balance equation (Equation 2.1 and Equation 2.2). Figure 2.5 shows a typical set of results obtained in a conventional fluidized bed of Silica R974, where both the pressure drop across the bed and the bed expansion at increasing gas velocities and decreasing gas velocities are presented. The pressure drop has been scaled with the actual measured weight of the bed per unit cross sectional area of the bed, whereas the bed height has been scaled with the height of the settled bed. It is clear from Figure 2.5 that the pressure drop increased
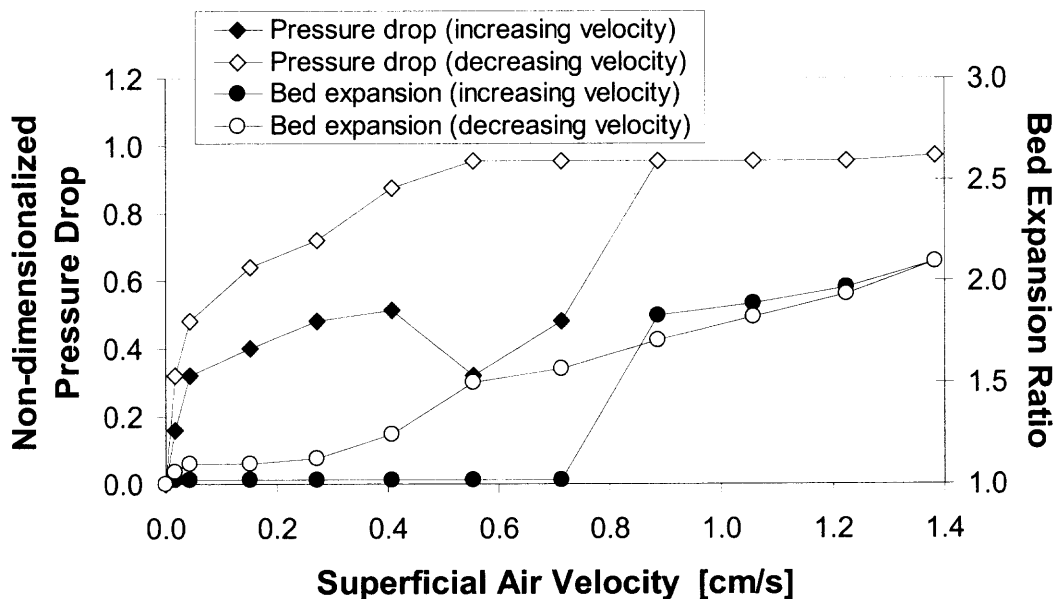
Figure 2.5 Pressure drop and bed expansion ratio as functions of air superficial velocity for Silica R974 in a conventional fluidized bed.

initially with gas velocity and then leveled off at high gas velocities. The velocity range between 0.4 and 0.7 cm/s represents the formation of a plug, the breakage of a plug and formation of channeling, and the final breakage of the channeling due to high velocity. In the plateau region, the scaled pressure drop is very close to the expected value of unity. With decreasing velocity, the bed is sufficiently loosened to fluidize more smoothly even at the lower gas velocities, as seen in Figure 2.5. In other words, decreasing velocity showed a small hysteresis in that smoother fluidization occurs once the bed is fluidized. Once the interparticle forces are disrupted, fluidization is easier to achieve than with a bed that has not been fluidized or is in the settled state. Appendix D shows results from all powders.

2.3.3   Minimum Fluidization Velocity

The minimum fluidization velocity is defined as the point at which the pressure drop begins to equal the weight of the bed per unit area. Typically, along with this definition comes the description of the bed expansion, which is generally accepted and understood to begin at the onset of fluidization or at the minimum fluidization velocity. However, for the fluidization of nanoparticles, the velocity at which the pressure drop begins to plateau is not always in sync with the bed expansion data. Often, a bed of nanoparticles, as seen in Figure 2.5 and Appendix D, will start to expand at a velocity lower than the minimum fluidization velocity. The velocity at which the bed begins to expand will be called the "minimum expansion velocity," u_{me}. The summary of results (minimum expansion and minimum fluidization velocities of each powder) is listed in Table 2.3. The velocities listed in Table 2.3 cannot be obtained from Equation 2.5 if the size of the

Table 2.3 Summary of Minimum Fluidization Velocity and Minimum Expansion Velocity for Each Powder from Conventional Fluidization Experiments

Powder	Minimum Fluidization Velocity [cm/s]	Minimum Expansion Velocity [cm/s]
Silica R974	0.5-0.6	~0.4
Silica R972	0.6-0.7	~0.7
Silica A300	~1.0	~0.3
Silica A90	~5.0	~0.7
Alumina C	~5.0	~4.5
Titania P25	3.0-3.5	~3.0

primary particle is used, demonstrating unequivocally that agglomerates were being fluidized and that agglomerate properties must be used in Equations 2.5 in order to obtain meaningful results.

2.3.4 Agglomerate Size

A Beckman Coulter counter (dry module) was used to determine the agglomerate size distribution of the as-received silica powder. Representative Coulter counter results for pre-experiment powder indicated a mean agglomerate size anywhere between 20–40 microns. This is highly suspect because large agglomerates of size on the order of millimeters (perhaps formed during storage) could be observed visually. These contradictory results, which are shown in Figure 2.6, suggest that the agglomerates are in general so fragile that any measurement method involving direct contact with the sample is not effective and reliable. It is conjectured that the agglomerates were broken up during the course of the Coulter counter size distribution measurements, leading to agglomerate sizes anywhere between 20–40 microns. Very similar results are found when analyzing the agglomerates in an Aerosizer as well. The Aerosizer, in its vacuum and sampling mode, is probably breaking the porous agglomerates just as the Coulter
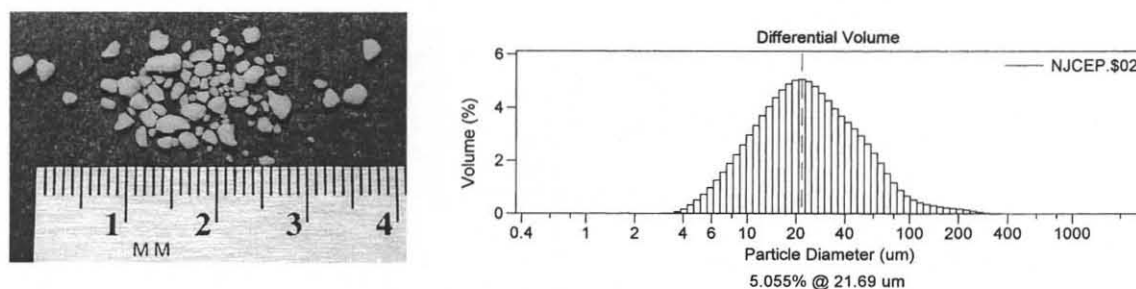
Figure 2.6 Photograph of sieved-out agglomerates (left) and the incongruous Beckman Coulter Counter results of the same sieved-out agglomerates (right).

Counter did during its measurement process. Agglomerate samples were aspirated out of the bed at different heights of the expanded fluidized bed and examined under SEM. As shown in Figure 2.6, the agglomerate sizes averaged about 20 microns. Similar sizes were obtained when samples were taken by dipping an SEM analysis disc directly into the fluidizing bed. The agglomerates appeared very porous and fragile and are believed to have broken (into sub-agglomerates) during their removal from the bed and/or during sample preparation for the SEM. A sketch of the agglomerate as the author envisions it is drawn in Figure 2.7. As discussed later, the agglomerate size estimated from pressure drop and bed height data in fluidization experiments was considerably larger, on the order of a hundred microns.

Given the fragile nature of the agglomerates, it is reasonable to expect that an equilibrium between agglomerate breakage and agglomerate formation is reached during the process of fluidization. Therefore, the true agglomerate size can be found only from measuring the agglomerates dynamically as fluidization is occurring. The use of a high-speed digital camera with an extremely short exposure time and a laser beam was used to observe and investigate the dynamic agglomerate size in situ. At least 500 images were taken for each powder. Nine images of typical results of the camera and laser for Silica R974 are shown in Figure 2.8. Bright spots indicate agglomerates

directly in line with the laser beam and therefore are focused. Grayer spots indicate agglomerates that are not quite in focus. The dark spots in the agglomerate images indicate a certain degree of porosity that the laser light was able to support the method of size estimation discussed in the following sections. The results from the other powders are summarized in Table 2.4 and images of the other powders are shown in Appendix B. It is important to note that the results listed in Table 2.4 for Titania P25 were sampled from a smaller sampling, which may lead to an error in accuracy. To measure the agglomerate size, all captured images were imported into Adobe Photoshop where the exact number of pixels was measured for each agglomerate individually. Since the focus, magnification, and other parameters of the camera were known, the number of pixels obtained could then be converted into a length.

primary agglomerates (1-4 microns)
Each primary agglomerate is made
up of chains and nets of nanoparticles.

sub agglomerates (10-50 microns)

in situ fluidized agglomerate size
(100 - 400 microns)
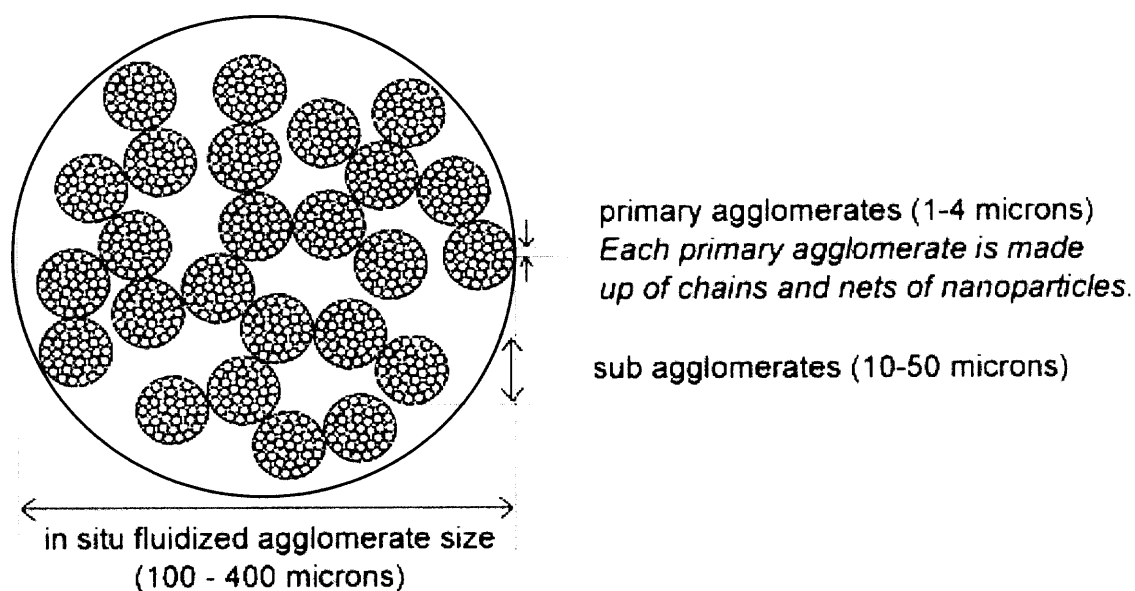
Figure 2.7 A sketch of the agglomerate (inspired by Cook, 1989).
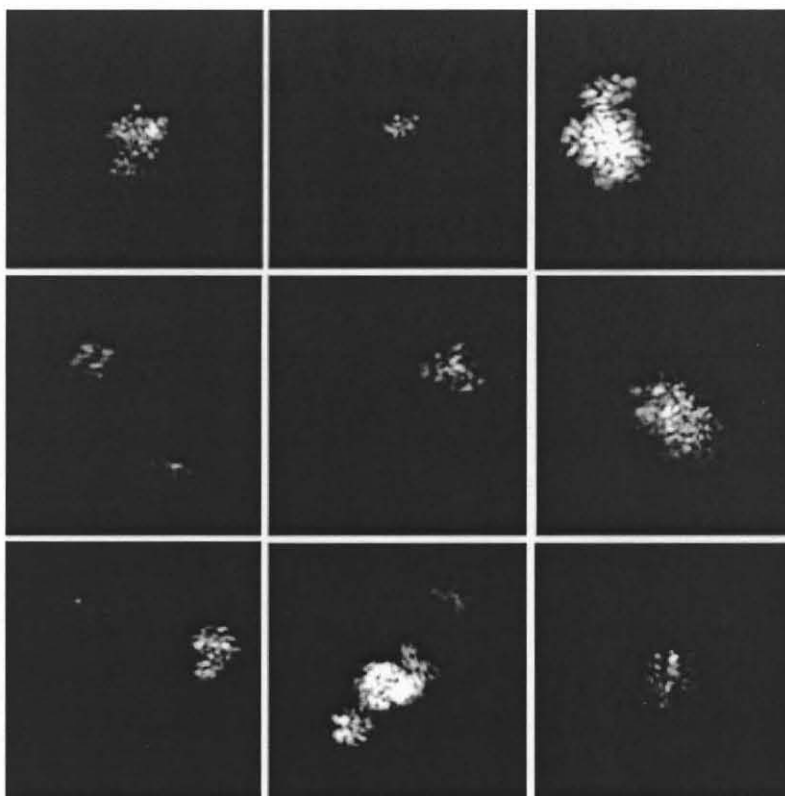
Figure 2.8 Nine laser and camera results capturing agglomerates in a conventional fluidized bed. Each shot is 1.1 mm in height and width.

Table 2.4 Summary of Size Analysis of In-Situ Agglomerate Images from Conventional Fluidization Experiments

Powder	Mean diameter [microns]
Silica R974	234.3
Silica R972	238.7
Silica A300	236.9
Silica A90	334.7
Alumina C	421.9
Titania P25	147.2

Because the behavior of nanoagglomerate fluidization was so liquid-like with practically no bubbling, the Richardson–Zaki (R-Z) approach, usually valid for homogeneous liquid–solid sedimentation and fluidization, is used in the analysis described below. To estimate the agglomerate density and porosity in terms of its size, we use the

fractal model suggested by Valverde et al. (2001b) and further explored by Castellanos et al. (2001). Agglomerates composed of fine particles typically have fractal structures (Valverde et al., 2001b). The number of primary particles, N, in an agglomerate of radius, r_a, can be expressed as (Friedlander, 2000)

$$N = k \left(\frac{r_a}{r_p} \right)^{D_f} \tag{2.7}$$

where k is a prefactor (commonly set to unity), D_f is the fractal dimension, and r_p is the radius of the primary particle. The images seen in Figure 2.8 are very reminiscent of a simulated model of a fractal agglomerate made of several thousands of primary particles by Schaefer et al. (1988), as depicted in Figure 2.9.
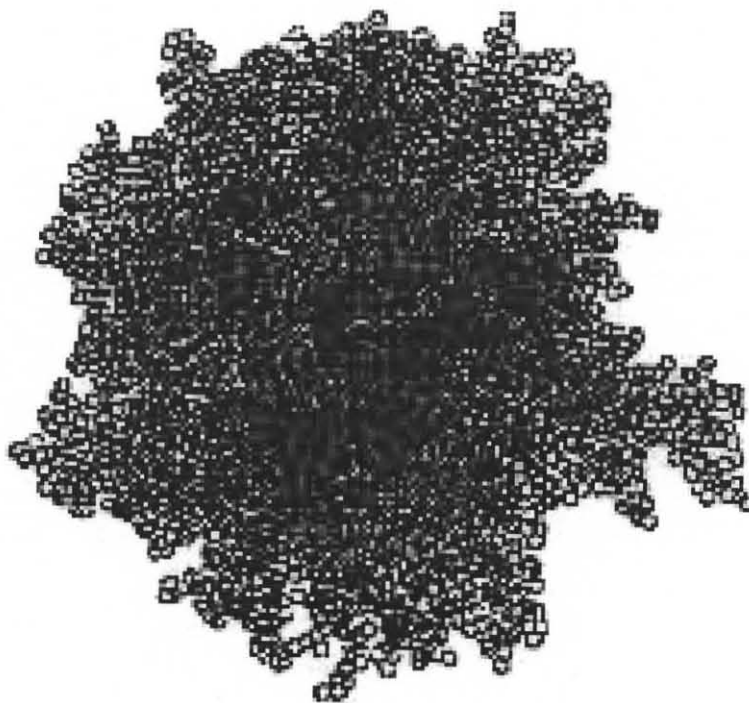
Figure 2.9 Simulated ($D_f = 2.5$) cluster-monomer ballistically grown three-dimensional aggregate containing 10^4 primary particles.
(Shaefer et al., 1988)

Assuming that the agglomerates are spherical, the mass of an agglomerate is

$$m_a = \frac{4}{3} N \pi r_p^3 \rho_p = \frac{4}{3} \pi r_a^3 \rho_a \tag{2.8}$$

Equation 2.7 and Equation 2.8 can be combined to obtain

$$\frac{\rho_a}{\rho_p} = N^{1-(3/D_f)} \tag{2.9}$$

It then follows that

$$\phi_e = \phi N^{(3/D_f)-1} \tag{2.10}$$

The Stokes settling velocities of a primary particle (V_0) and that of an agglomerate (v_a) are

$C(2\rho_p r_p^2 g / 9\mu)$ and $2\rho_a r_a^2 g / 9\mu$, respectively, where C is the Cunningham correction

factor, which applies for particles less than 1 micron in diameter (Seinfeld, 1986). These

velocities can be combined with Equation 2.7 to obtain

$$v_a = \frac{V_o}{C} \frac{\rho_a}{\rho_p} \left(\frac{r_a}{r_p}\right)^2 = v_o N^{1-(1/D_f)} \tag{2.11}$$

where $v_o = 2\rho_p r_p^2 g / 9\mu$. Using Equation 2.10 and Equation 2.11, and the R-Z equation,

$$\frac{u}{v_a} = \varepsilon_e^n \tag{2.12}$$

where n is the R-Z exponent, can be written as

$$u = v_o N^{1-(1/D_f)} (1 - \phi N^{(3/D_f)-1})^n \tag{2.13}$$

For each value of u, ϕ was determined from the measured bed height. Equation 2.13

indicates that a plot of $(u/v_o)^{1/n}$ vs. ϕ for a reasonable value of n would yield a linear

relationship with a y-intercept b, equal to $N^{[1-(1/D_f)](1/n)}$ and a slope m, equal to

$-bN^{(3/D_f)-1}$. The radius of the agglomerate can then be calculated from

$$r_a = r_p \sqrt{-mb^{n-1}}$$ (2.14)

The estimated value of 2.60 for the fractal dimension of Silica R974 agglomerates in a conventional fluidized bed is close to that for diffusion-limited aggregation (that is, 2.5) (Friedlander, 2000). This D_f value led to a calculated diameter size of 341 microns, which will be discussed in the following section. The fractal dimensions for all powders are listed in Table 2.5. With the exception of Titania P25 that had a small sample space, in comparison to the experimental measured values listed in Table 2.4, the calculated values listed in Table 2.5 are very reasonable. Given that such an aggregation mechanism is reasonable for the extremely fine primary particles used in this study, the fractal dimension

Table 2.5 Summary of Calculated Fractal Dimensions and Agglomerate Sizes for Each Powder from Conventional Fluidization Experiments

Powder	D_f	d_a [microns]
Silica R974	2.60	341
Silica R972	2.60	314
Silica A300	2.64	276
Silica A90	2.65	187
Alumina C	2.66	371
Titania P25	2.70	422

estimated from the bed height data and the above analysis is very encouraging. However, the estimated agglomerate diameter is much larger than the SEM experimentally measured value, which SEM photographs (see Figure 2.10), showed to be about the order of 10 microns, but in good agreement with the bright agglomerates seen in Figure 2.8, obtained by photographing the surface of the bed using a high-speed digital camera with an extremely short exposure time. It is suspected that considerable breakage of the fragile porous agglomerates took place (into sub-agglomerates) when the particles were aspirated out of the bed and/or prepared for the samples for SEM analysis. This is a possible

explanation of why the experimental SEM agglomerate sizes were much smaller than those estimated from the fractal analysis. AFM analysis was used to attempt to measure the force required to break an agglomerate. Unfortunately, due to the very fragile nature of the agglomerate and the small size, it was difficult to know exactly where the tip of the AFM is.
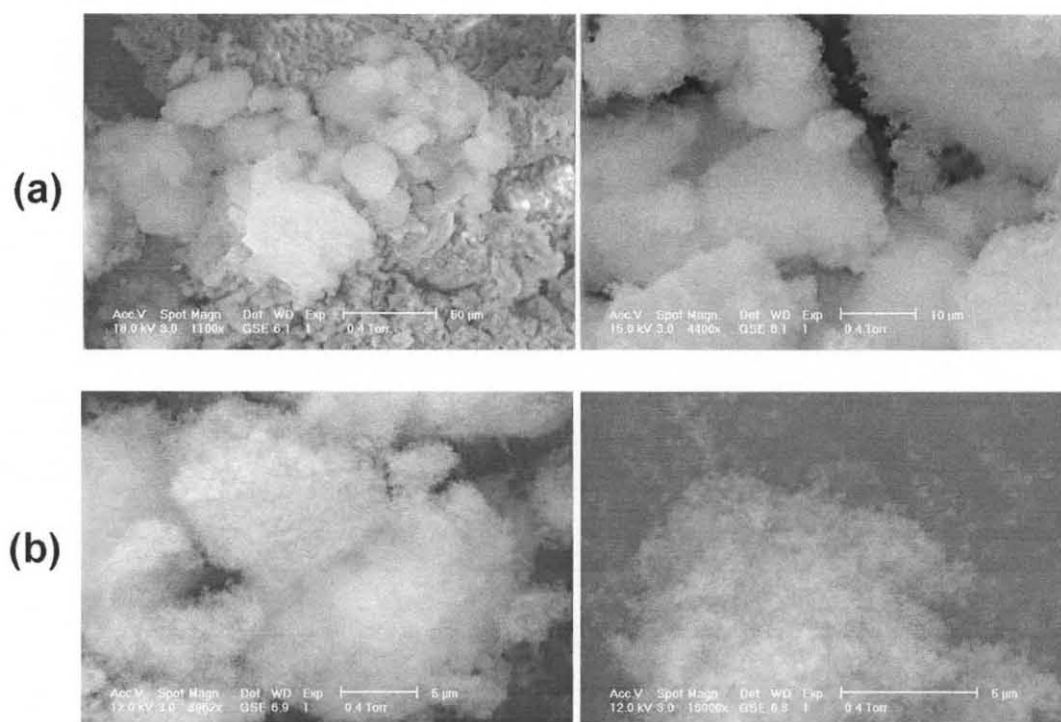
Figure 2.10 SEM images of (a) out-of-the-bag agglomerates and (b) samples taken from a conventional fluidized bed.

A fractal analysis (coupled with the R-Z equation) was performed for the bed-expansion data from the conventional fluidization work of Wang et al. (2002). This research group used Aerosil R972, which is very similar to Aerosil R974, used in our experiments. For R-Z exponents of 3.5, 4.0, 4.5, and 5.0, the D_f values were found to be

2.53, 2.54, 2.55, and 2.55 and the radii of the agglomerates calculated were 140, 135, 130, and 126 microns, respectively.

2.3.5 Voidage

Using Equation 2.6 and inputting 0.03 and 2.2 g/cm^3 for the bulk density of a settled bed and primary nanoparticle density, respectively, one finds that $\varepsilon \sim 0.9864$. Thus, the bed of nanoparticles was already highly fluffy even before fluidization. As the bed expands, ε increases to >0.99. The sub-agglomerates themselves, discussed in the previous section, were very porous, as seen from the high-resolution SEM and TEM image in Figure 2.11.
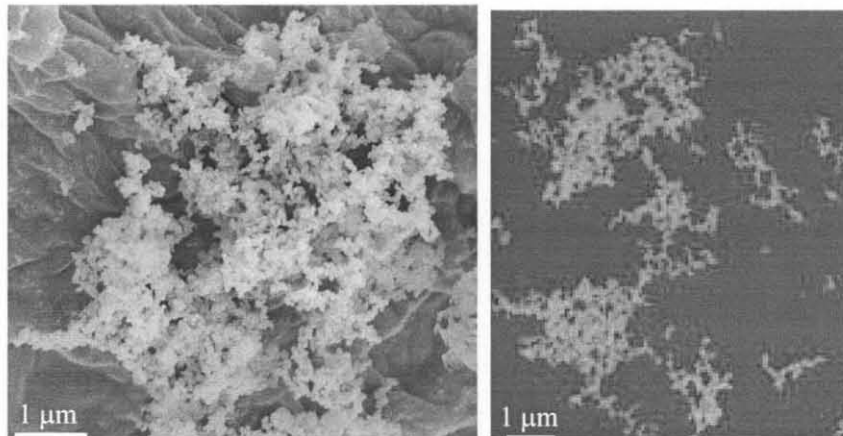
Figure 2.11 High-resolution SEM (left) and TEM (right) image of silica agglomerates.

The apparent density of the agglomerates and the fraction of bed volume occupied by the agglomerates are denoted by ρ_a and ϕ_e, respectively. It then follows that $\phi\rho_p = \phi_e\rho_a$. The void space between the agglomerates, represented as a fraction of the bed volume, is expressed as $\varepsilon_e = 1 - \phi_e$. The porosity inside the agglomerates (ε_{agg}) is simply equal to $1 - \rho_a/\rho_p$. The challenge lies in the estimation of ρ_a and ε_e from the experimental data. Chaouki et al. (1985) and Wang et al. (2002) assumed that

$$\varepsilon_e = 1 - \frac{H_o}{H_{exp}} \qquad (2.15)$$

Equation 2.15 is problematic because it assigns a value of zero to ε_e for a settled bed (that is, when $H_o = H_{exp}$). With the approach described in the previous section to estimate ρ_a and ε_e, originally presented by Valverde et al. (2001b) and Castellanos et al. (2001), and using an agglomerate diameter of 147 microns, found from the fractal analysis described in the previous section for Titania P25, and the experimental pressure drop data, ε_e was estimated at various gas velocities through the Blake–Kozeny equation (Ergun equation at low Reynolds numbers), as follows:

$$\frac{\Delta P}{H} g_c = 150 \frac{(1 - \varepsilon_e)^2}{\varepsilon_e^3} \frac{\mu u_o}{(\phi_s d)^2} \qquad (2.16)$$

Table 2.6 compares the values of ε_e determined through the three methods mentioned above: (1) the modified Richardson–Zaki analysis, which used only the bed-expansion data; (2) the pressure drop data, which assumed an agglomerate size estimated from the Richardson–Zaki analysis; and (3) the simple approach used by Chaouki et al. (1985) and Wang et al. (2002) (that is, Equation 2.15). Table 2.6 corresponds to the data presented earlier in Figure 2.5. It is clear from Table 2.6 that the values of ε_e determined by the first two methods are close to each other (except at the lower end of voidage), which lends further support to the fractal approach.

It could have been demanded that both the pressure drop and bed-expansion data be satisfied accurately by the model and allowed the agglomerate size to vary (slightly) with gas velocity. Such an exercise revealed that the agglomerate size decreases slightly as the gas velocity is increased, which is physically reasonable. The third method, using

Equation 2.15, did not give as reasonable values of ε_e because the values of $H/H_o < 2$, and

gave very small (and unphysical) values of ε_e.

Table 2.6 Summary of Interagglomerate Voidages Calculated from the Modified Richardson-Zaki Method, Blake-Kozeny Equation, and Equation 2.15 for Silica R974

U (cm/s)	ε_e (Modified Richardson–Zaki)	ε_e (Blake–Kozeny Equation)	$\varepsilon_e = 1 - H_0/H_{exp}$
0.89	0.582	0.649	0.453
1.06	0.594	0.669	0.470
1.22	0.611	0.686	0.491
1.38	0.634	0.702	0.522

For comparison, the values of ε_e estimated from the data by Wang et al. (2002),

assuming a value of 5 for the R-Z exponent, are summarized in Table 2.7. Also listed are

the values of ε_e obtained by Wang et al. (2002) by using Equation 2.15. Wang et al. (2002)

also performed experiments with other nanoparticles. Aerosil 300, for example, whose

apparent density and primary particle size are listed as 37 kg/m^3 and 7 nm, respectively, did

not exhibit high (>2) bed-expansion ratios. They applied Equation 2.15 and obtained ε_e

values summarized in Table 2.8. The minimum fluidization velocities found by Wang et

al. (2002) were higher than those found in this dissertation mostly likely due to the fact that

they did not sieve their particles. Thus, they were fluidizing much larger agglomerates, on

the order of millimeters. When a fractal analysis of the same data was performed,

assuming that n = 5, more reasonable estimates for ε_e were obtained (see Table 2.8). This

example shows that Equation 2.15 cannot be used to estimate ε_e when the bed expansion is

low but is a fair approximation for bed expansions > 2.

Table 2.7 Interagglomerate Voidages Obtained from Modified Richardson–Zaki Method and Equation 2.15 for Aerosil R972*

u (cm/s)	ε_e (Modified Richardson–Zaki)	$\varepsilon_e = 1 - H_0/H_{exp}$
1.45	0.735	0.643
1.70	0.772	0.692
2.15	0.797	0.726
2.40	0.819	0.756
2.70	0.835	0.778

*Wang et al. (2002).

Table 2.8 Interagglomerate Voidages Obtained from Modified Richardson–Zaki Method and Equation 2.15 for Aerosil 300*

u (cm/s)	ε_e (Modified Richardson–Zaki)	$\varepsilon_e = 1 - H_0/H_{exp}$
3.00	0.783	0.329
3.49	0.801	0.383
3.90	0.816	0.429
4.70	0.849	0.535
5.50	0.885	0.643
6.25	0.902	0.697

*Wang et al. (2002).

2.4 Conclusions

The main purpose of these conventional fluidization experiments was to provide a basis for comparison when fluidizing the same nanoparticles under different conditions and with assistance. It was shown that nanosized silica could be fluidized in the form of stable, very porous agglomerates at relatively high superficial velocities. A modified Richardson–Zaki approach combined with an assumption of fractal agglomerates was successfully applied to analyze the bed-expansion data reported here, from which we estimated the agglomerate size, other agglomerate properties, and the interagglomerate voidage. Voidages were independently checked with those calculated from the

Blake-Kozeny equation and were found to be in good agreement. The pressure drop

data were found to be consistent with agglomerate size determined in this manner.

CHAPTER 3

VIBRATING FLUIDIZED BED

3.1 Introduction and Theory

Vibration intensity is defined as the ratio of vibrational acceleration to gravitational acceleration,

$$\Gamma = A\omega^2/g, \tag{3.1}$$

where A is the amplitude of vibration and $\omega = 2\pi f$.

Erdesz and Mujumdar (1986) claimed that for micron sized particles, the minimum fluidization velocity, pressure drop, and bed porosity all are non-linear functions of the vibration intensity (Equation 3.1). As described in Chapter 1, Yoshida et al. (1965), Mori et al. (1990), Dutta and Dullea (1991), Jaraiz et al. (1992), Marring et al. (1994), and Noda et al. (1998) found similar results. These groups introduced various expressions for pressure drop and minimum fluidization velocity that differed from Equation 2.2 and Equation 2.5, both detailed in Chapter 2. However, it must be noted that these theories are for cohesive particles that are a few microns and above in diameter, which are different from the nanoparticle agglomerates. The parameter that must be considered for nanoparticle agglomerates is not only the porosity of the bed from the relatively high bed expansions, but also the porosity of the agglomerates themselves. The actual size of the fluidized nanopowder agglomerates is in the regime of group A and B particles, which makes the application of the expression for plateau pressure drop (Equation 2.2), for example, quite applicable.

3.2   Experimental Setup, Materials, and Procedure

A schematic of the vibrofluidized bed is shown in Figure 3.1.   The bed was mounted on top of a Ling Dynamic System vibrator, which can produce AC vertical sinusoidal waves with accelerations up to 5.5g (where g is the acceleration attributed to gravity) measured by a piezoelectric accelerometer.   The frequency, f, of vibration could be varied from 30 to 200 Hz.   Preliminary results were obtained from a vertical, cylindrical, glass bed of 6.25 cm in diameter with a glass distributor of 10 microns in pore size.   All other results were obtained using a vertical, cylindrical, acrylic bed of 6 cm in diameter with 6 layers of wire meshes of 40 microns in pore size as the distributor.   The layers of wire mesh with pore sizes of 40 microns were used to reduce the pressure drop across the distributor relative to the bed and to promote any channeling, spouting, and plugging that might occur.   In this way, the effect of vibration was much clearer and the measurement of pressure drop across the bed was more accurate.   Equipped along the length of the chamber was a series of ports for sampling and pressure measurements.   Pressure measurements were made with a pressure transducer (Omega), as depicted in Figure 3.1. Water manometers (Dwyer Mark II) were also used for verifying pressure drop measurements.

The powder bed was placed above the wire mesh distributor, through which the compressed, bone-dry air flowed.   Bone-dry air was used to minimize any humidity effects since liquid bridges between agglomerates can significantly alter the behavior of fluidization.   The amount of each powder used for the following results are as follows: 10.0 grams of Silica R974, 10.0 grams of Silica R972, 11.0 grams of Silica A300, 15.0 grams of Silica A90, 14.0 grams of Alumina C, and 40.0 grams of Titania P25.   The
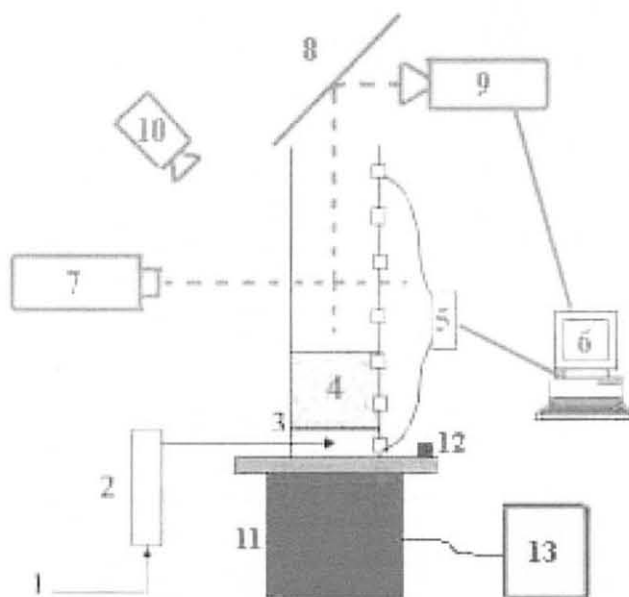
Figure 3.1 Schematic of the vibrofluidized bed. 1: Compressed air; 2: rotameter; 3: distributor; 4: fluidized bed; 5: pressure transducer; 6: computer; 7: laser generator; 8: mirror; 9: CCD camera; 10: digital camera; 11: vibrator; 12: accelerometer; 13: inverter.

column used was the lexan tube with a diameter of 6.25 cm. Electrostatic effects from using dry air can be decreased with static-eliminator aids such as the DC-nozzle provided by Tantec, Inc. A DC-nozzle ionizes the flowing air and achieves static-neutralization. Large agglomerates that may have formed from packaging, storage, and transportation were removed by sieving the as-received powders before each experiment through a 500 micron sieve. Flow rate was measured by rotameters (Gilmont). Visualization apparatus is the same as described in Section 2.2. Properties of the powders used for the vibrofluidization experiments were the same as those used for the conventional fluidization experiments, listed in Table 2.2. All powders are hydrophilic except for R974 and R972, which were surface treated with dimethyldichlorosilane (DDS) to induce hydrophobicity.

To start a typical vibrofluidization experiment, an amount (10.0 grams of Silica R974, 10.0 grams of Silica R972, 11.0 grams of Silica A300, 15.0 grams of Silica A90, 14.0 grams of Alumina C, or 40.0 grams of Titania P25) of powder from a sieved batch was carefully measured and placed inside the chamber. The initial height was recorded after waiting approximately 15 minutes for the bed to settle completely. The desired vibration parameters were set and turned on. The flow rate was increased incrementally and the corresponding pressure drop was recorded along with observations of fluidization behavior and expanded height. Once a definite plateau was reached, the flow rate was decreased incrementally and the corresponding pressure drop, expanded height, and behavior were recorded. At each incremental superficial velocity, sufficient time was given for the bed to reach its true state since it would take a certain amount of time for the bed to stop expanding from an increase in flow rate. Flow rate, pressure drop, vibrational acceleration, frequency and bed height measurements, as well as visual observation of the fluidization behavior for each experiment were all recorded. For each experiment, the vibrational intensity, which, as seen in Equation 3.1, is a function of frequency and amplitude, were varied. Similarly to the conventional fluidization experiments, at each velocity, the macroscopic and microscopic properties were recorded with a digital camera and CCD camera, respectively. Sampling methods from conventional fluidization experiments remained the same.

3.3 Results and Discussion

3.3.1 Fluidization Behavior

It was observed experimentally that mechanical vibration helped break up the channeling and spouting in a bed of nano-sized powders. Figure 3.2 illustrates typical experiments for each powder. Based on empirical observations, Geldart et al. (1973) determined that particles whose diameter is smaller than 30 μm and density difference is smaller than 1000 kg/m^3, classified as group C powders, are difficult to fluidize in a conventional gravity-driven fluidized bed. Generally, these powders would form cracks, channels, or lift as a solid plug when exposed to a fluidizing gas at low superficial gas velocity. This behavior is mainly caused by the strong interparticle (van der Waals) forces. The importance of these interparticle forces relative to the weight of the particle increases as the surface to volume ratio increases and may significantly exceed the external mechanical forces (such as that due to gravity) to which the particles are subjected. The mechanical agitation of vibration is able to provide enough energy to disrupt these interparticle forces that commonly give rise to the characteristic group C behavior, as illustrated in Figure 3.2. However, Figure. 3.2 is only typical of Silica R974. The behavioral results of all powders for 3 "g" are summarized in Table 3.1, where C = channeling, P = plugging, J = jetting/spouting, B = bubbling fluidization, and S = smooth fluidization, L = low velocity, ~ 0.15 cm/s, M = medium velocity, ~ 0.71 cm/s, and H = high velocity, ~ 1.38 cm/s. Beds of Silica R972, Silica A90, and Alumina C were more prone to the formation of bubbles around 75 and 100 Hz. The photographic results for 1.5 and 4.5 "g" and other powders are in Appendix A.

Silica R974

Silica R972

Silica A300

Silica A90

Alumina C

Titania P25

     (a)   (b)   (c)   (d)   (e)   (f)
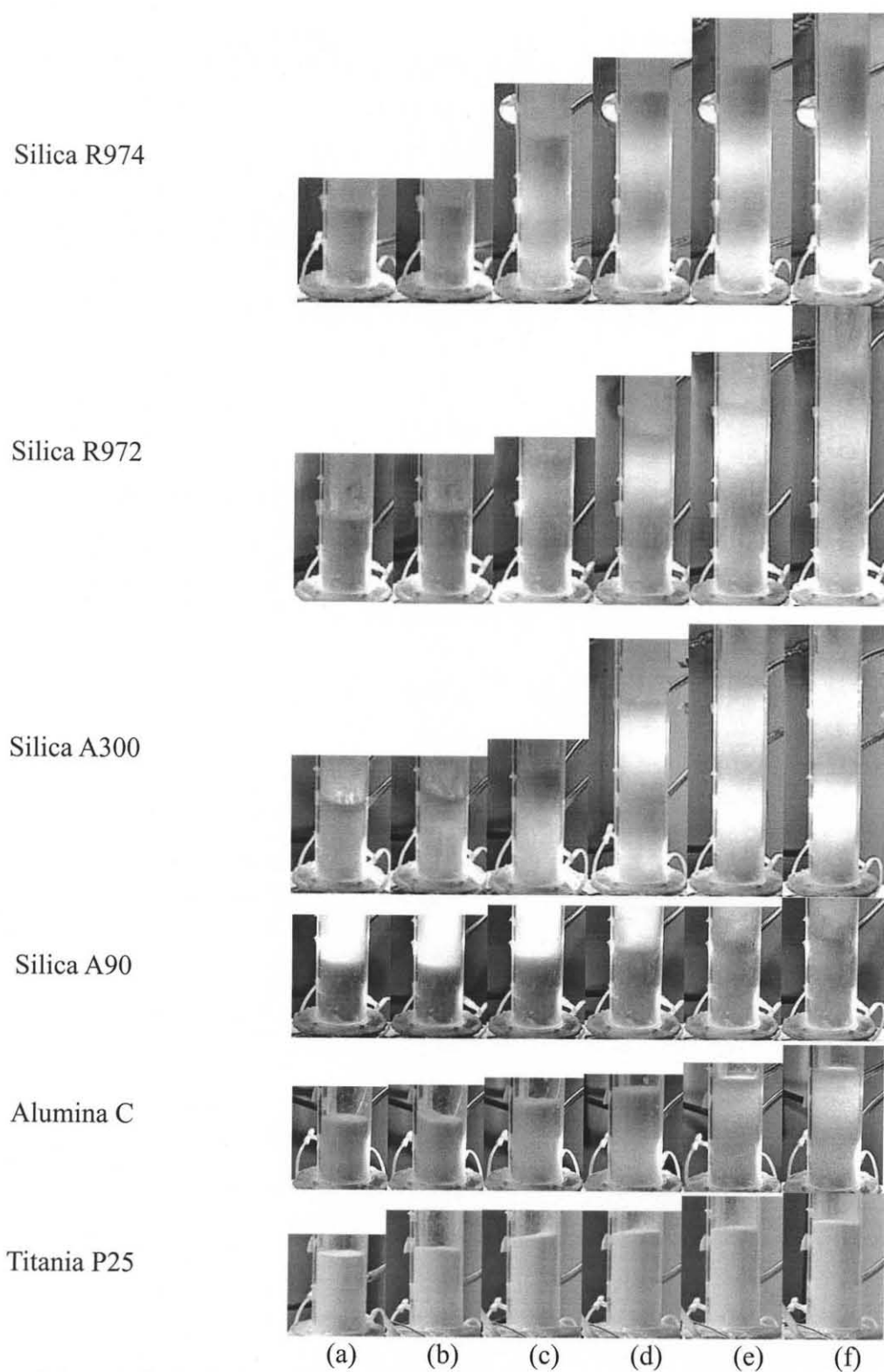
Figure 3.2 Typical photographs of vibrated experiments in a lexan tube of 6.25 cm with a wire mesh distributor at $\Gamma=3$, f=50 Hz with flow rates of (a) 0 cm/s, (b) 0.15 cm/s, (c) 0.41 cm/s, (d) 0.71 cm/s, (e) 1.06 cm/s, (f) 1.38 cm/s.

Table 3.1 Summary of Behavioral Results for All Powders at $\Gamma = 3$

Powder	R974			R972			A300			A90			AluC			P25		
Velocity	L	M	H	L	M	H	L	M	H	L	M	H	L	M	H	L	M	H
30 Hz	S	S	S	S	S	S	S	S	S	S	S	S	S	S	B	S	S	B
50 Hz	S	S	S	S	S	S	C	S	S	S	S	S	J	S	S	S	S	S
75 Hz	S	S	S	S	B	B	S	S	S	S	S	B	J	S	S	S	S	S
100 Hz	S	S	S	S	S	B	J	S	S	S	S	B	S	B	B	S	S	S
150 Hz	S	S	S	S	S	S	J	S	S	J	S	S	J	S	S	S	B	S
200 Hz	S	S	S	J	S	S	P	B	S	S	S	S	S	S	S	S	B	S

Another interesting result in terms of fluidization behavior was that, although beds were not initially (before application of vibration) fluidizable with low-flow-rate aeration alone, the bed of the hydrophobic powders (Silica R974 and Silica R972) appeared to have a short-term memory after vibration was applied. This memory effect was apparent in an experiment where the bed was first fully fluidized with vibration and aeration, and then was allowed to settle down by turning off the vibration and aeration. This settled bed of these hydrophobic powders could then be fluidized by aeration alone as long as it was done within a few minutes, which is not what one would expect given the Geldart group C character of the primary particles. Thus, once the bed was fluidized, the interparticle networks in the original sample were disrupted and the resulting agglomerates did not form strong cohesive networks for several minutes, even after the bed was allowed to settle. However, if the bed was left longer than a few minutes in its rest state, it became difficult to fluidize the bed at the same low flow rates.

Additionally, once the bed was fluidized with the aid of vibration and aeration, the vibration could be turned off and the bed would remain expanded and fluidized for a considerable amount of time (~30 h). Figure 3.3 shows a comparison between the settling of a fully expanded bed of Silica R974 after (1) aeration was left on and vibration was turned off and (2) both aeration and vibration were turned off. Without both vibration and aeration, the bed collapsed to its initial height within 2 min. Based on the above experimental observations, it is conjectured that once the interparticle forces are disrupted for hydrophobic powders, it takes a finite time to approach the original undisturbed conditions. Although identical experiments were conducted, the hydrophilic powders (Silica A90, Silica A300, Alumina C, and Titania P25) did not exhibit the same memory effects. This is possibly due to the fact that the hydrophilic powders are more sensitive to any moisture in the air and lab. Without the vibrational agitation, the beds of the hydrophilic powders become unstable due to the higher sensitivity of moisture. The mechanical agitation is needed to skirmish the factors that make the bed instable.

Generally, when airflow was coupled with sufficient vibration ($\Gamma = (A\omega^2)/g > 1$), the channels would close, the spouting would stop, and/or the solid plug would break up. Increasing vibrational intensity, Γ, weakly affected bed height. At high vibration frequencies (f >100 Hz) and airflow rate, relatively large bubbles could be seen (Figure 3.4) especially in beds of Silica R972, Silica A90, and Alumina C. At low frequencies (< 50 Hz), many of the bubbles appeared to break and dissipate throughout the bed forming microbubbles (estimated to be on the order of about 200μm). Bubbles were not seen to coalesce, grow or break the upper surface of the bed.
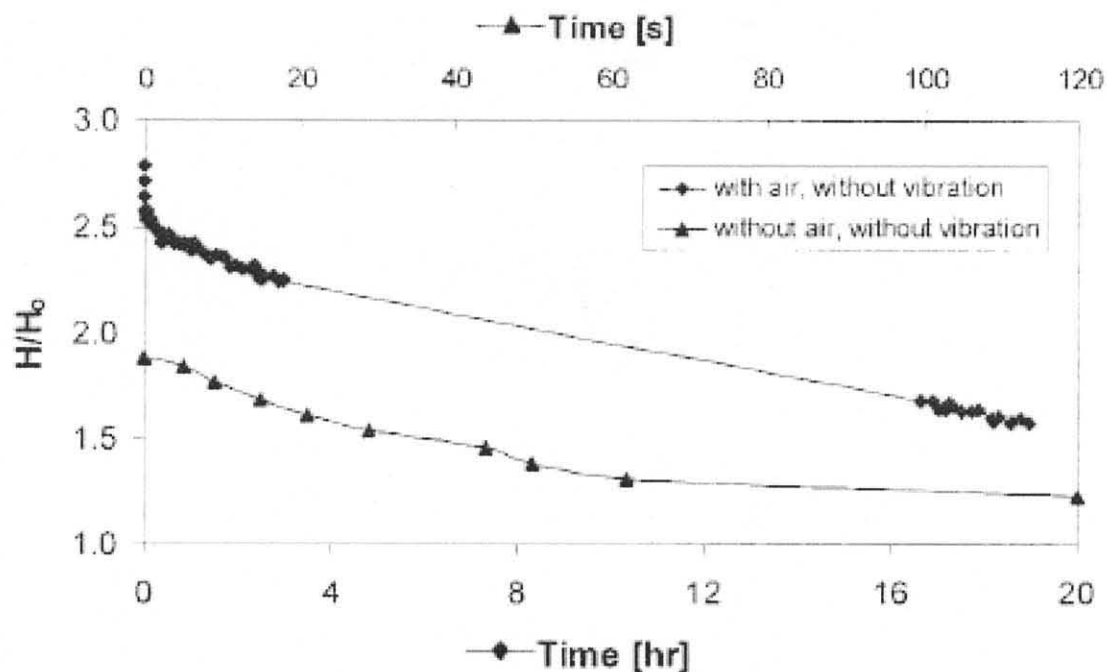
Figure 3.3 (♦) The bed was initially subjected to vibration (Γ=2, f = 50 Hz) and aeration at an air superficial velocity of 0.91 cm/s in the glass tube with a diameter of 6 cm and with a wire mesh distributor; at t = 0, the vibration was discontinued. (▲) The bed was initially subjected to vibration (Γ=2, f = 50 Hz) and aeration at an air velocity of 0.45 cm/s; at t = 0, both vibration and aeration were stopped.
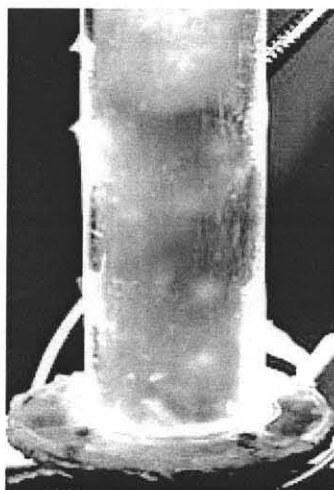
Figure 3.4 Bubbling fluidization of Silica A90 with vibration (Γ = 3, f = 75 Hz) in a 6.25 cm lexan tube with a wire mesh distributor.

At modest fluidization gas velocities, the surface of the bed was very smooth, there was no apparent disturbance from bubbles and practically no elutriation of particles was observed. At higher gas velocities, which depend on the different powders, the surface became unstable and elutriation of particles out of the tube could be observed. Appendix A shows photos of each of the powders at the different vibrational conditions at different velocities.

Figure 3.5 shows bed expansion rate at different Γ at a constant frequency of 50 Hz and constant superficial air velocity of 0.28 cm/s for Silica R974. In each of these experiments, the vibrational parameters were first set at the desired conditions, and then the aeration was turned on (at time $t = 0$) at the desired superficial velocity. The steady state bed expansion increased with increasing Γ, but appeared to become independent of Γ at sufficiently large values of Γ. In this series of experiments, the vibrational intensity was varied by changing the amplitude (A), while holding the frequency of vibration constant. This bed expansion behavior may be rationalized as follows: as the vibrational intensity was increased, the size of the agglomerate decreased at first and then became roughly independent of Γ. The scaled acceleration Γ was not the only vibrational parameter affecting steady state bed expansion. Figure 3.5 illustrates that the steady state bed expansion, at a constant superficial air velocity of 0.28 cm/s, depended on the frequency of vibration, even when Γ was maintained constant; however, no systematic trend was manifest. It was found that at higher values of Γ, the effect of vibration frequency on the steady state bed expansion decreased.

It is clear from Figure 3.5 that the rate at which the bed expanded depended on the vibrational parameters. Generally, for all the powders, the higher the frequency or the

lower the Γ, the slower the bed expanded. The rate of bed expansion was roughly the same for $\Gamma = 4 - 6$, but appreciably smaller at $\Gamma = 3$ (see Figure 3.5). As seen in Figure 3.5, the rates of bed expansion at frequencies of 50, 70 and 100 Hz were comparable, while those at 30 and 150 Hz suggest an inverse dependence on the frequency.
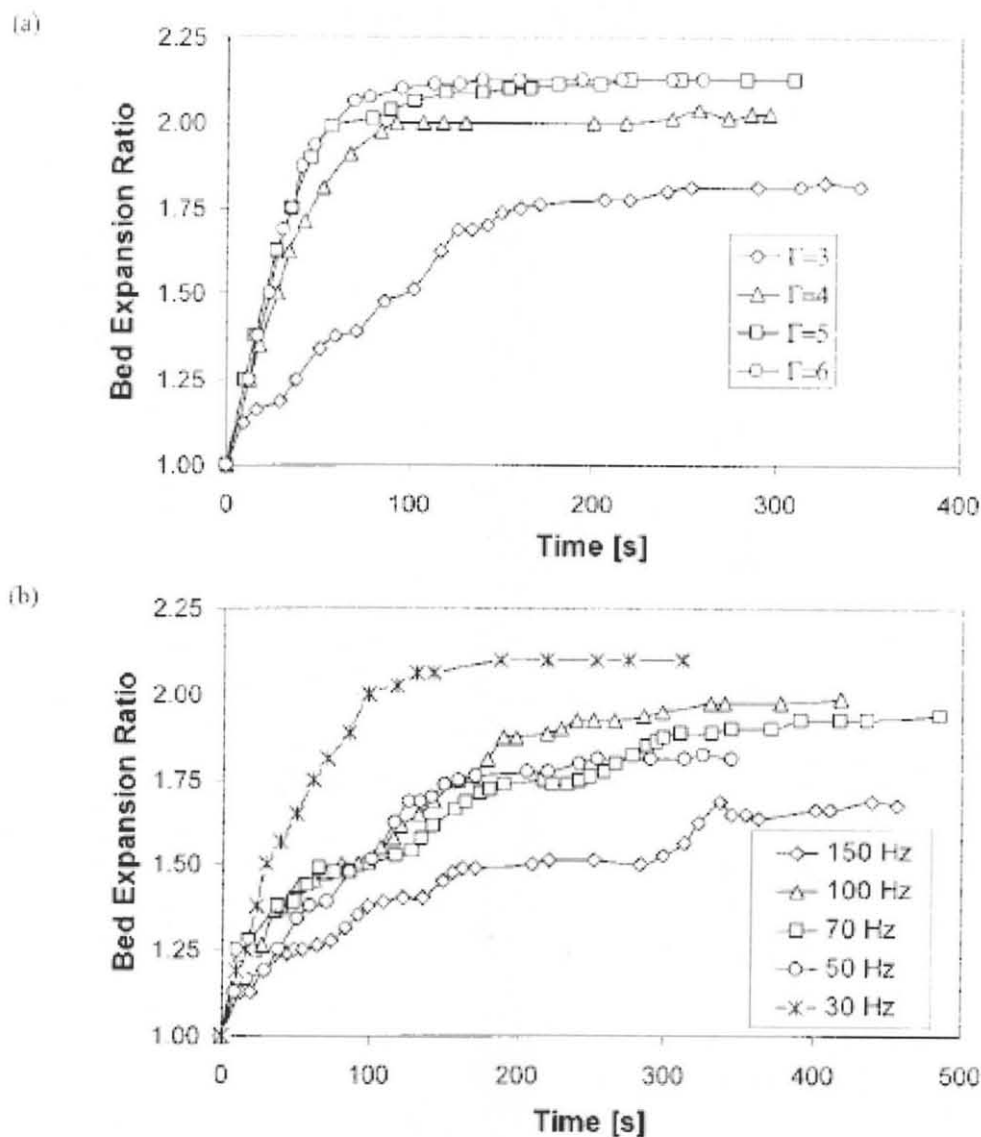
Figure 3.5 Plots of bed expansion ratio vs. time (a) for different Γ values at fixed frequency, f=50 Hz; (b) for different frequencies with $\Gamma = 3$.

3.3.2 Pressure Drop

In all of the experiments performed for all powders, the measured pressure drop across

the bed at high gas velocities approximately equaled the weight of the bed per unit cross

sectional area.   Figure 3.6 shows a typical set of results obtained in a vibrated fluidized

bed of Silica R974.   The results for the other powders (see Appendix A) are very similar

in that pressure drop approaches the weight of the bed and that there is considerable bed

expansion.   Each of the six nanopowders ((a) Silica R974, (b) Silica R972m (c) Silica

A300, (d) Silica A90, (e) Alumina C, and (f) Titania P25), where both the pressure drop

across the bed and the bed expansion at increasing gas velocities are presented.   The

pressure drop has been scaled with the actual measured weight of the bed per unit cross

sectional area of the bed, while the bed height has been scaled with the height of the

settled bed.   It is clear from Figure 3.6 that the pressure drop increased initially with gas
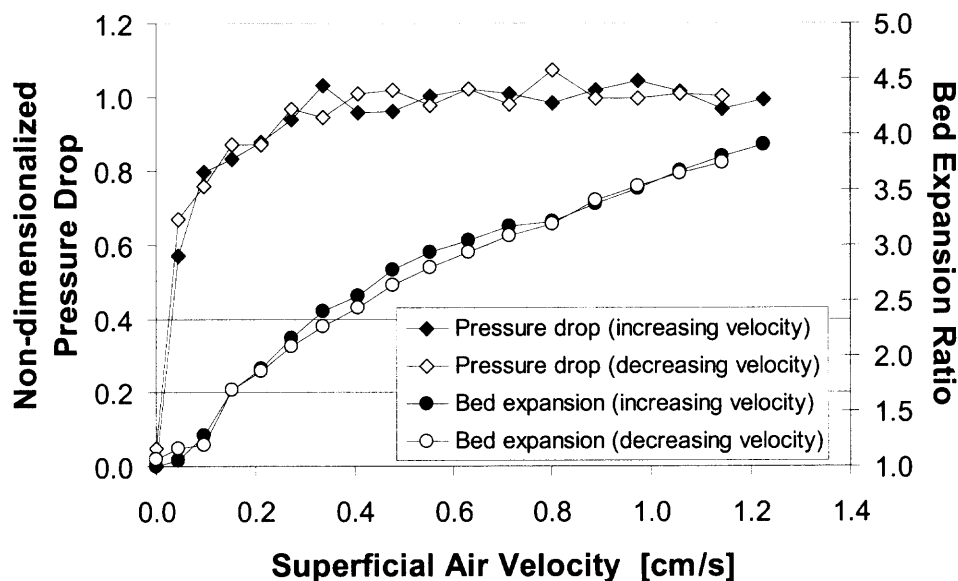
Figure 3.6   Pressure drop and bed expansion ratio as functions of air superficial velocity at $\Gamma = 3$, $f = 50$ Hz for Silica R974.

velocity and then leveled off at high gas velocities. In the plateau region, the scaled pressure drop is very close to the expected value of unity, as given by the familiar force balance (Wilhelm et al., 1948) equation

$$\frac{\Delta P}{H_{mf}} = \left(1 - \varepsilon_{mf}\right)\left(\rho_a - \rho_g\right)g \tag{3.2}$$

As stated in Chapter 2, a lower measured pressure drop than the weight of the bed given by Equation 3.2 could be due either to a loss of powder sticking to the wall, powder elutriation, or possibly to some non-uniformities in the gas flow due to the relatively porous distributor that was used in the experiments and a higher measured pressure drop could be due to wall friction and cohesion between the bed of particles with a layer of particles adhering to the distributor. Mutsers et al. (1977) were the first to suggest that additional terms may need to be included on the right hand side of Equation 3.2 to account for the higher pressure drop of cohesive powders. They developed a theory, which includes interparticle forces as well as wall friction. Liss et al. (1984) accounted for their high measured pressure drop in a fluidized bed, where the particles were cohesive due to liquid bridge formation, through a term $\dfrac{6S}{d_p}\left(1 - \varepsilon_{mf}\right)$, which was added to

Equation 1 on the right hand side. Here S is the cohesive stress, which is a function of temperature, composition, and particle size distribution.

Tasirin et al. (2001) found in their study of vibrofluidization of 15 to 34 μm particles that the pressure drop increased as the vibration intensity, Γ, increased. This is rather remarkable, as it implies that the consequence of vibration was a net force pointing downwards, which is not what one would expect intuitively. Erdesz et al. (1986), on the other hand, reported that the pressure drop decreased with increasing Γ. Mawatari et al.

(2002) found no appreciable change in pressure drop as a function of vibration intensity, Γ. While not shown, our study revealed only a weak effect of vibrational parameters on the constant (plateau) pressure drop obtained at high gas velocities. Thus, there is no clear consensus on the effect of vibration on pressure drop across the bed.

Wank et al. (2001) studied vibrofluidization of cohesive micron sized particles and proposed the following expression, which accounted for both interparticle forces and the effect of vibration:

$$\frac{\Delta P}{H_{mf}} = \left(1 - \varepsilon_{mf}\right)\left(\rho_a - \rho_g\right)g + \frac{6F_{CO}}{H_{mf}} - \left(1 - \varepsilon_{mf}\right)\left(Af^2\right)\rho_a \tag{3.3}$$

where F_{CO} represents the interparticle forces between particles. However, in our opinion, it is hardly realistic to hope to capture the effect of cohesion and vibration through such simple models. Cohesion between particles themselves cannot increase the required pressure drop, unless the particles adhere to boundaries and a resistance to bed expansion results through this adhesion. Consequently, justification for the cohesive force term must be made through an analysis of the interaction at the boundaries. The same is true for vibration.

Figure 3.6 also shows that the bed expansion behavior in some of these nanoparticle systems was different than that observed with Geldart group A particles where bed expansion begins only after the minimum fluidization velocity is exceeded. As soon as a vibrofluidized bed (with $\Gamma > 1$) was aerated, it began to expand even though the actual gas phase pressure drop was only a fraction of the bed weight per unit cross sectional area. As gas flow rate was increased, the bed continued to expand and this was accompanied by a systematic increase in the gas phase pressure drop. The bed expansion continued into the constant pressure drop regime. The overall bed expansion

could be in excess of five times the original height, and even at such dramatic bed expansion levels the quality of fluidization appeared to be smooth.

3.3.3 Minimum Fluidization Velocity

Based on an agglomerate size of about 50 microns, the Reynolds number is less than 1. The traditional expression for calculating the minimum fluidization velocity based on the Ergun equation for Re < 20 (Kunii et al., 1969) is

$$u_{mf} = \frac{(\phi_s d_p)^2}{150} \frac{\rho_p - \rho_g}{\mu} \left(\frac{\varepsilon_{mf}^3}{1 - \varepsilon_{mf}} \right) g \qquad (3.4)$$

where ϕ_s is the particle sphericity and ε_{mf} is the inter-particle voidage at minimum fluidization.   A number of studies (Mawatari et al., 2002; Noda et al., 1998; Tasirin et al., 2001; Erdesz et al., 1986) found that as the vibration intensity, Γ, increased, the minimum fluidization velocity decreased.   Here, minimum fluidization velocity refers to the lowest gas velocity for which the pressure drop across the bed becomes constant. However, in our experiments (with $\Gamma > 1$), frequency and other vibrational parameters had only a small effect on the minimum fluidization velocity, and this effect became unobservable as Γ was increased.

The minimum fluidization velocity in this study (based on the definition above) was determined to be around 0.3-0.4 cm/s for Silica R974, 0.3-0.4 cm/s for Silica R972, 0.3-0.4 cm/s for Silica A90, 0.3-0.4 cm/s for Silica A300, 0.3-0.5 cm/s for Alumina C, and 0.15-0.3 cm/s for Titania P25.   In comparison to the minimum fluidization velocities obtained from the conventional fluidized bed experiments, these velocities are much lower.   However, it is noted that the bed exhibited fluid-like properties as soon as

it started to expand at velocities that are not necessarily the minimum fluidization velocity. It is believed that one of the major differences between fluidization of nanoparticles in the form of nanoagglomerates and the fluidization of other group A or
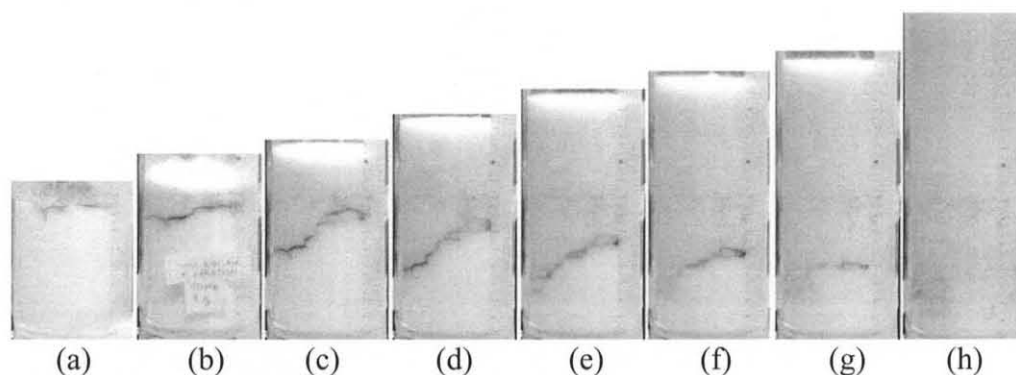
Figure 3.7 Progression of mixing of Silica R974 particles dyed with methylene blue during aerated vibrofluidization ($\Gamma=4$, f = 50 Hz) of 12 grams of Silica R974 in a glass tube of 6 cm in diameter with time (s): (a) 0, (b) 10, (c) 15, (d) 22, (e) 28, (f) 35, (g) 60, (h) 120. Aeration of a vibrated fluidized bed was started at t=0, and the figure panels show simultaneous bed expansion and mixing.

group B particles is that a fluid-like behavior occurs when the bed of nanoparticles begins to expand. This is evidenced by the mixing study, as shown in Figure 3.7, which consisted of a small layer of Silica R974 dyed with methylene blue atop a bed of Silica R974. The bed at a velocity lower than the velocity at which the pressure drop is entirely a plateau is completely mixed within 2 minutes. This suggests that when the bed expands, there is good circulation in the bed. The minimum expansion velocities, the minimum fluidization velocities obtained from conventional fluidized beds and from vibrofluidized beds are summarized in Table 3.2. For example, the bed of Silica R974 started to expand at a velocity as low as 0.1 cm/s. Such a minimum fluidization velocity cannot be obtained from Equation 3.4 if we use the primary particle size, demonstrating unequivocally that agglomerates were being fluidized and that agglomerate properties must be used in Equation 3.4 to obtain meaningful results.

Table 3.2 Summary of Minimum Fluidization Velocity and Minimum Expansion Velocity for Each Powder from Vibrofluidization Experiments

Powder	Minimum Fluidization Velocity [cm/s]	Minimum Expansion Velocity [cm/s]
Silica R974	0.3-0.4	0.05-0.1
Silica R972	0.3-0.4	0.05-0.1
Silica A300	0.3-0.4	0.05-0.1
Silica A90	0.3-0.4	0.05-0.1
Alumina C	0.3-0.5	0.05-0.1
Titania P25	0.15-0.3	0.05-0.1

3.3.4 Agglomerate Size

Since the behavior of nanoagglomerate fluidization was so liquid-like with practically no bubbling, the Richardson-Zaki (R-Z) approach, usually valid for homogeneous liquid-solid sedimentation and fluidization is employed in the analysis already detailed and described in Section 2.3.4. From this section, it was described that for each value of velocity, ϕ could be determined from the measured heights of the expanded bed. From the analysis, a plot of $(u/v_o)^{1/n}$ vs. ϕ for n = 5 (the Richardson-Zaki exponent is a function of Reynolds number, but is about 4.8 in the viscous flow regime) based on the experimental data given in Figure 3.6 is shown in Figure 3.8. The plot appears to be reasonably linear, lending support to the analysis described in Section 2.3.4.

Surprisingly, the fractal dimension, number of primary particles, and diameter of the agglomerates were found to be insensitive to the value of the Richardson – Zaki exponent in the range of n = 4 to 6 (see Table 3.3). The estimated values of the fractal dimensions and agglomerate size of each powder are summarized in Table 3.4. It appeared that powders with the higher bulk and / or particle densities had a slightly higher fractal dimension.

n=5.0
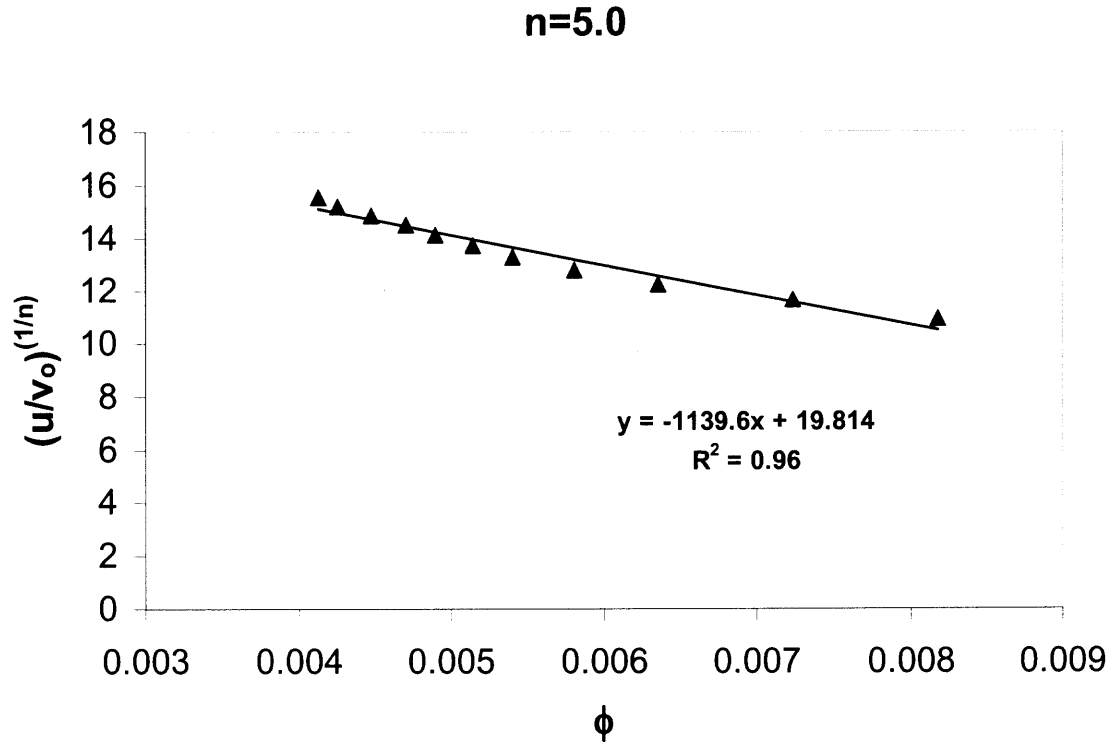
Figure 3.8   Plot of Equation 2.14 for n = 5.0 to obtain agglomerate size, density, and interparticle voidage for Silica R974 during vibrofluidization. R^2 is the square of the correlation from a simple linear regression model that measures the amount of variability in the observed data.

Table 3.3   Fractal Dimension (D_f), Number of Particles in an Agglomerate (N), and Agglomerate Diameter for Various Values of the Richardson – Zaki Exponent for Silica R974

n	D_f	N	Calculated Diameter (microns)
4.0	2.56	3.84E10	164
4.5	2.57	3.96E10	161
5.0	2.57	4.05E10	160
5.5	2.58	4.12E10	157
6.0	2.59	4.17E10	154

Table 3.4 D$_f$ and Agglomerate Size Values Evaluated at n=5 for Each Powder

Powder	D$_f$ value at n=5	d$_a$ [microns]
Silica R974	2.57	160
Silica R972	2.57	206
Silica A300	2.57	261
Silica A90	2.65	187
Alumina C	2.60	144
Titania P25	2.69	243

Table 3.5 Summary of Size Analysis of In-Situ Agglomerate Images from Vibrofluidization Experiments

Powder	Mean diameter [microns]
Silica R974	177.0
Silica R972	234.4
Silica A300	178.8
Silica A90	222.4
Alumina C	166.4
Titania P25	216.1

The estimated value of 2.57 for the fractal dimension of the Silica R974 agglomerates, for example, is close to that for diffusion-limited aggregation (namely, 2.5) (Friedlander, 2000). As such an aggregation mechanism is reasonable for the extremely fine primary particles used in our study, the fractal dimension estimated from the bed height data and the above analysis is very encouraging. However, the estimated agglomerate diameter from this analysis is much larger than the experimentally measured value (see Table 3.5), which SEM photographs, showed to be approximately 30 microns, but in good agreement with the bright agglomerates seen in Figure 3.9 obtained by photographing the surface of the bed using a high-speed digital camera with an extremely
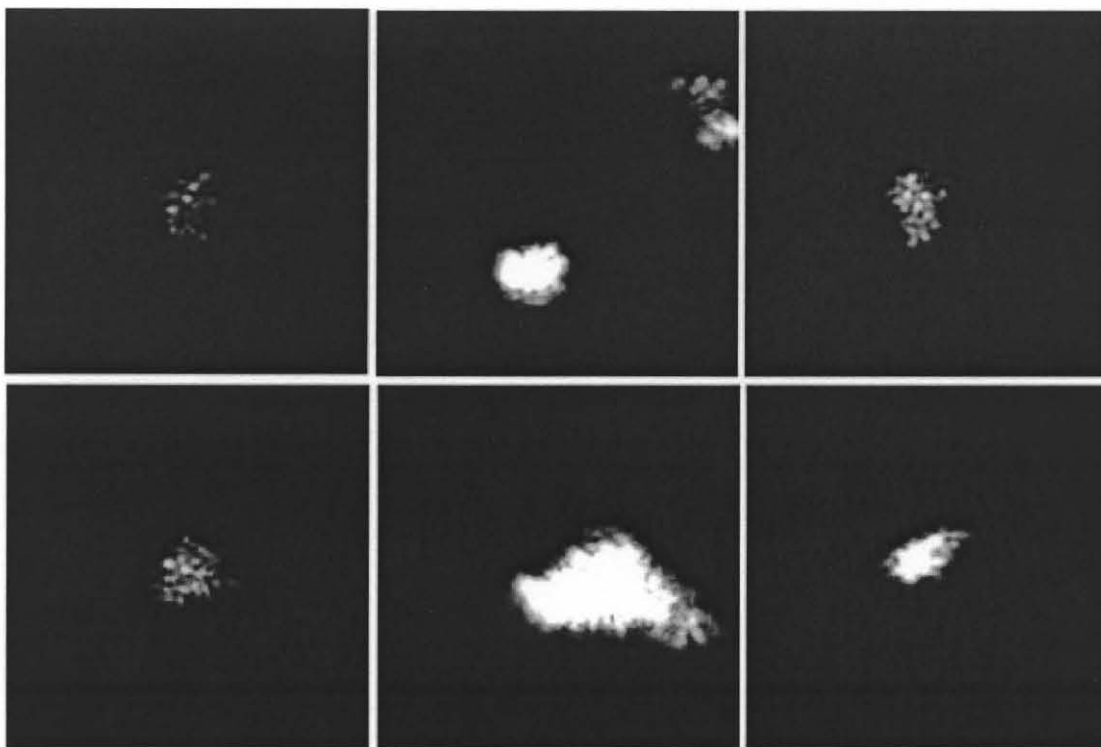
Figure 3.9 Six laser and camera results capturing Silica R974 agglomerates in an aerated vibrofluidized bed. Each shot is 1.1 mm in height and width. Images of other powders are in Appendix B.

short exposure time. We suspect that considerable breakage of the fragile porous agglomerates took place when we aspirated the particles out of the bed and/or prepared the samples for SEM analysis. This might explain why the experimental SEM agglomerate sizes were much smaller than those estimated from the fractal analysis.

3.3.5 Voidage

Since agglomerates were being fluidized, it is important to carefully label the various ways in which one can define voidage. The overall voidage, ε, is defined as the fraction of the total bed volume occupied by the fluid.

$$\varepsilon = 1 - \frac{\rho_b}{\rho_p} \qquad (3.5)$$

Here, ρ_p and ρ_b denote the density of the primary nano-particles and the apparent density of the bed, respectively. The volume fraction of primary particles in the bed, ϕ, is then equal to $1 - \varepsilon$. Using 0.03 g/cm^3 and 2.2 g/cm^3 for the bulk density of a settled bed and primary nanoparticle density, respectively, one finds that $\varepsilon \sim 0.9864$ for Silica R974, Silica R972, and Silica A300. Voidages for Silica A90, Alumina C, and Titania P25 are 0.9823, 0.9881, and 0.9711, respectively. Thus, the bed of nanoparticles was already highly fluffy even before fluidization. As the bed expands, the voidages for Silica R974, Silica R972, and Silica A300, for example, increase to above 0.99.

The agglomerate themselves were very porous (see the high resolution SEM image shown in Figure 2.9). The apparent density of the agglomerates and the fraction of bed volume occupied by the agglomerates are denoted by ρ_a and ϕ_e, respectively. It then follows that $\phi \, \rho_p = \phi_e \, \rho_a$. The void space between the agglomerates, represented as a fraction of the bed volume, $\varepsilon_e = 1 - \phi_e$. The porosity inside the agglomerates, ε_{agg}, is simply equal to $1 - \rho_a/\rho_p$.

The challenge is to estimate ρ_a and ε_e from the experimental data. As stated in the previous chapter, Chaouki et al. (1985) and Wang et al. (2002) assumed that

$$\varepsilon_e = 1 - \frac{H_o}{H_{exp}} \qquad (3.6)$$

Equation 3.6 is problematic as it assigns a value of zero to ε_e for a settled bed (i.e., when $H_0 = H_{exp}$). However, for expanded bed values higher than twice the initial height, Equation 3.6 is a sufficient approximation.

Using the agglomerate diameters obtained from the modified Richardson-Zaki analysis (on the order of 100 microns) and the experimental pressure drop data, ε_e was estimated at various gas velocities through the Blake-Kozeny equation (Ergun equation at low Reynolds numbers)

$$\frac{\Delta P}{H}g_c = 150\frac{(1-\varepsilon_e)^2}{\varepsilon_e^3}\frac{\mu u_o}{(\phi_s d)^2} \tag{3.7}$$

Table 3.6 compares the values of ε_e determined through the three methods mentioned above, namely (a) the modified Richardson – Zaki analysis which only used the bed expansion data, (b) the pressure drop data which assumed an agglomerate size estimated from the Richardson – Zaki analysis and (c) the simple approach employed by Chaouki et al. (1985) and Wang et al. (2002) (i.e., Equation 3.6). Table 3.6 corresponds to the data presented earlier in Figure 3.6 for Silica R974. Results from other powders are listed in Appendix C. It is clear from Table 3.6 that the values of ε_e determined by the first two methods are close to each other (except at the lower end of voidage), which lends further support to the fractal approach. It could have been demanded that both the pressure drop and bed expansion data be satisfied accurately by the model and allowed the agglomerate size to vary (slightly) with gas velocity. This revealed that the agglomerate size decreases slightly as the gas velocity is increased, which is physically reasonable.

The third method, using Equation 3.6 gave quite reasonable values of ε_e for values of $H/H_0 > 2$ (Table 3.6), but gave very small (and unphysical) values of ε_e at lower gas velocities.

Table 3.6 Summary of Interagglomerate Voidages Calculated from the Modified Richardson–Zaki Method, Blake–Kozeny Equation, and Equation 2.15 for Silica R974

u (cm/s)	ε_e (Modified Richardson–Zaki)	ε_e (Blake–Kozeny Equation)	$\varepsilon_e = 1 - H_0/H_{exp}$
0.149	0.529	0.526	0.400
0.207	0.584	0.566	0.469
0.268	0.634	0.602	0.534
0.331	0.666	0.632	0.574
0.399	0.689	0.657	0.603
0.469	0.704	0.677	0.623
0.542	0.718	0.700	0.641
0.619	0.729	0.709	0.655
0.700	0.742	0.724	0.671
0.785	0.755	0.738	0.688
0.870	0.763	0.741	0.697

3.4 Conclusions

It was demonstrated that nanosized powders (Silica R974, Silica R972, Silica A300, Silica A90, Alumina C, and Titania P25) could be easily and smoothly fluidized in the form of stable, very porous agglomerates with negligible elutriation with the aid of vibration and aeration. Vibration helped to break up typical group C behavior and allowed the bed to be fluidized at much lower gas velocities and with much improved bed expansion and fluidization quality. Because the bed remained fluidized for a considerable amount of time with only air flow after vibration was turned off for the hydrophobic powders, vibration appeared to be necessary only initially to disrupt interparticle networks, after which aeration was sufficient to sustain the hydrophobic bed in a fluidized and expanded state for an extended period of time at relatively low gas velocities. For hydrophilic powders, vibration was needed to sustain fluidization. Without vibration, the hydrophilic powders appeared to return to typical group C behavior. A modified Richardson–Zaki approach combined with an assumption of

fractal agglomerates was successfully applied to analyze the bed-expansion data reported here, from which the agglomerate size, other agglomerate properties, and the interagglomerate voidage were estimated. The pressure drop data were found to be consistent with agglomerate size determined in this manner.

CHAPTER 4

MAGNETICALLY ASSISTED FLUIDIZED BED

4.1   Introduction and Theory

The fluidization of nanoparticles using magnetic assistance is a novel idea.   As stated in

Chapter 1, some groups, such as Rosensweig et al. (1981), Zhu and Li (1996), and Thivel

et al. (2004), have fluidized magnetic particles themselves in a magnetic field but not

used magnetic particles to help aid the fluidization of other types of particles.   However,

this work has established the concepts that in the presence of magnetic intensity, bubble

size and overall gas bypassing decrease.   Thus, fluidization quality should improve.   It

will be seen that the magnetic particles give a similar type of excitation that vibration

provides to break up interparticle forces for certain nanopowders to allow the bed to

expand and fluidize.   The fluidization theory should remain the same as described in

Chapter 2.

4.2   Experimental Setup, Materials, and Procedure

A schematic of the magnetically assisted fluidized bed is shown in Figure 4.1.   The

magnetically assisted fluidized bed is very similar to the conventional fluidized bed

except for the added electromagnetic coils.   All beds used were simple, vertical

conventional beds with a cylindrical, acrylic, transparent chamber with a distributor

whose purpose is to distribute the fluidizing medium through the chamber.   The

distributor was composed of layers of wire mesh with 40 micron pores.   Equipped along

the length of the chamber was a series of ports for sampling and pressure measurements. As done in the conventional and vibrational fluidization experiments, pressure measurements were made with a pressure transducer (Omega), as depicted in Figure 4.1. Water manometers (Dwyer Mark II) were also used for verifying pressure drop measurements. The powder bed was placed above the distributor, through which the compressed, bone-dry air flowed. Bone-dry air was used to minimize any humidity effects since liquid bridges between agglomerates can significantly alter the behavior of fluidization. As with all previous fluidization experiments, large agglomerates that may have formed from packaging, storage, and transportation were removed by sieving the as-received powders before each experiment through a 500 micron sieve. However, this is the only mode of fluidization assistance that can fluidize nanoparticles smoothly without having to sieve the powders first since the magnetic particles can break large agglomerates that may have formed during handling and storage. This is one of the major advantages of using magnetic assistance. The powders used are the same as those used in Chapter 2 and Chapter 3, summarized in Table 2.2. Flow rate was measured by rotameters (Gilmont). The visualization apparatus was the same as described in Chapter 2 and Chapter 3.

The electromagnetic coils were placed near the bottom of the bed, above the distributor. Magnetic particles, made of barium ferrite and 1.4 mm in average diameter, were placed inside the chamber along with the powder bed. When the magnetic field is turned on, the magnetic particles vigorously move around in the direction of the magnetic field and spin but do not fluidize together with the powder. The magnetic field intensity, measured by a Gaussmeter, was about 100 to 150 Gauss at the center of the chamber.

To start a typical fluidization experiment with magnetic assistance, a similar procedure is followed as the procedure for conventionally fluidized experiments, as detailed in Chapter 2. The few differences are that the magnetic particles, the weight of which is equal to the weight of the powder bed used (but a much smaller volume), are placed inside the chamber with the powder bed and that the field generator coils are turned on when beginning the experiment. The lexan chamber with a diameter of 6.25 cm was used for all experiments. Distributor material was the wire mesh as described in Chapter 2. The amount of powder used for the experiments were as follows: 10.0 grams of Silica R974, 10.0 grams of Silica R972, 11.0 grams of Silica A300, 15.0 grams of Silica A90, 14.0 grams of Alumina C, and 40.0 grams of Titania P25.
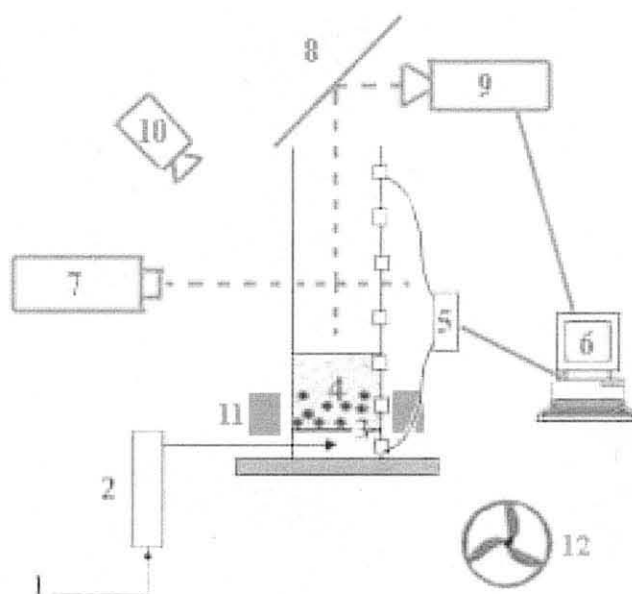
Figure 4.1 Schematic of the magnetically assisted fluidized bed. 1: Compressed air; 2: rotameter; 3: distributor; 4:fluidized bed with magnetic particles; 5: pressure transducer; 6: computer; 7: laser generator; 8: mirror; 9: CCD camera; 10: digital camera; 11: magnetic coils; 12: fan to cool down magnetic coils.

4.3   Results and Discussion

4.3.1   Fluidization Behavior

It was observed experimentally that with the aid of magnetic excitation, a bed of nanoparticles, depending on the powder properties, can be smoothly fluidized without bubbles. Some powders did not successfully fluidize with magnetic assistance and instead clumped into a hard cake, which with time immobilized the movement of the magnetic particles. An example can be seen in Figure 4.2 where Silica A300 was able to fluidize smoothly with high bed expansion and in Figure 4.3 where Titania P25 was not able to fluidize well with magnetic assistance.

Silica R974, Silica R972, and Silica A300 had high bed expansion, at least 3 times the settled bed height. Silica A90, Alumina C, and Titania P25 all had poor bed expansion and eventually solidified into hard agglomerates or into a cake. Silica A90, Alumina C, and Titania P25 all have higher bulk or particle densities than the other three particles used. These particles are not as fluffy or light and as a result, might be more susceptible to being compacted by the collisions of the magnetic particles. In a way, the magnetic particles also serve as another layer of a distributor and since the magnetic particles are so large, they could cause a relatively poor distribution of air; they are also heavy and therefore greatly increase the inertia of the system. This explains why none of these particles, even Silica R974, Silica R972, and Silica A300, could be fluidized without the coils turned on.
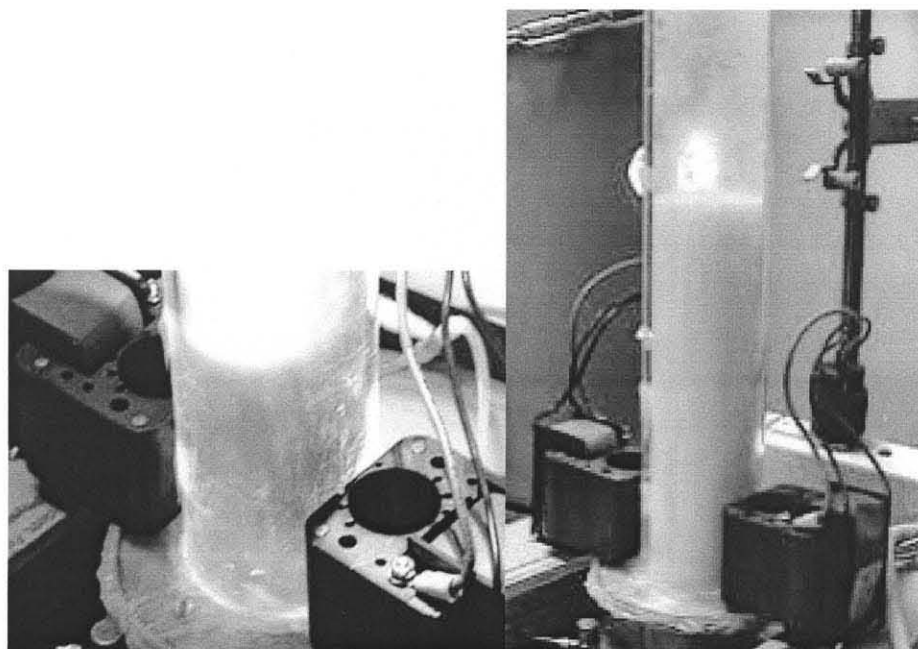
Figure 4.2 Effect of magnetic assistance on an aerated bed of Silica A300. (left): without the coils powered on, (right): with the coils powered on.
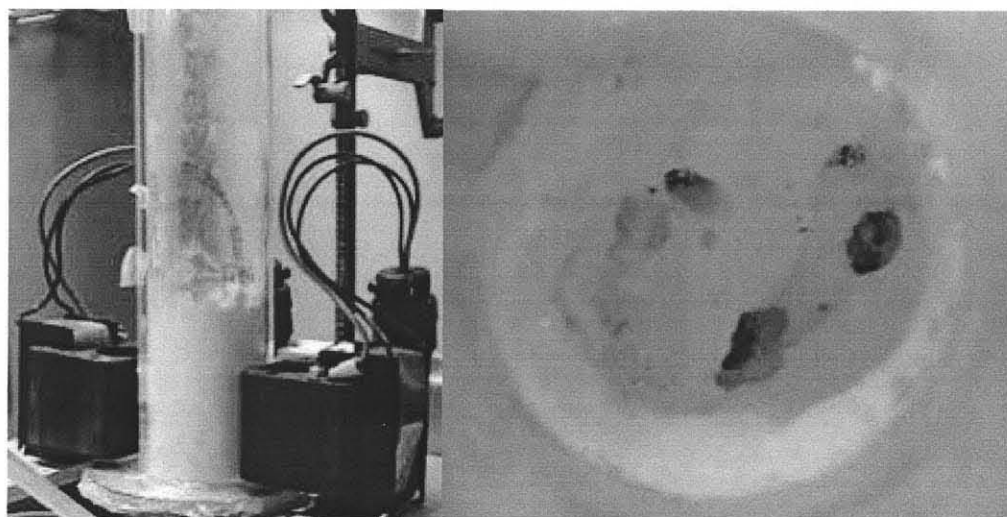
Figure 4.3 Effect of magnetic assistance on an aerated bed of Titania P25. (left): with coils powered on, (right): photo taken from above the bed looking down onto the surface of the bed which has compacted into a hard cake by the magnetic particles.

4.3.2 Pressure Drop

The pressure drop results were interesting in that unity was not always obtained (see Figure 4.4). For Silica R974 and Silica A300, the measured pressure drop was 95% and 85% of the weight of the bed per unit cross sectional area. Also seen from Figure 4.4, the pressure drop results from Silica R972 showed good agreement to unity (Equation 2.1 and Equation 2.2). Silica A90, Alumina C, and Titania P25 did not fluidize due to compaction from the collisions of the magnetic particles and thus, pressure drop results are not applicable. The pressure drop across the magnetic particles was found to be negligible as was the pressure drop through the distributor. Upon closer visual inspection, the bed appeared to have interesting flow characteristics. The bottom of the bed would be very vigorous since it was the location of the movement of the magnetic particles. Above this area, the behavior of the bed was very smooth and less vigorous than at the bottom. In regards to the pressure drop for Silica R974 and Silica A300, a reason that the pressure drop did not equal one could be attributed to the agglomerates near the bottom of the bed not completely participating in the fluidization. Also, the complete collection of powders after a magnetically assisted fluidization experiment was difficult due to some compaction near the distributor and thus, could lead to an inaccuracy in pressure drop measurements. Some might be compacted against the wall, for example. Figure 4.4 shows some typical pressure drop and bed expansion data for Silica R974, Silica R972, and Silica A300. Plots for other powders are shown in Appendix D.
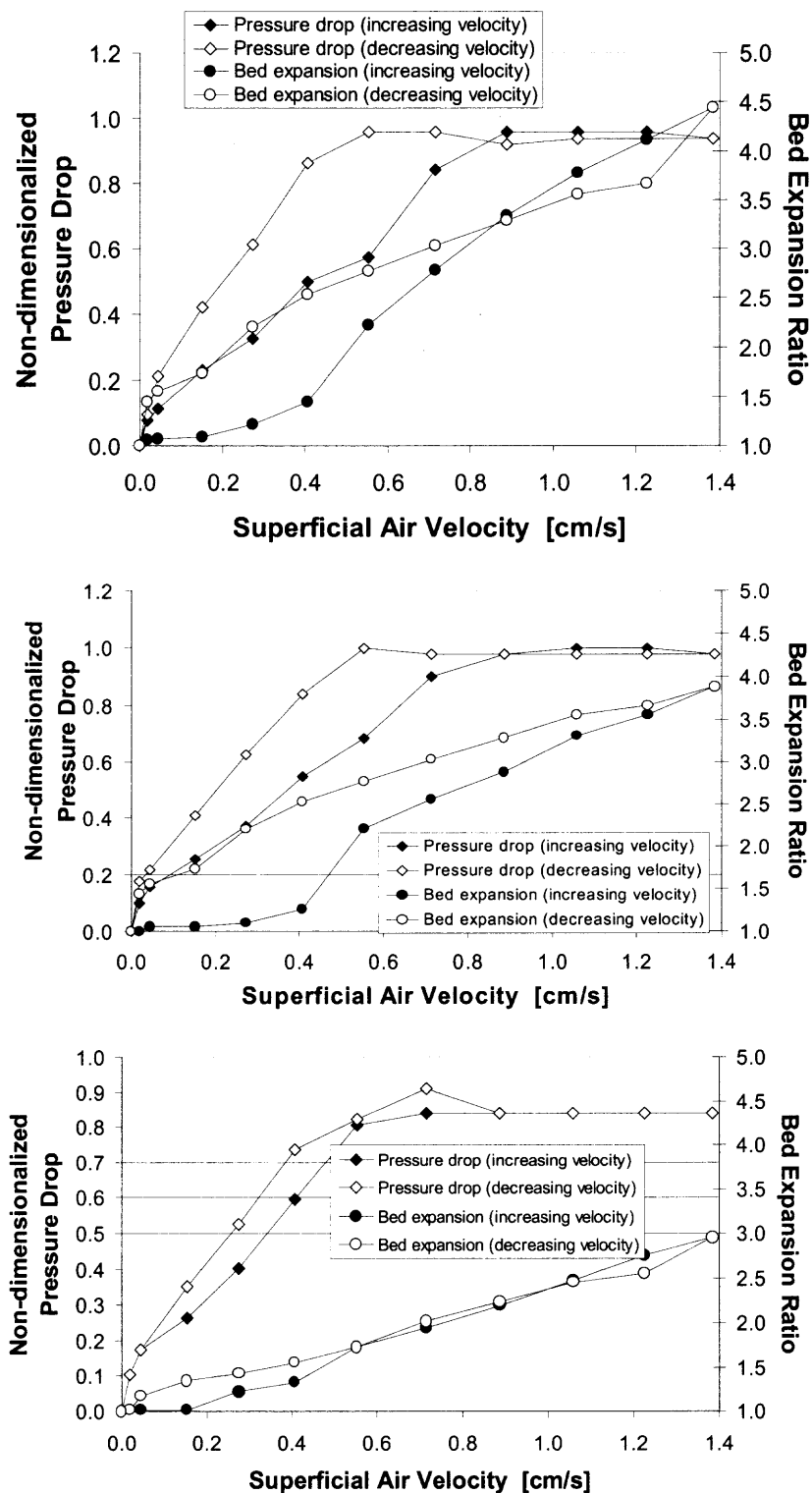
Figure 4.4 Pressure drop and bed expansion ratio as functions of air superficial velocity for a fluidization experiment of Silica R974 (top), Silica R972 (center), Silica A300 (bottom) with magnetic assistance in a lexan tube with a diameter of 6.25 cm and a wire mesh distributor (weight of magnetic particles equaled the weight of the particle bed).

4.3.3 Minimum Fluidization Velocity

As stated previously, the minimum fluidization velocity is defined as the point at which the pressure drop begins to equal the weight of the bed per unit area. For Silica R972, since the pressure drop plateau did equal the weight of the bed, this definition of minimum fluidization can be directly followed. For Silica R974 and Silica A300, a pseudo minimum fluidization velocity was defined at the point where the pressure drop begins to plateau regardless of its relation to the bed weight. These minimum fluidization velocities and the minimum expansion velocities for Silica R974, Silica R972, and Silica A300 are summarized in Table 4.1.

Table 4.1 Summary of Minimum Fluidization Velocities and Minimum Expansion Velocities from Fluidization Experiments with Magnetic Assistance

Powder	Minimum Fluidization Velocity [cm/s]	Minimum Expansion Velocity [cm/s]
Silica R974	~0.5-0.7	~0.2-0.3
Silica R972	~0.5-0.7	~0.2-0.3
Silica A300	~0.5-0.7	~0.2-0.3

4.3.4 Agglomerate Size

The bed expansions for Silica R974, Silica R972, and Silica A300 were high and their fluidization very smooth, which made the data very good for the fractal analysis and modified Richardson-Zaki method employed in previous chapters and detailed in Section 2.3.4. From the analysis, a plot of $(u/v_o)^{1/n}$ vs. ϕ for n = 5 (the Richardson-Zaki exponent is a function of Reynolds number, but is about 4.8 in the viscous flow regime) based on the experimental data given in Figure 4.4 is shown in Figure 4.5. The plot for each powder appears to be reasonably linear, lending further support to the analysis described

n=5.0
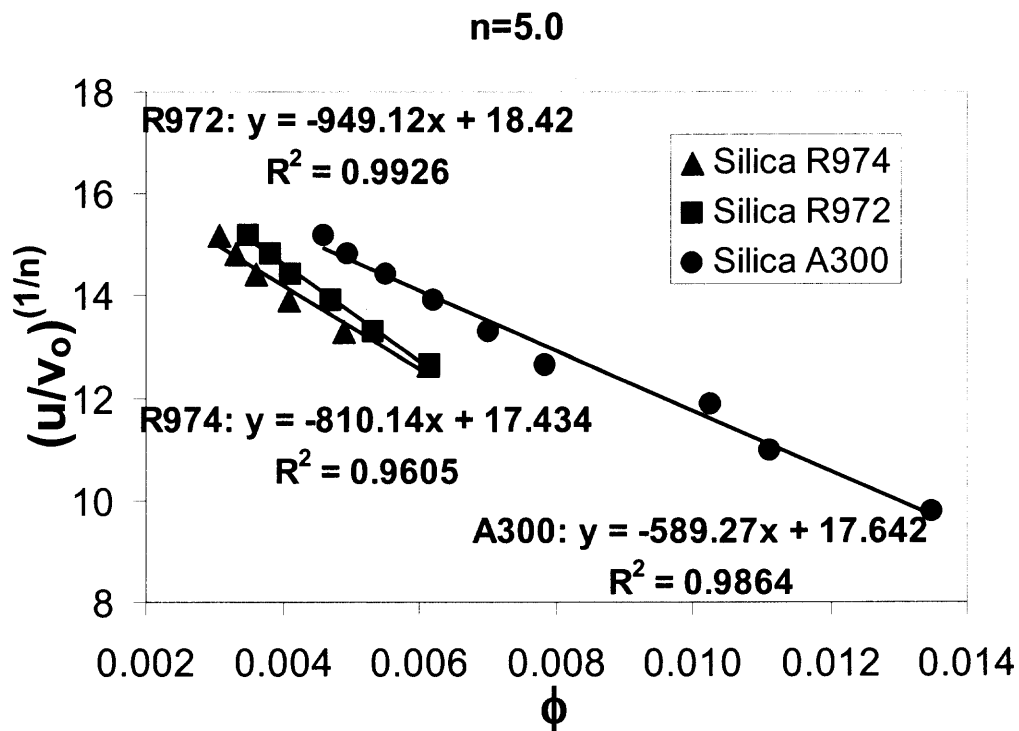
Figure 4.5 Plot of Equation 2.14 for n = 5.0 to obtain agglomerate size, density, and interparticle voidage for Silica R974, Silica R972, and Silica A300 during fluidization with magnetic assistance. R^2 is the square of the correlation from a simple linear regression model that measures the amount of variability in the observed data.

in Section 2.3.4. The estimated values of the fractal dimensions and agglomerate size of Silica R974, Silica R972, and Silica A300 are summarized in Table 4.2. The D_f values of 2.58, 2.57, and 2.61 obtained for the three powders are close to 2.5, which is associated with diffusion-limited aggregation. The results summarized in Table 4.2 are intuitively consistent; since the magnetic particles are breaking up the large agglomerates at the bottom of the bed, it is logical to conclude that the overall agglomerate sizes would be smaller than without external forces as aids. For comparison, summarized in Table 4.3 and Table 4.4 are the data from Table 4.2 and the results obtained from Chapter 2 (conventional) and Chapter 3 (vibration). Also of note is that the fractal dimension

remains relatively constant. The agglomerate size results match well with in-situ images taken, which resulted in sizes ranging from 80 to 200 microns. It should be noted that when applying the modified Richardson-Zaki method and fractal analysis, the slope and y-intercept from such plots as Figure 4.5 were very sensitive to the number of points chosen from the raw data. Generally, the points from the onset of bed expansion and thereafter are used for the modified Richardson-Zaki method and fractal analysis.

Table 4.2 D_f and Agglomerate Size Values Evaluated at n=5 for Silica R974, Silica R972, and Silica A300 from Fluidization Experiments with Magnetic Assistance

Powder	D_f value at n=5	d_a [microns]
Silica R974	2.58	138
Silica R972	2.57	167
Silica A300	2.61	121

Table 4.3 Summary of D_f (at n=5) for Silica R974, Silica R972, and Silica A300 from Fluidization Experiments with No Assistance (conventional), with Vibration, and with Magnetic Assistance

Powder	Conventional Fluidized Bed	Aerated Vibrofluidized Bed	Magnetically Assisted Fluidized Bed
Silica R974	2.60	2.57	2.58
Silica R972	2.60	2.57	2.57
Silica A300	2.64	2.57	2.61

Table 4.4 Summary of d_a [microns] results for Silica R974, Silica R972, and Silica A300 from Fluidization Experiments with No Assistance (conventional), with Vibration, and with Magnetic Assistance

Powder	Conventional Fluidized Bed	Aerated Vibrofluidized Bed	Magnetically Assisted Fluidized Bed
Silica R974	341	160	138
Silica R972	314	206	167
Silica A300	276	178	121

4.3.5 Voidage

It is clear from the compaction in the beds of Silica A90, Alumina C, and Titania P25, that the characteristic of the bed changes drastically and that as a result, the voidage in the bed is also very different compared to pre-experiment conditions. Table 4.5 compares the values of ε_e determined through the three methods used previously, namely (a) the modified Richardson – Zaki analysis which only used the bed expansion data, (b) the pressure drop data which assumed an agglomerate size estimated from the Richardson – Zaki analysis and (c) the simple approach employed by Chaouki et al. (1985) and Wang et al. (2002) (i.e., Equation 3.8). Table 4.5 corresponds to the data presented earlier in Figure 4.4 for Silica A300. Results from other powders are listed in Appendix E.

Table 4.5 Summary of Interagglomerate Voidages Calculated from the Modified Richardson–Zaki Method, Blake–Kozeny Equation, and Equation 2.15 for Silica R974 during fluidization with magnetic assistance

u (cm/s)	ε_e (Modified Richardson–Zaki)	ε_e (Blake–Kozeny Equation)	$\varepsilon_e = 1 - H_0/H_{exp}$
0.55	0.715	0.766	0.550
0.71	0.772	0.773	0.640
0.89	0.810	0.794	0.700
1.06	0.832	0.816	0.735
1.22	0.846	0.831	0.757
1.38	0.857	0.845	0.775

4.4 Conclusions

This chapter showed that another force (magnetic excitation), other than vibration or mechanical agitation, could help fluidize nanoparticles. This leads to the idea that nanoparticles simply need to have their interparticle forces disrupted whether it be through vibration, acoustics, or magnetic assistance. It was also shown that for the

experimental setup and conditions used in this chapter, the magnetic assistance did not work on every powder. It should be noted that wire meshes were used as the distributor for the experiments described in this chapter and that flow characteristics may play a large role in determining whether magnetic assistance can improve fluidization quality. Using a sintered metal distributor, for example, has shown that the compaction of Silica A90 is significantly lessened (Yu, 2004). In the setup used for this chapter, the magnetic particles appeared to crush some of the heavier particles (Silica A90, Alumina C, Titania P25) into hard agglomerates or a cake. The forces leading to agglomeration were obviously much stronger than those leading to deagglomeration. Thus, one of the goals is to find a balance between agglomeration and deagglomeration rates to smoothly fluidize porous nano-agglomerates and the role of distributor can be one of the factors affecting this balance. In conclusion, the magnetic assistance is a very unique method to improve fluidization. While vibration, acoustics, rotation, and others have been used to improve fluidization quality for micron sized powders, magnetic assistance has never been used in the fashion presented in this chapter. One of the biggest advantages of using magnetic assistance is the elimination of the need to sieve particles. Any large agglomerates can be easily broken by the magnets spinning and colliding around in the magnetic field.

CHAPTER 5

ROTATING FLUIDIZED BED

5.1 Introduction and Theory

A rotating fluidized bed (RFB) is somewhat different than the fluidized beds used in Chapter 2 (conventional fluidization), Chapter 3 (aerated vibrofluidization), and Chapter 4 (magnetically assisted fluidization). For example, the setup of the bed is very different in that the rotating fluidized bed is simply a cylindrical distributor, which rotates about its axis whereas the bed for conventional, vibrational, or magnetic fluidization setups are vertical tubes with a distributor near the bottom. The centrifugal forces can be varied because the bed can be rotated at different speeds. When the rotating fluidized bed is spun, the powders line the wall of the distributor. The fluidizing air then enters the distributor radially to start fluidizing the powders layer by layer. As stated in Chapter 1, several groups (Mutsers and Rietema, 1977; Levy et al., 1978; Takahashi et al., 1984; Chang et al., 1985; Kao et al., 1987; Chen, 1987; Watano et al., 1993; Tardos et al., 1998; Watano et al., 1999; Qian et al., 2001; Qian et al., 2001; Zhu et al., 2003; Matsuda et al., 2001; Ding et al., 2002; Watano et al., 2004; Arastoopour et al., 2004) studied rotating fluidized beds, also known as centrifugal fluidized beds. Each of these studies was about powders whose diameters were no smaller than a few microns. Matsuda et al. (2001, 2002) fluidized micron sized glass beads and nanosized titania in a rotating fluidized bed as described in Chapter 1. Their results will be detailed in the discussion section. The work of Matsuda et al. (2001, 2002) and this chapter are among the first studies to describe the fluidization of nanoparticles in a rotating fluidized bed. However,

the general theory for rotating fluidized beds has been established and will be described below.

For Geldart group A or B powders, Kao et al. (1987) found that the average minimum fluidization velocity can be calculated by equating the pressure drop across the fixed bed to that of the fluidized bed, which is expressed in Equation 5.1.

$$\frac{u_{mf}\rho_f d_p}{\mu} = \left[\left(33.7\frac{c_2}{c_1}\right)^2 + 0.0408\frac{\rho_f\left(\rho_p - \rho_f\right)d_p^3\varpi^2}{\mu^2}\frac{c_3}{c_1}\right]^{\frac{1}{2}} - 33.7\frac{c_2}{c_1} \tag{5.1}$$

$$\text{where}\quad \begin{aligned} c_1 &= r_o^2\left(1/r_i - 1/r_o\right) \\ c_2 &= r_o\ln\left(r_o/r_i\right) \\ c_3 &= \left(r_o^2 - r_i^2\right)/2 \end{aligned}$$

The radii are explained as follows: r_i is the inner surface radius and r_o is the distributor radius. Since the powders experience a centrifugal force, the velocity required to fluidize the powders will be higher than in a conventional gravity-driven bed. This means that the pressure drop equation (Equation 2.1, Equation 2.2) needs to incorporate the centrifugal force. The more rigorous equations from the work of Chen et al. (1986) were simplified by Kao et al. (1987) to produce expressions for the pressure drop. The pressure drop in the fixed bed region can be expressed by

$$\Delta P = \phi_1 u_o r_o \ln\left(r_o/r_i\right) + \phi_2 u_o^2 r_0^2 \ln\left(1/r_i - 1/r_o\right) \tag{5.2}$$

$$\text{where}\quad \begin{aligned} \phi_1 &= \frac{150\left(1-\varepsilon\right)^2\mu}{\varepsilon^3\left(\phi_s d_p\right)^2} \\ \phi_2 &= \frac{1.75\left(1-\varepsilon\right)\rho_f}{\varepsilon^3\phi_s d_p} \end{aligned}$$

And the pressure drop in the fluidized bed region can be expressed by

$$\Delta P = (1 - \varepsilon)(\rho_s - \rho_f)\omega^2 (r_0^2 - r_i^2)/2 \qquad\qquad (5.3)$$

For typical group A and B powders, fluidization often appears to occur layer by layer in rotating fluidized beds (Kao et al., 1999). As the superficial air velocity increases, the inner layer (closest to the center of the rotating, cylindrical chamber) of powder, which feels less centrifugal force than the outer layer (closest to the distributor), is fluidized first. A particle closer to the axial center of the chamber will have a velocity higher than a particle near the distributor. Also associated with proximity to the center is higher drag forces and less centrifugal forces. Figure 5.1 shows an example of a plot of pressure drop and velocity that evidences such layer by layer fluidization. The curve in between the linear packed bed region and the fluidized region where the pressure drop is plateau represents the partial fluidization that occurs in the bed of glass particles. Layer by layer, starting from the top layer of the powder down to the layer near the distributor, becomes fluidized with increasing superficial velocity. When the bed is fully fluidized, the differential pressure plateaus.
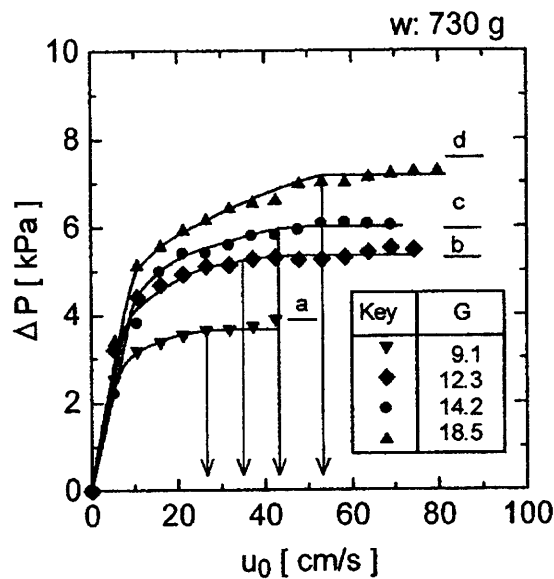

Figure 5.1 Pressure drop of 200 micron glass beads with various rotational speed. (Matsuda et al., 2001)

5.2 Experimental Setup, Materials, and Procedure

A schematic of the rotating fluidized bed apparatus is illustrated in Figure 5.2. Figure 5.3 is a photograph of the unit. For the rotating fluidized bed apparatus, clean, dry, compressed air at 120 psig passes through a Pitot tube to accurately measure the flow rate. Flow rate was also measured with flowmeters (Gilmont, Omega). Depending on the rotational speed, the appropriate flowmeter was used. The air passes through a tangential inlet into the rotating fluidized bed so that the flow can be as uniform as possible in the radial direction when entering through the distributor to fluidize the nanoparticles. The outer chamber, inlet, and outlet chamber are constructed of polycarbonate to enhance visibility. The outer chamber, houses and supports the distributor, as well as acts as the plenum for the fluidizing medium to flow. The woven stainless steel distributor, whose pore size is 100 microns, diameter is 3.625 inches, and length is 3.750 inches, rotates at a desired speed anywhere between 0 and 2000 RPM by a motor. Four settings were used: 300, 600, 900, and 1200 RPM, which is equivalent to a centrifugal acceleration of 6, 25, 56, and 100 "g," respectively. A piece of wire mesh of 10 microns in pore size was placed at the fluid exit inside the unit so that any elutriated powders could be retained.

The pressure drop was measured with a pressure transducer and when possible, verified with a water tube manometer. The powder used was Silica R974 (Degussa) whose properties are listed in Table 2.2. A digital camera is used to record the fluidization behavior. Unfortunately, the high-speed laser and CCD camera were unable to take successful photos to measure in situ agglomerate size due to the design requirements of the RFB. Measurements of superficial gas velocity and pressure drop

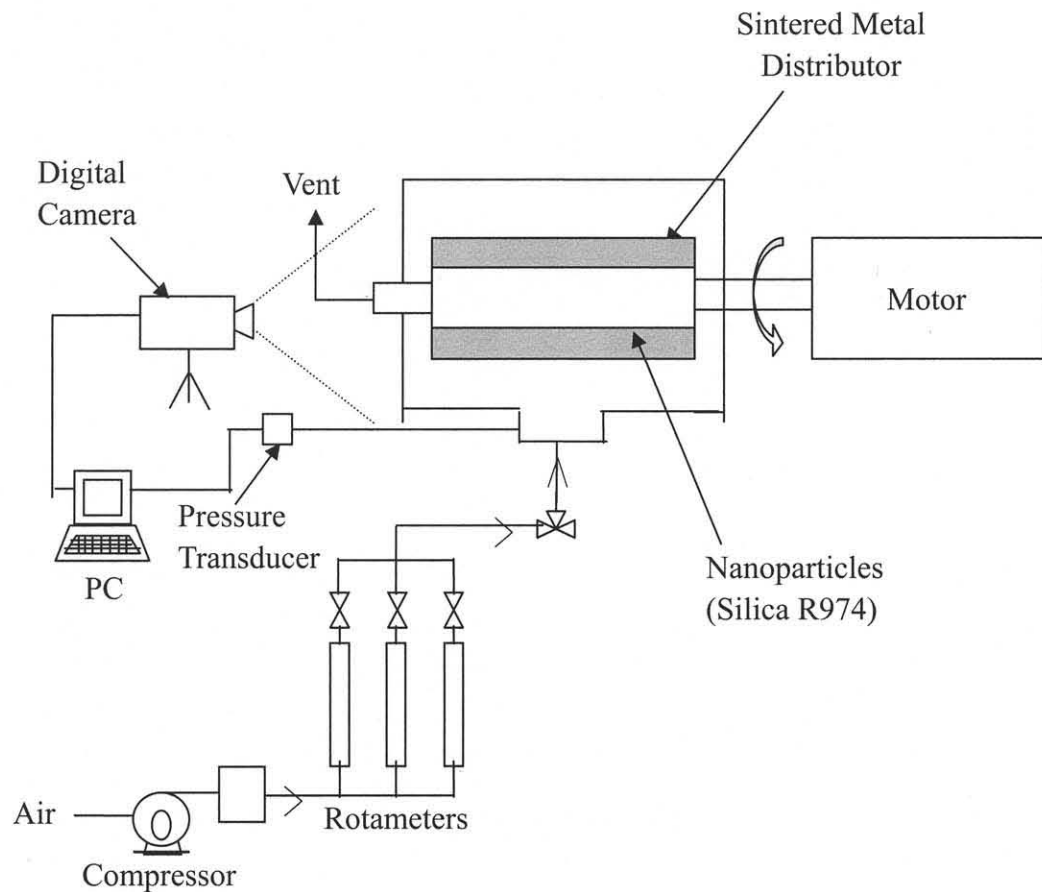**Figure 5.2** Schematic of the rotating (centrifugal field) fluidized bed system.
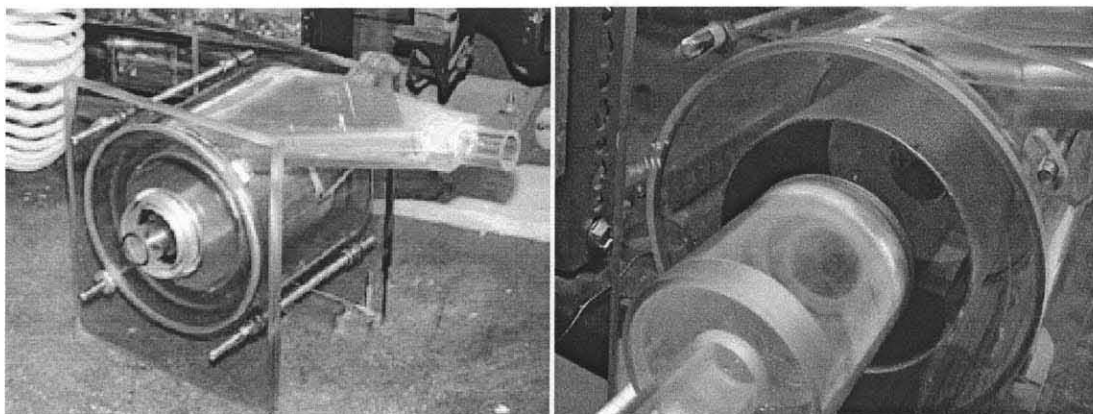

Figure 5.3 Photographs of the rotating (centrifugal field) fluidized bed unit without the exit vent attached (left) and with the exit vent attached (right).

data across the bed are collected and recorded in a PC. Only Silica R974 powder was used in these experiments, the properties of which are summarized in Table 2.2.

To start a typical experiment, an amount of Silica R974 was sieved through a 500 micron mesh and carefully measured. The powder is then placed into the chamber and the unit is properly sealed to prevent powder leakage. The motor is started and set to the desired speed and a few minutes are allowed for the powders to line the walls evenly. The flow rate is incrementally increased and pressure drop and bed behavior are recorded. The digital video footage is used to measure bed expansion through Adobe Photoshop. When the images and video data are imported into Adobe Photoshop, the bed heights are measured in pixels with the Adobe Photoshop measurement tool and then converted into a length. Each experiment was repeated thrice and the data were averaged.

5.3   Results and Discussion

5.3.1   Fluidization Behavior

Upon increasing velocity, the bed expands from its packed state (see Figure 5.4 and Figure 5.5). Small surface instabilities occurred sometimes and could be attributed to small bubbles. Due to the centrifugal force, the bed compacts before fluidizing air enters the bed. As a result, it is slightly easier to see a smoother fluidization with decreasing velocity after increasing velocity. The experiment serves to break up the compaction and once fluidized, the bed is less likely to be susceptible to cracks and channels at the lower velocities. At higher velocities however, the surface becomes less clear and some powders start to elutriate out to the vent. Since the bed is relatively small, only 2.5 grams of powder were used for all experiments since any more powder

would restrict the range of velocities that can be used without elutriation occurring. However, a 10-gram experiment was conducted for clarity of observation (see Figure 5.5). The higher the centrifugal force, the higher the velocity is needed to obtain similar bed expansions that were observed from experiments at lower centrifugal forces.

(a) **(b)** **(c)**

Figure 5.4 Photographs of 2.5 grams of silica nanopowder (a) in a pre-experiment state, (b) in an RFB spun at 1200 RPM without aeration, and (c) in an RFB spun at 1200 RPM with aeration.

(a) **(b)** **(c)**

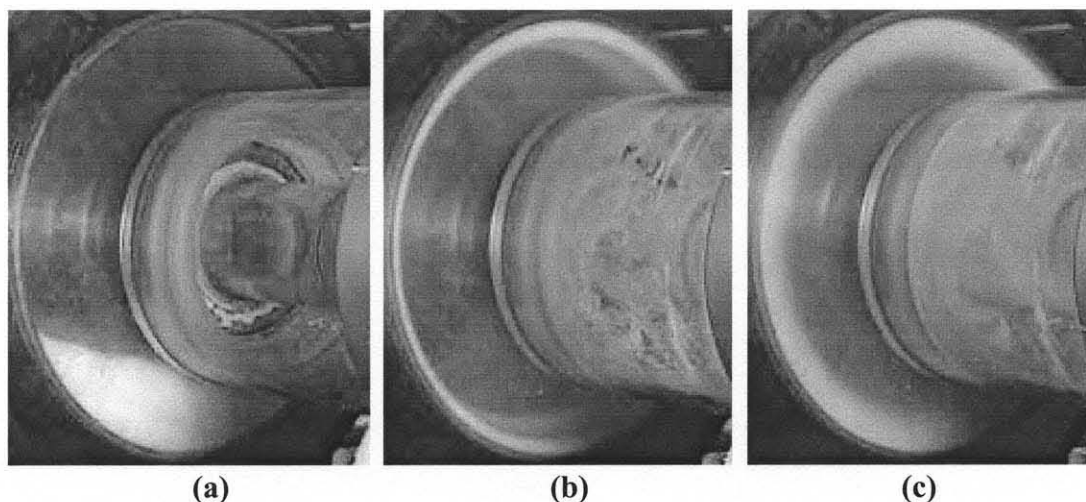**Figure 5.5** Photographs of 10 grams of silica nanopowders (a) in a pre-experiment state, (b) in an RFB spun at 1200 RPM without aeration, and (c) in an RFB spun at 1200 RPM with aeration.
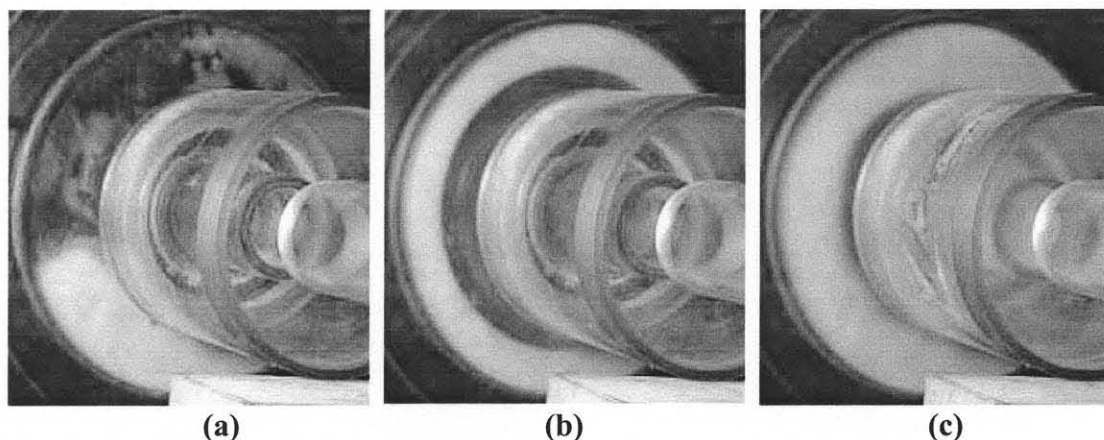
5.3.2 Pressure Drop

As with all fluidization experiments with pressure taps located below the distributor, the pressure drop across the distributor must be subtracted out of the full pressure drop. Since one of the pressure taps is located near the inlet of the air flow, before the distributor, the pressure drop across an empty bed at different rotational speeds must be measured and used to correct for the pressure drop across the powder bed. Despite this correction and the correction for centrifugal force in Equation 5.3, the measured pressure drop was much higher than expected. It has been conjectured that the theory presented by Kao et al. (1987), which assumed flow only in the radial direction might not be completely valid for the experiments, performed and might have to be corrected for tangential flow effects such as Coriolis forces and other effects (Quevedo, 2003). However, the pressure drop did plateau which indicates that the bed was fluidized. Absolute pressure drops for each RPM used for both the empty bed and a powder bed are shown in Figure 5.6. While it can be seen from this figure that the pressure drop across the distributor is much higher than the pressure drop across the powder bed, the instrumentation to measure differential pressure was sensitive enough to measure the pressure drop associated with the powder bed. The total pressure drop measured had to have the pressure drop of the distributor subtracted in order to obtain the pressure drop across the powder bed. Non-dimensionalized with the weight of the bed per unit cross sectional area is shown in Figure 5.7. According to Quevedo (2003), the higher the rotational speed, the effects of Coriolis forces decrease and the non-dimensionalized pressure drop when fluidized (i.e., the plateau region) should approach unity. The results presented here concur with the theory presented by Quevedo (2003). It should

be noted in that in Figure 5.7, the slopes of the pressure drops at the different rotational speeds before the minimum fluidization velocity (i.e., in the packed bed region) are different which is contrary to typical results from group A or group B powders. Matsuda et al. (2001) obtained very similar results, shown in Figure 5.8, which also showed higher pressure drops than expected. The smaller slopes with increasing rotational speed are counter-intuitive since a smaller slope means a lower voidage (see Ergun equation). One would assume that under higher centrifugal forces, the bed of porous nanoagglomerates would become more compact, which means that the voidage in the bed would decrease, not increase. A possible error could arise from the large discrepancy between the pressure drop associated with the distributor and that of the powder bed. However, as seen from Figure 5.8, Matsuda et al. (2001) obtained similar results in that slope decreased with increasing rotational speed. This is contrary to the findings from Watano et al., (1999) and from Quevedo (2003) who both obtained the opposite trend. Clearly, a more in depth study is needed to investigate the reasons for these findings. The design of the RFB unit may play a large role. The RFB unit used for this chapter and the unit used by Matsuda et al. (2001) were considerably smaller than the unit used by Watano et al. (1999) for example. Perhaps, the flow characteristics in smaller beds are much more complicated than those in larger beds.
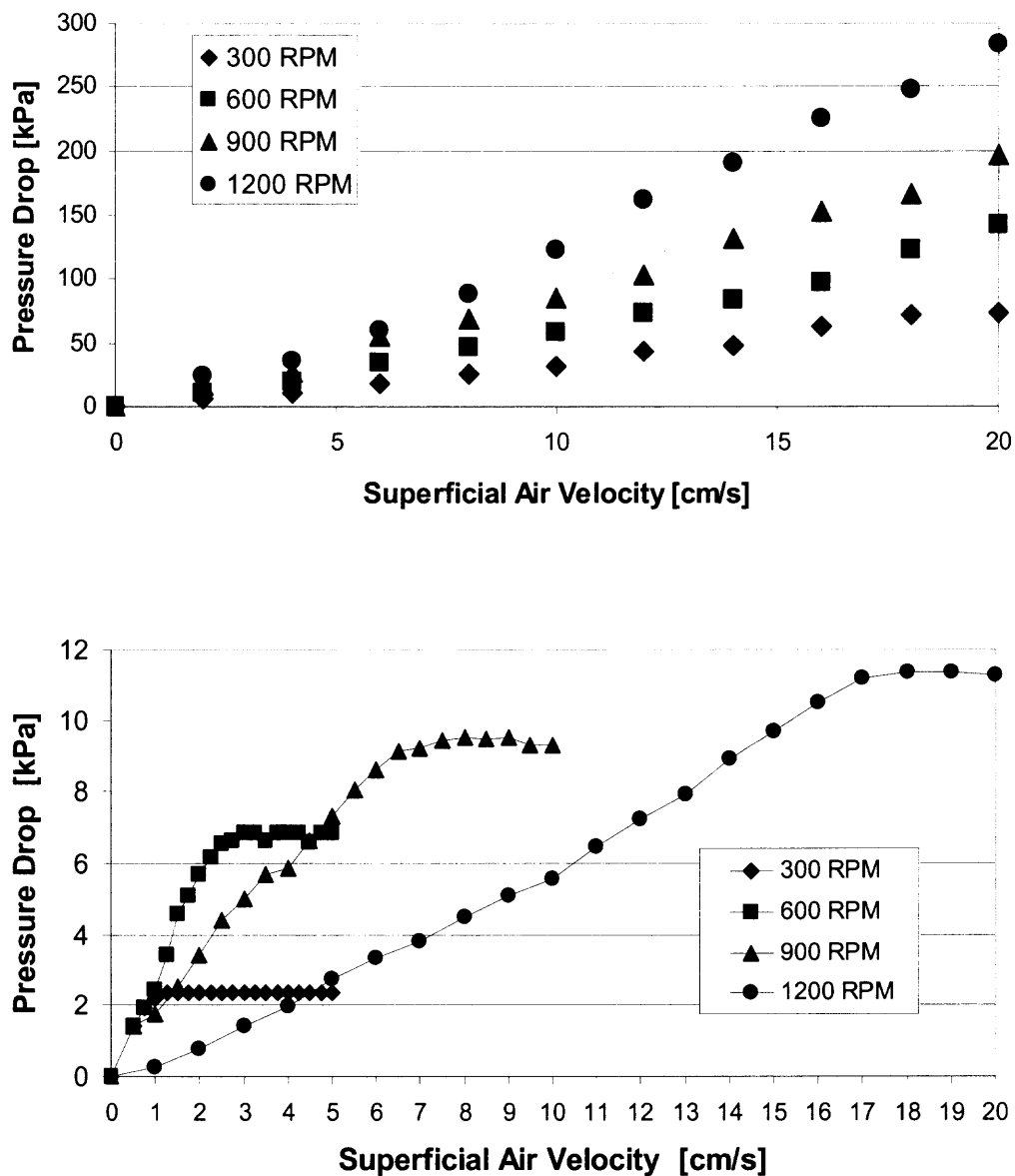
Figure 5.6   Pressure drop and bed expansion ratio as functions of air superficial velocity at 300, 600, 900, and 1200 RPM for an empty bed (top) and for a powder bed with the distributor pressure subtracted (bottom).
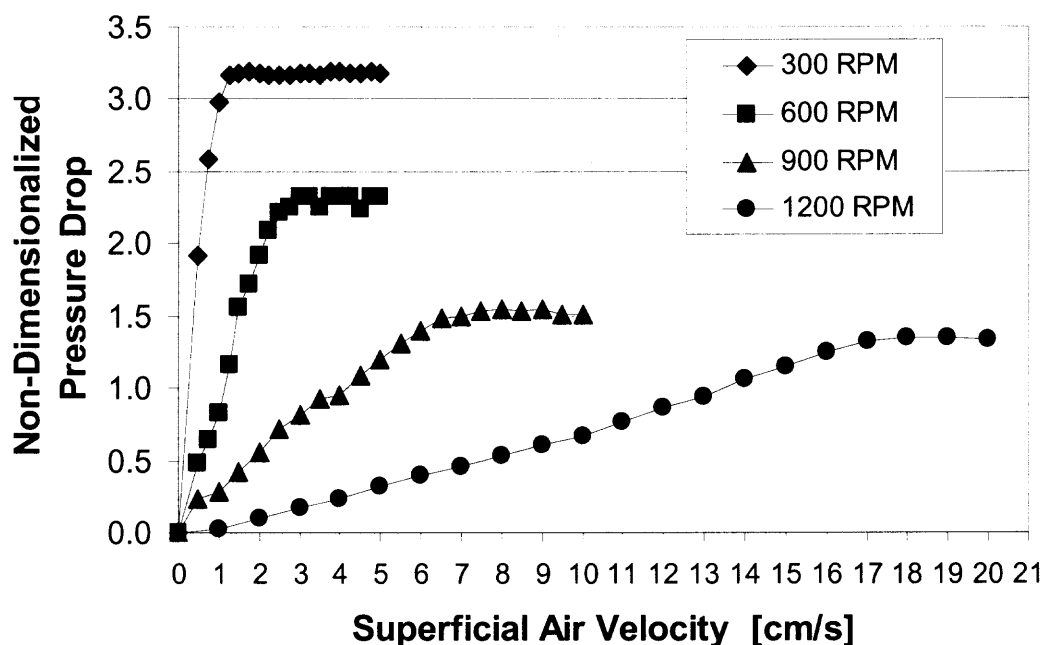
Figure 5.7 Non-dimensionalized pressure drop (with Equation 5.3) and bed expansion ratio as functions of air superficial velocity at 300, 600, 900, and 1200 RPM.
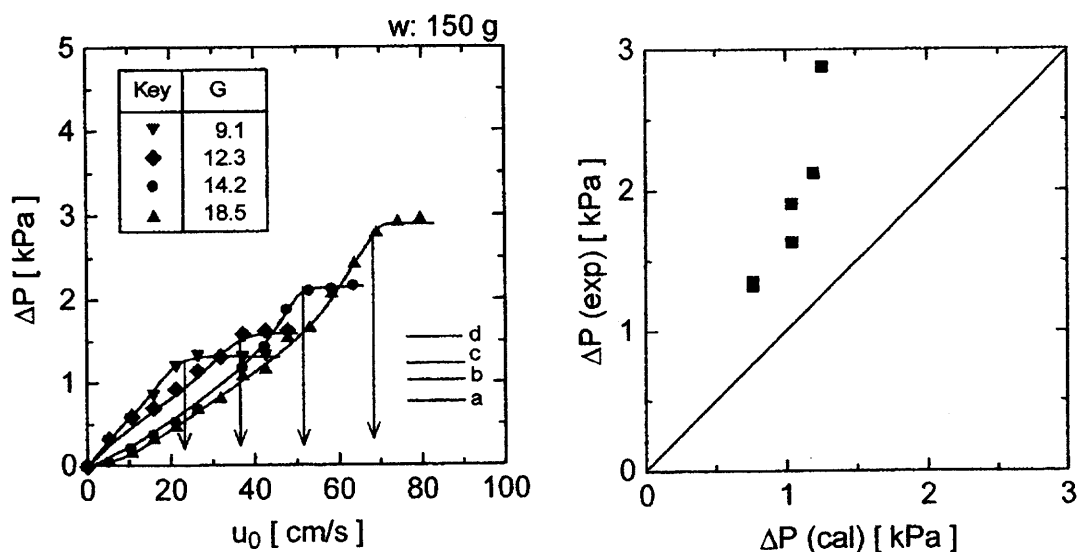

Figure 5.8 Pressure drop of 7 nm titania particles at various G (left) and comparison between calculated and experimental values of pressure drop (right).
(Matsuda et al., 2001)

5.3.3 Minimum Fluidization Velocity

The minimum fluidization velocity is plotted as a function of G in Figure 5.9. The limited data appeared to be somewhat linear with G. The minimum fluidization velocity here is the velocity at which the pressure drop begins to plateau.
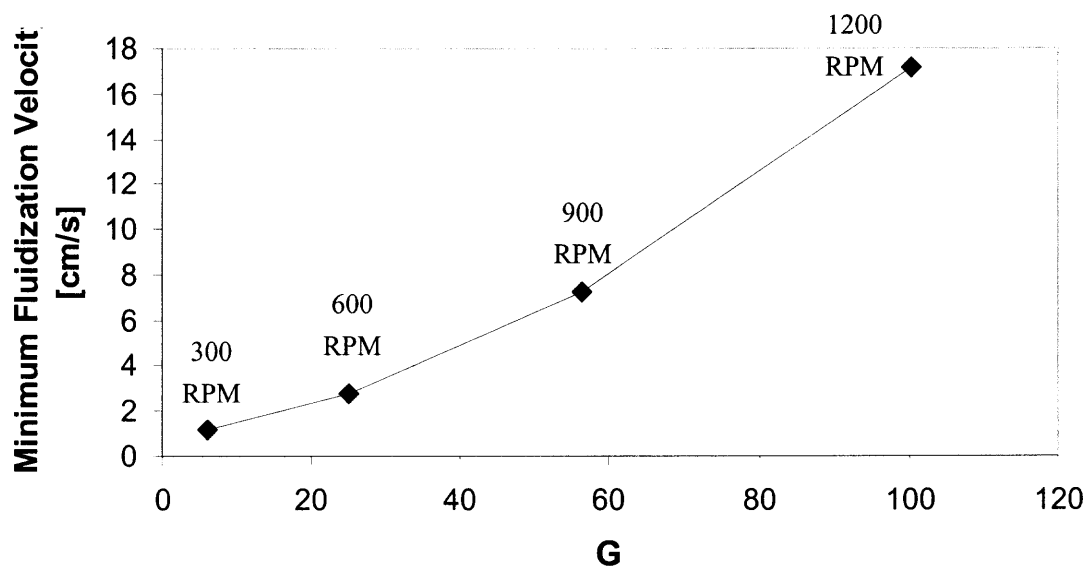
Figure 5.9 Minimum fluidization velocity plotted with G.

5.3.4 Agglomerate Size

Since the bed expansion data, which are plotted in Figure 5.10, was known, the modified Richardson-Zaki and fractal analysis, detailed in Chapter 2, can be applied. For a Richardson-Zaki exponent of 5, the plots of ϕ vs. $(u/V_o)^{1/n}$ were plotted (see Figure 5.11), from which the fractal dimension (D_f) and agglomerate size (d_a) were calculated and are summarized in Table 5.1. The theory suggested that agglomerate size tended to decrease with G. This supports the idea that as G increases and the size of the agglomerates decreases, the fluidization quality should be improved. In addition, the

Figure 5.10   Bed expansion ratio plotted with superficial air velocity plotted at 300, 600, 900, and 1200 RPM.

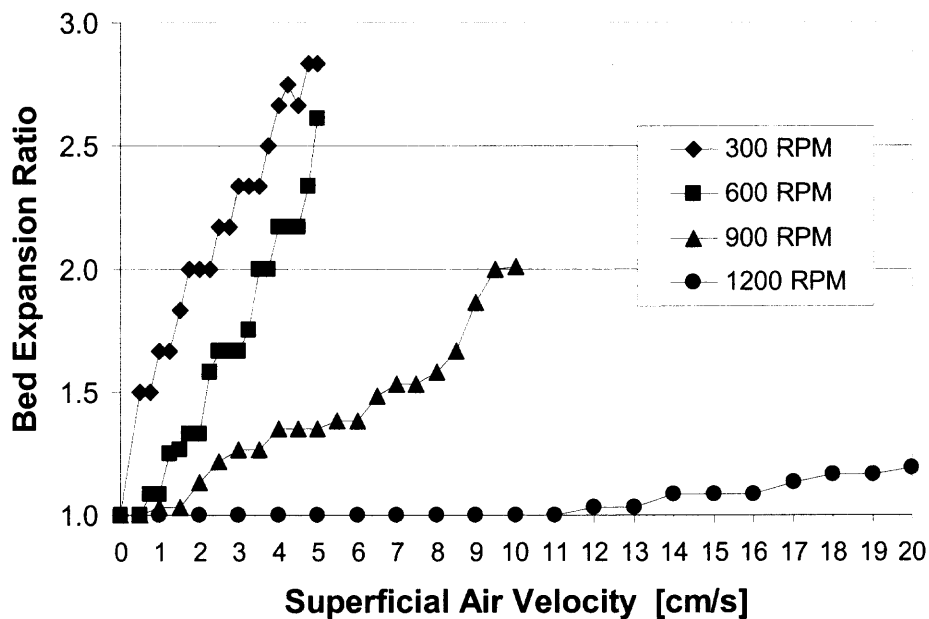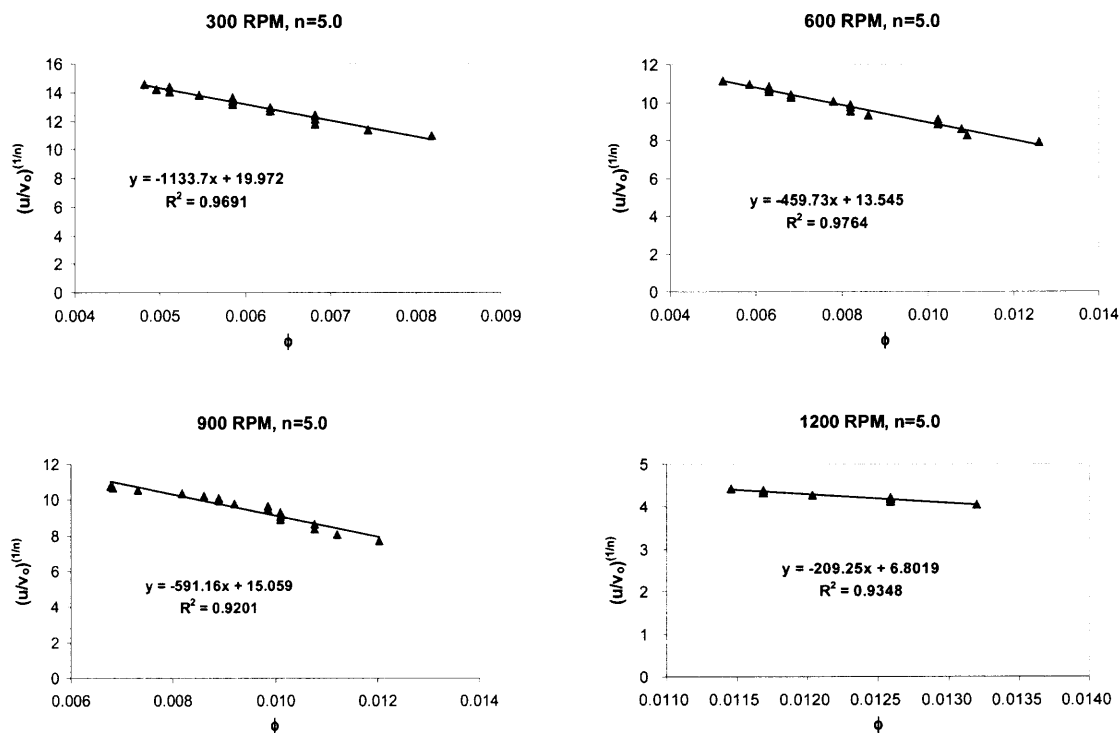**Figure 5.11**   Plots of ϕ vs. $(u/V_0)^{1/n}$ for each rotational speed.

Table 5.1 D_f and Agglomerate Size Values Evaluated at n=5 for Each G

G	D_f value at n=5	d_a [microns]
6 (300 RPM)	2.58	215
25 (600 RPM)	2.57	63
56 (900 RPM)	2.57	88
100 (1200 RPM)	2.47	11

higher centrifugal and shear forces could be breaking the large agglomerates into smaller ones. Unfortunately, due to the design requirements of the RFB, a laser and CCD camera could not be situated such that clear images of in situ agglomerates could be taken for comparison. The results of Matsuda et al. (2001), however, concur that agglomerate sizes decrease with increasing G.

5.3.5 Voidage

According to Figure 5.6, the slopes of each experiment before the plateau pressure drops are different which implies that voidages in the bed are different for the different cases of G. The theory presented by Kao et al. (1987) applies only to Group A and B powders; thus the voidage will remain constant in the packed bed regime (before the bed becomes fluidized). Since the bed expansions (especially at high rotating speeds) were not very high, the method to calculate voidage presented by Wang et al. (2002) did not produce reasonable voidages. However, the voidages calculated by the modified Richardson - Zaki method as described in Chapter 2, did give reasonable results. Figure 5.12 shows a plot of these voidages vs. superficial air velocity at each G. It can be seen from the figure that the higher the G, the less voidage there is which rings true since higher G tends to cause compaction.
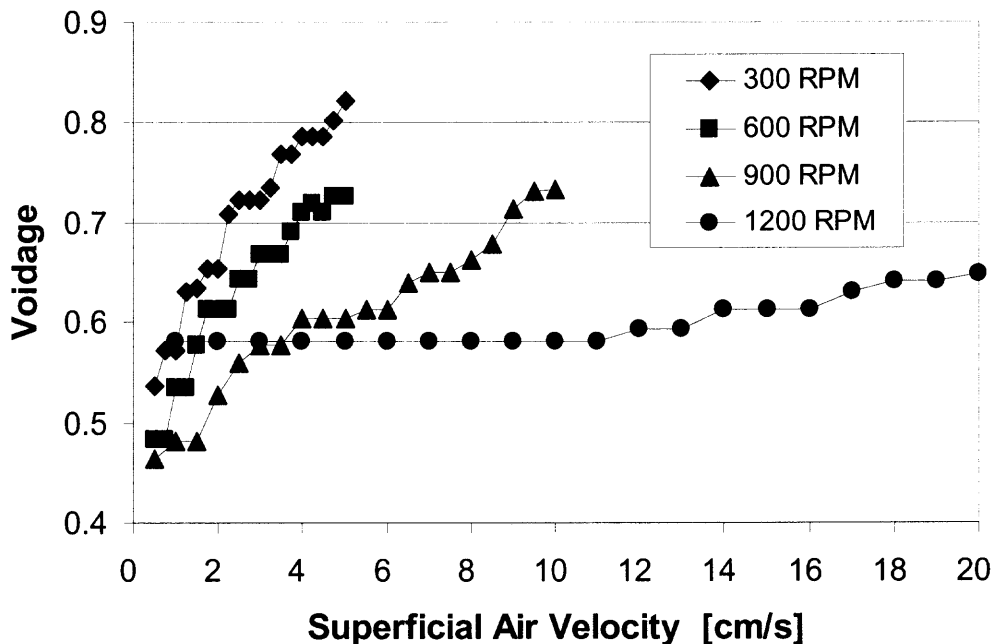
Figure 5.12 Voidage calculated by the modified Richardson-Zaki method plotted with superficial velocity.

5.4 Conclusions

It was clearly demonstrated that the silica nanoparticles can be fluidized in a rotating fluidized bed with considerable bed expansion (at the lower rotating speeds), which is not observed for the fluidization of micron sized powders. The modified Richardson-Zaki method and fractal analysis were applied and suggested very reasonable results for agglomerate size, voidage, and fractal dimension. The advantages of using a rotating fluidized bed include higher air flow rates, high shear, and elimination of wall effects. Smaller agglomerate sizes were calculated for higher G values, where shear forces are high. Future work should include a method for measuring agglomerate sizes in situ so that calculated results can be compared.

CHAPTER 6

SUPERCRITICAL FLUIDIZED BED

6.1 Introduction and Theory

The idea of fluidizing nanoparticles under supercritical conditions is quite novel and studies pertaining to it, if any prior to this dissertation, are not found in the literature. It has been observed that dense fluid systems such as gases at very high pressure and liquids fluidize solid particles as if they were Geldart group A particles. As the gas pressure is increased, borderline Geldart group B systems behave more like Geldart group A systems. It is also known that increasing density or viscosity usually decreases minimum fluidization velocity as well as terminal velocity (Knowlton, 1977; Werther, 1983). However, Rowe (1984) conducted a study that showed that small particles (<100 microns) and systems where Re < 2, the minimum fluidization velocity is independent of pressure. An increase in temperature means a decrease in density, but for gases, an increase in viscosity. And it is thought that the minimum fluidization velocity would decrease with an increase in temperature. Like Knowlton (1977) and Werther (1983), Abrahamsen and Geldart (1980) also found that by increasing the density and viscosity of the gas, the fluidization system becomes more aeratable as if it were a liquid-solid fluidization and thus the behavior of fluidization becomes more smooth and bubbleless. Equipped with this knowledge, the fluidization of nanoparticles at high pressure seemed very promising and a behavioral study was conducted.

6.2   Experimental Setup, Materials, and Procedure

Figure 6.1 shows different angles of the fluidized bed chamber that was used in the experiments.   The chamber, made of 0.4 cm thick plastic, 3.2 cm x 3.2 cm (square cross section), and 19.65 cm in height, was securely placed above a sintered metal distributor with pores that are less than 3 microns in size.   The distributor and bed chamber were secured to another plastic piece to fit a high-pressure stainless steel vessel.   The stainless steel vessel, pictured in Figure 6.2, was 8.25 cm in inner diameter, 25 cm in inner height, with three small quartz windows that were 1.5 cm in diameter and located 15 cm from the top of the vessel.

A pressure transducer was used to measure the pressure drops across the bed and distributor.   A thermocouple and a pressure gauge were used to measure temperature and pressure of the vessel, respectively.   There were several valves installed such that the inlet and outlet tubes can be used simultaneously or not in sync.   This was necessary so when pressurizing the system, the bed can be pressurized from both ends (underneath the bed and above the bed).   A mass flow pump, whose maximum was 25 kg/hr, and flow meter were used to measure the flow rate of CO_2 and various pressure gauges and thermocouples were located at several other places in the system such as the refrigerating system to cool the CO_2.   With each flow setting, the pump processed CO_2 in a pulsating manner which made for non-continuous flows.   The critical temperature and pressure for CO_2 are 31 C and 73.9 bars, respectively.   A digital camera was used to record what was seen through the windows.   The powders used for these experiments were Silica R974, Silica A300, and Silica A90 whose properties are listed in Table 2.2.   All particles used were sieved through a 500 micron sieve and 2.5 grams of each powder were used

for each run. This amount of powder (2.5 grams) corresponded to a height of approximately 4 cm in the pressurized fluidization chamber. The surface of the powder bed was located right below the viewing window. In this way, the initial stages of fluidization can be clearly viewed and recorded through the window.

To start an experiment, the CO_2 tank is opened and is led to a refrigerant system where the CO_2 is cooled so that it is in the liquid state and easily pumpable in the mass flow pump. The CO_2 is then heated to a desired temperature, in this case 40 degrees Celsius. Appropriate valves are turned to start pressurizing the fluidization system. The stainless steel vessel is pressurized extremely slowly from both below and above the distributor to prevent any disturbance to the bed. Pressurizing from below the distributor would prematurely fluidize or disturb the bed before the desired conditions are met. Pressuring from above the distributor would compact the bed which is an undesirable start for a fluidization experiment. Once the bed is pressurized to the desired pressure (105, 160, or 230 bars) and the vessel temperature is stable, the CO_2 is set to flow at a low velocity. The vessel pressure is maintained with a manual back pressure regulator (BPR). At each flow rate, the BPR must be used to regulate the pressure of the vessel. The pressure drop and the behavior of the bed (if seen through the window) are recorded at each flow rate.
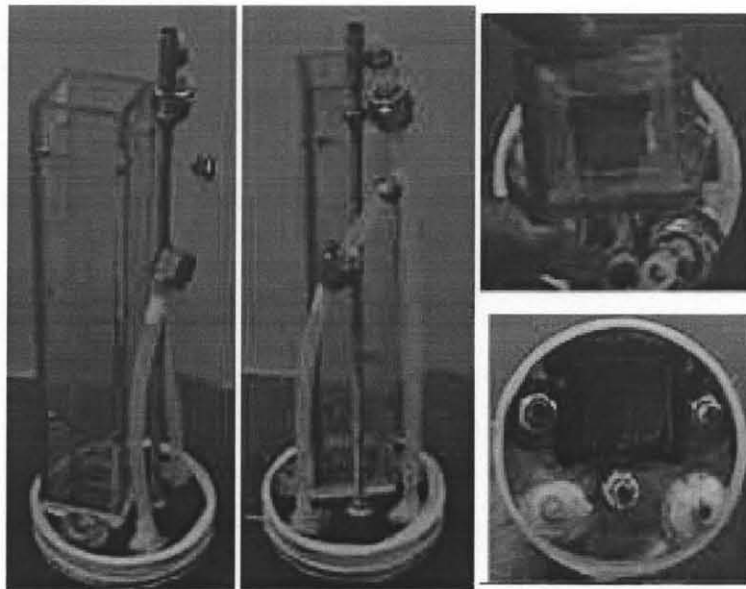
Figure 6.1 Photographs of different views of the fluidization chamber bed, which is placed in a stainless steel vessel (see Figure 6.2).
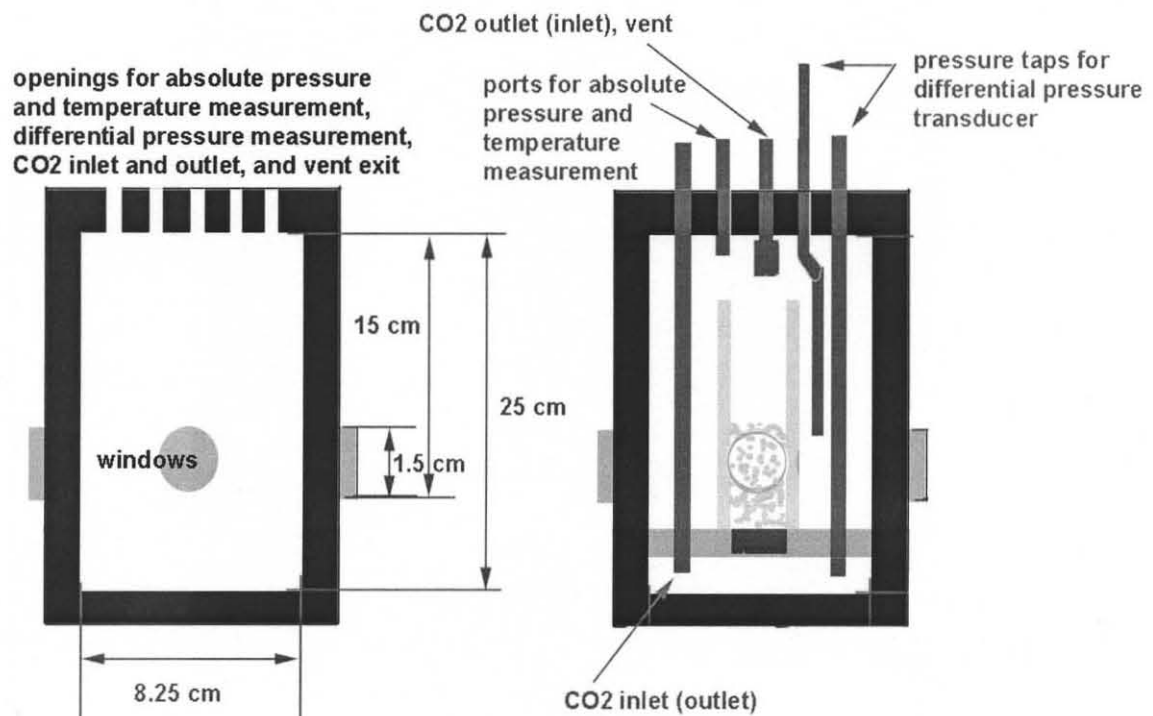

Figure 6.2 Sketch of stainless steel vessel (left) and of the vessel with the square fluidized bed chamber, see Figure 6.1, situated inside (right).

6.3 Results and Discussion

As stated in Chapter 1, there were a few groups who fluidized micron sized particles under supercritical conditions. Marzocchella and Salatino (2000) fluidized group A and B powders with CO_2 at pressures from ambient to supercritical. They found that the region of homogenous fluidization is broader as the fluid density increases, or in other words, as pressure increases. According to this group, supercritical conditions allowed for the bed to be fluidized at a lower fluidization velocity and thus had a higher bed voidage according to the Richardson and Zaki (1954) equation $u=u_o\varepsilon^n$. The lower minimum fluidization velocities and overall smoother fluidization were taken advantage of in the supercritical coating experiments conducted by Schreiber et al. (2002).

The pressure drop data obtained here was rather incongruous to the fluidization theory available. The beds appeared very fluidlike and smoothly fluidized yet the pressure drop data did not plateau. This might perhaps be due to the limitation of the flowmeter. The pressure drop across the distributor was of course subtracted out of the total pressure drop measured. The expected plateau pressure drop was calculated to be 0.239 mbar for a 2.5 gram bed of powders in a 3.2 cm X 3.2 cm square bed. Figure 6.3 shows the pressure drop data obtained. While visual observations indicated smooth fluidization and vigorous movement of the nanoagglomerates starting at low velocities, the measured pressure drop did not appear to plateau, as stated previously. It is not certain that the pressure drop for a supercritical experiment should follow conventional fluidization theory. Nonetheless, for comparison, pressure drops per bed height ($\Delta P/H$) for the "packed bed region" were calculated by the Blake-Kozeny equation for voidages
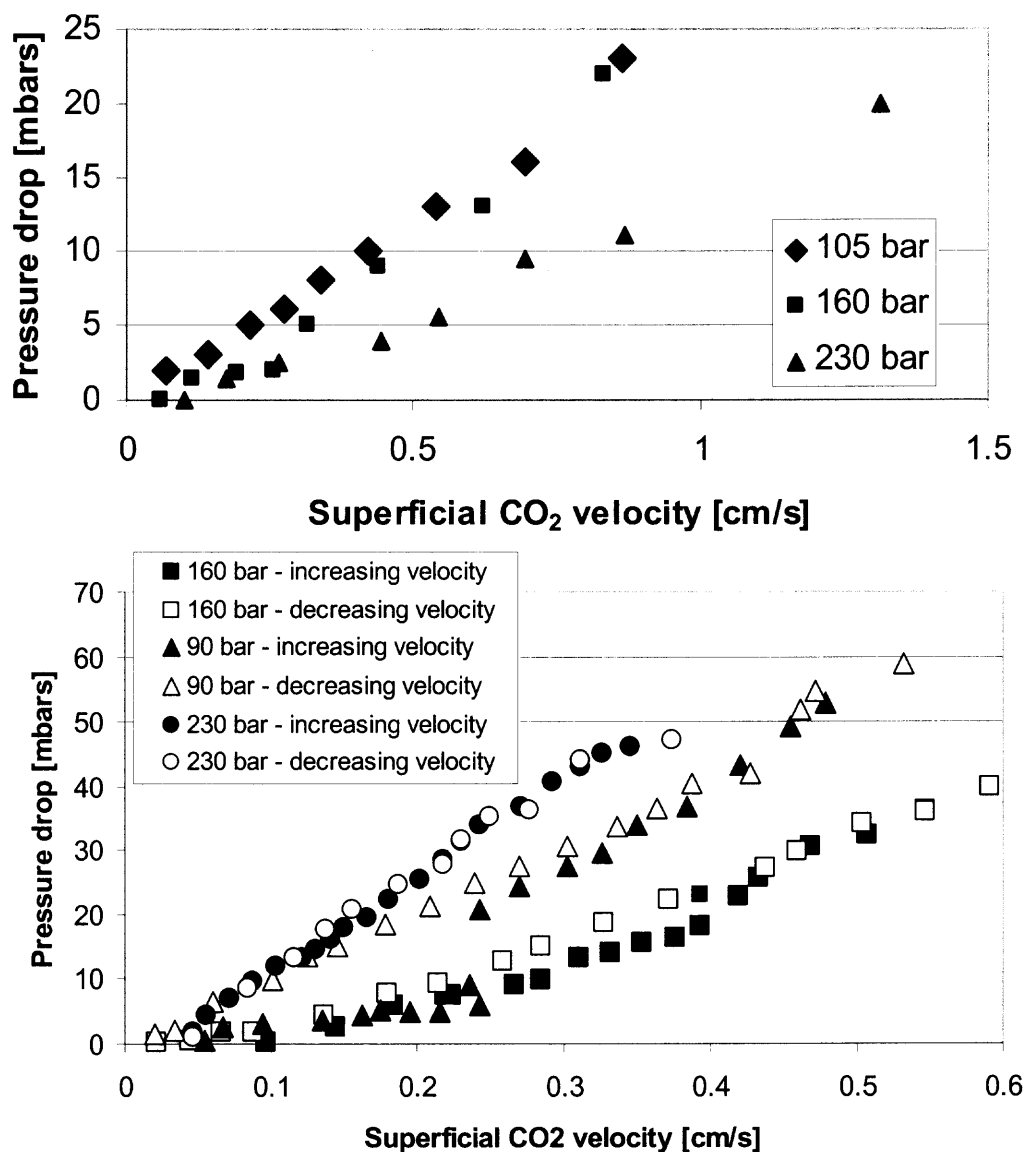
Figure 6.3 Pressure drop vs. mass flow rate of the empty bed (top) and of Silica A90 (bottom).

of 0.5, 0.6, and 0.7 and are plotted in Figure 6.4. Given that the weight of the bed accounts for 0.239 mbar and that the initial height is 4 cm, the expected value for $\Delta P/H$ at fluidization conditions is roughly 0.598 mbar/cm, which is the cut-off point for the plots shown in Figure 6.4. With bed expansion data, this value can be more accurately calculated and thus, it is strongly recommended that for future experiments, another bed
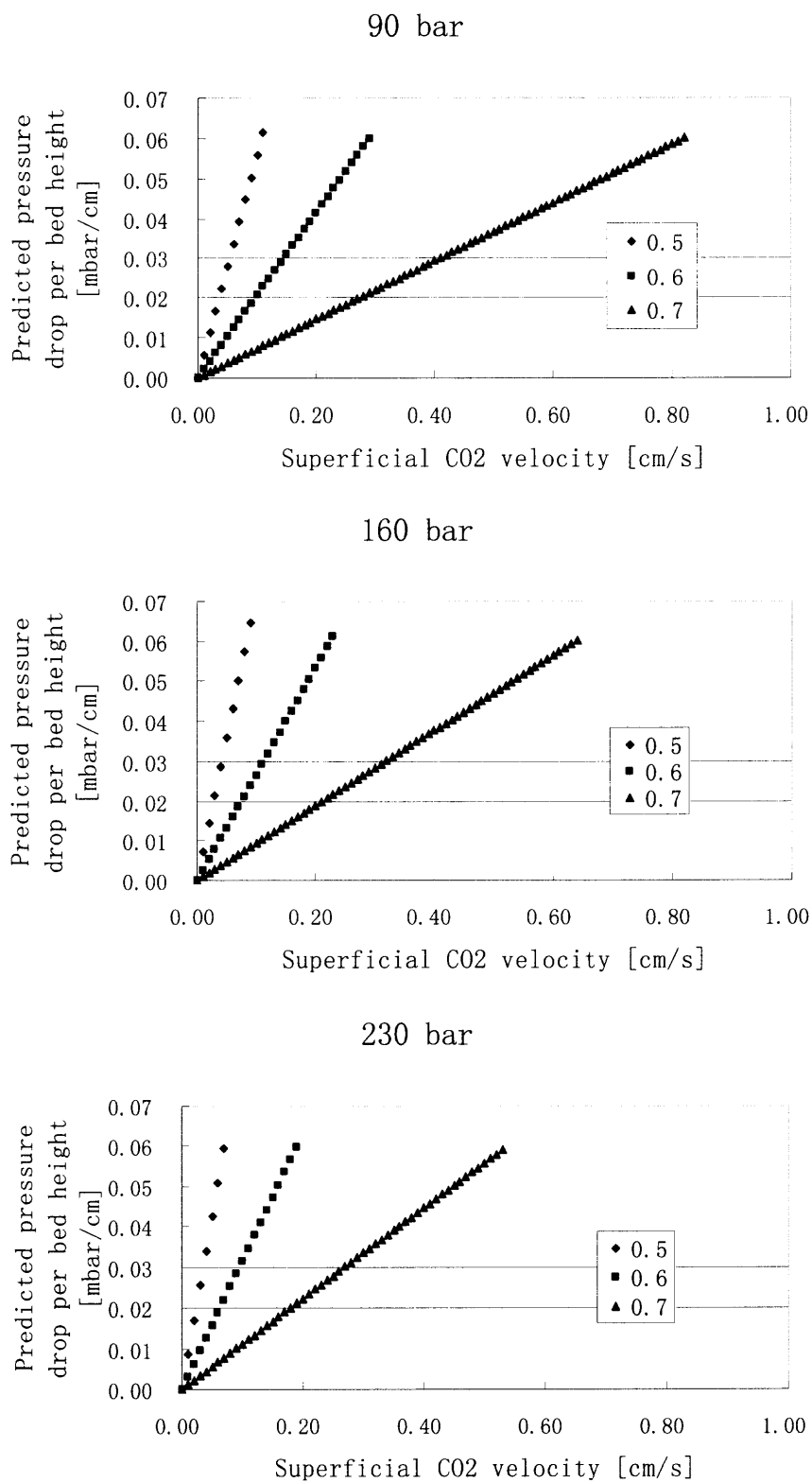
90 bar

160 bar

230 bar

Figure 6.4 $\Delta P/H$ vs. superficial CO_2 velocity as predicted by the Blake-Kozeny equation for $\varepsilon = 0.5$, 0.6, and 0.7 at 105 bar (top), 160 bar (center), and 230 bar (bottom).

be designed with a full length window so bed expansion may be measured. As a summary, the predicted minimum fluidization velocities are given in Table 6.1. In comparison to visual observations, the beds appeared fluidized at roughly 0.2 cm/s and thus, the values calculated for a voidage of 0.6 appear to be more accurate than a voidage of 0.5 or 0.7.

Table 6.1 Summary of Predicted Minimum Fluidization Velocities at ε = 0.5, 0.6, and 0.7 at 105, 160, and 230 bars

	$\varepsilon = 0.5$	$\varepsilon = 0.6$	$\varepsilon = 0.7$
105 bar	0.11 cm/s	0.29 cm/s	0.82 cm/s
160 bar	0.08 cm/s	0.22 cm/s	0.64 cm/s
230 bar	0.07 cm/s	0.19 cm/s	0.53 cm/s

The pulsing flow did not appear to hinder fluidization and in fact, inspires the idea that pulsing flow could help improve fluidization in general. The pulsing flow was reminiscent of a low-intensity vibration, which has been shown to clearly improve quality of fluidization (see Chapter 3). Figure 6.5 shows photos of what an experiment looked like when it was prepared for a mixing study. The mixing study, with carbon black, showed promising results in that every experiment resulted in a well-mixed sample after processing. The subsequent figures (Figures 6.6 through 6.13) are the collection of images obtained for Silica 90, Silica R974, and Silica A300 at 105, 160, and 230 bars, all at 40°C. At these pressures, the densities of CO_2 are approximately 0.620, 0.805, and 0.871 g/mL, respectively and the viscosities are 5.92 X 10^{-6}, 7.60 X 10^{-6}, 9.00 X 10^{-6} Pa s, respectively. Overall, smooth fluidization with good mixing was observed and less nanoagglomerates in the freeboard region was noted at higher pressures.
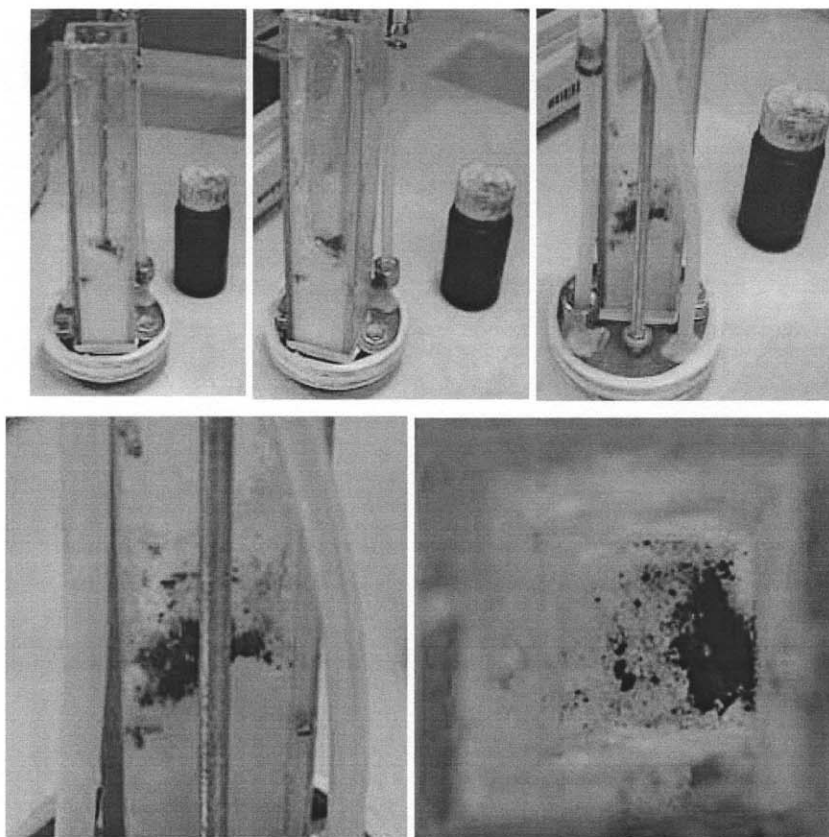
Figure 6.5 Photographs of preparation for mixing experiments with carbon black.
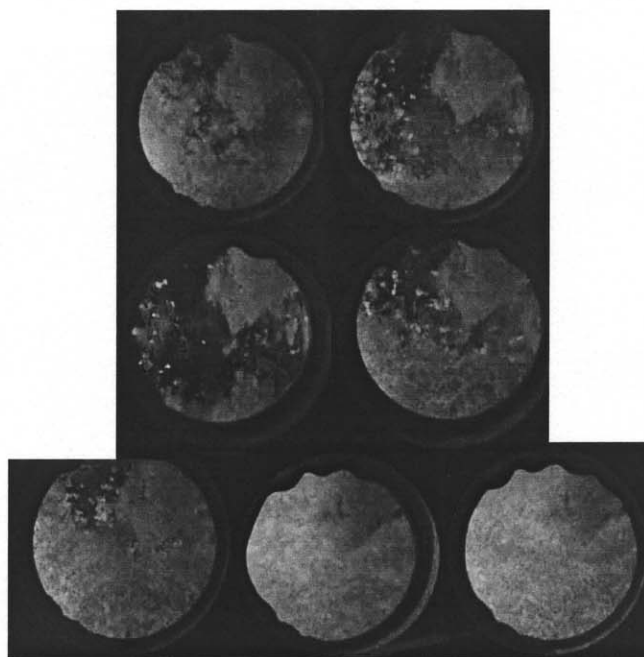

Figure 6.6 Photographs of Silica A90 at 105 bar. From left to right: 7, 7.1, 5.3, 8.0, 9.0, 12.0, 16.0 kg/hr (0.306, 0.311, 0.232, 0.350, 0.394, 0.525, 0.700 cm/s, respectively).
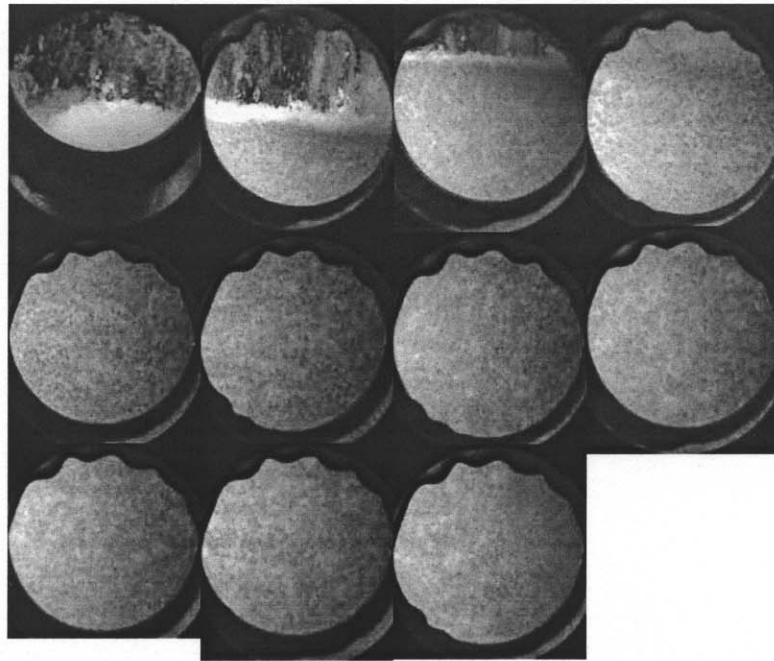
Figure 6.7 Photographs of Silica A90 at 160 bar. From left to right: 4.2, 6.1, 6.5, 7.1, 8.6, 9.0, 9.5, 10.0, 10.7, 11.6, 13.5 kg/hr (0.142, 0.206, 0.219, 0.239, 0.290, 0.303, 0.320, 0.337, 0.361, 0.391, 0.455 cm/s, respectively).
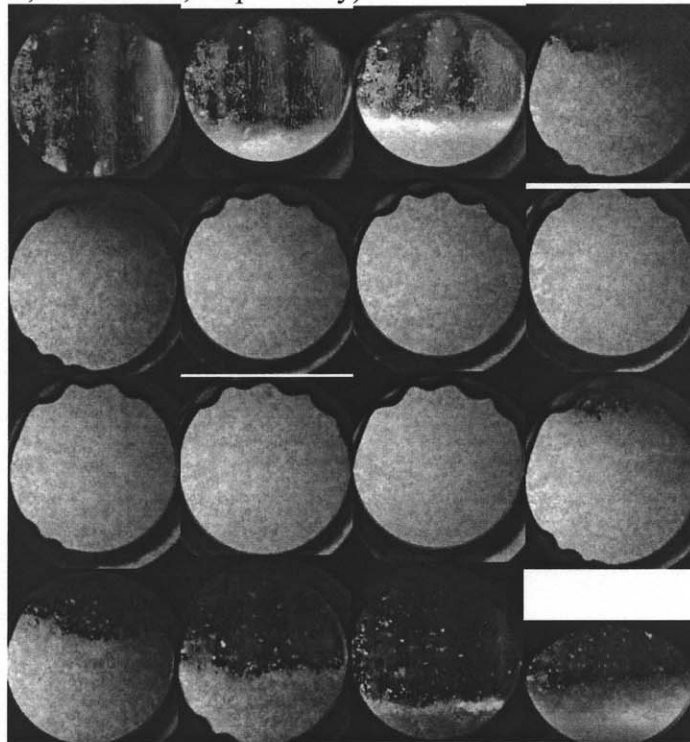

Figure 6.8 Photographs of Silica A90 at 230 bar. From left to right: 1.5, 5.0, 5.8, 6.5, 7.0, 7.4, 7.8, 8.7, 9.4, 10.0, 10.5, 12.0, (and for decreasing velocity) 8.0, 7.4, 7.0, 6.0, 4.0 kg/hr (0.047, 0.156, 0.181, 0.202, 0.218, 0.230, 0.243, 0.271, 0.293, 0.311, 0.327, 0.374, 0.249, 0.230, 0.218, 0.187, 0.125 cm/s, respectively).
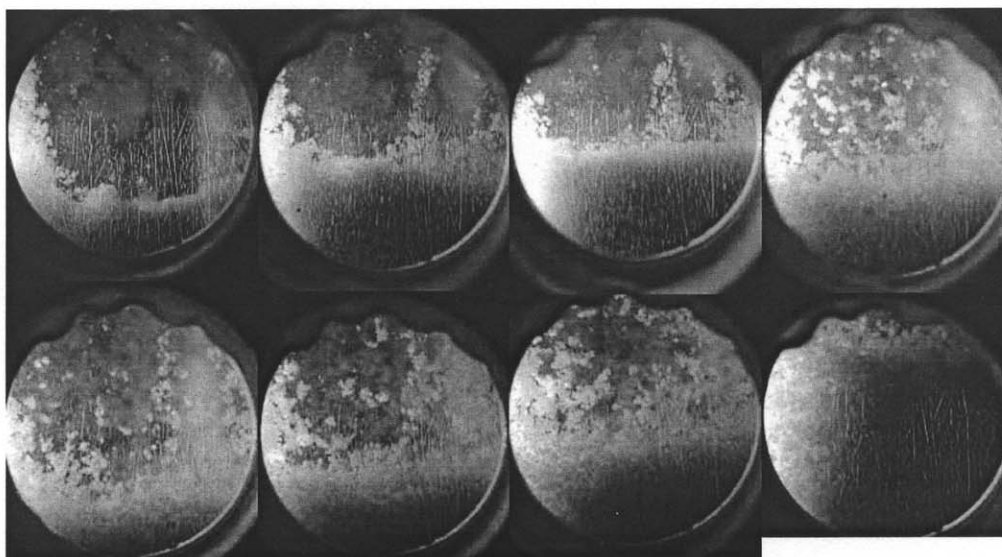
Figure 6.9 Photographs of Silica A90 and CB at 105 bar. From left to right: 0.6, 1.9, 2.9, 3.0, 3.1, 4.4, 4.8, 5.5 kg/hr (0.026, 0.083, 0.127, 0.131, 0.136, 0.193, 0.210, 0.241 cm/s, respectively).
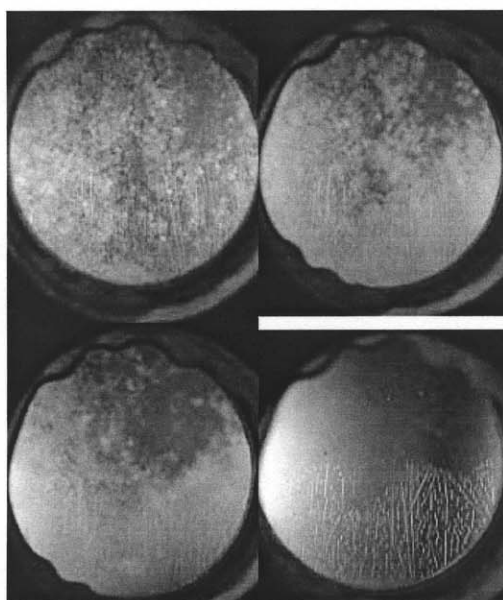

Figure 6.10 Photographs of Silica A300 at 105 bar. From left to right: 1.5, 4.0, 6.0, 8.0 kg/hr (0.066, 0.175, 0.263, 0.350 cm/s, respectively).
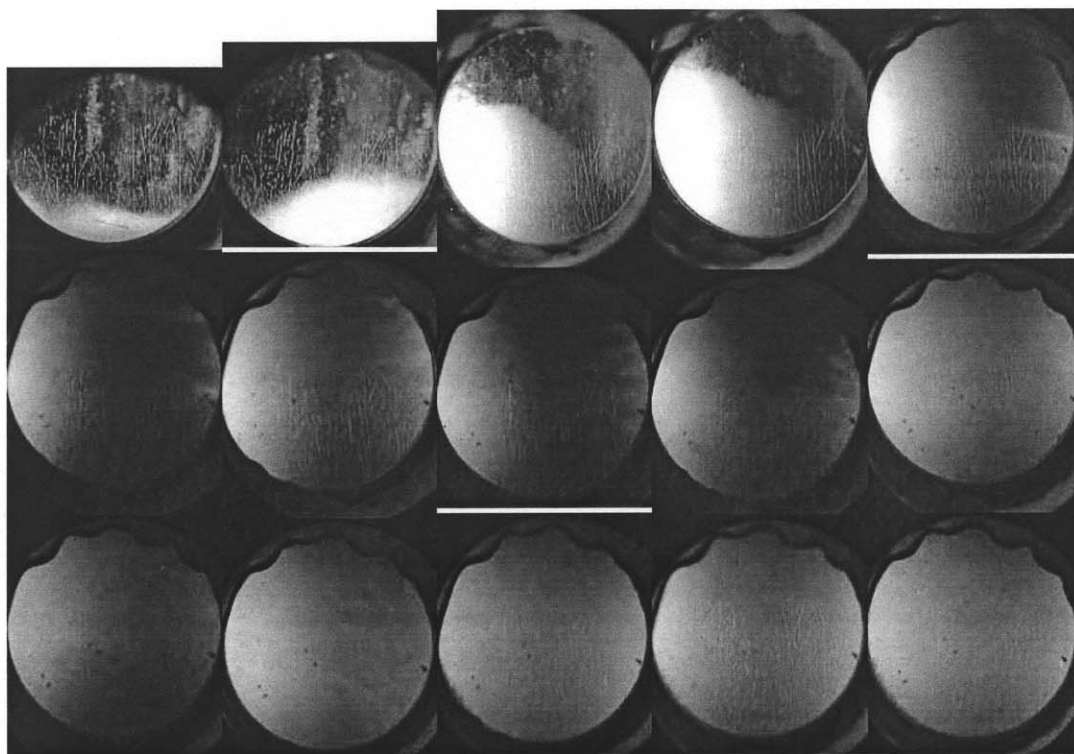
Figure 6.11 Photographs of Silica A300 at 230 bar. From left to right: 1.0, 1.4, 1.9, 2.0, 2.3, 2.5, 2.6, 3.0, 3.5, 5.5, 6.9, 7.4, (and for decreasing velocity) 6.2, 5.5, 4.5 kg/hr (0.031, 0.044, 0.059, 0.062, 0.072, 0.078, 0.081, 0.093, 0.109, 0.171, 0.215, 0.230, 0.193, 0.171, 0.140 cm/s, respectively).
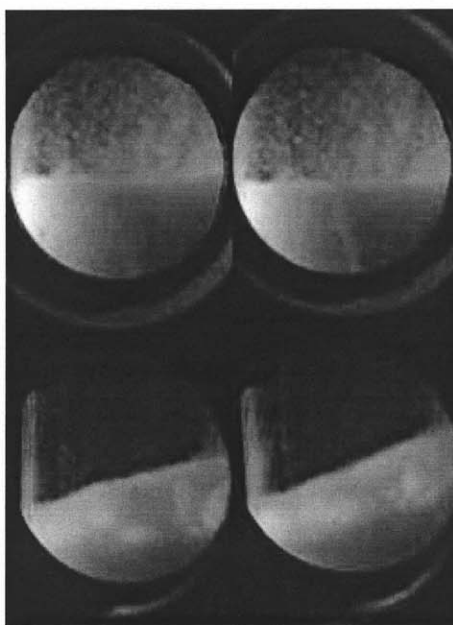

Figure 6.12 Photographs of Silica R974. From left to right: pre-experiment photo, pre-experiment photo with small channel from pushing in apparatus, 0.4 kg/hr (0.018 cm/s) at 105 bar, 1.2 kg/hr (0.053 cm/s) at 105 bar.
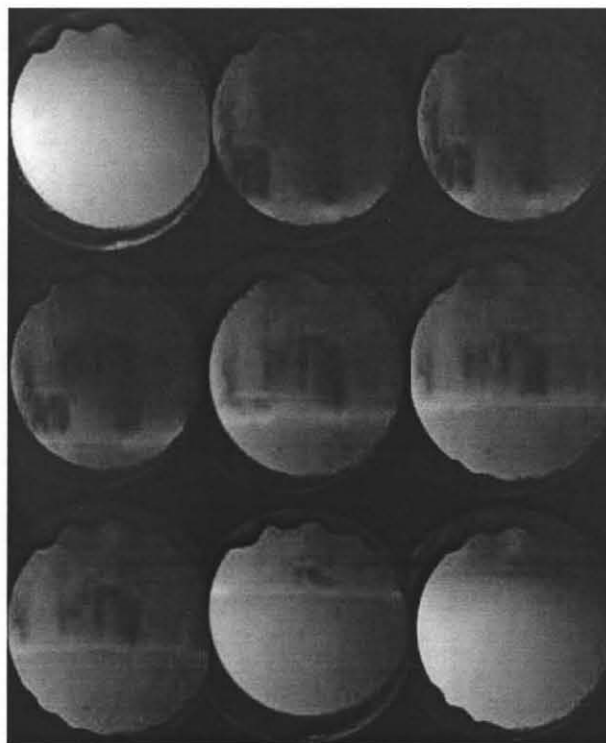
Figure 6.13 Photographs of Silica R974. From left to right: pre-experiment / loading at 1.01325 bar, and at 160 bars: 1.0, 1.2, 2.0, 2.1, 2.2, 2.3, 2.4, 2.5 kg/hr (0.034, 0.040, 0.067, 0.071, 0.074, 0.078, 0.081, 0.084 cm/s, respectively).

6.4 Conclusions

It was experimentally observed that nanoparticles can be smoothly fluidized under supercritical conditions. The visual observations showed that a substantial bed expansion occurs and that the number of agglomerates in the freeboard region is significantly decreased at higher pressures. The results from the mixing studies supported that the powder was being fluidized. A better design, especially with a long window so all of the bed can be seen, is necessary. Once all the parameters and values can be accounted for, applications such as mixing and coating of nanoparticles under supercritical conditions can be examined more thoroughly.

CHAPTER 7

APPLICATIONS OF NANOPARTICLES AND FLUIDIZED BEDS

7.1 Mixing

Sanderson and Rhodes (2001) used a common technique of utilizing tracer particles to observe the flow of particles within fluidized beds. They used various bed diameters to observe the scaling behavior of active particle motion and solids downflow velocity. They determined that tracer particle size and bed material must be matched in order to obtain the predicted particle circulation rate. Formisani et al. (2004) studied the fluidization behavior of mixtures of two dissimilar solids in the 100 to 800 micron range. They showed that minimum fluidization velocity is no longer relevant in these systems, and that such systems must be characterized by a velocity range, bounded by initial and final fluidization velocities. They also demonstrated that particle size ratio and mixture composition determine the segregating behavior of the mixture, more so than the density difference of the materials.

Given some of these previous studies and the data shown in this dissertation, the idea to mix different nanoparticles together in a fluidized bed is very promising. To test the idea, a small amount of silica was dyed blue with methylene blue for mixing/tracer experiments. The dyed powder was placed in the oven for at least 24 hours to remove as much moisture as possible and then was used as tracer particles to observe during the fluidization of nanoparticles. Carbon black and molybdenum oxide were among other particles used for tracer and mixing studies.

Figure 3.6 shows the progression of mixing of a small layer of dyed-blue particles

placed at the top of the vibrated fluidized bed of Silica R974. Within a few minutes, the entire bed turned blue and appeared well mixed. Figure 7.1 shows another similar experiment but with carbon black instead of methylene blue dyed particles shown in Figure 3.6, showing that particles of a different composition and density can also be mixed well. From the tracer studies, it was seen that the particle movement follows down along the walls and up again through the center of the bed. This cycle is illustrated in Figure 7.2.
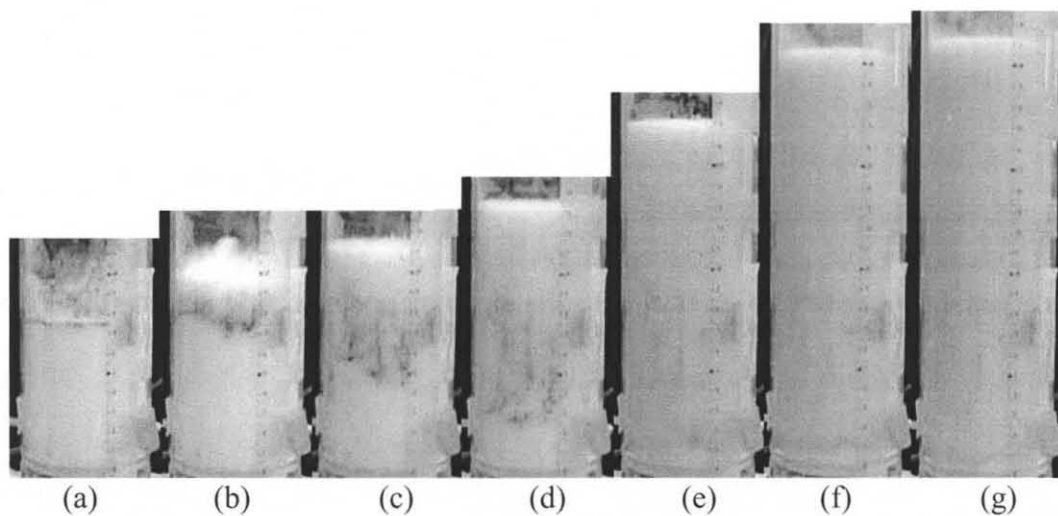

| (a) | (b) | (c) | (d) | (e) | (f) | (g) |

Figure 7.1 Progression of mixing of carbon black particles during aerated vibrofluidization (Γ=3, f = 50 Hz) of Silica R974 with time (s): (a) 0, (b) 7, (c) 13, (d) 18, (e) 25, (f) 36, (g) 63. Aeration of a vibrated fluidized bed was started at t=0, and the figure panels show simultaneous bed expansion and mixing.
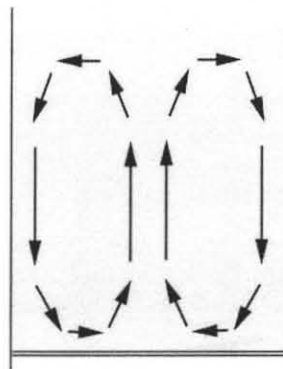

Figure 7.2 Direction of circulation of powders in the fluidized bed.

Silica R974 was also mixed with Titania P25 in the vibrated assisted fluidized bed. The two powders were layered in one set of experiments as shown in Figure 7.3. The layering did not make a significant difference in quality of mixing as opposed to having one powder above the other in the bed. It is believed that the agglomerates are dynamic, i.e., they do not retain their integrity during fluidization and that they break and form again
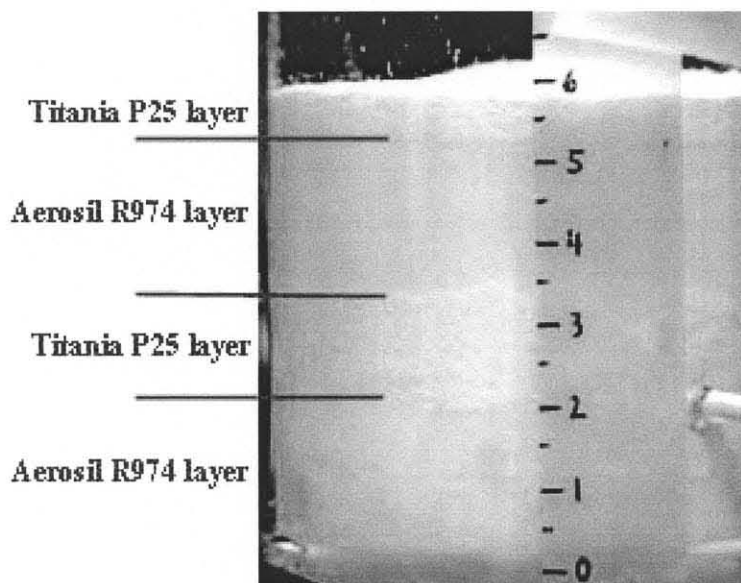

Figure 7.3 Photograph of layers of Titania P25 and Aerosil Silica R974, prepared for a mixing experiment.

rapidly, thus resulting in intimate mixing. The degree of mixing was very high, which is supported by several SEM/EDX and TEM/EELS analyses shown in Figure 7.4 and Figure 7.5. Titania P25, due to is crystalline structure, is generally brighter and whiter than Silica R974 in the SEM images, which has been verified by EDX analyses. The images in Figure 7.4 and Figure 7.5 show that the agglomerates were well mixed and EDX, SEM, TEM images show evidence of mixing on the nanoscale, indicating that vibrofluidization could be used to mix agglomerates of different species of nanoparticles.
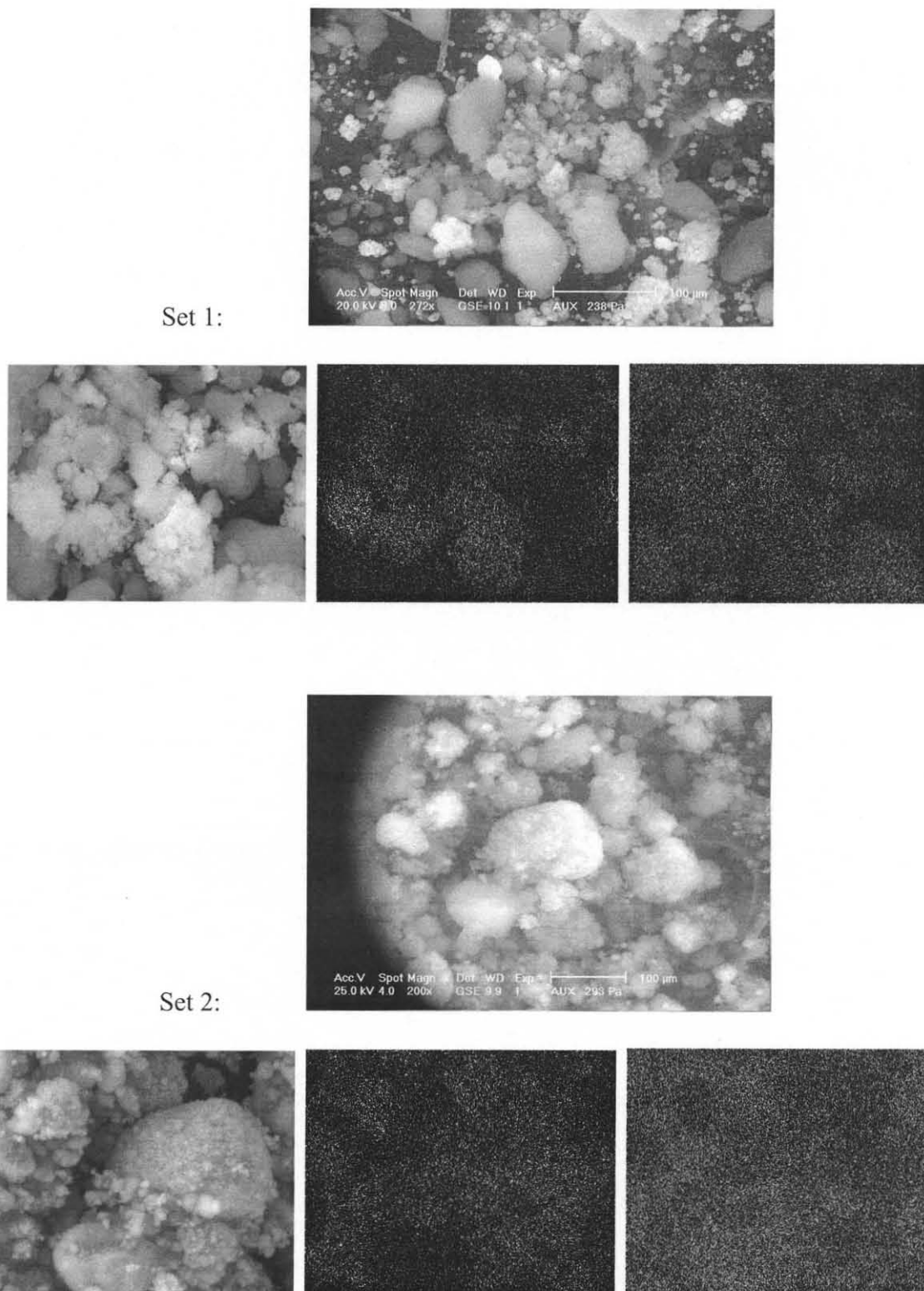
Set 1:

Set 2:

Figure 7.4 Two sets of SEM and EDX analyses of the mixture between Silica R974 and Titania P25. In each set: (Top): original SEM image, (Bottom right): image used for EDX analysis, (Bottom center): particles of Titania P25, (Bottom right): particles of Silica R974.
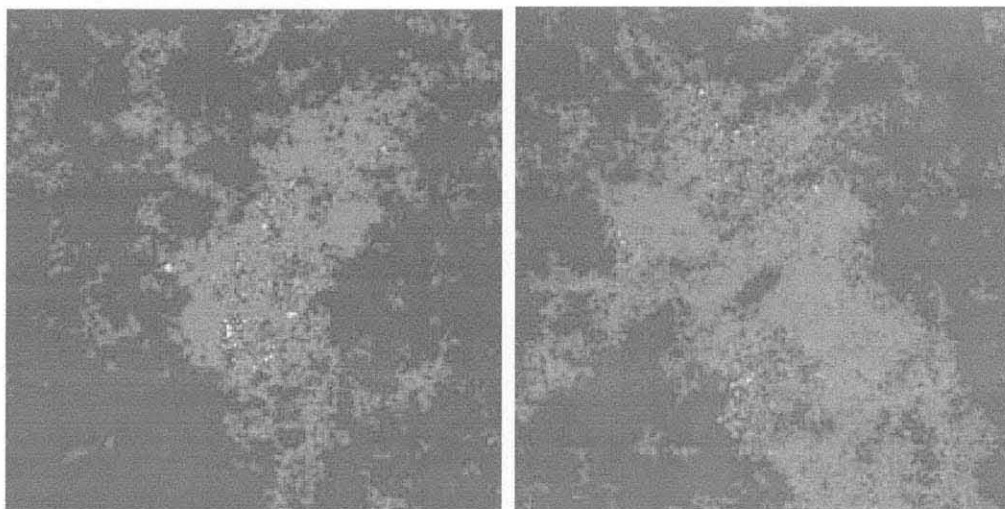
Figure 7.5 TEM analyses of the mixture between Silica R974 and Titania P25 from vibrofluidization experiments ($\Gamma = 3$, f = 50 Hz).
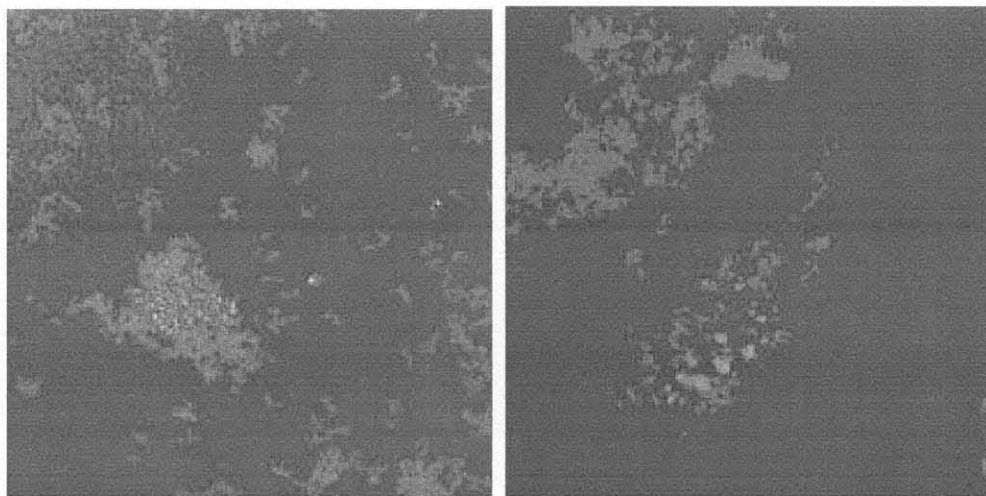
Figure 7.6 TEM analyses of the mixture between Silica R974 and Titania P25 from magnetically assisted fluidization experiments.

Figure 7.6 shows TEM images from mixing experiments of Silica R974 and Titania P25 in a magnetically assisted bed. The images are similar to those from Figure 7.5 and make it difficult to quantify exactly which method of fluidization is the better mixer over the other. Hand shaken mixtures and conventional fluidization showed poor intimate mixing on the nanoagglomerate level, which indicates that the presented methods of

assisted fluidization of nanoparticles do indeed offer an advantage. Although there is evidence of nano-scale mixing (see Figure 7.5 and Figure 7.6), further research is needed to systematically determine on which length scale intimate mixing of different species of nanoparticles can be achieved.
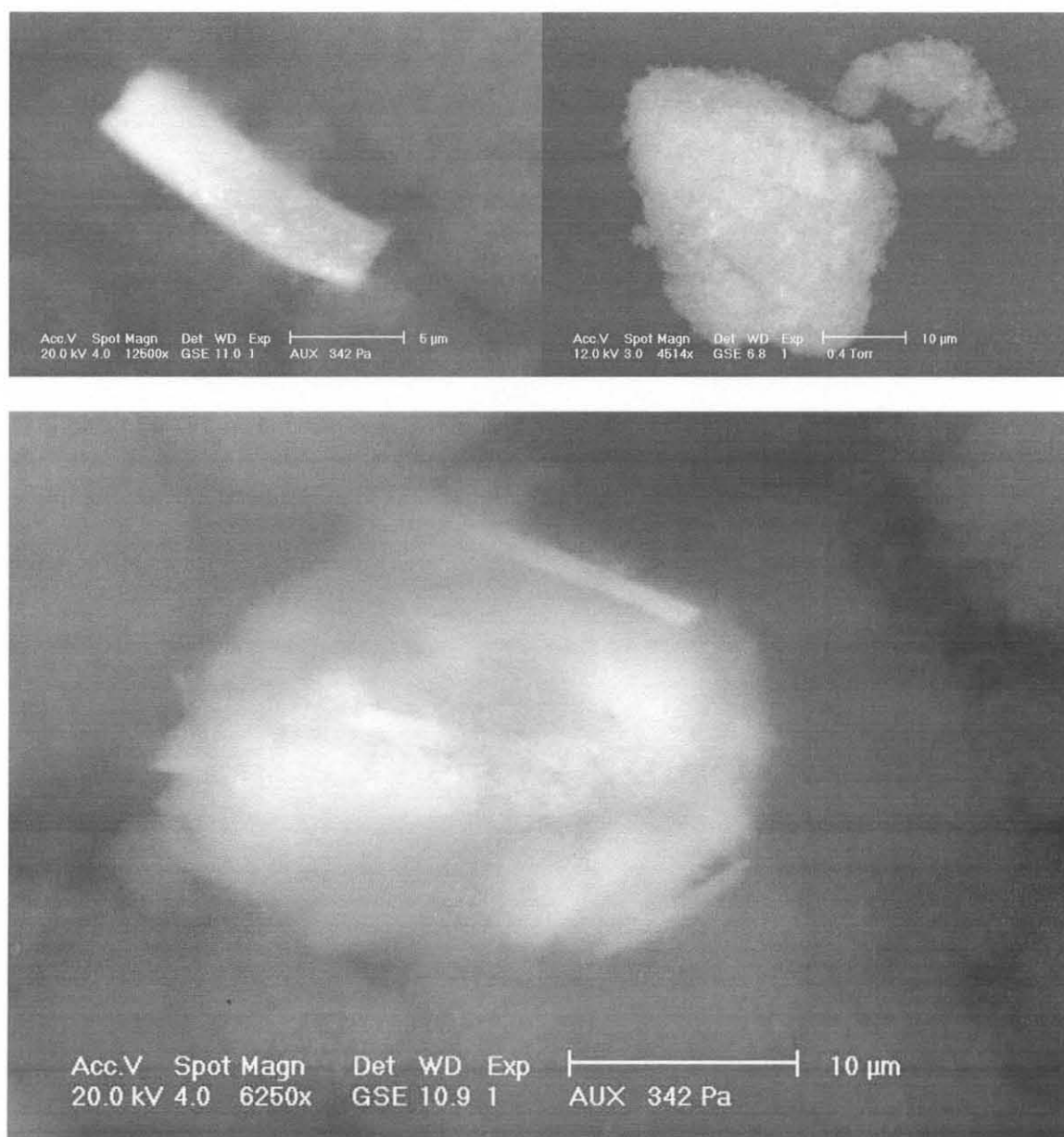

Figure 7.7 SEM analysis of Molybdenum Oxide (top left), Silica R974 agglomerate (top right), and an agglomerate showing the mixture between Silica R974 and Molybdenum Oxide from vibrofluidization experiments.

7.2 Filtration

Since the nanoagglomerates are very porous, there is a significant amount of surface area for its size. In this way, it is believed that the pores could possibly retain aerosols such as dust or mist. There are no studies available in the literature that examine porous nanoagglomerates as a filter media. However, there are several studies that research filter media for filtration of aerosols.

Smith (1993), for example, studied the progress and acceptance rates of rigidized filter media, which can preserve their surface area despite continuous pulse cleaning. Smith found that rigidized filters accounted for a small portion of the market at the time, but predicted that their use would grow rapidly, and highlighted the conditions under which the rigidized media outperformed traditional media.

Kanaoka and Kishima (1997) studied the accumulation and release of 1.9 micron mean diameter dust particles in a ceramic filter by measuring the pressure drop across the filter under various conditions. They identified three stages of accumulation in which the dust first forms a dense layer, followed by a loose layer, followed by a final layer of average density. The efficiency of dust expulsion during the cleaning process was found to depend on the density of the dust layers and pressure of the cleaning air.

Maus and Umhauer (1997) examined the efficiency of fibrous filter media on biological and non-biological particles in the range of 0.5 to 30 microns, both theoretically and experimentally. Their apparatus used a high-pressure xenon lamp and optical particle counters to measure the number of particles before and after the filter. They found that non-biological and biological particles of the same size behaved similarly under the test conditions, and that the measured efficiencies matched well with

their theoretical models.

Yu and Liu (2004) applied a fractal analysis to model the permeability of porous media. Their model shows that the relative permeability depends on saturation of the media, a pore fractal dimension, and a tortuosity fractal dimension. These fractal dimensions allowed the model to represent the complex structures of pores in some porous media by two metrics.

Marre, et al. (2004) created a simple and effective model of sintered granular membrane filters to estimate filtration efficiency. By approximating the filter shape as a rectangular lattice and tuning the model with parameters representing the structural tortuosity and effective kinetic coefficient of particle adsorption, the model provides accurate estimates without the computational complexity of more sophisticated models.

For this dissertation, a simple experiment was setup to test the principle of using the porous nanoagglomerates as the filter media themselves. A flat, packed bed (1/4" x 6" x 6") of Alumina C nanoagglomerates was used to flow aerosol through, as depicted in Figure 7.8. Dried silicon carbide (~0.5 microns in diameter) was used as the aerosol,
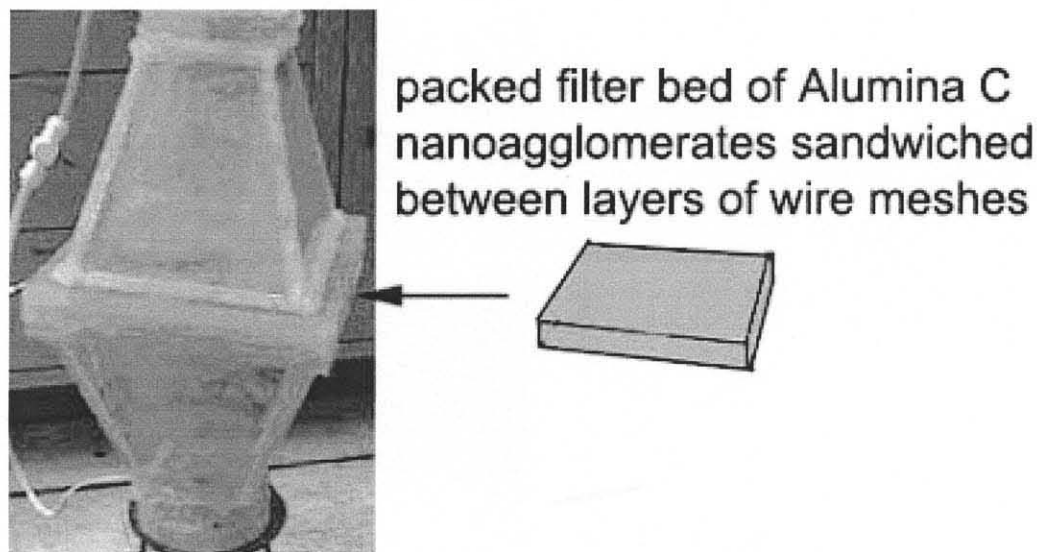

packed filter bed of Alumina C nanoagglomerates sandwiched between layers of wire meshes

Figure 7.8 Photograph and schematic of filtration experiment.

which was sent through a Sympatec RODOS particle disperser and then into the bed. Silicon carbide is brown in color and Alumina C is white in color, which made differentiating between the two easy. Particle size distributions before and after the filter were measured with an Aerosizer and the simple test proved somewhat successful in that over 90% of aerosols were retained in the nanoagglomerates. Evidence of successful filtration can be seen in Figure 7.9 where the region before the filter is covered with aerosol particles and the region after the filter is relatively clear of SiC particles. The post-experiment filter material was analyzed with an SEM and EDX. Figure 7.10 shows these results, where the bright spots and grayer spots have been verified by the EDX to be SiC and Alumina particles, respectively. Since this is not a fluidization
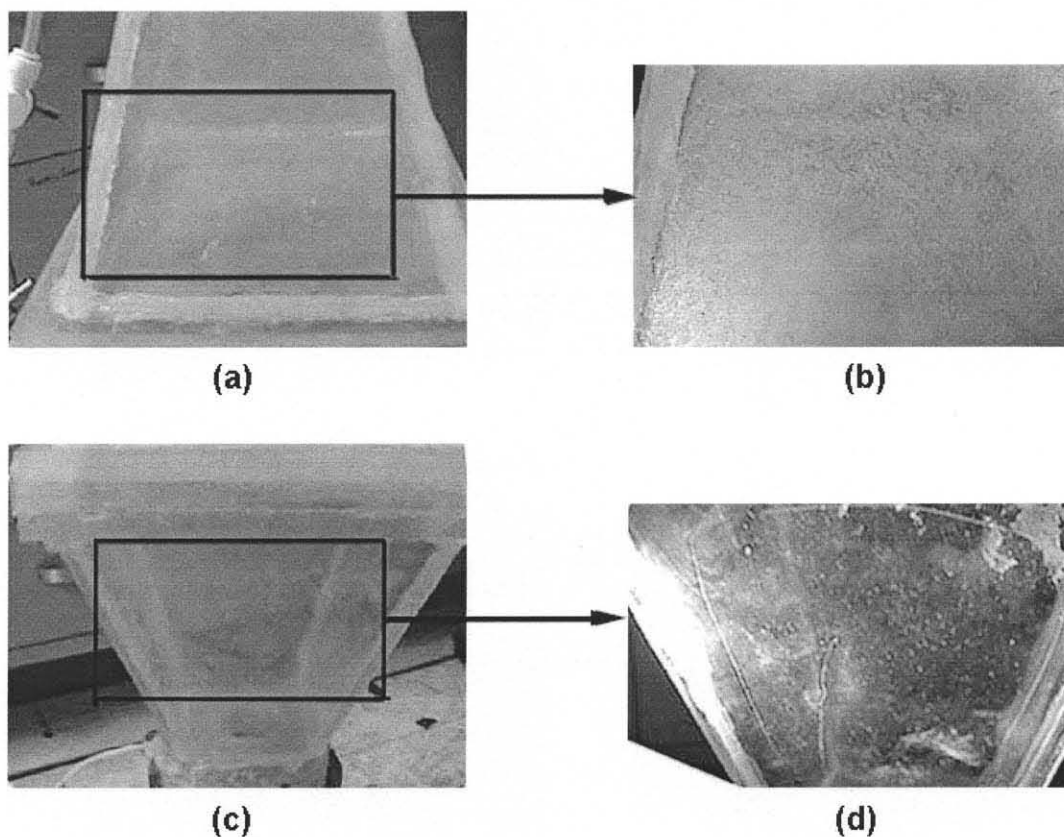

Figure 7.9 Photographs of (a) the area before the filter, (b) a close-up view of the area before the filter, (c) the area after the filter, and (d) a close-up view of the area after the filter.
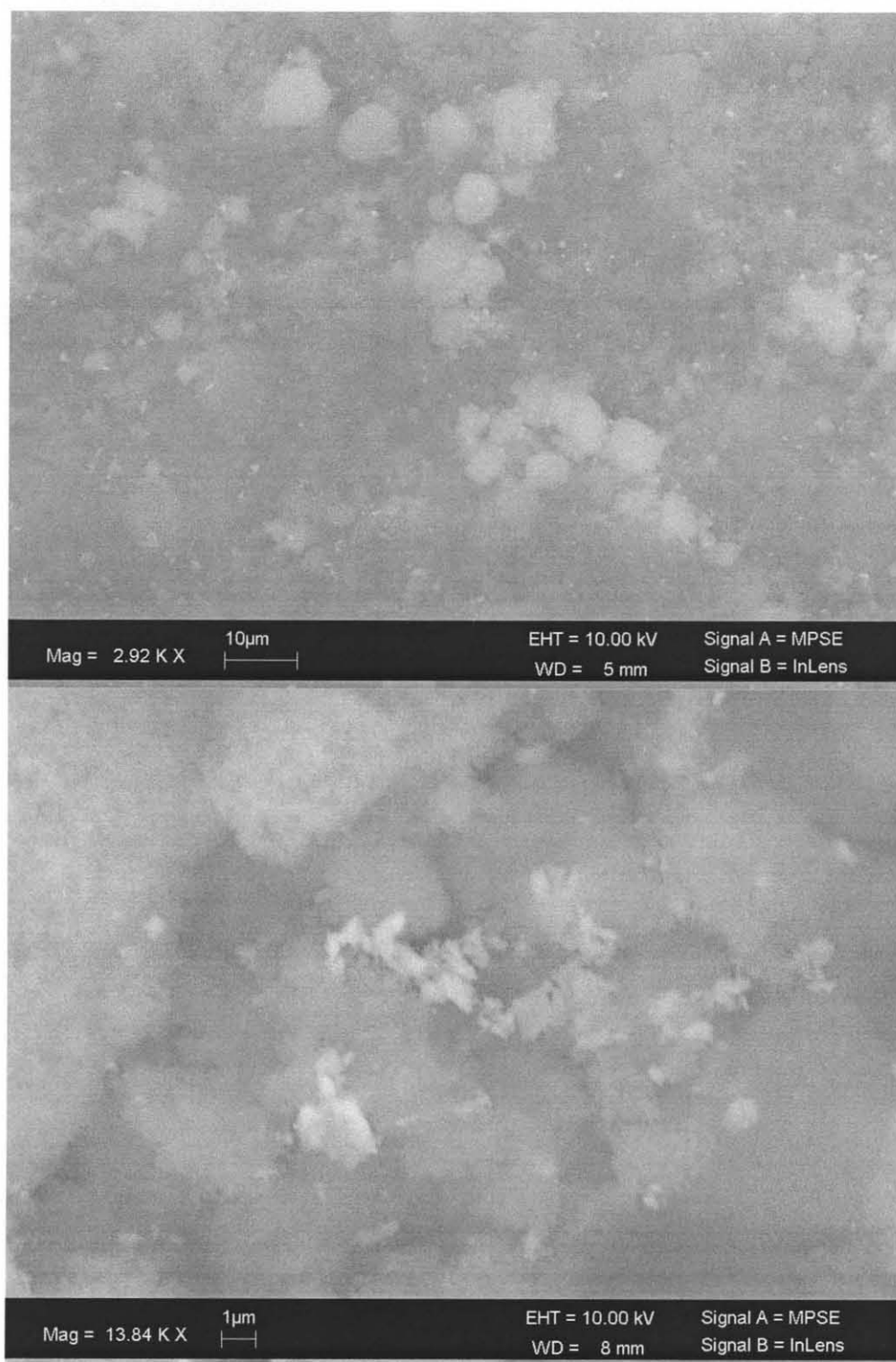
Mag = 2.92 K X   10µm

EHT = 10.00 kV   Signal A = MPSE
WD = 5 mm   Signal B = InLens

Mag = 13.84 K X   1µm

EHT = 10.00 kV   Signal A = MPSE
WD = 8 mm   Signal B = InLens

Figure 7.10 SEM images of post-experiment filter material containing SiC particles (brighter, whiter spots). Grayer agglomerates are Alumina C agglomerates.

experiment, it is out of the scope of the dissertation. However, the idea of using a fluidized bed as the filter should not be dismissed and should be investigated. Other powders should be investigated as well such as Silica R974 whose agglomerates are extremely porous and might be better suited for filtration applications.

It should be noted that nanoagglomerates pose very promising applications. The nanoagglomerates used in this dissertation are very unique in their low bulk density, high specific surface area, and high porosity (~99%). Thus, when used as a filtering media for liquid droplets (mist) the nanoagglomerates will tend to take in the fine droplets into the pores due to capillary action rather than retain them on their outer surface, greatly increasing the filtering capacity as compared to solid granular media. The high surface area poses another advantageous feature for several applications such as in catalysis.

7.3 Coating

The supercritical fluidization of nanoparticles is very promising for coating applications due to the higher pressure and temperature that make it ideal for polymer coatings. Although the in situ images could not show an agglomerate in the process of actually breaking or forming, it is believed that the equilibrium between the agglomerates breaking and forming does occur and is too fast for the CCD camera to capture. A study by Wank et al. (2004) strongly supports the theory that there is a mechanism occurring that involves the constant formation and breakage of agglomerates. Their telling results were from their particle size distribution analysis from their ALD (atomic layer deposition) experiments in a vibrofluidized bed under high pressure. Wank et al. (2004) coated 7-11 micron boron nitride particles through the ALD process in a vibrofluidized bed. In situ

agglomerate photos showed that the fluidized agglomerate sizes can be as large as over 300 microns. Yet, when the particles were analyzed under the SEM and TEM, they saw individual particles coated. They also saw that the size distribution was hardly different than the pre-processed particles. This strongly implies that during fluidization, the agglomerates continually break and re-form such that the ALD process can reach every particle on an individual basis. This makes the fluidization of nanoparticles quite a strong possibility for a method to coat nanoparticles. The various methods for enhancing the fluidization of nanoparticles presented in this dissertation which result in less bubbling, less gas bypassing and less elutriation would then be very good options to choose from when designing coating systems.

CHAPTER 8

CONCLUSIONS

8.1 Closing Remarks

The fluidization of ultrafine (<20 μm) particles, which are also known as Geldart group C particles, is possible due to the formation of nanostructures or agglomerates. The formation of agglomerates affects the bulk properties of the powder and is essential for many powder processes since agglomerates flow more easily, produce less dusting, and are easily dispersed into individual particles. From recent studies, the properties of the primary particles determine the properties of the agglomerates as well as the behavior of fluidization. Two different fluidization behaviors of nanoparticles have been observed thus far: agglomerate bubbling fluidization (ABF) and agglomerate particulate fluidization (APF). At low superficial gas velocities, a bed of cohesive powders is in the channeling or plug formation mode. When the superficial gas velocity is raised, however, the bed is disrupted to form agglomerates of different sizes. If bubbles are seen and vigorous fluidization of the agglomerates takes place, the type of fluidization is ABF. If bubbles are not seen and smooth, liquid-like fluidization of the agglomerates takes place with very high bed expansion ratios, the type of fluidization is APF. These different modes of nanoagglomerate fluidization were coined by Wang et al. (2002).

It was shown in this dissertation that nanoparticles fluidize in the form of agglomerates and that the quality of fluidization can be significantly enhanced with external forces. The external forces should not be limited to vibration, magnetic assistance, and rotation and the variation in conditions should not be limited to increasing

pressure and temperature. There are other forces such as acoustic waves or gas pulsing that can be just as suitable for certain systems of powders. The key find is that it was clearly observed that fluidization assistance such as vibration helped to disrupt the interparticle forces that are prevalent in group C powders such as the nanoparticles used in this study. The nanoparticles with higher bulk or particle properties tended to exhibit Geldart group B (bubbling, ABF) fluidization behavior and the nanoparticles with lower bulk and particle properties tended to exhibit Geldart group A fluidization behavior (aeratable, APF). Using a modified Richardson-Zaki equation and fractal analysis, a model was derived to estimate agglomerate size during fluidization. The results were in close agreement with experiments for all the possible methods of fluidizing nanoparticles except the rotating bed results where experimental verification of the theory could not be done.

The knowledge of the different fluidization phenomena in conventional, vibrating, magnetically assisted, rotating fluidized beds as well as under supercritical conditions will be extremely useful in several applications and processes. Such processes, as mentioned in Chapter 1, include the production of homogenous nanomixtures, nanostructured materials, and coating of nanoparticles to obtain materials with tailored properties. The ultimate goal of this nanoparticle fluidization research is to apply the results from novel techniques and methods to the processing of nanoparticles. Efforts from the experimental and modeling standpoints must be combined to have a fundamental understanding of nanoparticle fluidization and consequently, to make major advancements in this emerging field of nanotechnology.
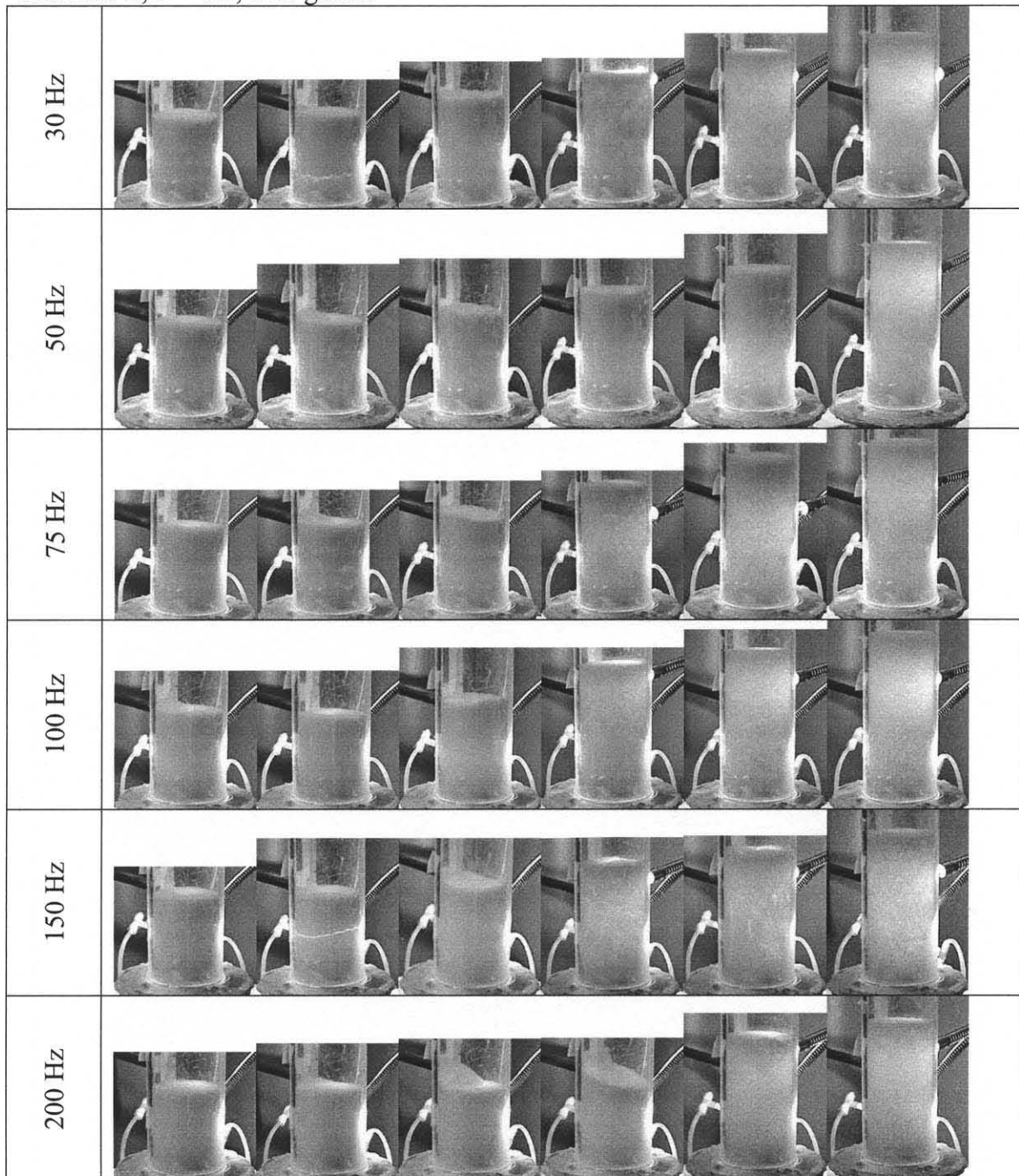
8.2 Recommendations

More particles of more variety in particle and bulk properties should be tested. However, with the current knowledge of nanoparticle fluidization, the applications areas should also be pursued. Scale-up issues should be considered and thus, experimental setups on a pilot scale or larger, would help deepen and clarify the experimental results and theories presented here. The supercritical experiments should be redesigned so that the entire bed could be seen as visual observation is one of the most valuable pieces of information when trying to describe fluidization. Also the pressure drop across the bed at supercritical pressures must be measured more accurately. Filtration experiments should also be tried in a fluidized bed instead of a packed bed and many different nanoagglomerates should be tested.
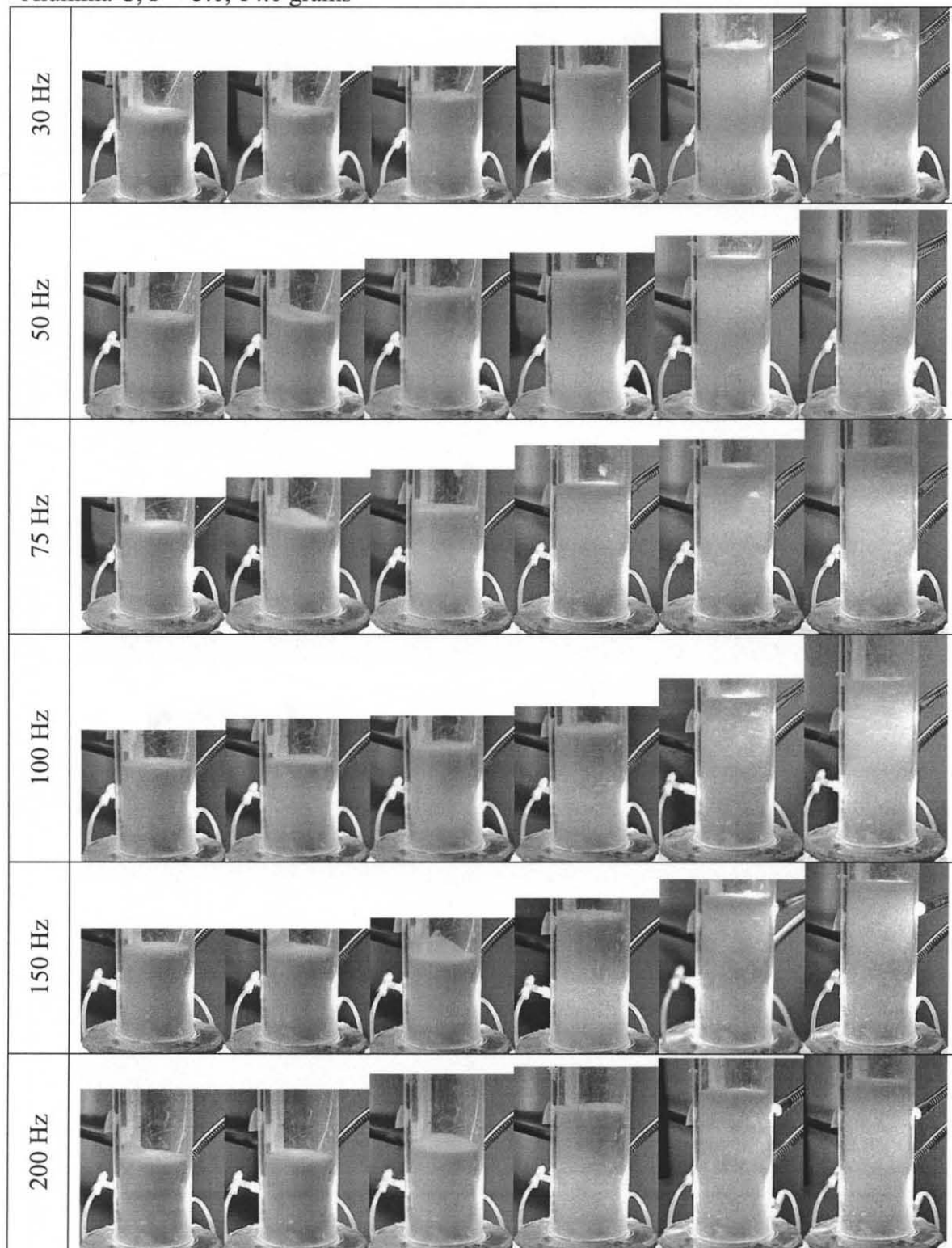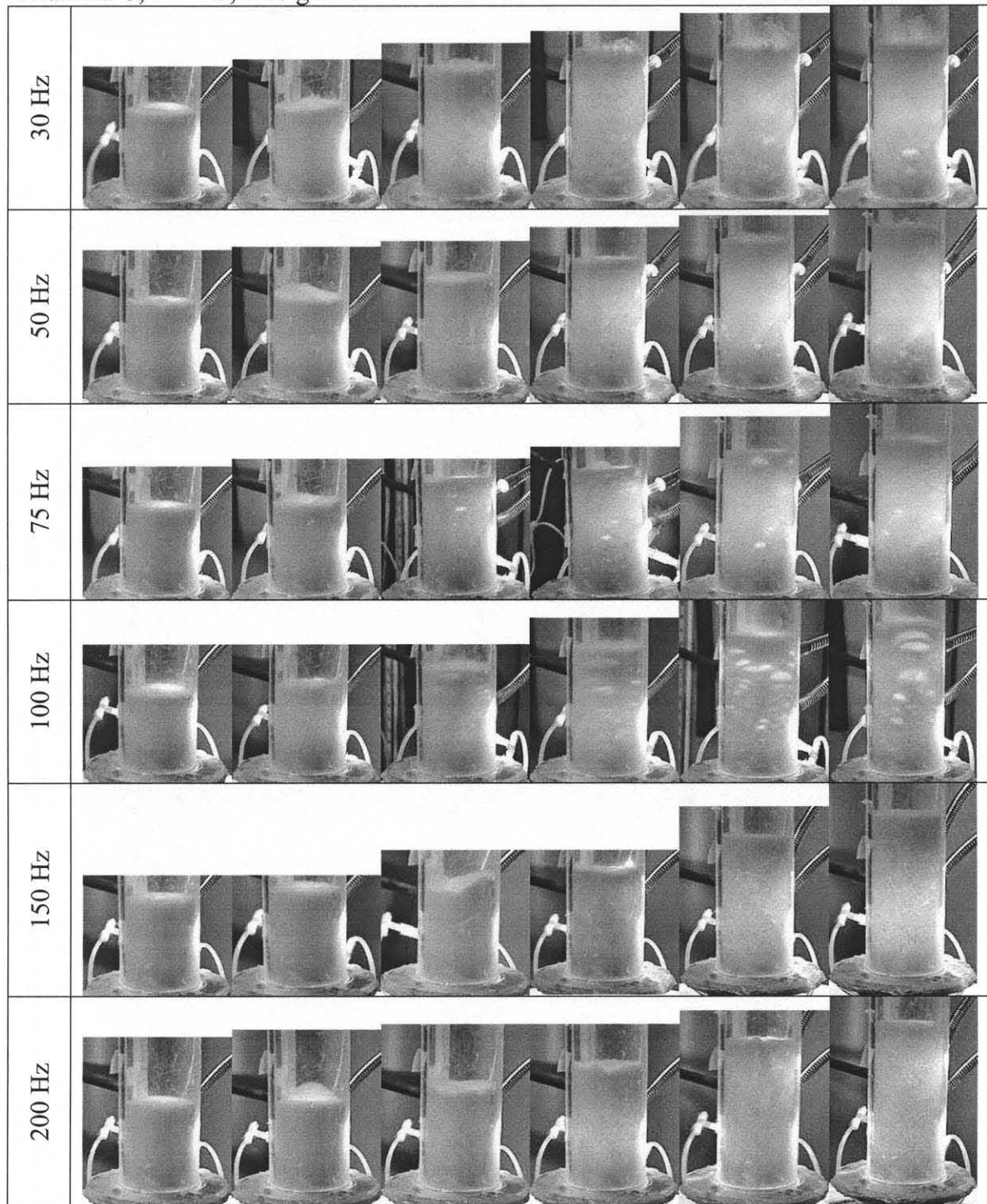
APPENDIX A

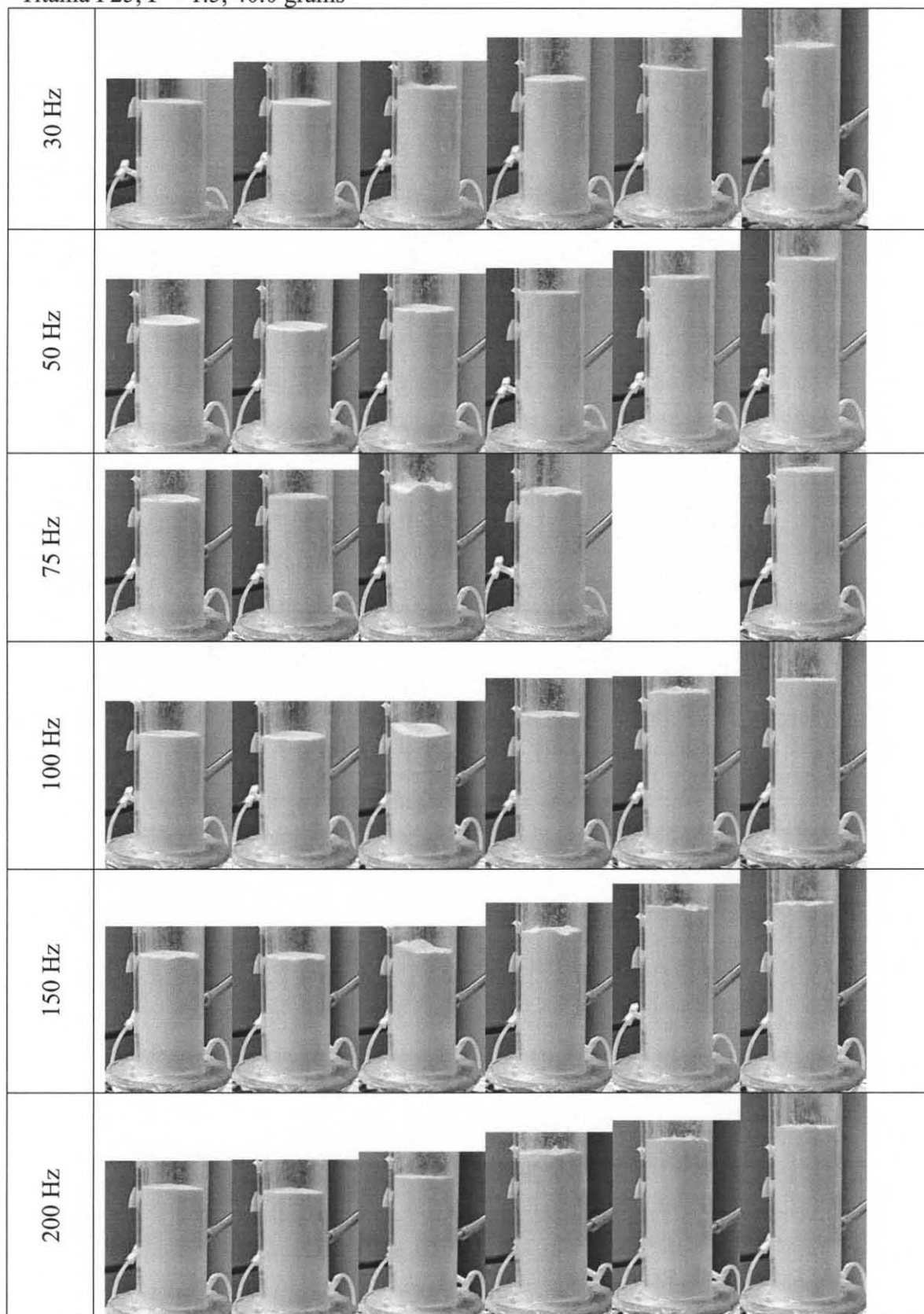## TYPICAL PHOTOGRAPHS OF VIBRATED EXPERIMENTS

The following images are of vibrated experiments with flow rates of (left to right) 0, 0.15, 0.41, 0.71, 1.06, and 1.38 cm/s. Chamber material was lexan and distributor material was wire mesh.
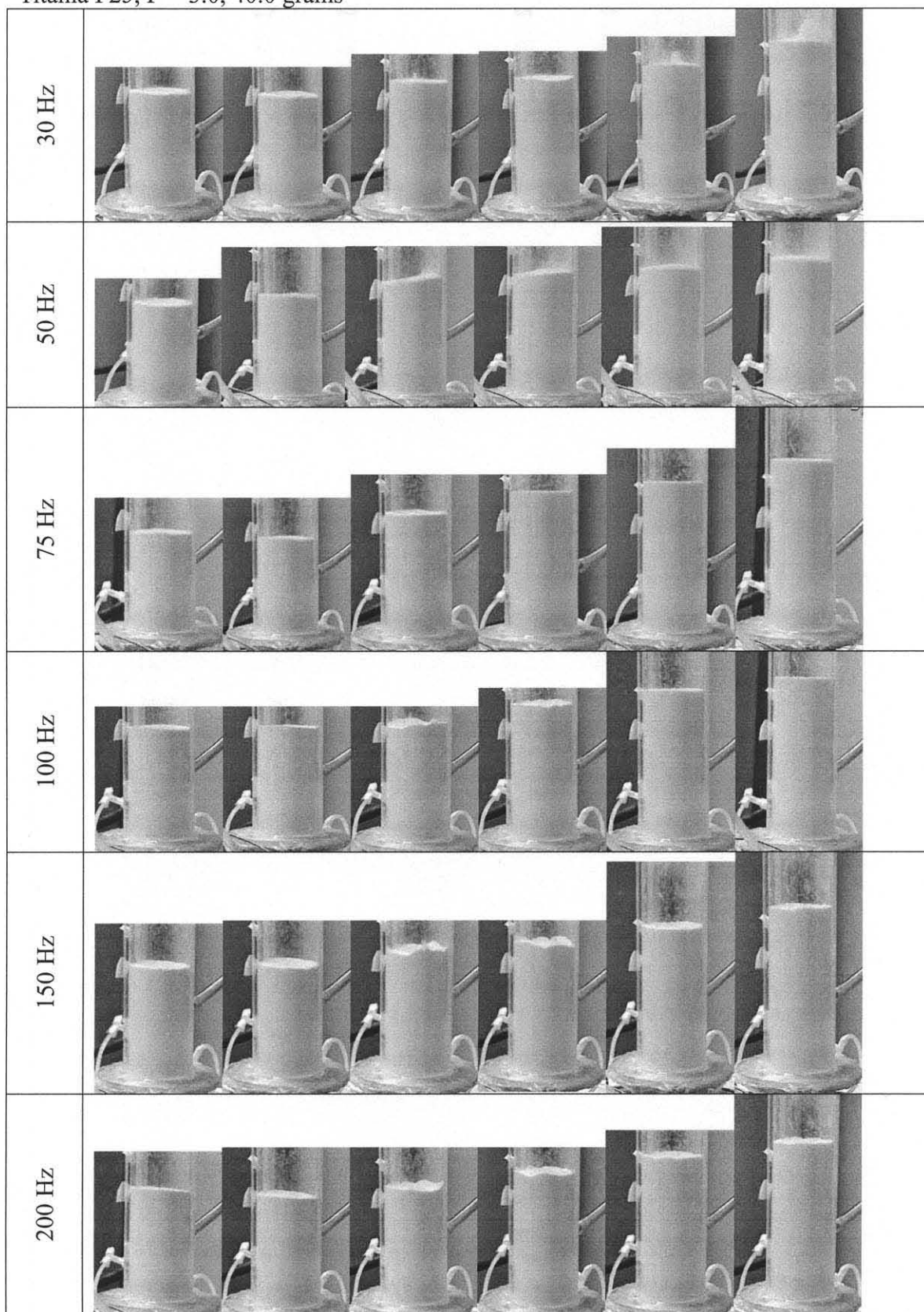
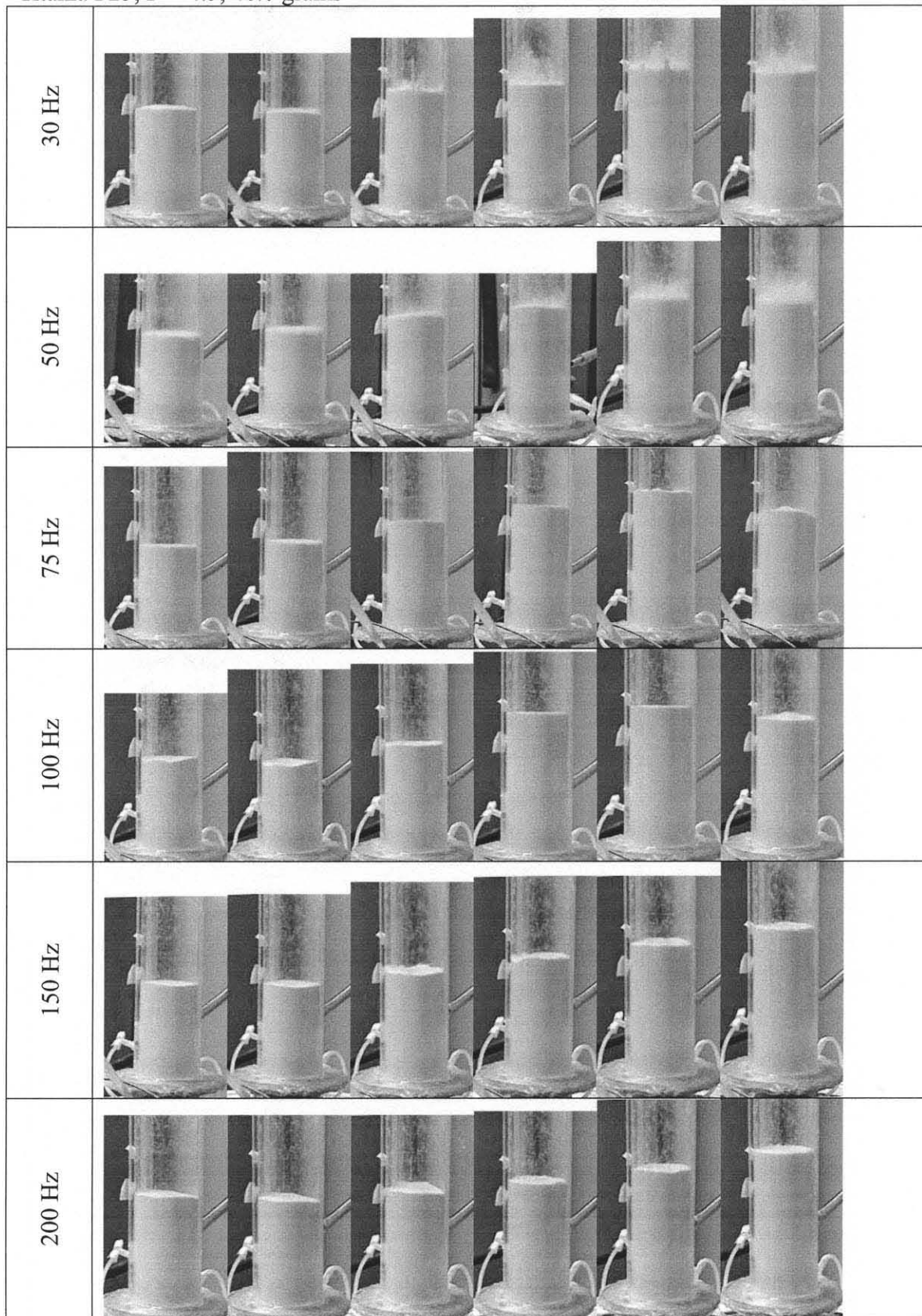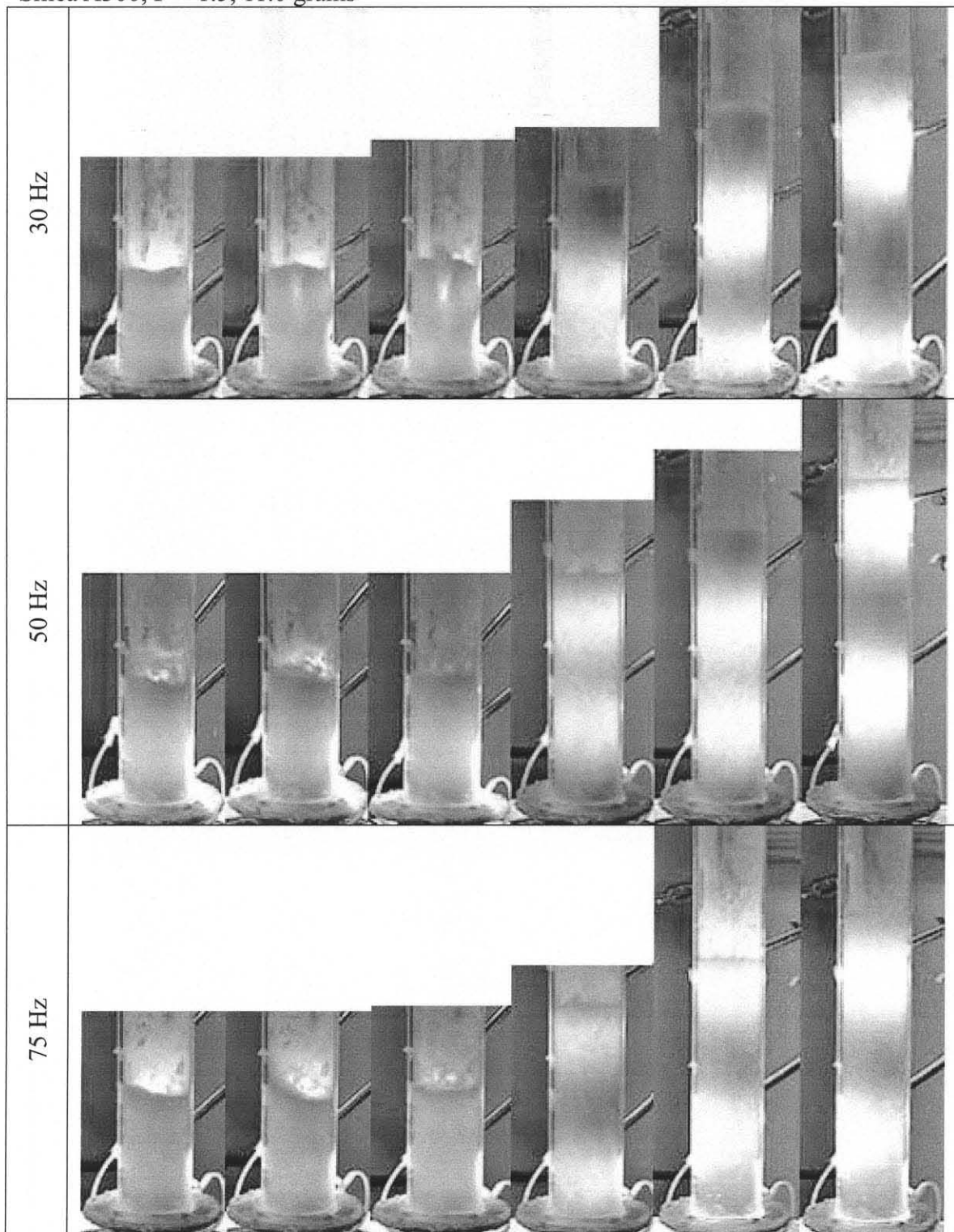Alumina C, $\Gamma = 1.5$, 14.0 grams

Alumina C, Γ = 3.0, 14.0 grams

Alumina C, Γ = 4.5, 14.0 grams

Titania P25, Γ = 1.5, 40.0 grams

Titania P25, Γ = 3.0, 40.0 grams

156

Titania P25, Γ = 4.5, 40.0 grams

157

Silica A300, Γ = 1.5, 11.0 grams
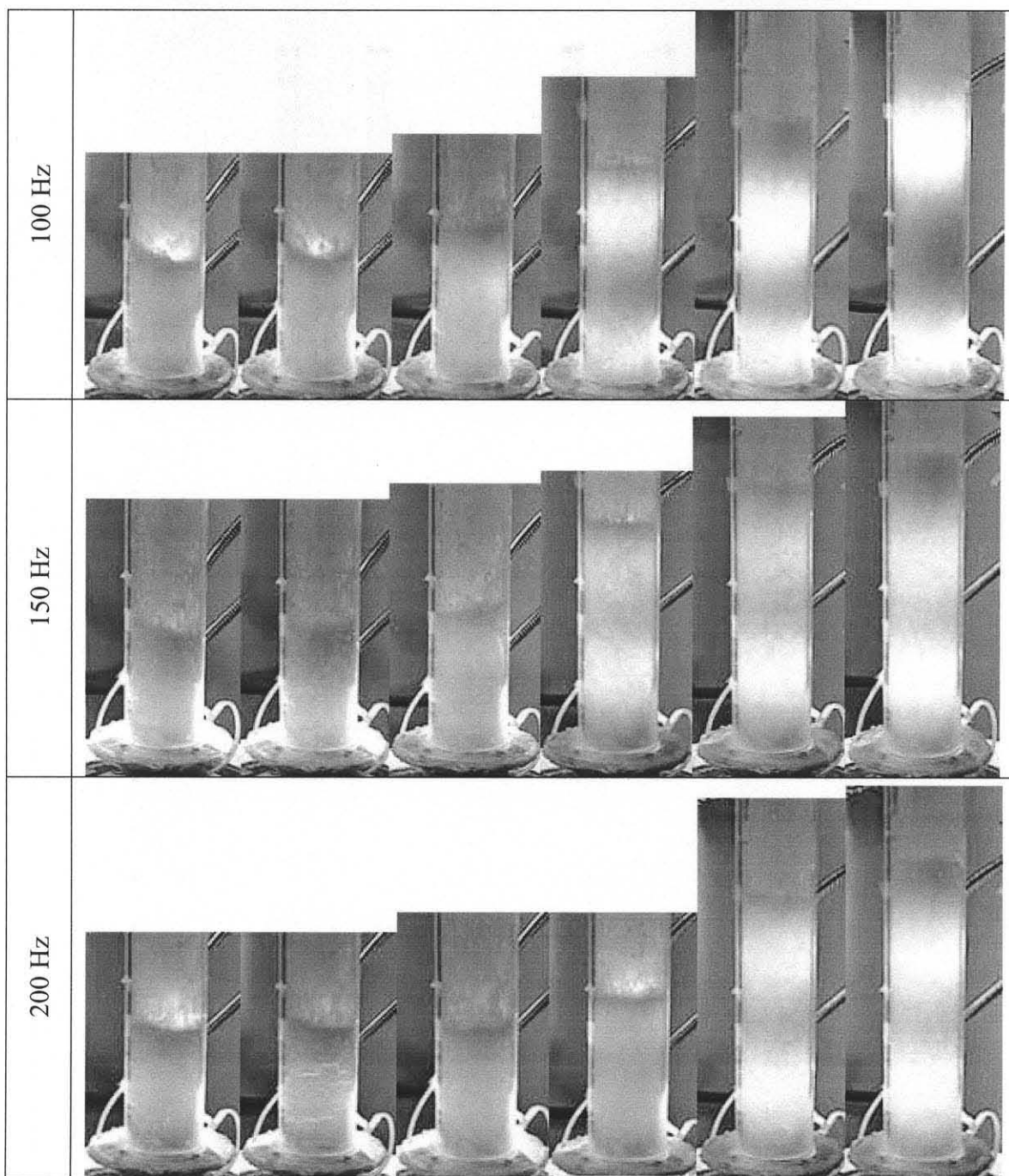
Silica A300, Γ = 3.0, 11.0 grams
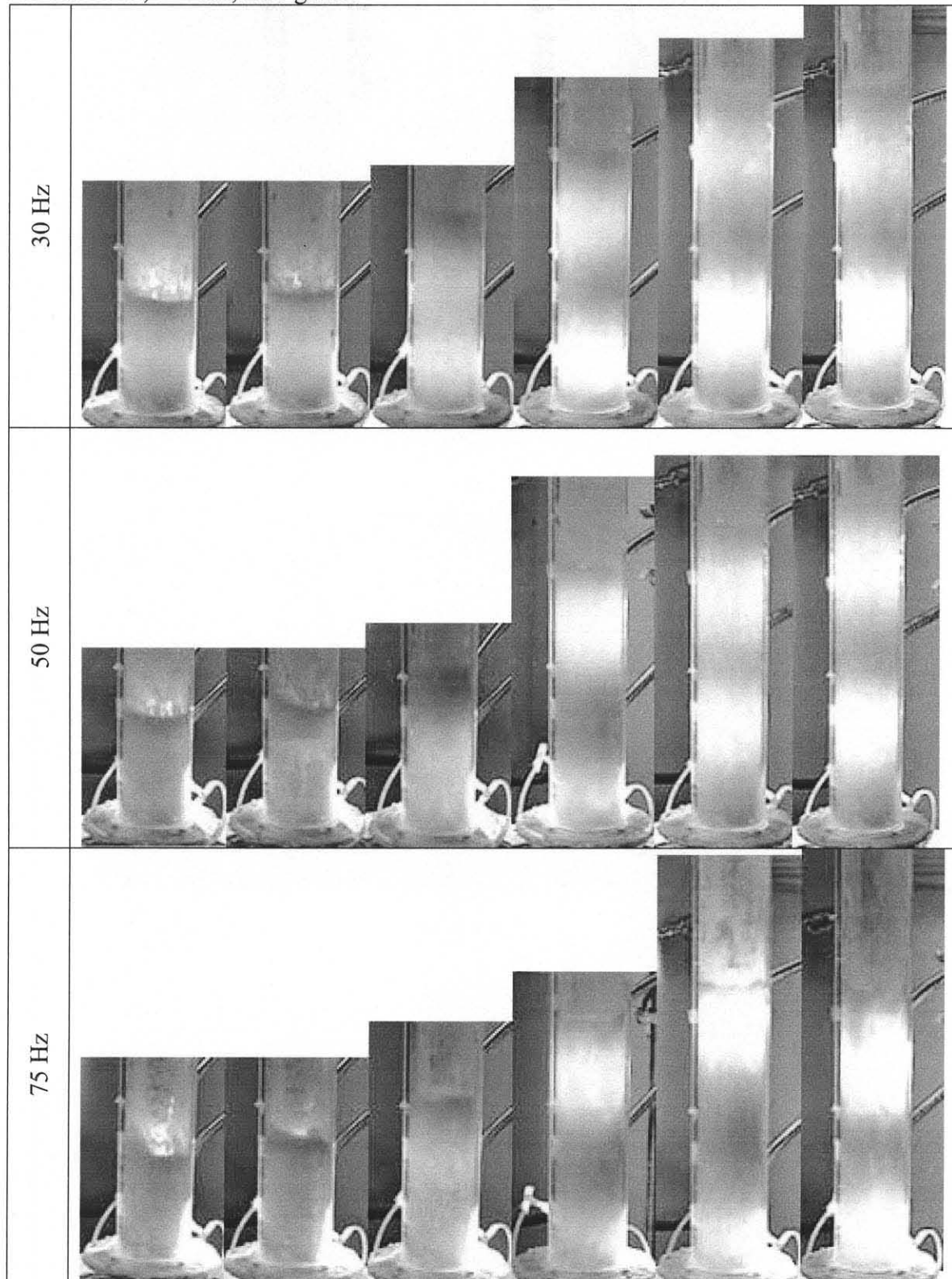
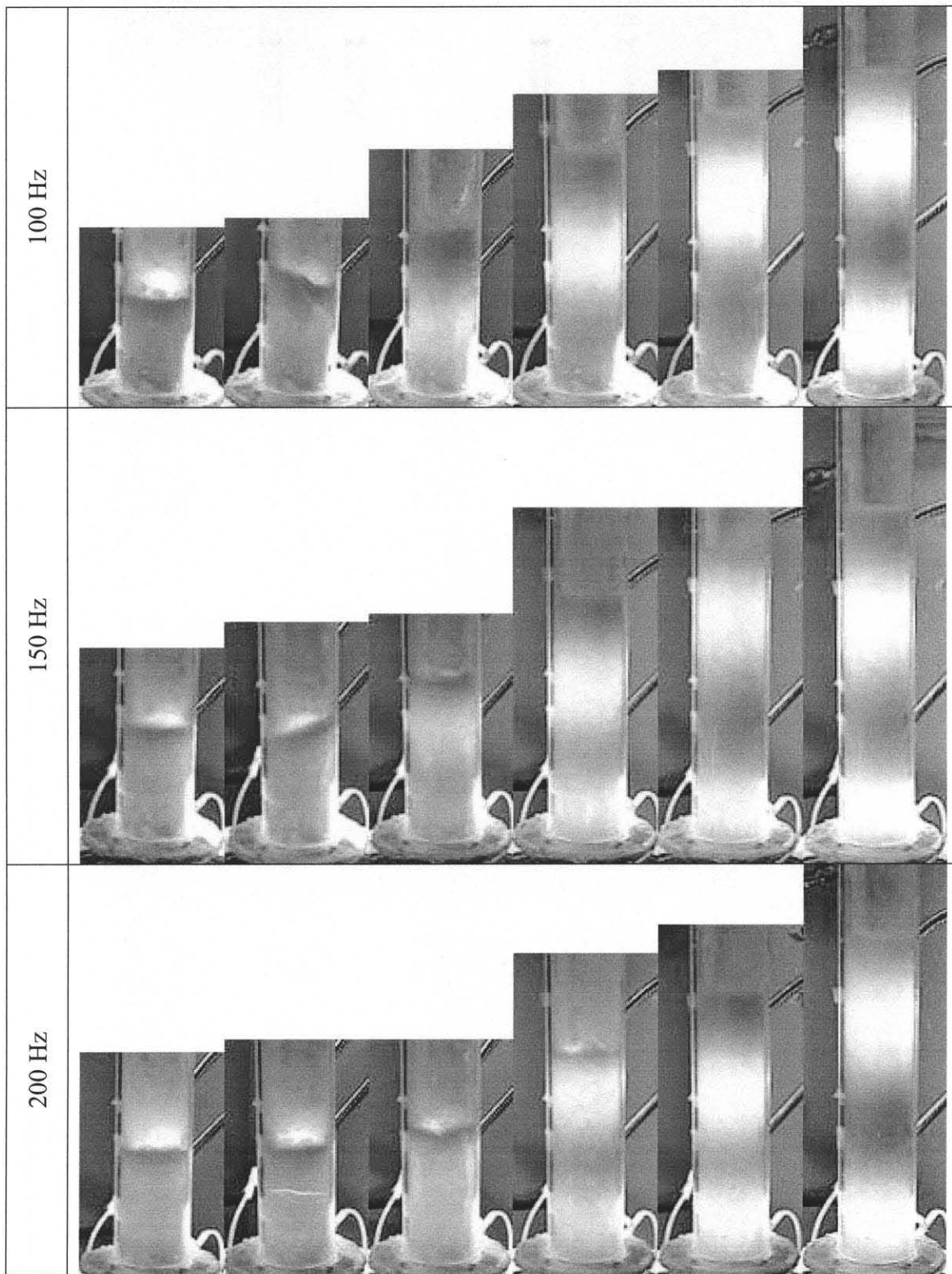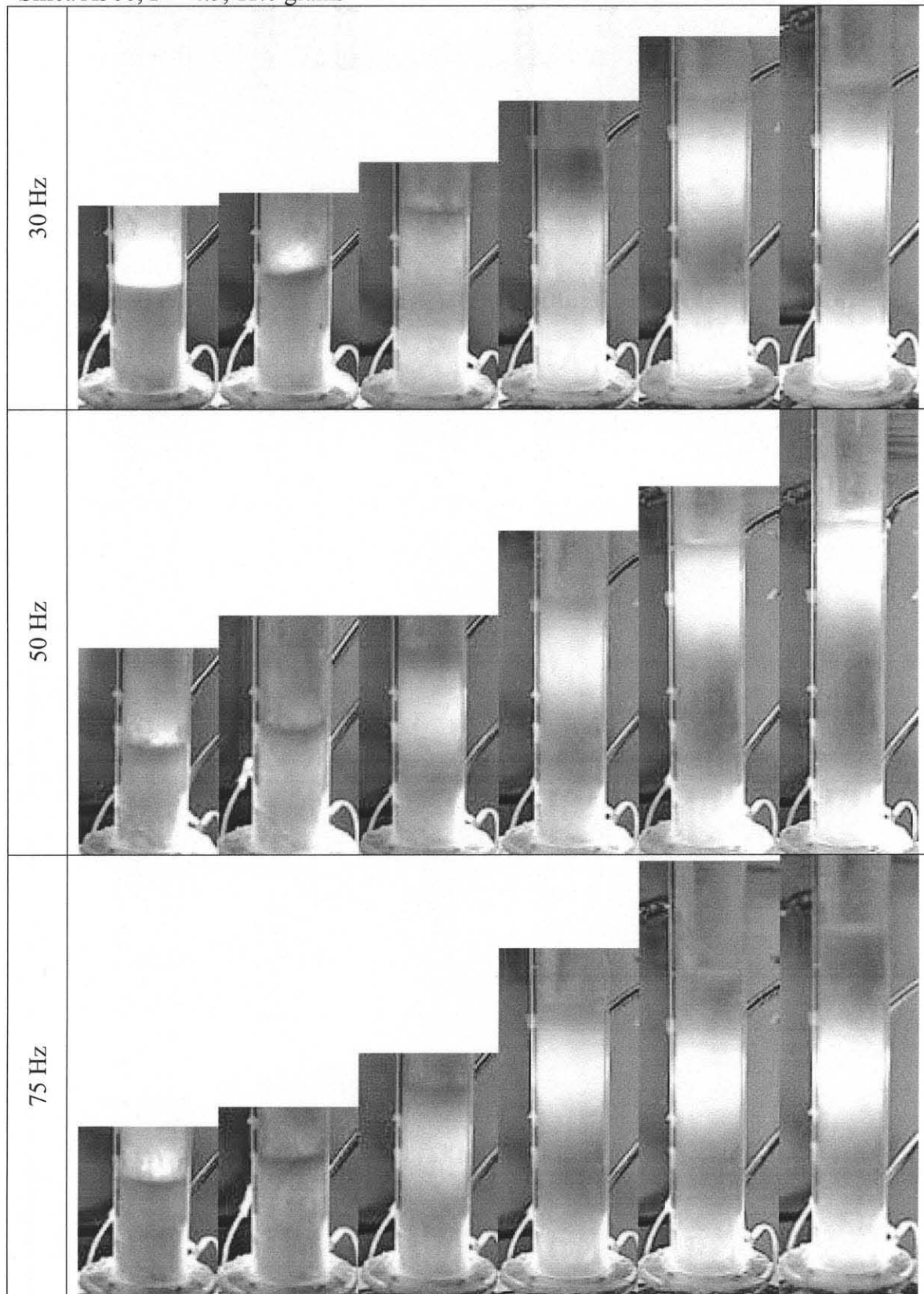Silica A300, Γ = 4.5, 11.0 grams
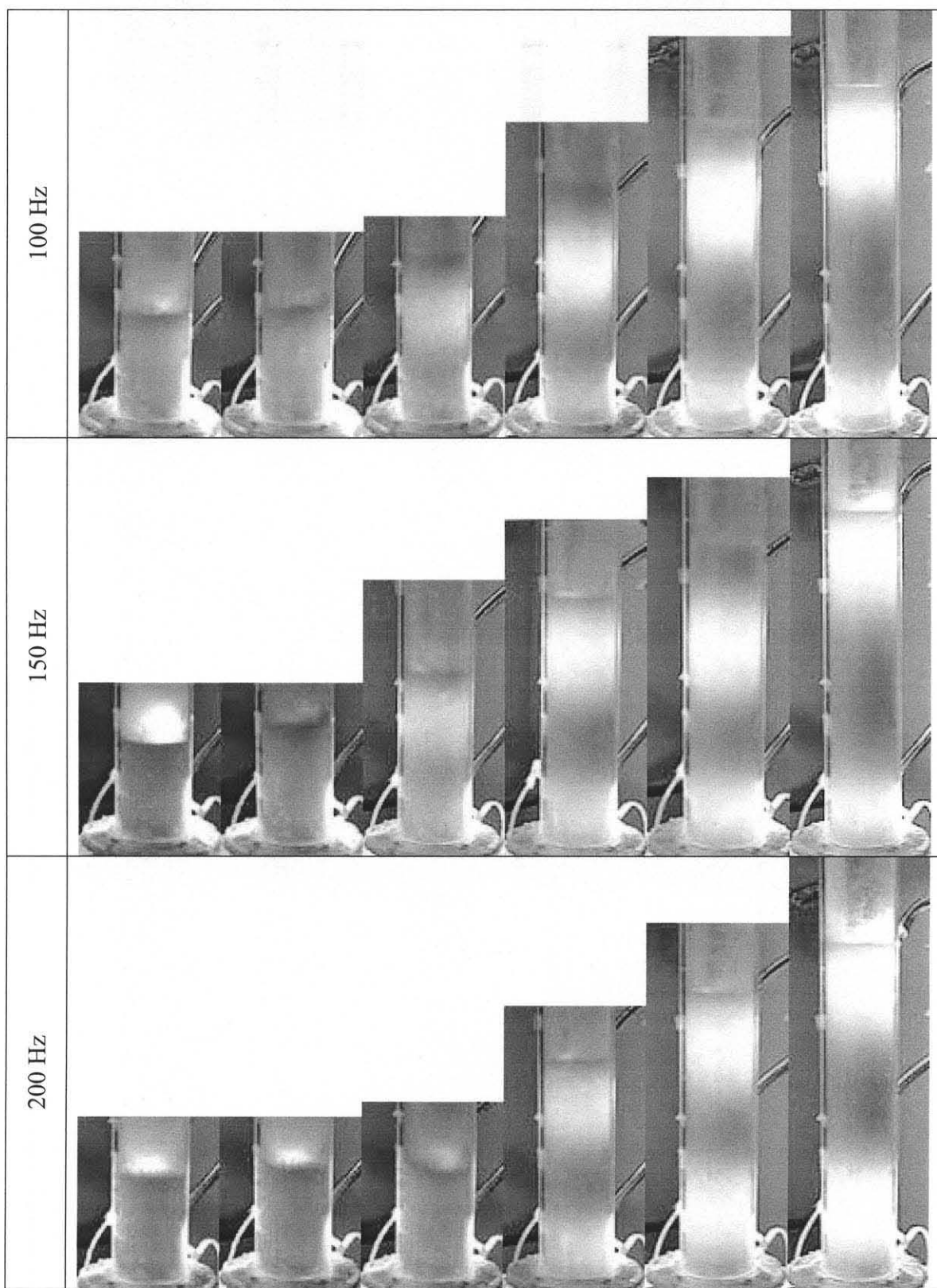
Silica A90, Γ = 1.5, 15.0 grams
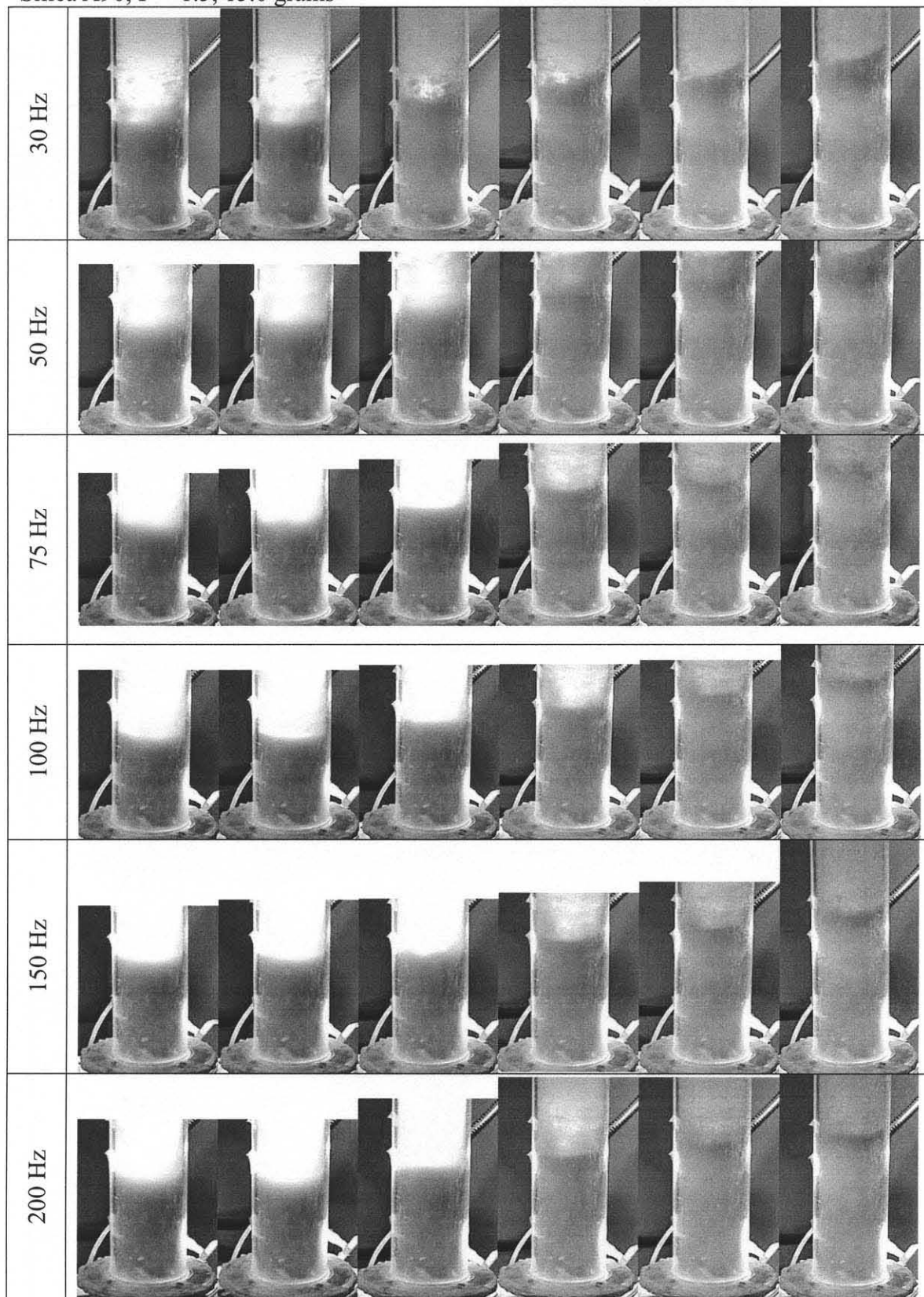
Silica A90, $\Gamma = 3.0$, 15.0 grams
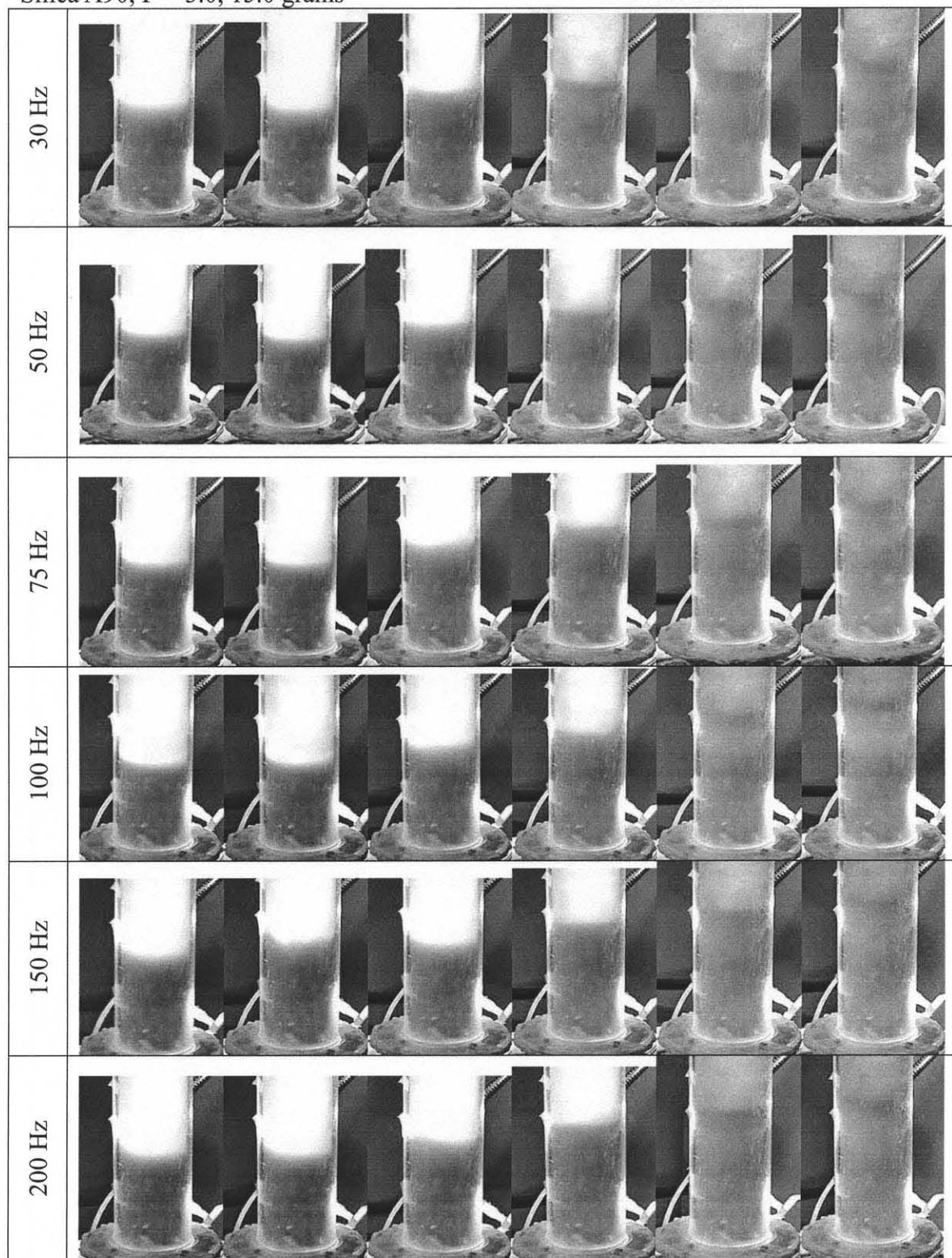
Silica A90, $\Gamma = 4.5$, 15.0 grams

Silica R972, Γ = 1.5, 10.0 grams

100 Hz

150 Hz

200 Hz
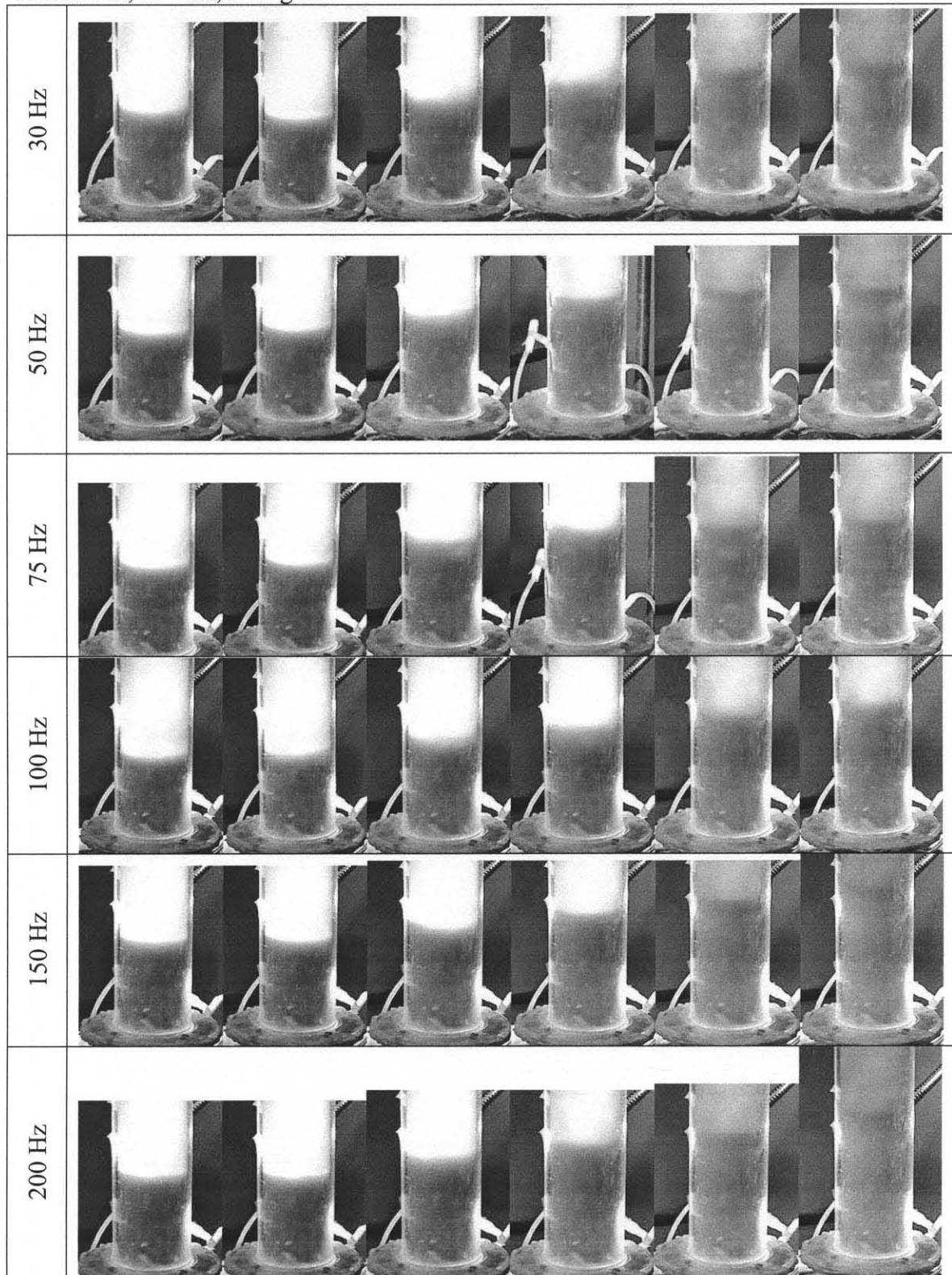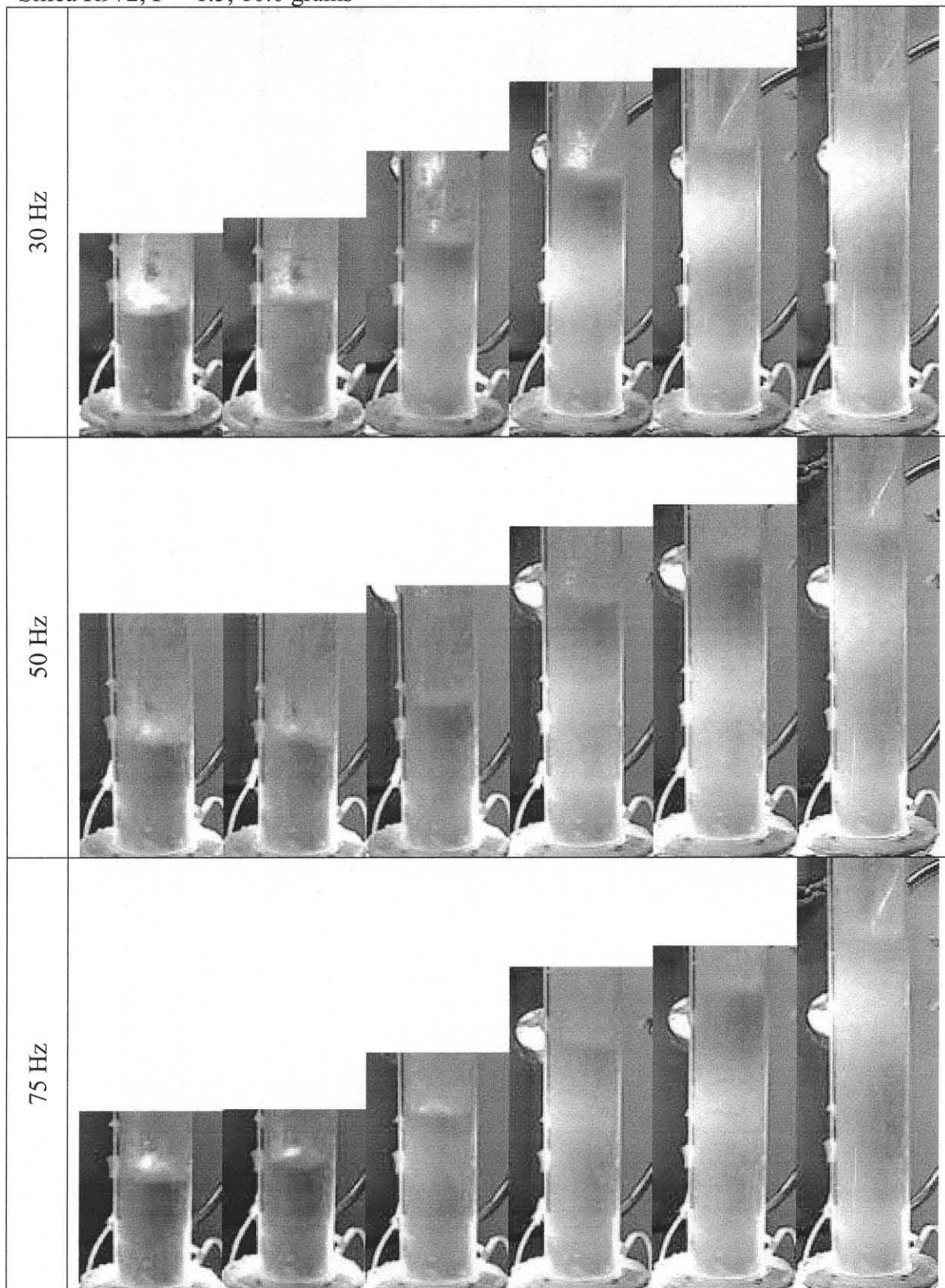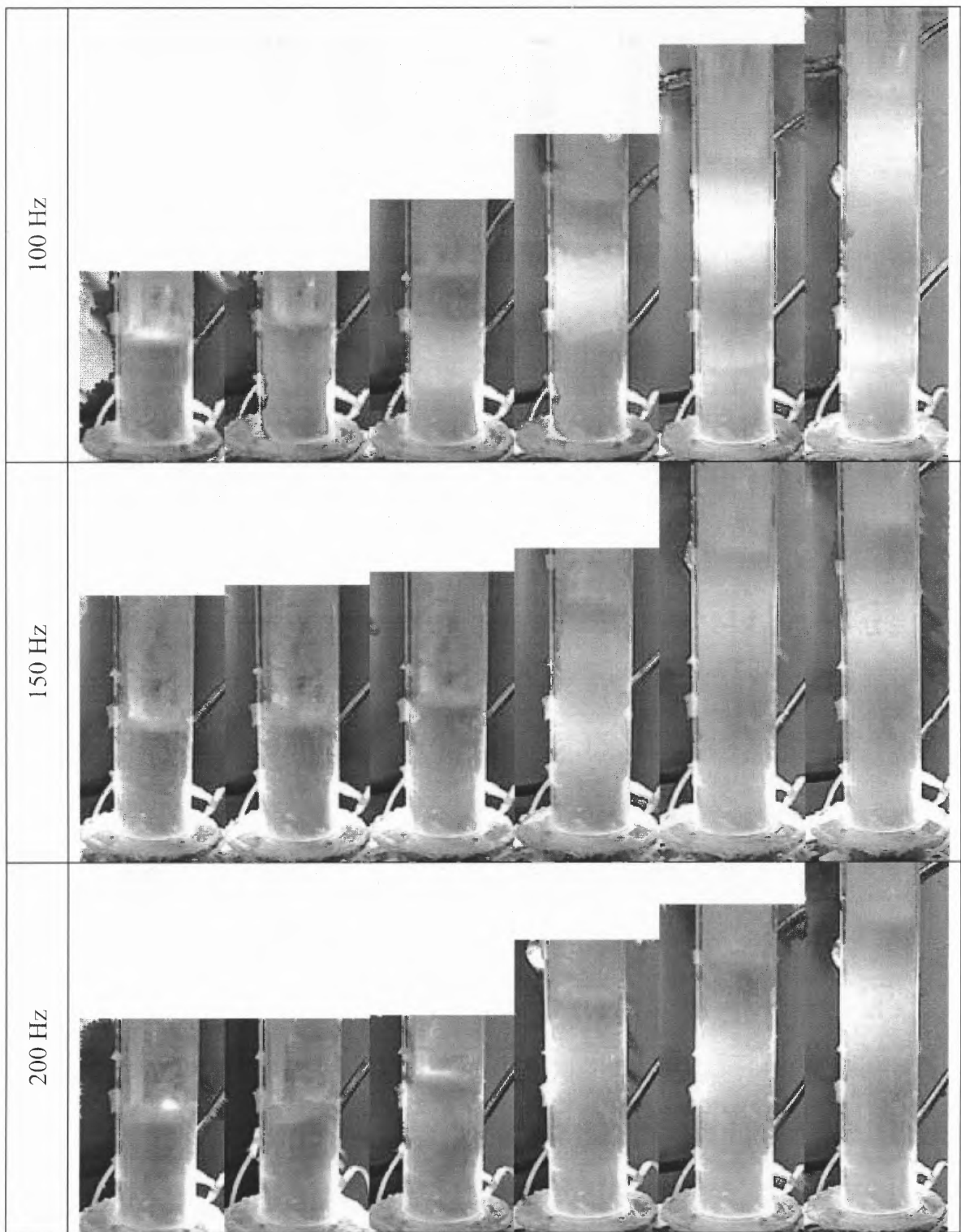
Silica R972, Γ = 4.5, 10.0 grams
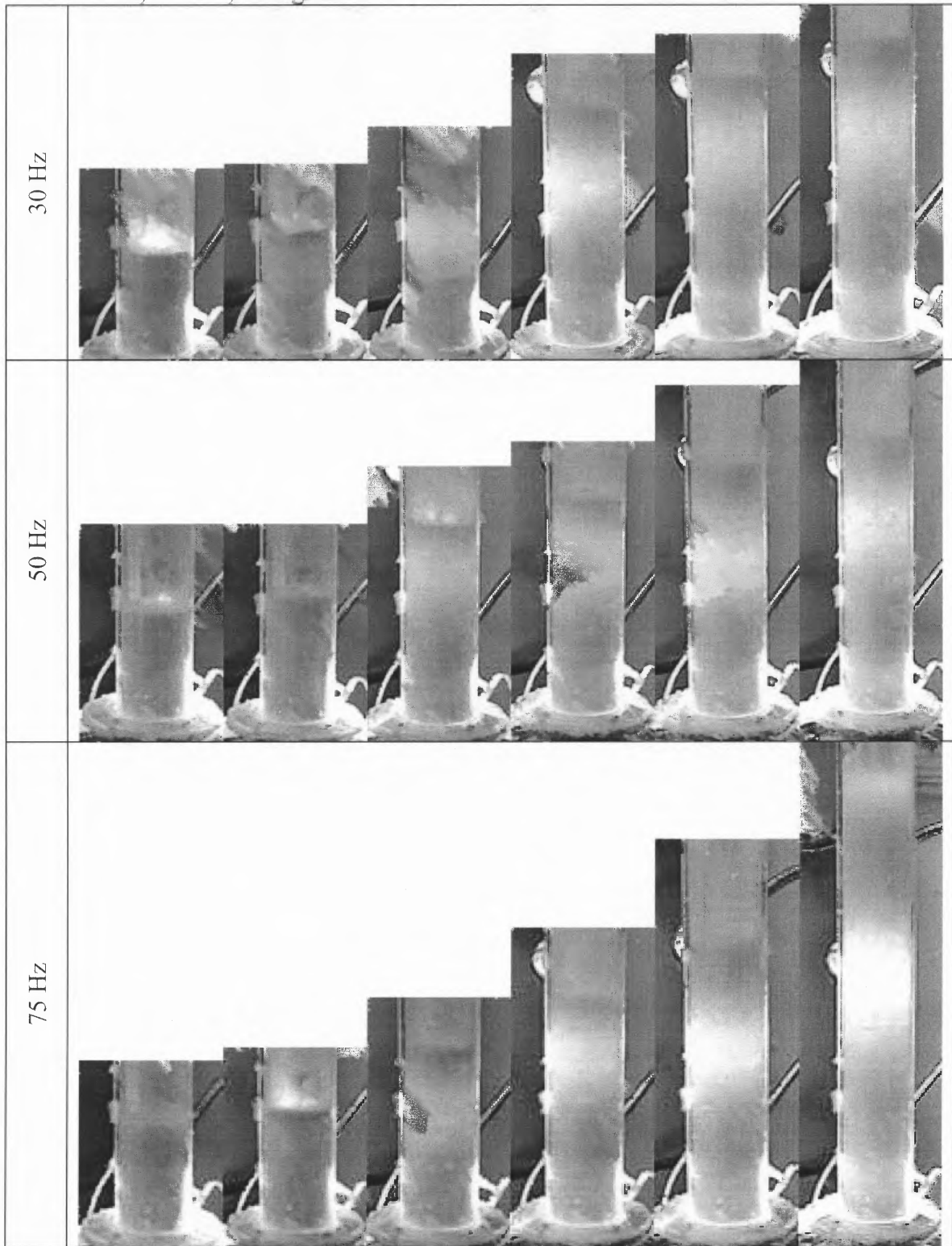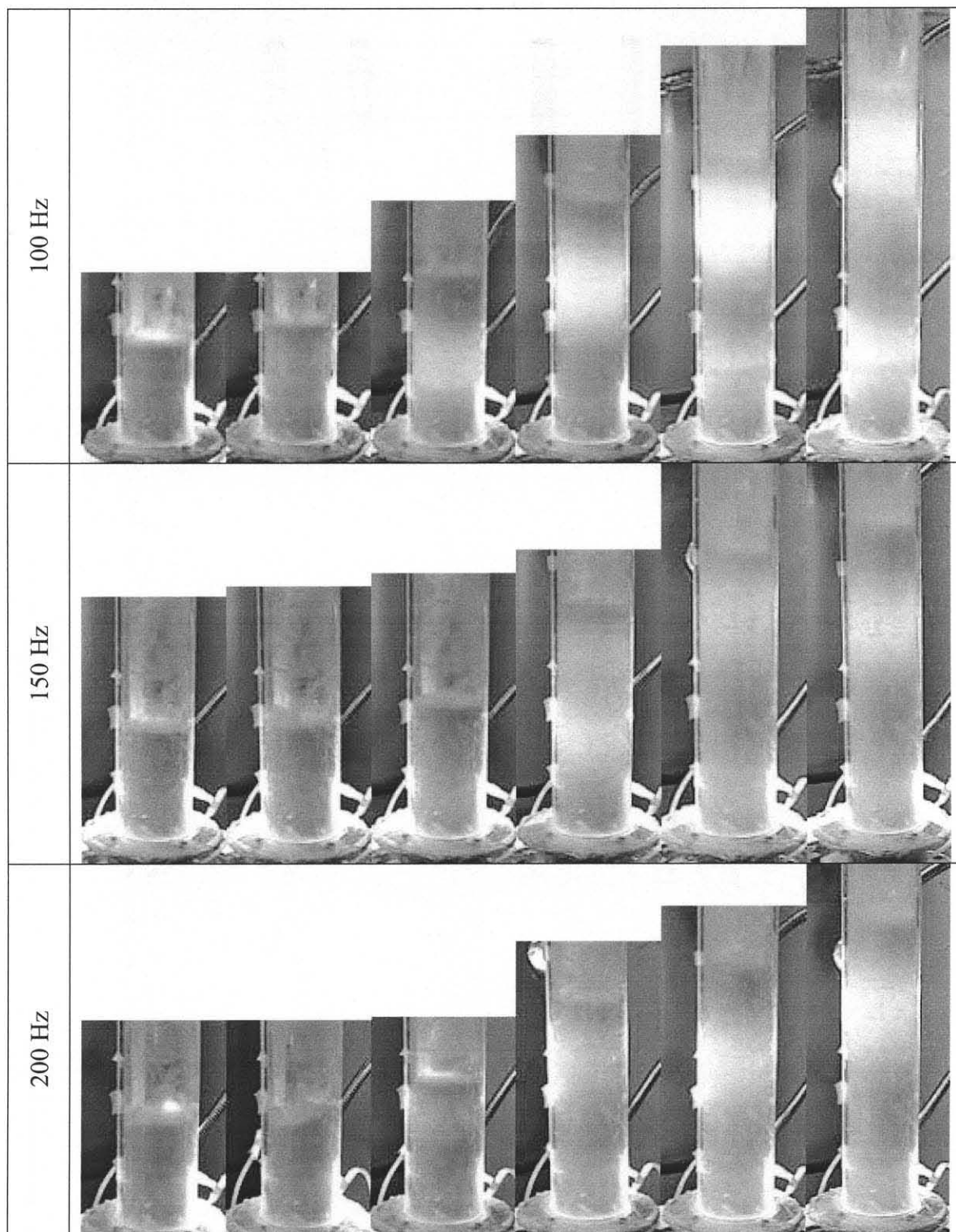
Silica R972, Γ = 4.5, 10.0 grams
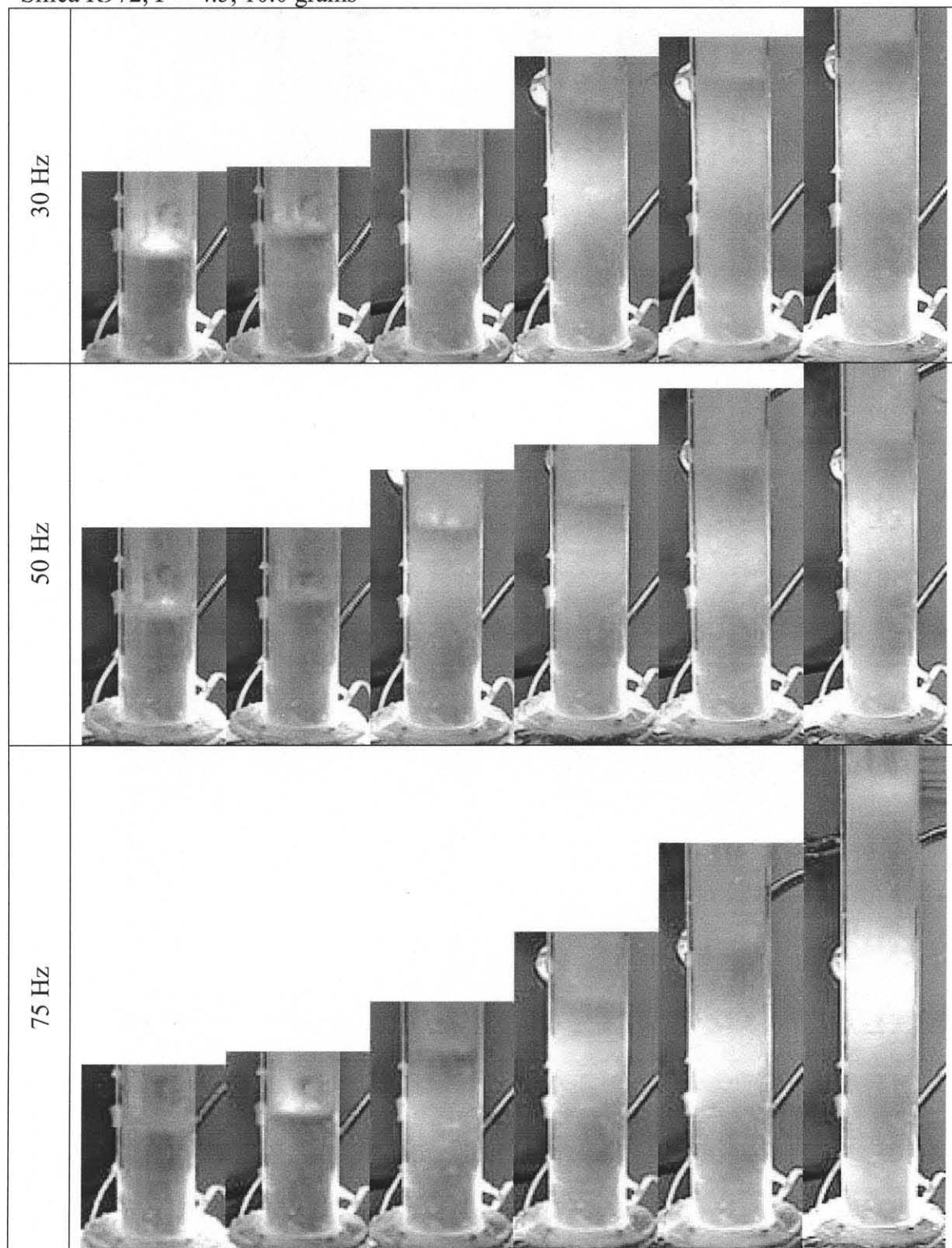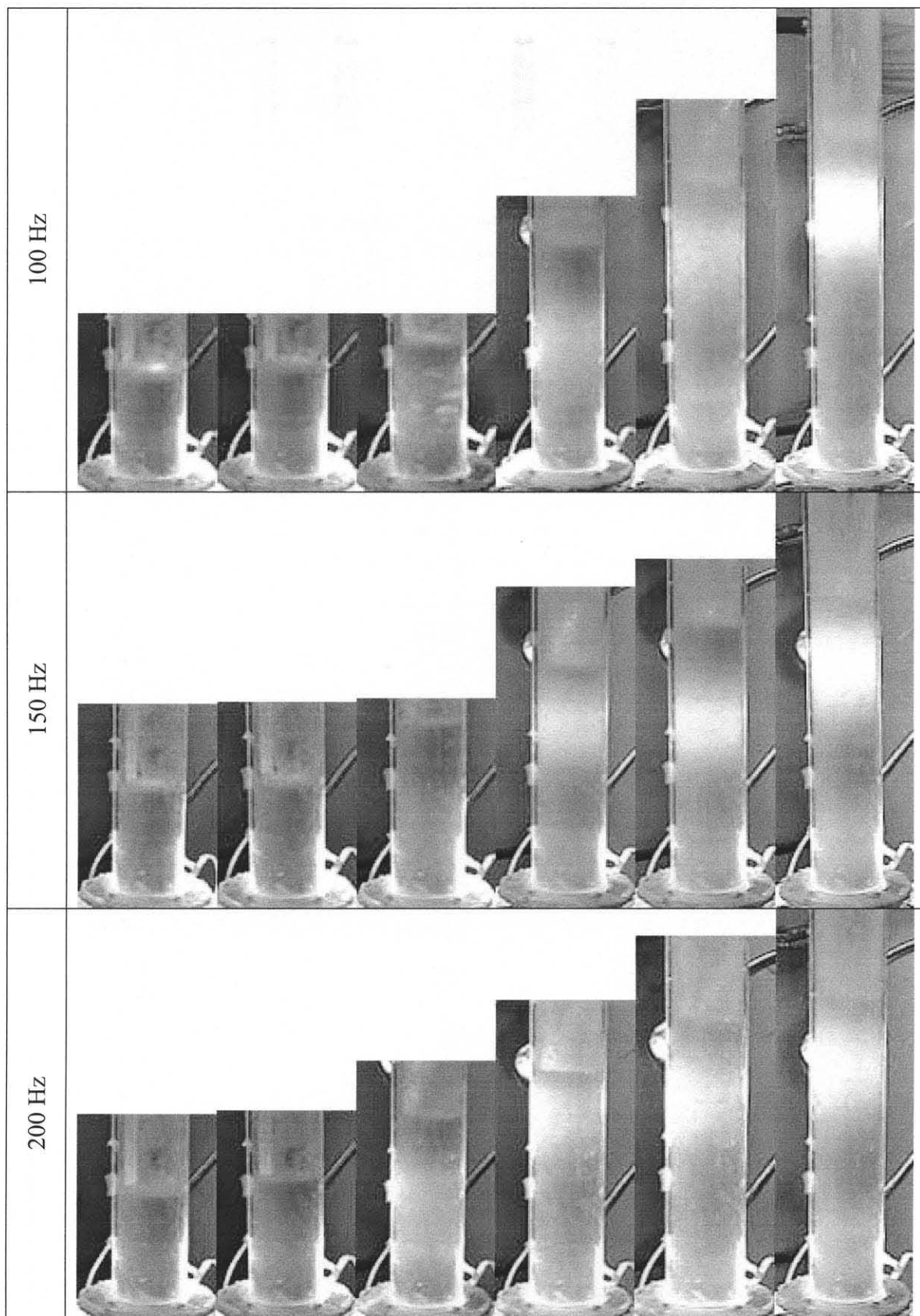
APPENDIX B

LASER AND CCD CAMERA IMAGES

The following are images from the laser and CCD camera system. The results capture nanoagglomerates in a conventionally fluidized bed and in an aerated vibrofluidized bed ($\Gamma = 3$, f = 50 Hz). Each shot is 1.1 mm in height and width.

Aerosil R974 agglomerates in a conventionally fluidized bed
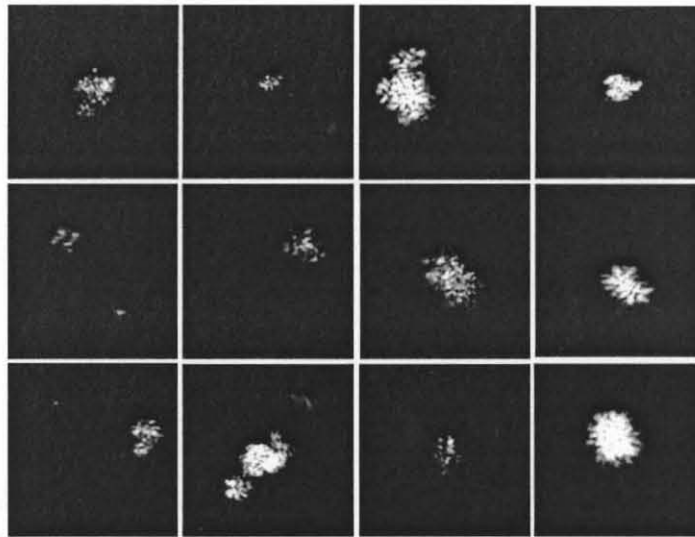
Aerosil R974 agglomerates in a vibrofluidized bed
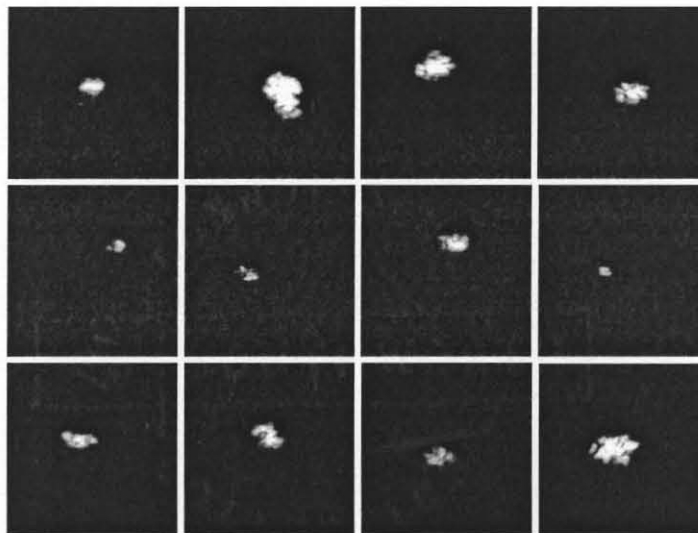
Aerosil R972 agglomerates in a conventionally fluidized bed
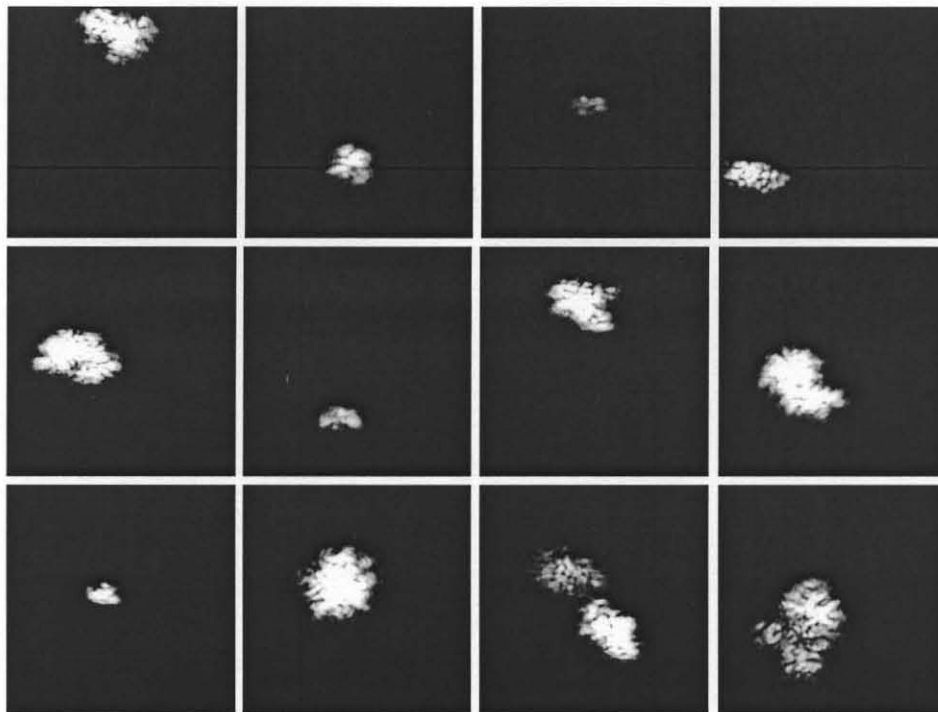
Aerosil R972 agglomerates in a vibrofluidized bed
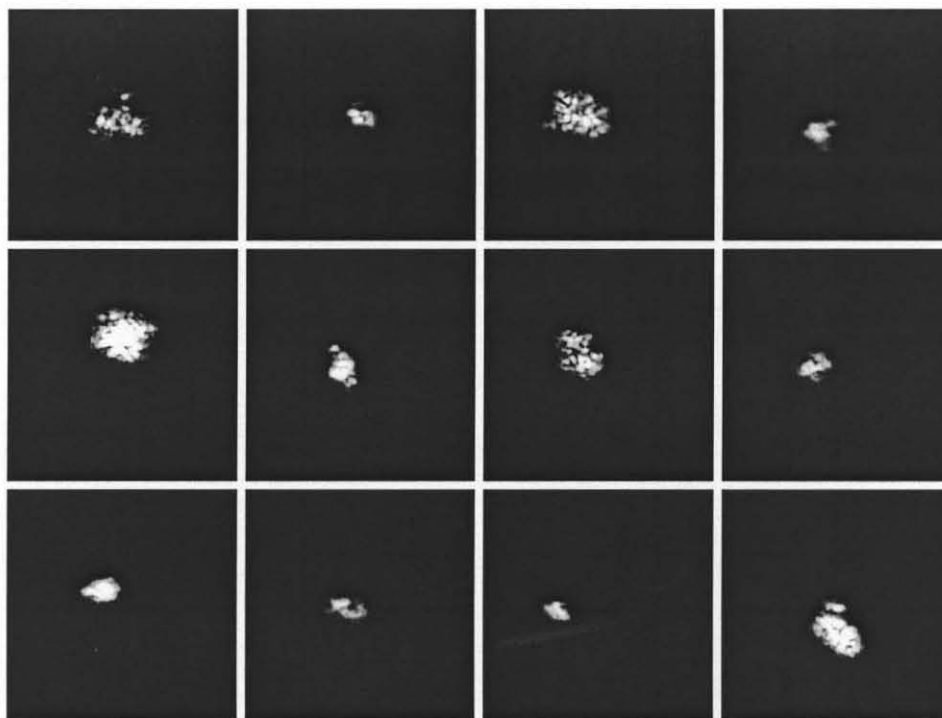
Aerosil 300 agglomerates in a conventionally fluidized bed
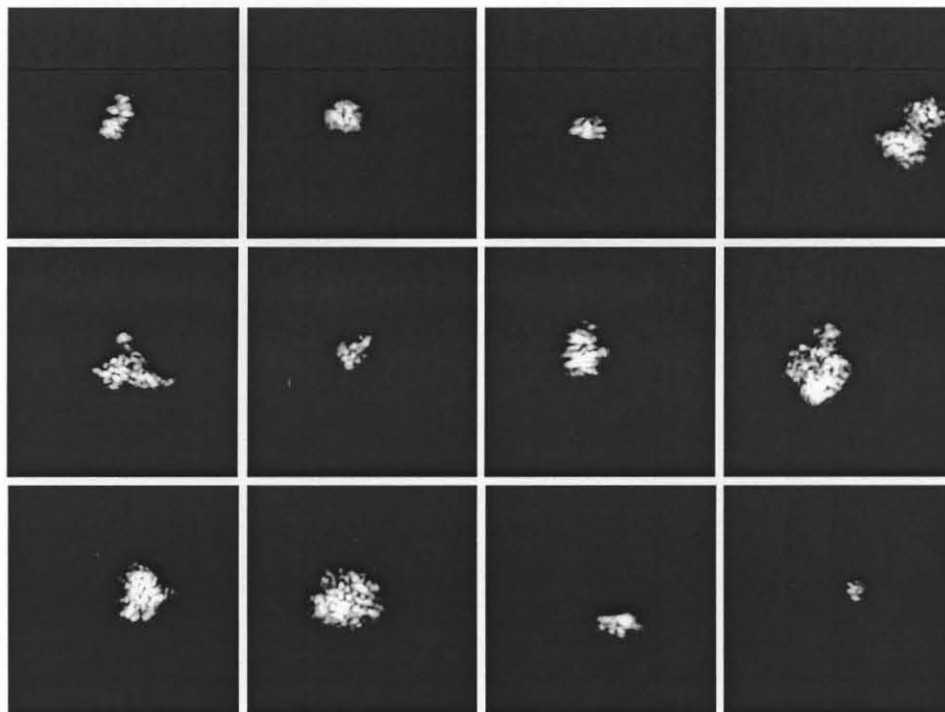
Aerosil 300 agglomerates in a vibrofluidized bed
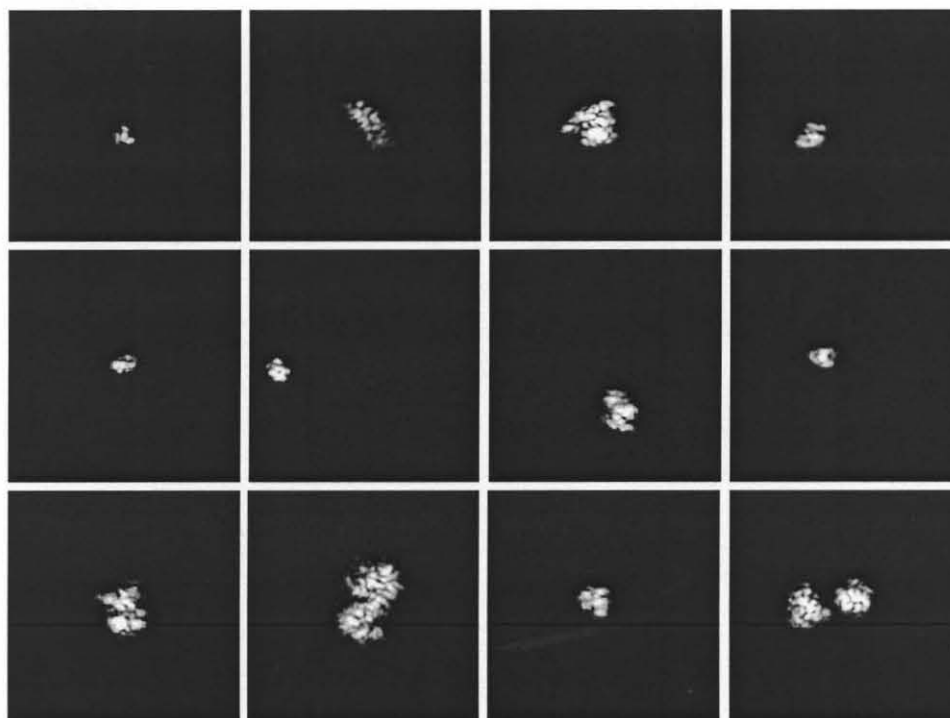
Aerosil 90 agglomerates in a conventionally fluidized bed
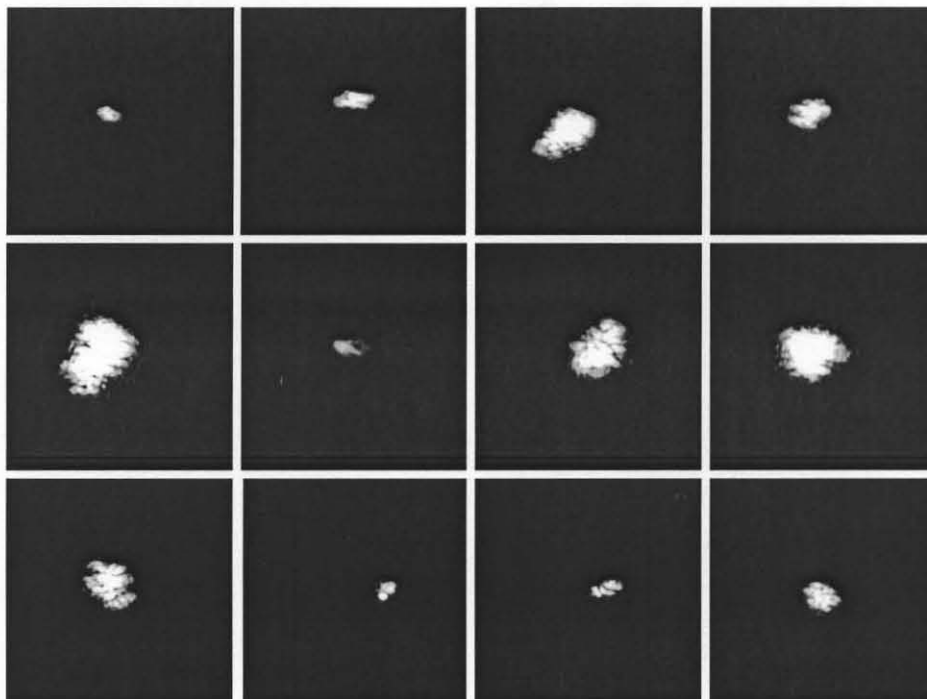
Aerosil 90 agglomerates in a vibrofluidized bed
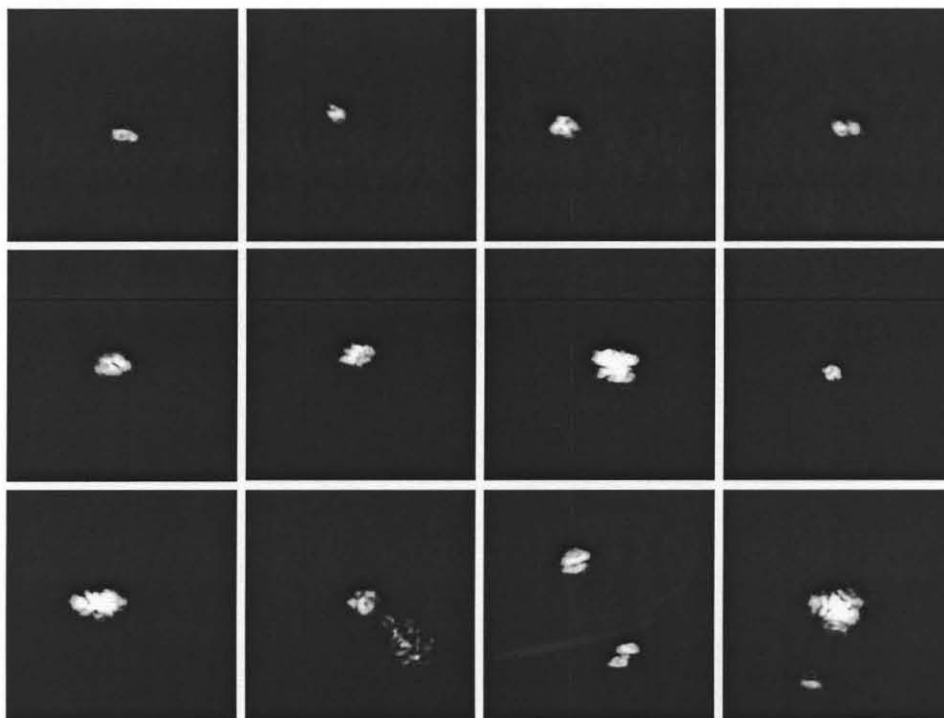
Alumina C agglomerates in a conventionally fluidized bed
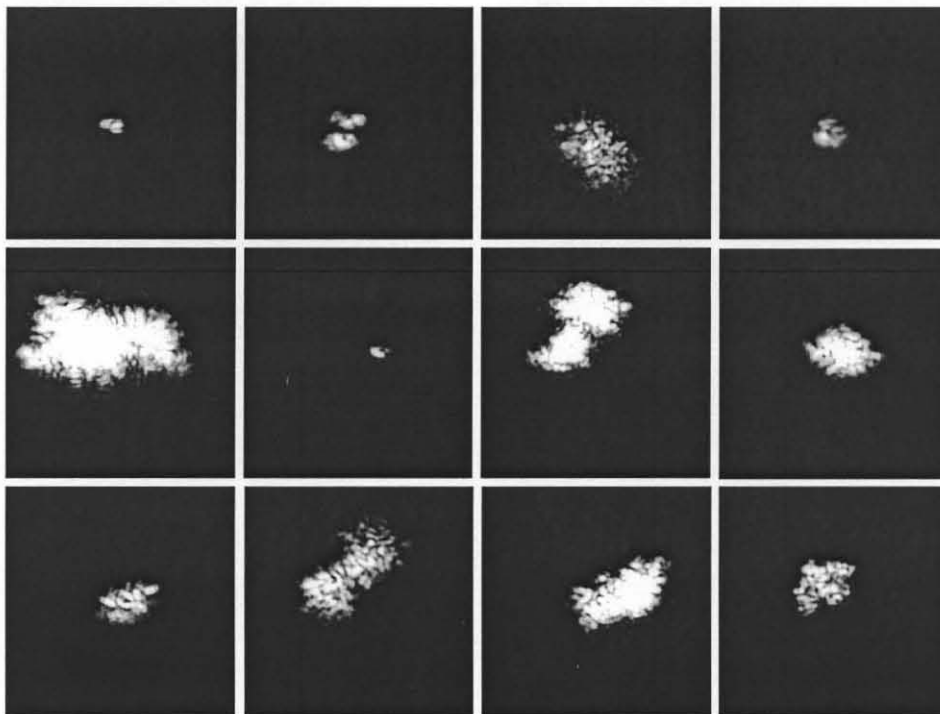
Alumina C agglomerates in a vibrofluidized bed
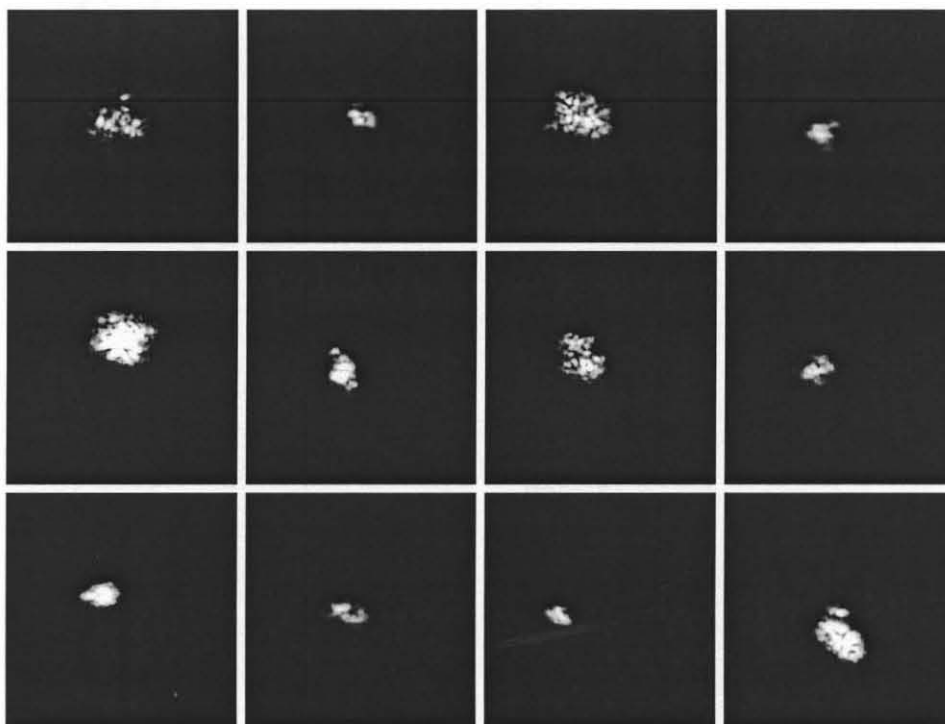
Titania P25 agglomerates in a conventionally fluidized bed
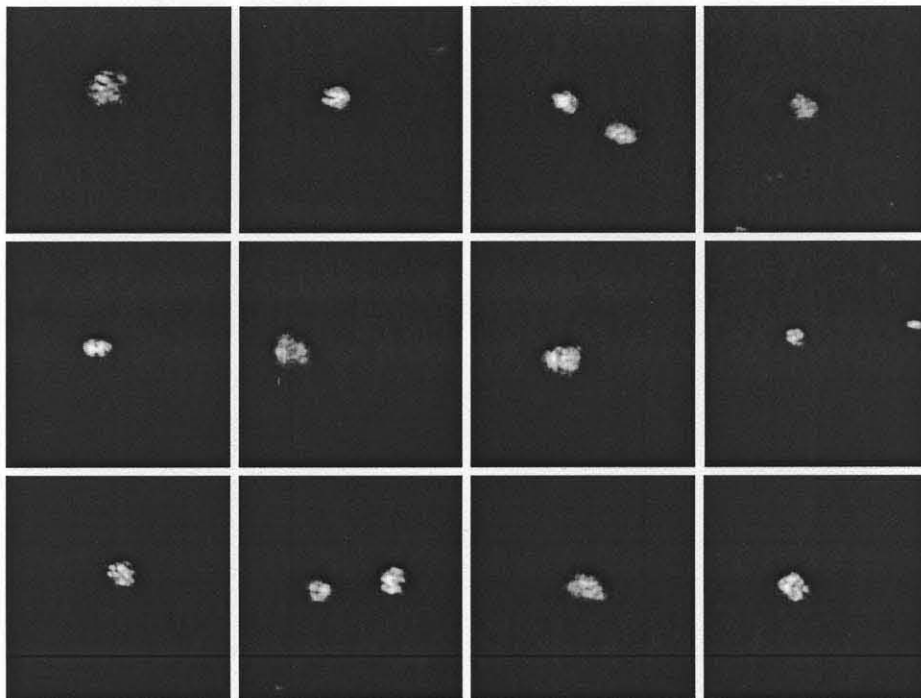
Titania P25 agglomerates in a vibrofluidized bed
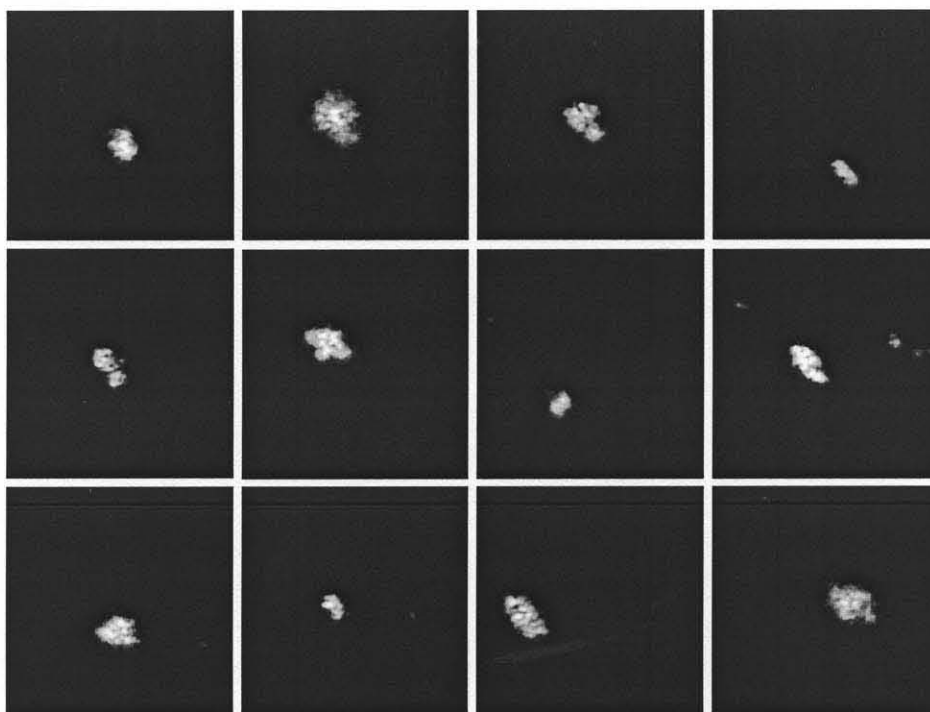
APPENDIX C

SUMMARY OF INTERAGGLOMERATE VOIDAGES
IN VIBRATED EXPERIMENTS

The following is a summary of the interagglomerate voidages calculated from the modified Richardson-Zaki method, Blake-Kozeny Equation, and Equation 2.15 during vibrofluidization ($\Gamma = 3$, $f = 50$ Hz).

Silica R974

u (cm/s)	ε_e (Modified Richardson–Zaki)	ε_e (Blake–Kozeny Equation)	$\varepsilon_e = 1 - H_0/H_{exp}$
0.15	0.529	0.526	0.400
0.21	0.584	0.566	0.469
0.27	0.634	0.602	0.534
0.33	0.666	0.632	0.574
0.40	0.689	0.657	0.603
0.47	0.704	0.677	0.623
0.54	0.718	0.700	0.641
0.62	0.729	0.709	0.655
0.70	0.742	0.724	0.671
0.79	0.755	0.738	0.688
0.87	0.763	0.741	0.697

Silica R972

u (cm/s)	ε_e (Modified Richardson–Zaki)	ε_e (Blake–Kozeny Equation)	$\varepsilon_e = 1 - H_0/H_{exp}$
0.27	0.483	0.480	0.400
0.41	0.567	0.538	0.497
0.55	0.606	0.580	0.543
0.71	0.634	0.614	0.575
0.89	0.648	0.639	0.591
1.06	0.660	0.659	0.605
1.22	0.664	0.673	0.610
1.38	0.677	0.688	0.625

Silica A300

u (cm/s)	ε_e (Modified Richardson–Zaki)	ε_e (Blake–Kozeny Equation)	$\varepsilon_e = 1 - H_0/H_{exp}$
0.04	0.314	0.369	0.000
0.15	0.376	0.480	0.091
0.27	0.428	0.540	0.167
0.41	0.608	0.615	0.429
0.55	0.688	0.667	0.545
0.71	0.718	0.701	0.588
0.89	0.746	0.729	0.630
1.06	0.762	0.749	0.653
1.22	0.771	0.764	0.666
1.38	0.779	0.778	0.677

Silica A90

u (cm/s)	ε_e (Modified Richardson–Zaki)	ε_e (Blake–Kozeny Equation)	$\varepsilon_e = 1 - H_0/H_{exp}$
0.27	0.580	0.462	0.101
0.41	0.619	0.521	0.184
0.55	0.619	0.542	0.184
0.71	0.619	0.573	0.184
0.89	0.623	0.598	0.192
1.06	0.660	0.627	0.273
1.22	0.686	0.649	0.328
1.38	0.683	0.659	0.322

Alumina C

u (cm/s)	ε_e (Modified Richardson–Zaki)	ε_e (Blake–Kozeny Equation)	$\varepsilon_e = 1 - H_0/H_{exp}$
0.15	0.556	0.528	0.008
0.21	0.566	0.564	0.031
0.27	0.573	0.573	0.046
0.34	0.592	0.610	0.088
0.41	0.603	0.620	0.114
0.48	0.603	0.633	0.114
0.55	0.603	0.645	0.114
0.63	0.603	0.653	0.114
0.71	0.708	0.693	0.347
0.80	0.776	0.727	0.500
0.89	0.778	0.729	0.504
0.97	0.778	0.745	0.504
1.06	0.785	0.750	0.519
1.14	0.786	0.761	0.523
1.22	0.788	0.767	0.527
1.31	0.786	0.772	0.523
1.38	0.792	0.782	0.536

Titania P25

u (cm/s)	ε_e (Modified Richardson–Zaki)	ε_e (Blake–Kozeny Equation)	$\varepsilon_e = 1 - H_0/H_{exp}$
0.55	0.411	0.537	0.174
0.71	0.429	0.541	0.182
0.89	0.444	0.541	0.182
1.06	0.462	0.545	0.189
1.22	0.483	0.576	0.244
1.38	0.496	0.579	0.250

APPENDIX D

PRESSURE DROP AND BED EXPANSION DATA

The following are plots of non-dimensionalized pressure drop and bed expansion ration vs. superficial air velocity for the different modes of fluidization.

Silica R974 - Conventional Fluidized Bed
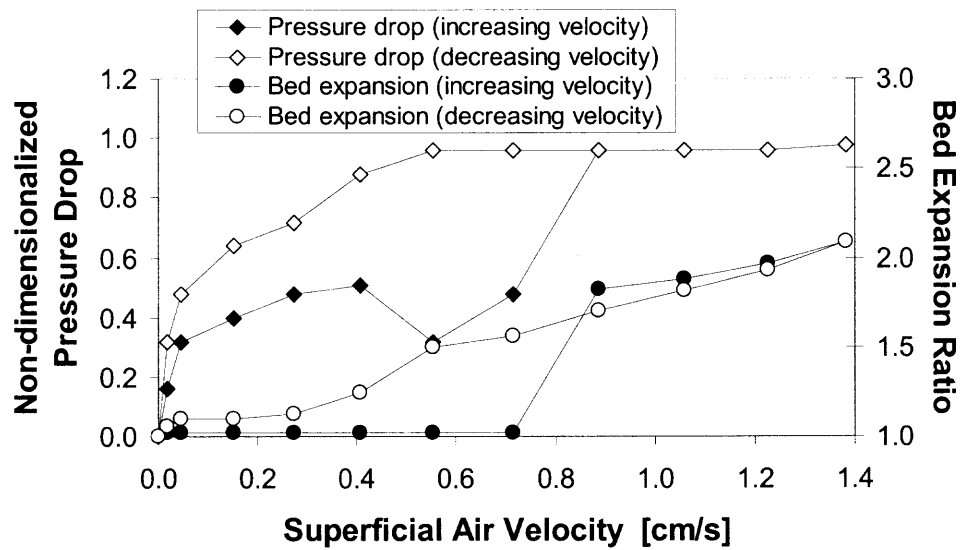
Silica R974 - Vibrofluidized Bed (Γ = 3, f = 50 Hz)
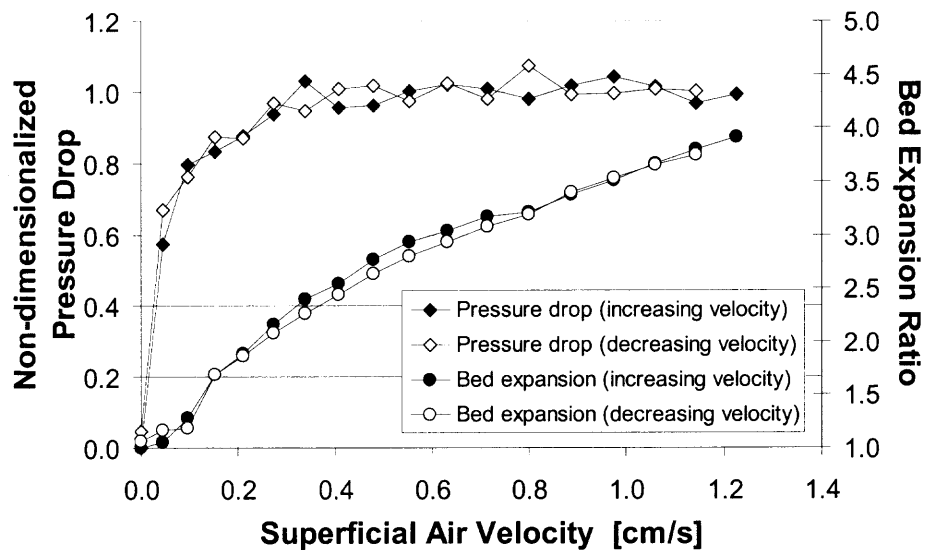
Silica R974 - Magnetically Assisted Fluidized Bed
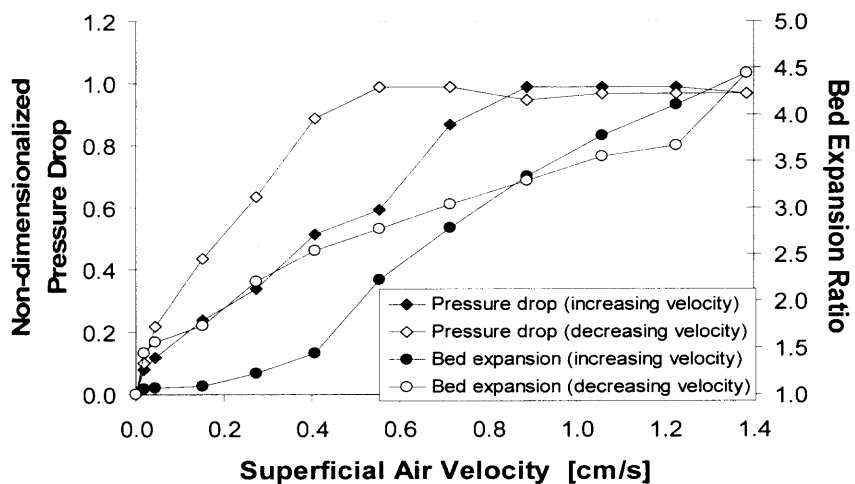
Silica R972 - Conventional Fluidized Bed
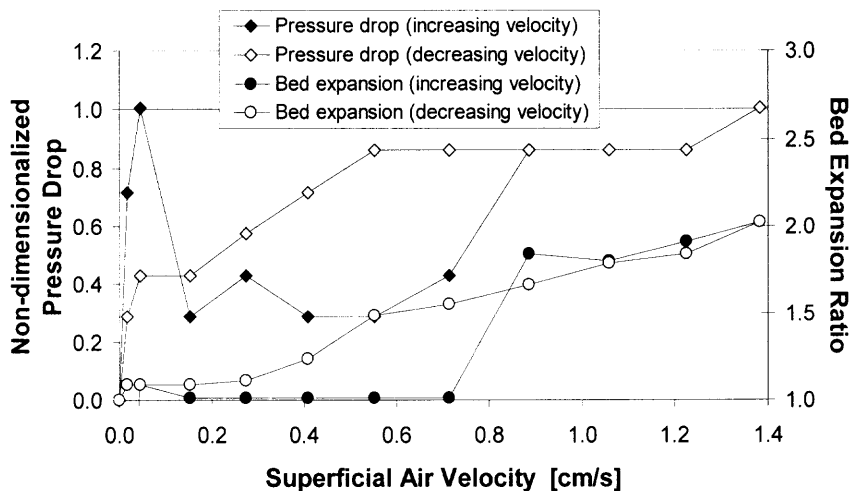
Silica R972 - Vibrofluidized Bed ($\Gamma = 3$, f = 50 Hz)
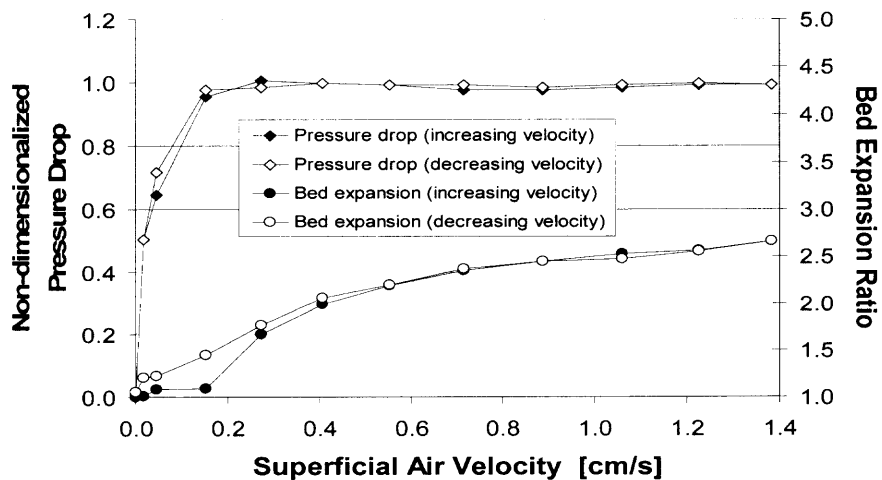
Silica R972 - Magnetically Assisted Fluidized Bed
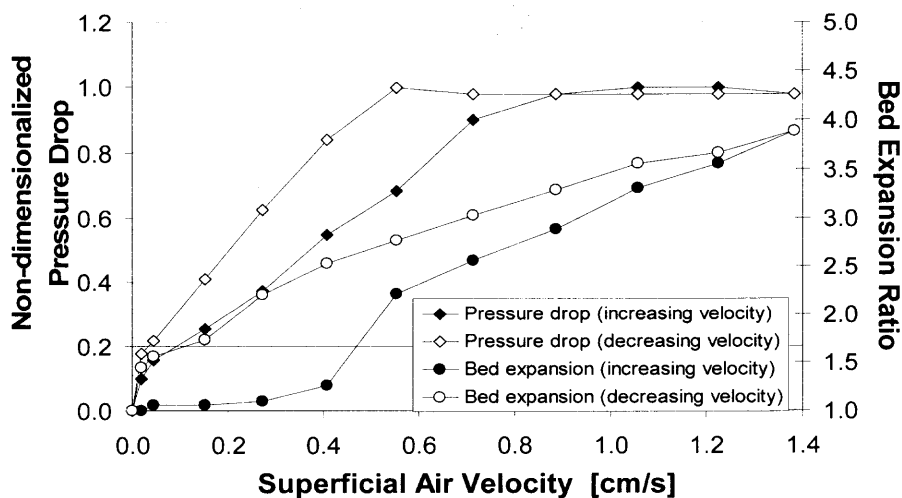
Silica A300 - Conventional Fluidized Bed
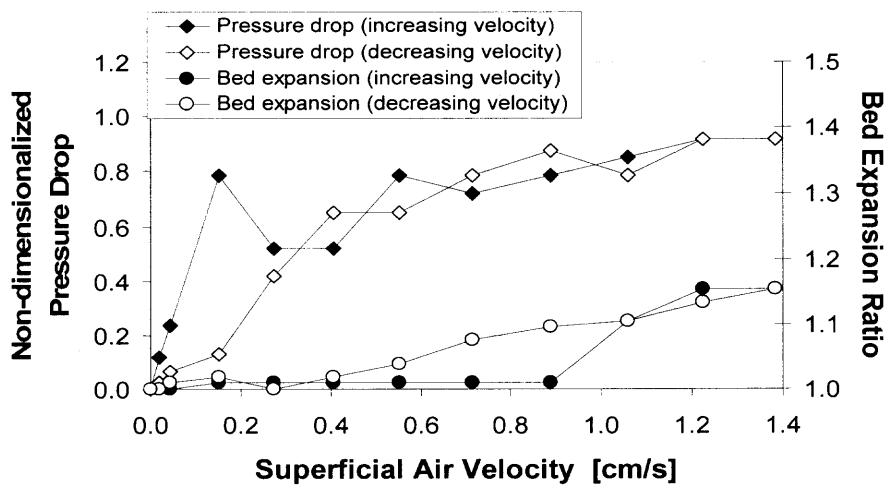
Silica A300 - Vibrofluidized Bed ($\Gamma = 3$, f = 50 Hz)
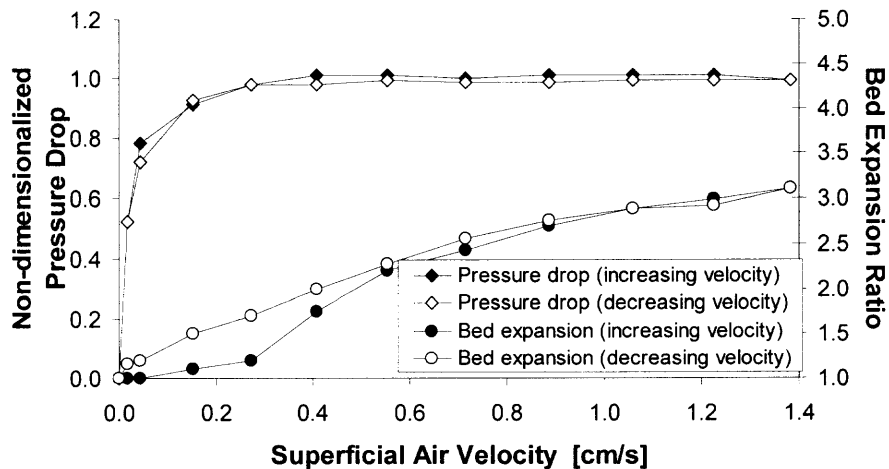
Silica A300 - Magnetically Assisted Fluidized Bed
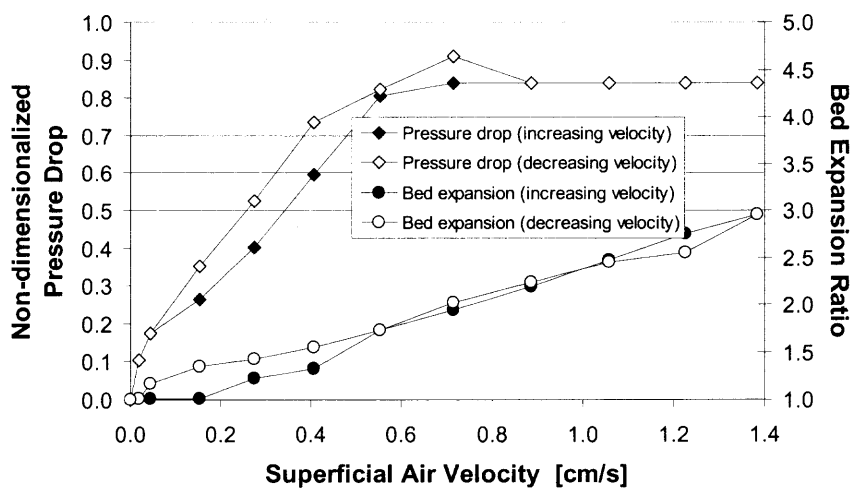
Silica A90 - Conventional Fluidized Bed
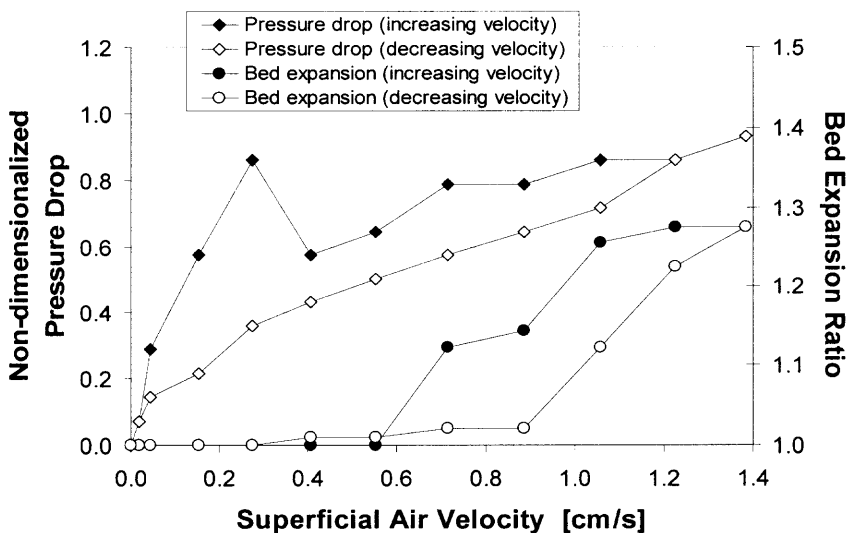
Silica A90 - Vibrofluidized Bed ($\Gamma = 3$, $f = 50$ Hz)
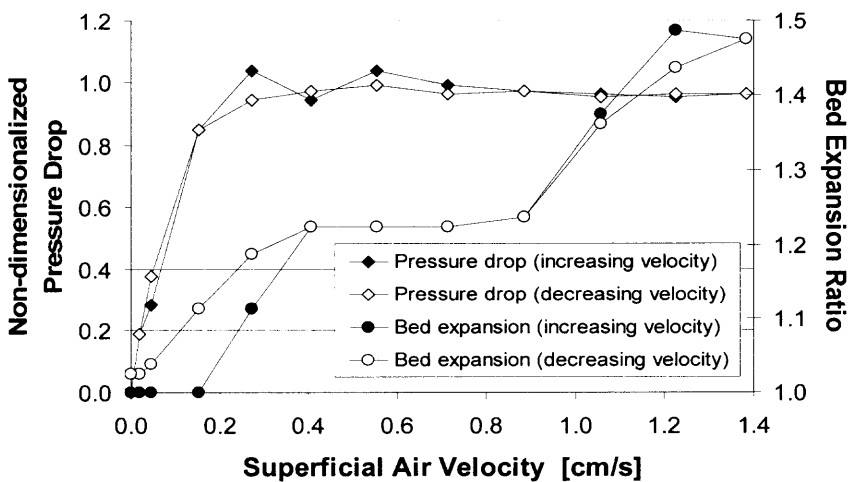
Alumina C - Conventional Fluidized Bed
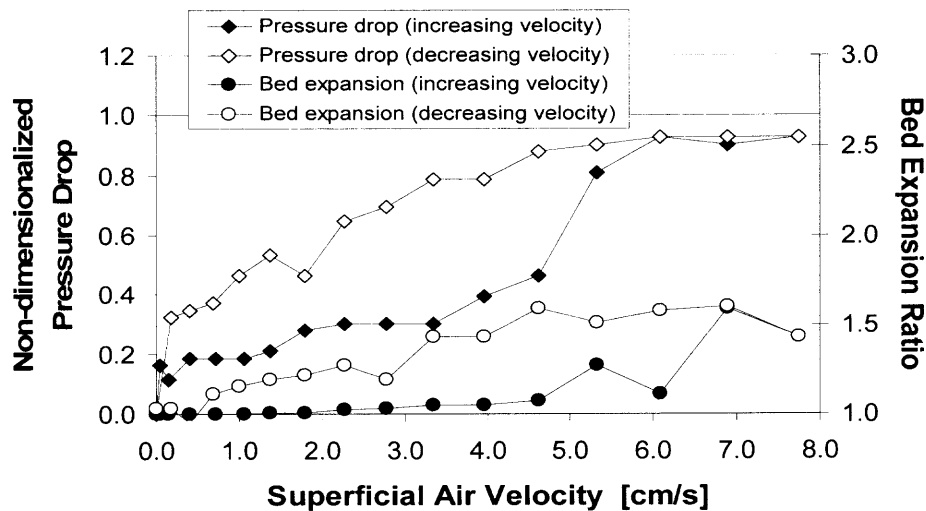
Alumina C - Vibrofluidized Bed ($\Gamma = 3$, f = 50 Hz)
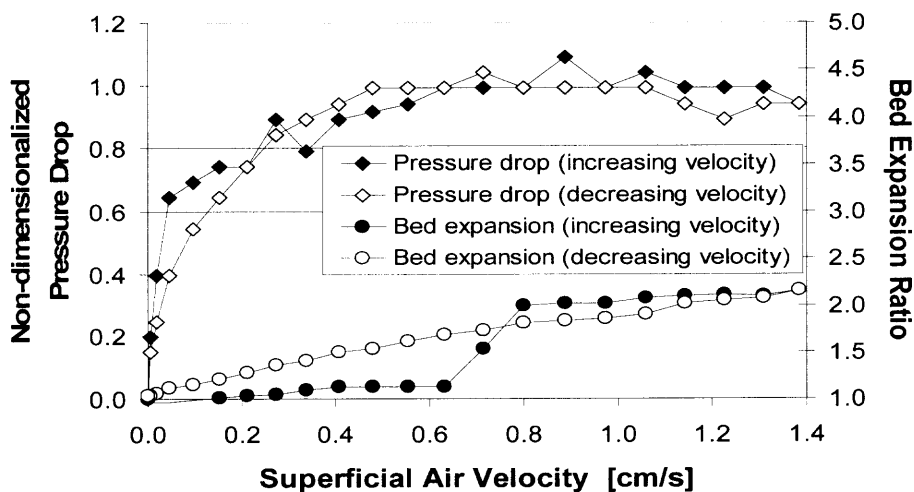
Titania P25 - Conventional Fluidized Bed
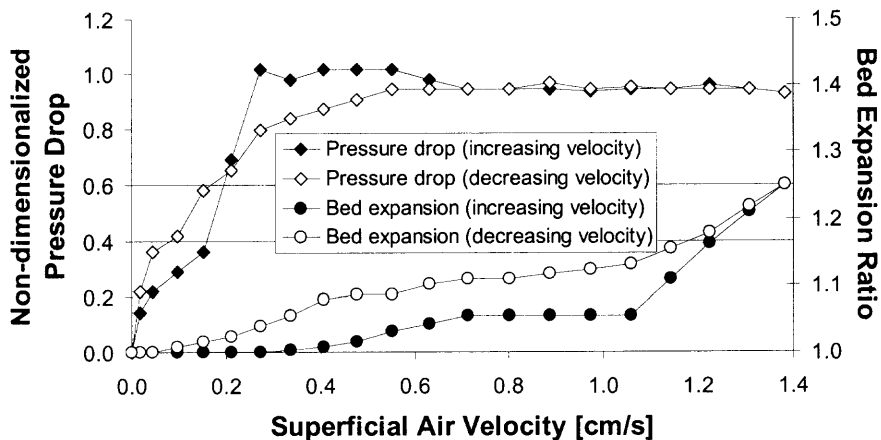
Titania P25 - Vibrofluidized Bed ($\Gamma = 3$, f = 50 Hz)
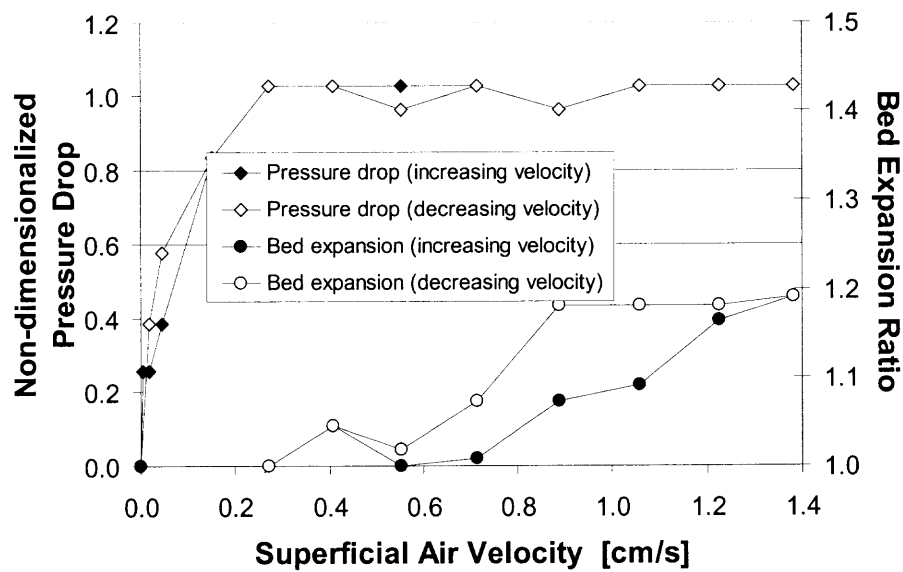
APPENDIX E

SUMMARY OF INTERAGGLOMERATE VOIDAGES
IN MAGNETICALLY ASSISTED EXPERIMENTS

The following is a summary of the interagglomerate voidages calculated from the modified Richardson-Zaki method, Blake-Kozeny Equation, and Equation 2.15 during fluidization with magnetic assistance.

Silica R974 during fluidization with magnetic assistance, weight of magnets = 10.0 grams

u (cm/s)	ε_e (Modified Richardson–Zaki)	ε_e (Blake–Kozeny Equation)	$\varepsilon_e = 1 - H_0/H_{exp}$
0.55	0.766	0.715	0.550
0.71	0.773	0.772	0.640
0.89	0.794	0.810	0.700
1.06	0.816	0.832	0.735
1.22	0.831	0.846	0.757
1.38	0.845	0.857	0.775

Silica R972 during fluidization with magnetic assistance, weight of magnets = 10.0 grams

u (cm/s)	ε_e (Modified Richardson–Zaki)	ε_e (Blake–Kozeny Equation)	$\varepsilon_e = 1 - H_0/H_{exp}$
0.55	0.682	0.7200	0.548
0.71	0.725	0.7326	0.609
0.89	0.757	0.7528	0.654
1.06	0.788	0.7764	0.698
1.22	0.802	0.7930	0.719
1.38	0.819	0.8097	0.743

Silica A300 during fluidization with magnetic assistance, weight of magnets = 11.0 grams

u (cm/s)	ε_e (Modified Richardson–Zaki)	ε_e (Blake–Kozeny Equation)	$\varepsilon_e = 1 - H_0/H_{exp}$
0.15	0.549	0.541	0.010
0.27	0.628	0.576	0.183
0.41	0.657	0.585	0.246
0.55	0.737	0.613	0.424
0.71	0.765	0.645	0.484
0.89	0.792	0.677	0.544
1.06	0.816	0.705	0.595
1.23	0.835	0.727	0.637
1.38	0.846	0.744	0.662

REFERENCES

Abrahamsen, A. R., and D. Geldart, "Behavior of gas-fluidized beds of fine powders part I. homogeneous expansion," *Powder Technology,* **26,** 35-46 (1980).

Arastoopour, H., A. Ahmadzadeh, and F. Teymour, "Fluidization behavior of rotating fluidized beds," *Fluidization XI: Proceedings of the Eleventh Engineering Foundation Conference on Fluidization,* Engineering Foundation, New York, (2004).

Benge, G. G., and A. M. Squires, "Microreactor simulating reaction scene in turbulent fluid bed of group A powder: 1. axial gas dispersion," *AIChE Symposium Series – Developments in Fluidization and Fluid-Particle Systems,* **91,** 119-127 (1995).

Bird, R. B., W. E. Stewart, E. N. Lightfoot, Transport Phenomena, John Wiley & Sons, Inc. (1960).

Castellanos, A., J. M. Valverde, A. T. Perez, A. Ramos, and P. K. Watson, "Flow regimes in fine cohesive powders," *Physical Review Letters,* **82,** 1156-1159 (1999).

Castellanos, A., J. M. Valverde, and M. A. S. Quintanilla, "Aggregation and sedimentation in gas-fluidized beds of cohesive powders," *Physical Review E,* **64,** 041304 (2001).

Castellanos, A., J. M. Valverde, and M. A. S. Quintanilla, "Fine cohesive powders in rotating drums: Transition from rigid-plastic flow to gas-fluidized regime," *Physical Review E,* **65,** 061301 (2002).

Chaouki, J., C. Chavarie, and D. Klvana, "Effect of interparticle forces on the hydrodynamic behavior of fluidized aerogels," *Powder Technology,* **43,** 117 (1985).

Chapman, S., and T. Cowling, The Mathematical Theory of Non-Uniform Gases; an Account of the Kinetic Theory of Viscosity, Thermal Conduction, and Diffusion in Gases, Cambridge Univ. Press, England (1970).

Chen, S. B., and A. Cai, "Hydrodynamic interactions and mean settling velocity of porous particles in a dilute suspension," *Journal of Colloid and Interface Science,* **217,** 328-340 (1999).

Chen, Y.-M., "Fundamentals of a centrifugal fluidized bed," *AIChE Journal,* **33,** 722-727, (1987).

Chirone, R., L. Massimilla, and S. Russo, "Bubble-free fluidization of a cohesive powder in an acoustic field," *Chemical Engineering Science*, **48,** 41-52 (1993).

Chitester, D. C., R. M. Kornosky, L.-S. Fan, J. P. Danko, "Characteristics of fluidization at high pressure," *Chemical Engineering Science,* **39,** 253-261 (1984).

Cook, R. F., "Effective-medium theory for the fracture of fractal porous media," *Physical Review B,* **39,** 2811-2814 (1989).

Davies, R., "Particle science and technology – a view at the millennium," *Powder Technology*, **119,** 45-57 (2001).

Ding, J., and D. Gidaspow, "A bubbling fluidization model using kinetic theory of granular flow," *AIChE Journal*, **36,** 523-538 (1990).

Ding, Y. L., R. Forster, J. P. K. Seville, and D. J. Parker, "Granular motion in rotating drums: bed turnover time and slumping-rolling transition," *Powder Technology,* **124,** 18-27 (2002).

Dutta, A. and L. V. Dullea, "Effects of external vibration and the addition of fibers on the fluidization of a fine powder," *AIChE Symposium Series - Advances in Fluidized Systems,* **87,** 38-46 (1991).

Elimelech, M., J. Gregory, X. Jia, and R. A. Williams, <u>Particle Deposition and Aggregation: Measurement, Modelling and Simulation,</u> Butterworth-Heinemann, Woburn, MA (1995).

Erdesz, K., and A. S. Mujumdar, "Hydrodynamic aspects of conventional and vibrofluidized beds – a comparative evaluation," *Powder Technology,* **46,** 167-172 (1986).

Ergun, S., "Determination of Geometric Surface Area of Crushed Porous Solids," *Analytical Chemistry,* **24,** 388-393, (1952).

Ergun, S., "Fluid Flow Through Packed Columns," *Chemical Engineering Progress,* **48,** 89-94, (1952).

Ergun, S., "Mass-Tranfer Rate in Packed Columns," *Chemical Engineering Progress,* **48,** 227-236, (1952).

Fan, L. T., C. C. Chang, Y. S. Yu, T. Takahashi, and Z. Tanaka, "Incipient fluidization condition for a centrifugal fluidized bed," *AIChE Journal,* **31,** 999-1006, (1985).

Fortes, A. F., P. Caldas, and J. V. Gallo, "Particle aggregation and the van der Waals forces in gas-solids fluidization," *Powder Technology,* **98,** 201-208 (1998).

Filippov, A. V., M. Zurita, and D. E. Rosner, "Fractal-like aggregates: relation between morphology and physical properties," *Journal of Colloid and Interface Science,* **229,** 261-273 (2000).

Finkers, I. H. J., and A. C. Hoffmann, "Invention for the fluidization of fine and sticky powders," http://www.fwn.rug.nl/chemeng/research/Disp/fluidiza/fluidiza.html.

Formisani, B., R. Girimonte, and M. Mortara, "Segregating fluidization of beds of two dissimilar solids: the effect of component concentration, density and size," *Fluidization XI: Proceedings of the Eleventh Engineering Foundation Conference on Fluidization,* Engineering Foundation, New York, (2004).

Friedlander, S. K., Smoke, Dust, and Haze: Fundamentals of Aerosol Dynamics, Oxford University Press, New York (2000).

Gidaspow, D., and J. Ding, "A semi-empirical model for fluidization of fine particles," *Indian Chemical Engineering,* **36,** 139-150 (1994).

Guo, Q., J. Werther, and E. Hartage, "The influence of the distributor pressure drop on the hydrodynamics of a circulating fluidized bed," *Fluidization XI: Proceedings of the Eleventh Engineering Foundation Conference on Fluidization,* Engineering Foundation, New York, (2004).

Hoffman, A. C., "Manipulating fluidized beds by using internals: fluidization with baffles," http:// www.fwn.rug.nl/chemeng/research/Disp/npt00/npt99.html.

Iwadate, Y., and M. Horio, "Agglomerating fluidization of wet powders – a numerical analysis -," *Fluidization IX: Proceedings of the Ninth Engineering Foundation Conference on Fluidization,* Engineering Foundation, New York, 293-300 (1998).

Iwadate, Y., and M. Horio, "Prediction of agglomerate sizes in bubbling fluidized beds of group C powders," *Powder Technology,* **100,** 223-236 (1998).

Iwadate, Y., Y. Ohwada, K. Nishii, H. Kamiya, and M. Horio, "Fluidization characteristics of fine powders treated with different adsorbate species," Advances in Multiphase Flow, Elsevier Science, 689-700 (1995).

Jaraiz, E., S. Kimura, and O. Levenspiel, "Vibrating beds of fine particles: estimation of interparticle forces from expansion and pressure drop experiments," *Powder Technology,* **72,** 23-30 (1992).

Jones, E. M., "One Small Step", *Appolo 11 Lunar Surface Journal*, (1995). Retrieved February 2004 from the World Wide Web: http://www.hq.nasa.gov/alsj/a11/a11.step.html

Judd, M. R., and R. Goosen, "Effects of particle shape on fluidisation characteristics of fine particles in the freely bubbling and turbulent regimes," *Fluidization VI: Proceedings of the Sixth Engineering Foundation Conference on Fluidization,* Engineering Foundation, New York, 41-48 (1989).

Jung, J., D. Gidaspow, "Fluidization of nano-sized particles," *Journal of Nanoparticle Research,* **4,** 483-497 (2002).

Kanaoka, C., and T. Kishima, "Observation of the process of dust accumulation on a rigid ceramic filter surface and the mechanism of cleaning dust from the filter surface," *Advanced Powder Technol.,* **10,** 417-426 (1999).

Kantorovich, I. I., and E. Bar-ziv, "Role of the pore structure in the fragmentation of highly porous char particles," *Combustion and Flame,* **113,** 532-541 (1998).

Kao, J., R. Pfeffer, and G. I. Tardos, "On partial fluidization in rotating fluidized beds," *AIChE Journal,* **33,** 858-1410 (1987).

Kaye, B. H., Powder Mixing, Chapman & Hall, London (1997).

Khan, A. R., and J. F. Richardson, "Pressure gradient and friction factor for sedimentation and fluidisation of uniform spheres in liquids," *Chemical Engineering Sciences,* **45,** 255-265 (1990).

Knowlton, T.M., "High Pressure Fluidization Characteristics of Several Particulate Solids: Primary Coal and Coal-Derived Materials," *AIChE Symposium Series,* **73,** 161 (1977).

Koch, C., Nanostructure Science and Technology, Kluwer Academic Publications, (1999).

Kono, H. O., S. Narasimhan, L. M. Richman, and T. Ohtake, "Flow properties of homogeneously aerated, expanded emulsion phase of fine powders (quasi-solid emulsion phase viscosity)," *Powder Technology,* **122,** 168-176 (2002).

Kunii, D., and O. Levenspiel, Fluidization Engineering, John Wiley & Sons, New York, (1969).

Kwauk, M., J. Li, and W. Yang, editors, *Fluidization X: Proceedings of the Tenth Engineering Foundation Conference on Fluidization,* United Engineering Foundation, New York (2001).

Larraz, R., "Influence of fractal pore structure in Claus catalyst performance," *Chemical Engineering Journal,* **86,** 309-317 (2002).

Liss, B., T. R. Blake, A. M. Squires, and R. Bryson, "Incipient defluidization of sinterable solids," *Fluidization IV: Proceedings of the Fourth Engineering Foundation Conference on Fluidization,* 249-256 (1984).

Lettieri, P., J. G. Yates, and D. Newton, "The influence of interparticle forces on the fluidization behaviour of some industrial materials at high temperature," *Powder Technology,* **110,** 117-127 (2000).

Leva, M., Fluidization, McGraw Hill, New York, (1959).

Levy, E., N. Martin, and J. Chen, "Minimum fluidization and startup of a centrifugal fluidized bed," Fluidization, Cambridge University Press, (1978).

Louge, M. Y., E. Mastorakos, and J. T. Jenkins, "The role of particle collisions in pneumatic transport," *Journal of Fluid Mechanics,* **231,** 345-359 (1991).

Malhotra, K., and A. S. Mujumdar, "Immersed surface heat transfer in a vibrated fluidized bed," *Ind. Eng. Chem. Res.,* **26,** 1983-1992 (1987).

Marre, S., J. Palmeri, A. Larbot, and M. Bertrand, "Modeling of submicrometer aerosol penetration through sintered granular membrane filters," *Journal of Colloid and Interface Science,* **270,** (2004).

Marring, E., A. C. Hoffmann, and L. P. B. M. Janssen, "The effect of vibration on the fluidization behaviour of some cohesive powders," *Powder Technology,* **79,** 1-10 (1994).

Marring, E., A. C. Hoffmann, and L. P. B. M. Janssen, "A study of the discharge of cohesive powders under simultaneous aeration and vibration," *Particulate Science and Technology,* **13,** 7-21 (1995).

Marzocchella, A., and Salatino, P., "Fluidization of solids with CO2 at pressures from ambient to supercritical," *AIChE Journal,* **46,** 901-910 (2000).

Mathiesen, V., T. Solberg, H. Arastoopour, and B. H. Hjertager, "Experimental and computational study of multiphase gas/particle flow in a CFB riser," *AIChE Journal,* **45,** 2503-2518 (1999).

Matsuda, S., H. Hatano, T. Muramoto, and A. Tsutsumi, "Modeling for size reduction of agglomerates in nanoparticle fluidization," *AIChE Annual Meeting,* Indianapolis, Indiana (2002).

Matsuda, S., H. Hatano, T. Muramoto, and A. Tsutsumi, "Particle and bubble behavior in ultrafine particle fluidization with high G," *Fluidization X: Proceedings of the Tenth Engineering Foundation Conference on Fluidization,* Engineering Foundation, New York, 501-508 (2001).

Maus, R., and H Umhauer, "Collection efficiencies of coarse and fine dust filter media for airborne biological particles," *J. Aerosol Sci.,* **28,** 401-415 (1997).

Mawatari, Y., T. Koide, Y. Tatemoto, S. Uchida, and K. Noda, "Effect of particle diameter on fluidization under vibration," *Powder Technology,* **123,** 69-74 (2002).

Mawatari, Y., Y. Tatemoto, and K. Noda, "Prediction of minimum fluidization velocity for vibrated fluidized bed," *Powder Technology,* **131,** 66-70 (2003).

Mori, S., A. Yamamoto, S. Iwata, T. Haruta, and I. Yamada, "Vibro-fluidization of group-C particles and its industrial applications," *AIChE Symposium Series Advances in Fluidization Engineering,* **86,** 88-94 (1990).

Morooka, S., K. Kusakabe, A. Kobata, and Y. Kato, "Fluidization state of ultrafine powders," *Journal of Chemical Engineering of Japan,* **21,** 41-46 (1988).

Mutsers, S. M. P., and K. Rietema, "The effect of interparticle forces on the expansion of a homogeneous gas-fluidized bed," *Powder Technology,* **18,** 239-248 (1977).

Mutsers, S. M. P., and K. Rietema, "Gas-solids fluidization in a centrifugal field. The effect of gravity upon bed expansion," *Powder Technology,* **18,** 249-256 (1977).

Narsimhan, G. "On a generalized expression for prediction of minimum fluidization velocity," *AIChE Journal,* **11,** 550-554 (1965).

Noda, K., Y. Mawatari, and S. Uchida, "Flow patterns of fine particles in a vibrated fluidized bed under atmospheric or reduced pressure," *Powder Technology,* **99,** 11-14 (1998).

Park, S., and G. Stephanopoulos, "Packed bed bioreactor with porous ceramic beads for animal cell culture," *Biotechnology and Bioengineering,* **41,** 25-34 (1993).

Pacek, A. W., and A. W. Nienow, "Fluidised bed granulation of tungsten carbide from powder," *ICHEME –International Symposium on Agglomeration,* **5,** 151-160 (1989).

Pacek, A. W., and A. W. Nienow, "Fluidization of fine and very dense hardmetal powders," *Powder Technology,* **60,** 145-158 (1990).

Paola, A., and Riccardo, C., "Effect of cohesive interparticle forces on minimum fluidization velocity at high temperatures," *Fluidization XI: Proceedings of the Eleventh Engineering Foundation Conference on Fluidization,* Engineering Foundation, New York, (2004).

Pell, M., Handbook of Powder Technology Volume 8: Gas Fluidization, Elsevier Science Publishers B. V., Amsterdam (1990).

Perry R., D. Green, Perry's Chemical Engineer's Handbook, 6th Edition (1994).

Piepers, H.W., Cottaar, E.J.E., Verkooijen, A.H.M., and Rietema, K., "Effects of Pressure and Type of Gas on Particle-Particle Interaction and the Consequences for Gas Solid Fluidization Behavior," *Powder Technology,* **37**: 55-70 (1980).

Pirard, R., C. Alie, J.-P. Pirard, "Characterization of porous texture of hyperporous materials by mercury porosimetry using densification equation," *Powder Technology,* **128,** 242-247 (2002).

Qian, G.-H., R. Pfeffer, H. Shaw, and J. G. Stevens, "Fluidization of group C particles using rotating fluidized beds," *Fluidization X: Proceedings of the Tenth Engineering Foundation Conference on Fluidization,* Engineering Foundation, New York, 509-516 (2001).

Qian, G.-H., I. Bagyi, I. W. Burdick, R. Pfeffer, and H. Shaw, "Gas-solid fluidization in a centrifugal field," *Particle Technology and Fluidization,* **47,** 1022-1034 (2001).

Quevedo, J. A., personal communication (September 2003).

Quintanilla, M. A. S., A. Castellanos, and J. M. Valverde, "Correlation between bulk stresses and interparticle contact forces in fine powders," *Physical Review E,* **64,** 031301 (2001).

Rhodes, M. J., X. S. Wang, A. J. Forsyth, K. S. Gan, S. Phadtajaphan, "Use of a fluidized bed in studying Geldart Group B to A treansition," *Chemical Engineering Science,* **56,** 5429-5436 (2001).

Rietema, K., "Powders, what are they?" *Powder Technology,* **37,** 5-23 (1984).

Rietema, K., The Dynamics of Fine Powders, Elsevier Science Publishers, England (1991).

Rietema, K., E. J. E. Cottaar, and H. W. Piepers, "The effect of interparticle forces on the stability of gas-fluidized beds – II. theoretical derivation of bed elasticity on the basis of Ven Der Waals forces between powder particles," *Chemical Engineering Science,* **48,** 1687-1697 (1993).

Richardson, J. F., and W. N. Zaki, "Sedimentation and Fluidization: Part I," *Trans. Instn Chem. Engrs,* **32,** 35-53 (1954).

Rosensweig, R. E., J. H. Siegell, W. K. Lee and T. Mikus, "Magnetically stabilized fluidized solids," *AIChE Symposium Ser.,* **77,** 8 (1981).

Rosner D. E., and Y. F. Khalil, "Particle morphology- and Knudsen Transition-effects on thermophoretically-dominated total mass deposition rates from 'coagulation-aged' aerosol populations," *J. Aerosol Sci,* **31,** 273-292 (2000).

Rowe, P.N., "The Effect of Pressure on Minimum Fluidization Velocity," *Chem. Eng. Sci.,* **39,** 173-174 (1984).

Sanderson, J., and M. Rhodes, "Hydrodynamic similarity of solids motion and mixing in bubbling fluidized beds," *AIChE Journal,* **49,** 2317-2327 (2003).

Schreiber, R., C. Vogt, J. Werther, and G. Brunner, "Fluidized bed coating at supercritical fluid conditions," *Journal of Supercritical Fluids,* **24,** 137-151 (2001).

Screiber, R., B. Reinke, C. Vogt, J. Werther, and G. Brunner, "High-pressure fluidized bed coating utilizing supercritical carbon dioxide," *Powder Technology,* **138,** 31-38 (2003).

Schaefer D. W., "Fractal models and the structure of materials," *MRS Bulletin,* **13,** 22-27 (1988).

Sinclair, J. L., and R. Jackson, "Gas-particle flow in a vertical pipe with particle-particle interactions," *AIChE Journal,* **25,** 1473-1486 (1989).

Smith, C. R., "Trends towards rigidised filtration media dust collectors," *Filtech Europa 93 Coneference,* Karlsruhe, Germany (1993).

Squires, A. M., "Microreactors simulating present (and future?) fluid beds," *Fluidization X: Proceedings of the Tenth Engineering Foundation Conference on Fluidization,* Engineering Foundation, New York, 15-26, (2001).

Squires, A. M., and G. G. Benge, "Microreactor simulating reaction scene in turbulent fluid bed of group A powder: 2. usefulness in fluid-bed reaction engineering," *AIChE Symposium Series – Developments in Fluidization and Fluid-Particle Systems,* **91,** 128-135 (1995).

Srivastava, A., K. Agrawal, S. Sundaresan, S. B. Reddy Karri, and T. M. Knowlton, "Dynamics of gas-particulate flow in circulating fluidized beds," *Powder Technology,* **100,** 173-182 (1998).

Srivastava, A., and S. Sundaresan, "Role of wall friction in fluidization and standpipe flow," *Powder Technology,* **124,** 45-54 (2002).

Takahashi, T., Z. Tanaka, A. Itoshima, and L. T. Fan, "Performance of a rotating fluidized bed," *Journal of Chemical Engineering of Japan,* **17,** 333-336, (1984).

Tang, P., and J. A. Raper, "Modelling the settling behaviour of fractal aggregates – a review," *Powder Technology,* **123,** 114-125 (2002).

Tardos, G. I., I. Khan, and D. G. Schaeffer, "Forces on a slowly rotating, rough cylinder in a Couette device containing a dry, frictional powder," *Physics of Fluids,* **10,** 335-341 (1998).

Tasirin, S. M. and N. Anuar, "Fluidization behavior of vibrated and aerated beds of starch powders," *Journal of Chemical Engineering of Japan,* **34,** 1251-1258, (2001).

Tasirin, S. M. N. Anuar, and F. Rodzi, "Entrainment of fines (group C particles) from fluidized beds," *Fluidization X: Proceedings of the Tenth Engineering Foundation Conference on Fluidization,* Engineering Foundation, New York, (2001).

Tchabalala, S. N., and A. M. Squires, "Effect of axial gas dispersion on MTO Light-Olefin yield: microreactor data," *AIChE Journal,* **42,** 2941-2947 (1996).

Thivel, P.-X., Y. Gonthier, P. Boldo, and A. Bernis, "Magnetically stabilized fluidization of a mixture of magnetic and non-magnetic particles in a transverse magnetic field," *Powder Technology,* **139,** 252-257 (2004).

Thomas, B., M. O. Mason, Y. A. Liu, and A. M. Squires, "Identifying states in shallow vibrated beds," *Powder Technology,* **57,** 267-280 (1989).

Thomas, B., and A. M. Squires, "Vibrated-bed microreactors simulating catalytic fluid beds: a feasibility study," *Proceedings of the Sixth Annual International Fluidization Conference,* Banff, Alberta, Canada (1989).

Thomas, B., and A. M. Squires, "Support for Faraday's view of circulation in a fine-powder Chladni heap," *Physical Review Letters,* **81,** 574-577 (1998).

Thomas, B., M. O. Mason, R. Sprung, Y. A. Liu, and A. M. Squires, "Heat transfer in shallow vibrated beds," *Powder Technology,* **99,** 293-301 (1998).

Thomas, B., M. O. Mason, and A. M. Squires, "Some behaviors of shallow vibrated beds across a wide range in particle size and their implications for powder classification," *Powder Technology,* **111,** 34-49 (2000).

Tong H., O. Qiu, and H. Li, "Fluidization characteristics of cohesive ultrafine particles in a conical bed," *Fluidization XI: Proceedings of the Eleventh Engineering Foundation Conference on Fluidization,* Engineering Foundation, New York, (2004).

Tsutsumi, A., S. Nakamoto, T. Mineo, and K. Yoshida, "A novel fluidized-bed coating of fine particles by rapid expansion of supercritical fluid solutions," *Powder Technology,* **85,** 275-278 (1995).

Valverde, J. M., A. Castellanos, P. Mills, and M. A. S. Quintanilla, "Effect of particle size and interparticle force on the fluidization behavior of gas-fluidized beds," *Physical Review E,* **67,** 051305 (2003).

Valverde, J. M., A. Castellanos, and M. A. S. Quintanilla, "Effect of vibration on the stability of a gas-fluidized bed of fine powder," *Physical Review E,* **64,** 021302-1 (2001).

Valverde, J. M., A. Castellanos, and M. A. S. Quintanilla, "Self-diffusion in a gas-fluidized bed of fine powder," *Physical Review Letters,* **86,** 3020-3023 (2001).

Valverde, J. M., M. A. S. Quintanilla, A. Castellanos, and P. Mills, "Experimental study on the dynamics of gas-fluidized beds," *Physical Review E,* **67,** 016303 (2003).

Valverde J. M., A. Ramos, A. Castellanos, and P. K. Watson, "The tensile strength of cohesive powders and its relationship to consolidation, free volume and cohesivity," *Powder Technology,* **97,** 237-245 (1998).

Van der Gulik, P. S., "Viscosity of carbon dioxide in the liquid phase," *Physica A,* **238,** 81-112 (1997).

Veale, C. R., Fine Powders: Preparation, Properties and Uses, John Wiley & Sons, Inc., New York, (1972).

Venkatesh, R. D., M. Grmela, and J. Chaouki, "Simulations of vibrated fine powders," *Powder Technology,* **100,** 211-222 (1998).

Vogt, C., R. Schreiber, J. Werther, and G. Brunner, "Influence of hydrodynamics on fluidized bed coating at supercritical fluid conditions," *Fluidization XI: Proceedings of the Eleventh Engineering Foundation Conference on Fluidization,* Engineering Foundation, New York, (2004).

Wang, Y., G. Gu, F. Wei, and J. Wu, "Fluidization and agglomerate structure of SiO2 nanoparticles," *Powder Technology,* **124,** 152-159 (2002).

Wang, Y., F. Wei, Y. Jin, and T. Luo, "Agglomerate particulate fluidization and E-particles," *Proceedings of CUChe-3*, (2000).

Wang, Z., M. Kwauk, and H. Li, "Fluidization of fine particles," *Chemical Engineering Science*, **53**, 377-395 (1998).

Wang, Z., X. Lu, and H. Li, "Modeling fluidized agglomerate size of cohesive particles," in press *Powder Technology*.

Wank, J. R., S. M. George, and A. W. Weimer, "Vibro-fluidization of fine boron nitride powder at low pressure," *Powder Technology*, **121**, 195-204 (2001).

Wank, J. R., S. M. George, and A. W. Weimer, "Nanocoating individual cohesive boron nitride particles in a fluidized bed by ALD," *Powder Technology*, **142**, 59-69 (2004).

Watano, S., H. Nakamura, K. Hamada, Y. Wakamatsu, Y. Tanabe, R. N. Dave, and R. Pfeffer, "Fine particle coating by a novel rotating fluidized bed coater," *Powder Technology*, **141**, 172-176 (2004).

Watano, S., R. Pfeffer, R. N. Dave, and W. Dunphy, "Dry particle coating by a newly developed rotating fluidized bed coater," *Advanced Technologies for Fluid-Particle Systems*, **95**, 112-116 (1999).

Watano, S., K. Terashita, and K. Miyanami, "Analysis of granulation process and determination of operational end point in a tumbling fluidized bed granulation," *Bulletin of University of Osaka Prefecture*, **41**, 47-56 (1993).

Webb, C., G. M. Black, and B. Atkinson, "Liquid fluidisation of highly porous particles," *Chem. Eng. Res. Des.*, **61**, 125-134 (1983).

Wen, C. Y., and Y. H. Yu, "A generalized method of solid particles," *Chem Eng. Progr.*, **44**, 201-217 (1948).

Werth, J. H., M. Linsenbuhler, S. M. Dammer, Z. Farkas, H. Hinrcihsen, K.-E. Wirth, and D. E. Wolf, "Agglomeration of charged nanopowders in suspensions," *Powder Technology*, **133**, 106-112, (2003).

Werther, J., "Fundamentals of Fluidized Bed Technology," *German Chemical Engineering*, **6**: 228-235 (1983).

Wu, R. M., and D. J. Lee, "Hydrodynamic drag force exerted on a highly porous sphere moving towards an impermeable plate," *Chemical Engineering Science*, **53**, 3571-3578 (1998).

Xu, C., Y. Cheng, and J. Zhu, "Fine particle fluidization - effects of mechanical/acoustic vibrations," *Fluidization XI: Proceedings of the Eleventh Engineering Foundation Conference on Fluidization,* Engineering Foundation, New York, (2004).

Xu, C., and J. Zhu, "Prediction of minimum fluidization velocity for fine particles of various degrees of cohesiveness and effects of mechanical/acoustic vibrations," *Fluidization XI: Proceedings of the Eleventh Engineering Foundation Conference on Fluidization,* Engineering Foundation, New York, (2004).

Yang, W.-C., D. C. Chitester, R. M. Kornosky, and D. L. Keairns, "A generalized methodology for estimating minimum fluidization velocity at elevated pressure and temperature," *AIChE Journal,* **31,** 1086-1092 (1985).

Yao, W., G. Guangsheng, W. Fei, and W. Jun, "Fluidization and agglomerate structure of SiO2 nanoparticles," *Powder Technology,* **124,** 152-159 (2002).

Yi, W., W. Ting-Jie, Y. Yi, and J. Yong, "Resonance characteristics of a vibrated fluidized bed with a high bed hold-up," *Powder Technology,* **127,** 196-202 (2002).

Yoshida, T., Y. Kousaka, and A. Yutani, "Gas-solid fluidized bed having mechanically vibrated gas distributor," *Kagaku Kogaku Chemical Engineering,* **29,** 875-879 (1965).

Youzhi, L., Z. Jiyu, and Z. Bijiang, "Separation of a binary particle mixture in a vibrating fluidized bed of dense medium," *Powder Technology,* **100,** 41-45 (1998).

Yu B., and W. Liu, "Fractal Analysis of permeabilities for porous media," *AIChE Journal,* **50,** 46-57 (2004).

Yu, H., F. Wei, Y. Wang, and G. Luo, "Hydrodynamics of carbon nanotubes in a nano-agglomerates fluidized bed," *Fluidization XI: Proceedings of the Eleventh Engineering Foundation Conference on Fluidization,* Engineering Foundation, New York, (2004).

Yu, Q., personal communication (July 2004).

Zhou, T., and H. Li, "Estimation of agglomerate size for cohesive particles during fluidization," *Powder Technology,* **101,** 57-62 (1999).

Zhou, T., and H. Li, "Force balancing modeling for agglomerating fluidization of cohesive particles," *Powder Technology,* **111,** 60-65 (2000).

Zhu, C., C. H. Lin, G. H. Qian, and R. Pfeffer, "Modeling of the pressure drop and flow field in a rotating fluidized bed," *Chemical Engineering Communications,* **190,** 1132-1154 (2003).

Zhu, C., G. Liu, Q. Yu, R. Pfeffer, R. N. Dave, C. H. Nam, "Sound assisted fluidization of nanoparticle agglomerates," *Powder Technology,* **141,** 119-123 (2004).

Zhu, Q., and H. Li, "Study on magnetic fluidization of group C powders," *Powder Technology,* **86,** 179-185 (1996).

Zurita-Gotor, M., and D. E. Rosner, "Effective Diameters for collisions of fractal-like aggregates: recommendations for improved aerosol coagulation frequency predictions," *J. Colloid Interface Sci.,* **255,** 10-26 (2002).